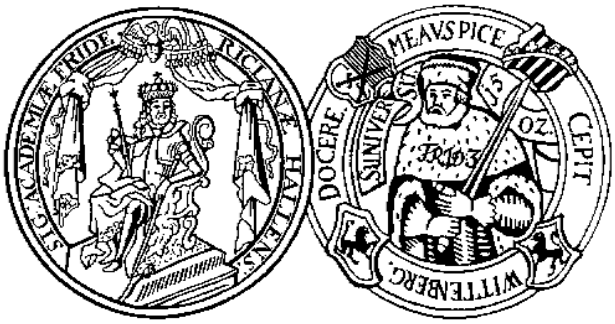

Structure Based Design, Synthesis and Characterization of Small Molecules as Inhibitors of Parasitic Targets

Dissertation

zur Erlangung des

Doktorgrades der Naturwissenschaften (Dr. rer. nat.)

der

Naturwissenschaftliche Fakultät I - Biowissenschaften

Martin-Luther-Universität Halle-Wittenberg

vorgelegt von

Theresa Bayer

geb. am 22. Oktober 1986 in Hamburg

Gutachter:

1. Professor Dr. Wolfgang Sippl

2. Professor Dr. Bodo Dobner

3. Professor Dr. Ralph Holl

Halle (Saale), 14. Januar 2021

Der traurigste Aspekt derzeit ist, dass die Wissenschaft schneller Wissen sammelt, als die Gesellschaft Weisheit.

Isaac Asimov

Für meine Familie

Table of content

Abbreviations

^{1}H-NMR	^{1}H-Nuclear Magnetic Resonance
Ag_2SO_4	Silver sulphate
Ar	Aryl-residue
$BrCH_2CO_2Me$	Methyl bromacetate
Bt	Benzotriazole
CH_3CN	Acetonitrile
DABCO	1,4-Diazabicyclo[2.2.2]octan
DMF	Dimethylformamide
DMSO	Dimethyl sulfoxide
DNA	Deoxyribonucleic acid
DPBS	Dulbecco's phosphate-buffered saline
eq	Equivalent
ESI	Electrospray-ionization
EtOH	Ethanol
FdL	Fluor de Lys®
h	Hour
HAT	Histone acetyl transferase
HBTU	***N,N,N',N'***-Tetramethyl-*O*-(1*H*-benzotriazol-1-yl)uronium hexafluorophosphate
HCl	Hydrochloric acid
HDAC	Histone deacetylase
HEK	Human embryonic kidney
*h*HDAC	Human Histone deacetylase
HPβCD	(2-Hydroxypropyl)-beta-cyclodextrin
HPLC	High pressure / performance liquid chromatography

$HSCH_2CO_2Me$	Methyl thioglycolate
K_2CO_3	Potassium carbonate
KOH	Potassium hydroxide
LC	liquid chromatography
MeOH	Methanol
MOE	Molecular Operating Environment
MPLC	Medium pressure liquid chromatography
MRM	multiple reaction monitoring
MS	Mass spectrometry
NAD	Nicotineamide adenine dinucleotide
NaOH	Sodium hydroxide
NH_2OTHP	*O*-(Tetrahydro-*2H*-phran-2-yl)hydroxylamine
PDB	Protein data bank
$Pd(OAc)_2$	Palladium(II) acetate
*Pf*HDAC1	*Plasmodium falciparum* histone deacetylase 1
PK	pharmacokinetics
PyBOP®	Benzotriazol-1-yl-oxytripyrrolidinophosphonium-hexafluorophosphat
PZQ	Praziquantel
RNA	Ribonucleic acid
RT	Room temperature
*sm*HDAC8	*Schistosoma mansoni* histone deacetylase 8
S. mansoni	*Schistosoma mansoni*
tcDAC2	*Trypanosoma cruzi* deacetylase 2
T.cruzi	*Trypanosoma cruzi*
THF	tetrahydrofurane

THP	Tetrahydropyran
TLC	Thin layer chromatography
Trityl	Triphenyl methyl
TSA	Trichostatin A
WHO	World Health Organisation

Table of figures

List of Tables

1 Introduction

1.1 Parasitic diseases

1.1.1 Schistosomiasis

Schistosomiasis is a parasitic disease which is caused by a flatworm of the genus *Schistosoma*. It is also known as bilharzias named after the German doctor Theodor Bilharz, who first reported the disease[1]. There are five schistosome species known that can infect humans, namely *Schistosoma mansoni*, *Schistosoma haematobium*, *Schistosoma intercalatum*, *Schistosoma japonicum* and *Schistosoma mekongi*, of which *S. mansoni* is the most widely spread species. Like all schistosomes it uses a freshwater mollusk (in the case of *S. mansoni: Biomphalaria sp.*) as an intermediate host[2–6]. Its cercariae penetrate human skin evolving into adult worms. After the first contact, the patient would develop little itchy pustules on the skin as an immunological reaction to the cercariae the penetrated the skin. This is commonly called swimmers itch or swimmers rash. After the cercariae reach the human blood stream they mature to be adult worm. The shorter male wraps around the longer but thinner female and they become an inseparable unit (see figure 1). Depending on the species the paired couple can lay one hundred or even up to one thousand eggs daily. Various serious symptoms including fatigue, myalgia, eosinophilia and fevers as well as chronic diarrhea, liver or lung fibrosis, bladder cancer, hepatosplenomegaly and encephalitis are a result of the body's reaction to the constant exposure to rejected schistosome eggs[2,7,8]. The eggs are excreted with the urine or feces of the host and can then if reaching fresh water again infect a mollusk as a

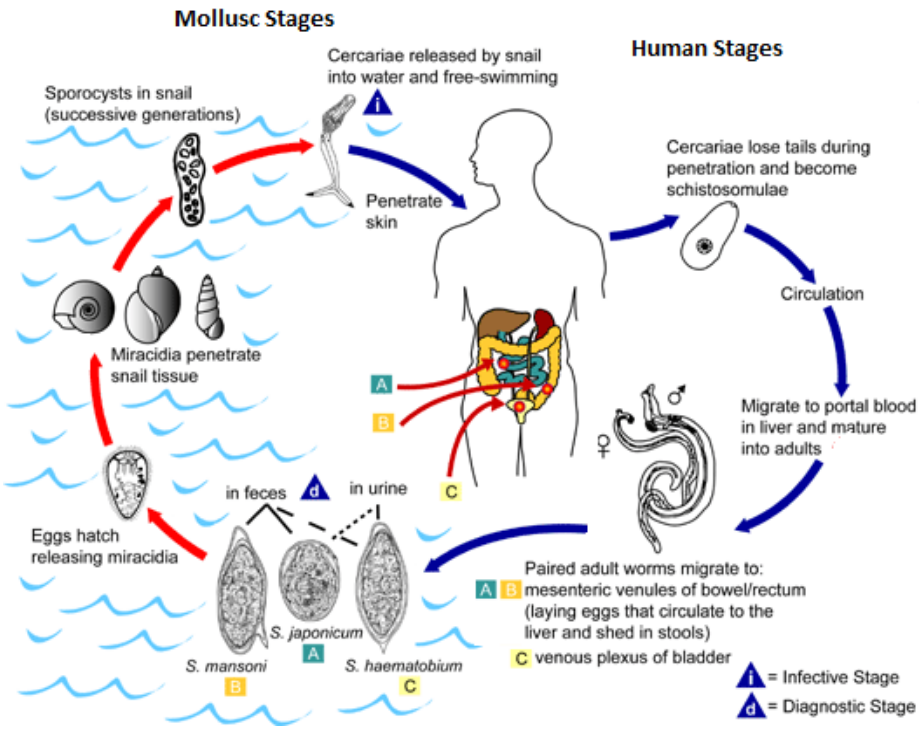

Figure 1 Lifecycle of Schistosomiasis (modified after CDC[123])

miracidium. Schistosomiasis is the second most important parasitic disease next to malaria. Worldwide more than 265 million individuals are infected[9] among whom 280 000 die annually[3,4]. To date, there is no effective vaccine available for schistosomiasis so the control of the disease relies on a single drug. The anthelmintic praziquantel (Biltricide®) is effective against all forms of human schistosomiasis and is well tolerated with no major negative side effects[10]. For this reason it is used in mass treatment programs, particularly in sub-Saharan Africa and has led to significant reductions in disease morbidity and mortality[2,4,10–12]. In 2014, more than 61 million people in 30 countries have received treatment with praziquantel[10,13]. Due to this intensive use, there have been reports of treatment failure from different regions[2,14,15]. Together with the demonstrated ease of inducing resistance in laboratory strains of the parasite, this emphasizes the need for alternative therapeutic strategies [2,10,14–18].

1.1.2 Chagas disease

Chagas disease is named after Carlos Chagas, a Brazilian physician who discovered it in 1909 it is caused by the protozoal parasite *Trypanosoma cruzi*. It is also referred to as American trypanosomiasis and is a potentially life threatening illness. In Latin America the disease is mostly transmitted through a vector which makes it a vector-borne disease. Humans can be infected through contact with the feces or urine of infected blood sucking triatomine bugs (see figure 2). Triatomine bugs are active at night biting exposed areas of skin and then defecate and urinate close to the bite. *T. cruzi* is transmitted to the human when infected feces get in contact with a skin damage (possibly caused by the vector's bite) or mucosal surfaces such as eyes or mouth.

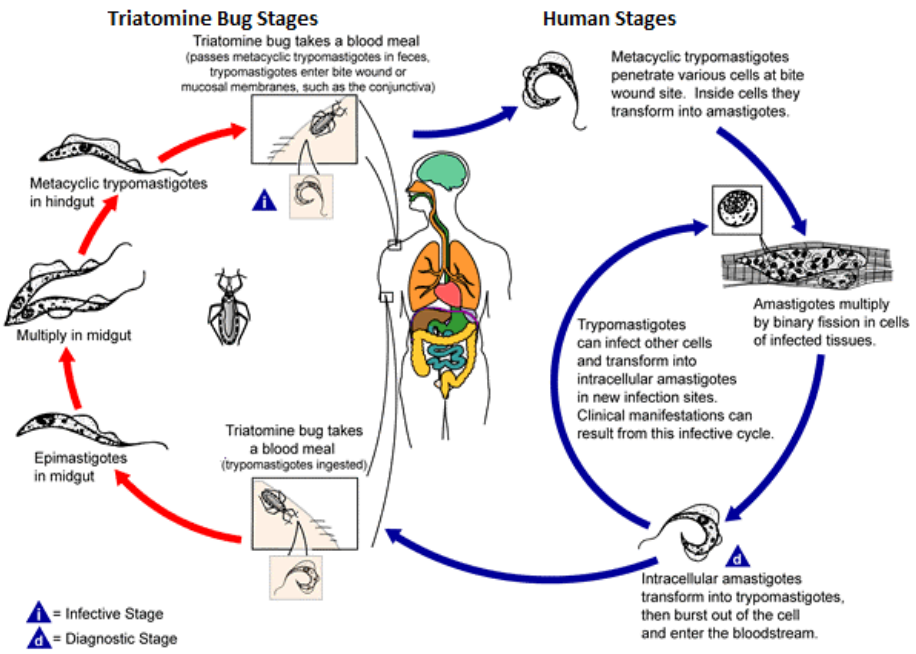

Figure 2 Trypanosoma cruzi (modified after CANTEY ET AL[124])

Different possibilities of infection with this parasite are by direct contact with contaminated blood (i.e. contaminated blood transfusions or congenital transmission during pregnancy or childbirth), organ transplantation from infected organ donors or laboratory accidents or even by consuming food which is contaminated with triatomine bug's waste[19].

The disease is subdivided into two phases, an initial acute phase which lasts for approximately two months and a chronic phase that succeeds the acute phase. During the acute phase the symptoms are usually mild or completely absent. However a high number of parasites circulate in the blood. Unspecific symptoms such as skin lesions or the so-called Romaña sign which is a unilateral painless swelling of an eyelid can help in the diagnosis of chagas disease. After the acute phase the parasites are not circulating in the blood but are rather hidden in the heart and / or digestive muscles. This causes cardiac disorders in approximately 30 % of the infected and digestive, neurological or mixed

symptoms in approximately 10 % of the patients. The different clinical symptoms may require specific treatment. The infection can lead to sudden death years after the first contact with contaminated material. The deaths are usually caused by arrhythmia or heart failure due to the parasitic colonization of the heart muscles[20].

There are two anti-parasitic drugs used in the therapy of chagas disease, benznidazole (Lafepe®) and nifurtimox (Lampit®). If applied during the acute phase both drugs are up to 100 % effective in curing *T. cruzi* infections. The more time has passed since the initial infection the more the efficacy of the both drugs diminishes[21]. Treatment is definitely indicated in children especially congenital cases. Also patients during the early chronic phase and those patients in whom the disease has been reactivated due to immunosuppression require treatment. Adult infected people should be offered treatment in order to prevent the progression and further transmission of the disease rather than expecting a complete cure[22,23]. The treatment requires up to two months and in approximately 40 % of the patients there can be adverse reactions. This should be weighed against the possible benefits of medical treatment of patients after the acute phase.

Worldwide estimates of 6-7 million people are infected with *T. cruzi*. The greater majority of the infected population is located in the endemic areas of numerous Latin American countries. There has been a shift of the epidemiological pattern from it being a mainly rural disease to increasing numbers of infections on the urban regions due to higher mobility of the people. Furthermore there have been increasing numbers of reported cases in the United States of America, Canada, several European countries and two Western Pacific countries[24].

Adding up all diagnosed and untreated and the estimated number of undiagnosed cases who are a reservoir for active vectorial and oral transmission approximately 75 million people are at risk of infection with chagas disease.

With no vaccine available vector control has been the most efficient prevention method for trypanosomiasis in Latin America. Transmission via infected blood transfusions or transplantation of infected organs can be prevented by blood screening with laboratory quality control[25]. Eradication of the disease would be fairly difficult due to the large reservoir of *T. cruzi* parasites in wild animals. Instead it is important to focus on eliminating transmission to humans and improve early diagnosis and treatment of infected individuals.[19]

1.1.3 Malaria

Malaria is a vector-borne parasitic infection that is transmitted by female Anopheles mosquitos (see figure 3). It can be caused by five different parasite of the genus *Plasmodium* (*P. falciparum*, *P. malariae*, *P. ovale*, *P. vivax* and *P. knowlesi*)[26,27]. In humans most infections are caused by *P. falciparum* (approximately 75% of infections) followed by P. vivax (approximately 20% of infections)[28].

In 2017 an estimated 219 million malaria infections occurred worldwide. The great majority of the infections occurred in Sub-Saharan African countries and South-East Asian countries followed by a small percentage that occurred in the Eastern Mediterranean region. In 2017 there were also approximately 435 000 deaths on account of malaria infections which makes malaria the most important parasitic disease worldwide[29].

The disease is transmitted by the bite of an infected Anopheles mosquito, then the parasite passes a human liver stage to then enter an erythrocytic cycle in the human blood stage (figure 3). First symptom usually occur after an incubation time of about 9 to 30 days and are unspecific flulike symptoms. Reoccurring fevers are the most characteristic symptom of malaria but also other symptoms like nausea, vomiting, myalgia, headaches and dizziness may show[30]. Neurological symptoms such as abnormal posturing, seizures, nystagmus, conjugate gaze palsy or coma can turn up in case of cerebral malaria[31]. A malaria infection can lead to serious complications especially if untreated or undiagnosed.

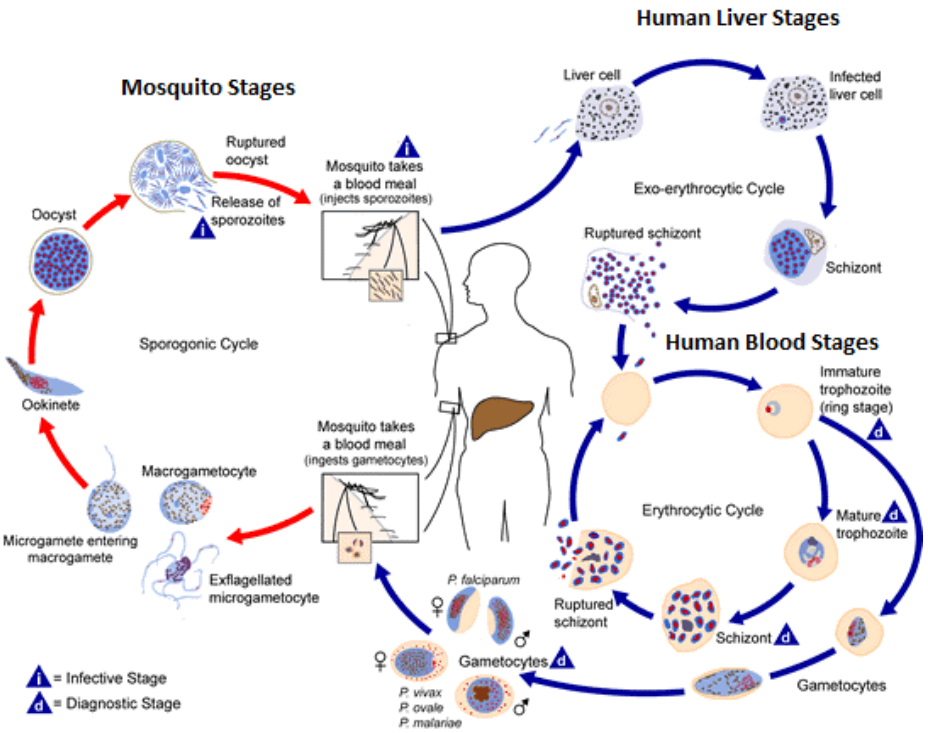

Figure 3 Lifecycle of Plasmodium sp. (modified after CDC[125])

One important attempt of malaria control is vector control. There are two main measures to vector control which summed up can be effective in reducing malaria transmission in certain regions. One is using insecticide treated nets (and ensuring that every individual at risk of malaria sleeps under an insecticide treated net). And the second one is indoor spraying with residual insecticides which can last up to 3-6 months[32].

There is also a variety of medical drugs that are used for prevention and treatment of malaria. The World Health Organization (WHO) recommends a treatment with artemisinin-based combination therapy possibly with and additional single dose of primaquine for all uncomplicated *P. falciparum* infections. *P. vivax* infections are to be treated with chloroquine of in case of chloroquine resistance also with artemisinin-based combination therapy. Additionally the infected should receive full primaquine treatment to prevent relapses. The severe malaria infections should be treated with intramuscular or intravenous administration of injectable artesunate for 24 hours followed by a 3-day therapy with artemisinin-based combination therapy[29].

Travelers visiting regions with the risk of malaria infection can either take preventive therapy or have stand by medication to take in case of signs of an infection. Preventive treatment mainly relies on three drugs / drug combinations namely mefloquine, doxycycline and atovaquon/proguanil (also known as Malarone®). Mefloquine is administered weekly but has a potential of psychological side effects like abnormal dreams, anxiety and depressed moods. Doxycycline is fairly low in cost and taken daily[33]. It should not be used by children younger than eight years and can cause indigestion and photosensitivity[34].

1.2 Epigenetics

Epigenetics is a field of biology; its name is derived from the Greek prefix “epi-” which means “over, around something, outside something” and genetics which is the study of genes, genetic variations and heredity in living organisms[35]. Epigenetics is defined as the inheritable change in gene expression and describes the differences in phenotypes without changing the genotypes[36]. This phenomenon enables the differentiation of cells and allows them to react to endogenous signals such as environmental influences or pathogens[37,38]. Epigenetic mechanisms are responsible for transcriptional control. They determine the time of DNA- replication and –repair[39]. On a molecular basis epigenetic mechanisms govern the dynamic balance between different states of covalent modifications to the DNA itself and the histone proteins around which the DNA is wrapped as well as non-histone proteins[40]. Covalent modifications to the DNA such as methylation or hydroxy methylation of cytosine in position 5 causes a silencing of a specific gene[41]. Covalent changes to the histone proteins have a broader variety of possible effects. They can either activate genes or suppress them[42,43]. The best investigated histone modifications are acetylation / deacetylation, methylation / demethylation and phosphorylation / dephosphorylation. However there are more mechanisms namely ubiquitinylation, ADP-ribosylation and SUMOylation[38,44]. These mechanisms govern the interactions of the great number of genes and enzymes. They regulate the cellular differentiation, the cell cycle as well as they are able to initiate the programmed cell death which is called apoptosis[15,44,45].

1.2.1 Histones modifying enzymes

DNA in eukaryotic cells is wrapped around alkaline proteins called histones. This highly organized structure enables the DNA to fit into the nucleus because it results in a very compact molecule (see figure 4). To date there are five different types of histone proteins known H1, H2A, H2B, H3 and H4[14,46]. Two of each of the core proteins (H2A, H2B, H3 and H4) form an octameric structure which is called a histone. One of these histones fits 146 base pairs which are wound around it like a spool[46–48]. The N-terminal tail regions contain numerous alkaline lysine and arginine residues. In physiological conditions these residues are protonated so they carry a positive charge. The positive charge allows electrostatic interactions with the negatively charged phosphate groups which form the backbone of the DNA together with deoxyribose. One histone with its associated DNA wrapped around it 1.65 times is called a nucleosome[47]. Nucleosomes are the smallest

subunits of the chromatin[15]. The nucleosomes are connected to one another with non-associated linker DNA[44,49].

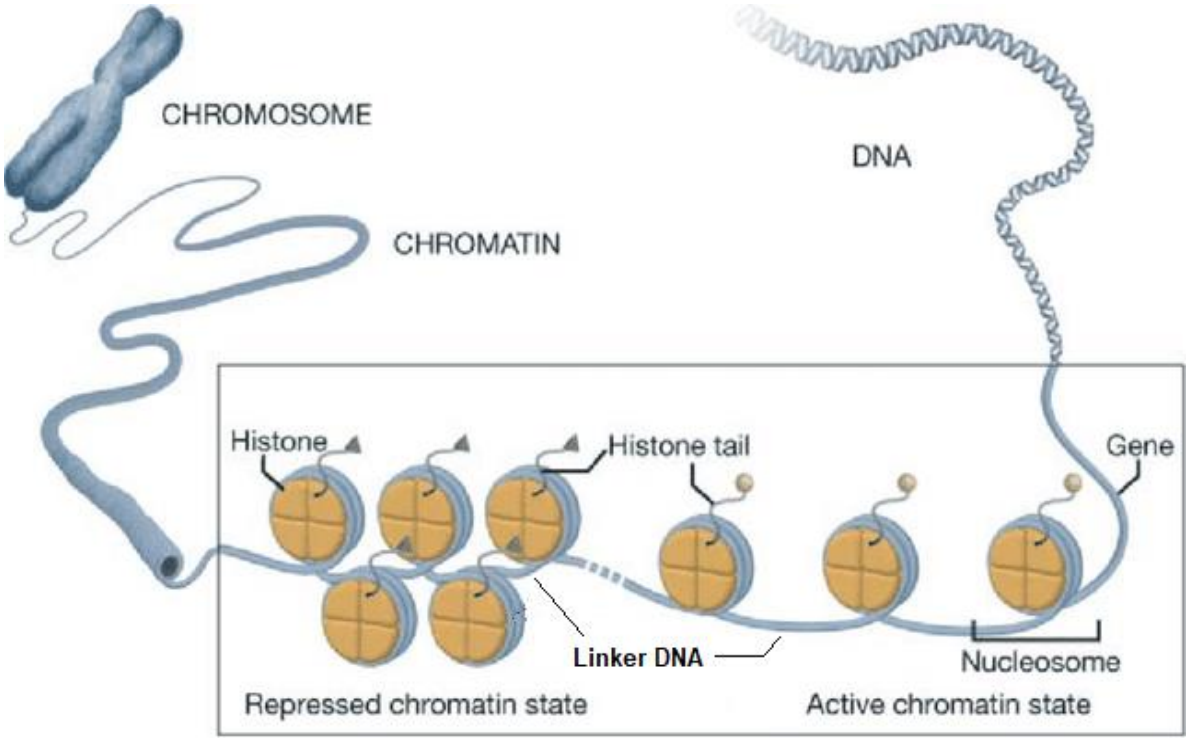

Figure 4 Chromatin structure of modified after PIETERMAN[49]

When the DNA is wrapped tightly around the histones genes cannot be transcribed, this repressed chromatin state is called hetero chromatin[49]. The positively charged amino acid residues of the histone tails make them accessible to posttranslational modifications such as acetylation or methylation[13–15,49]. Acetylation of the histone results in decreased interactions between the histones and the negatively charged DNA. The active chromatin state is described by a loosened DNA – histone packing which enables the transcription of genes. The chromatin in active state is also known as euchromatin[48]. The variable intensity interactions of histones and their associated DNA is dependent on various modifications to the histones. These modifications are controlled by certain enzymes which are summed up under the term histone modifying enzymes. The group of histone modifying enzymes is subdivided by the function of the respective group of enzymes. The *"writers"* add modifications to the histone tails. As outlined in figure 7 there are kinases adding phosphate residues, histone acetyl transferases (HATs) adding acetyl residues and histone methyl transferases (HMTs) adding methyl residues. The group of *"readers"* recognizes and interacts with the modifications for example acetylated lysine residues of the histone tails

are recognized by bromodomains whereas methylated lysine residues are recognized by *plant homeodomains* (PHDs). Consequently the *"erasers"* for example histone deacetylases (HDACs) or histone demethylases (HDMs) are enzymes that remove modifications from the histone tails[50].

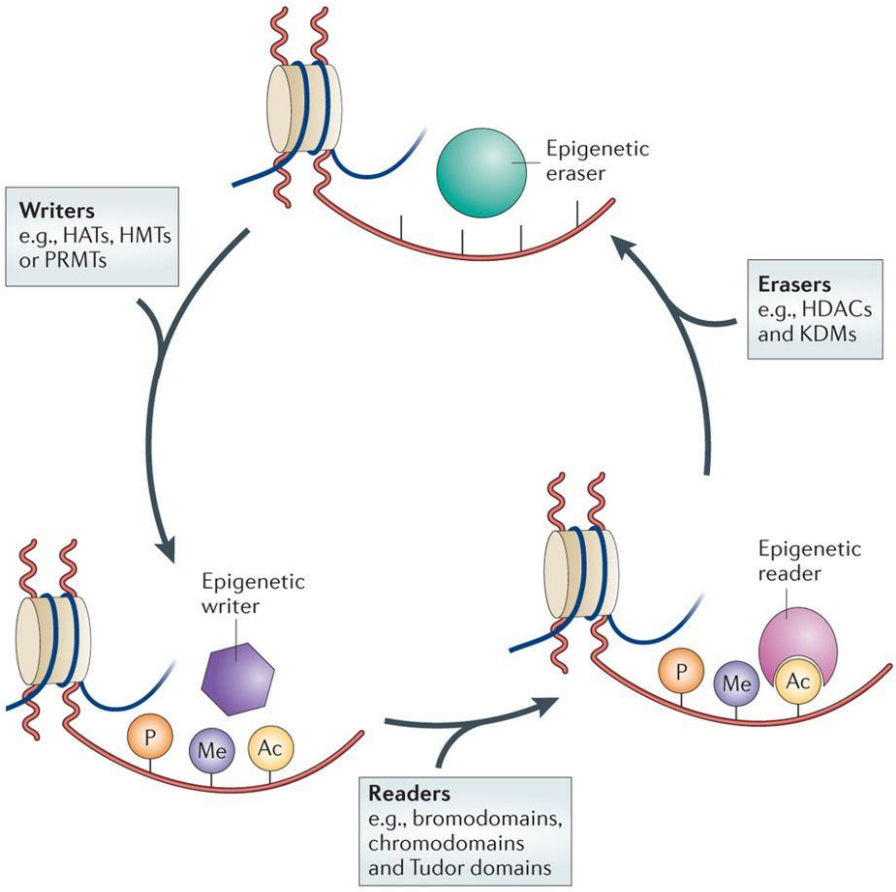

Figure 5 Histone modifying enzymes modified after FALKENBERG[50]

1.2.2 Histone deacetylases (HDACs)

Histone deacetylases are the natural antagonists of the histone acetyl transferases. They remove acetyl residues from lysine residues of histone tails. Additionally they are able to remove acetyl residues form other non-histone proteins, therefore they are also referred to as lysine deacetylases (KDACs). The state of acetylation of histones determines the degree of interaction with DNA and, therefore, the balance between heterochromatin, the condensed state and euchromatin, the open state of chromatin. With this switch function the family of histone deacetylases plays a key-role in regulation of genes being accessible to transcription or not[49–52] (figure 5 and 6).

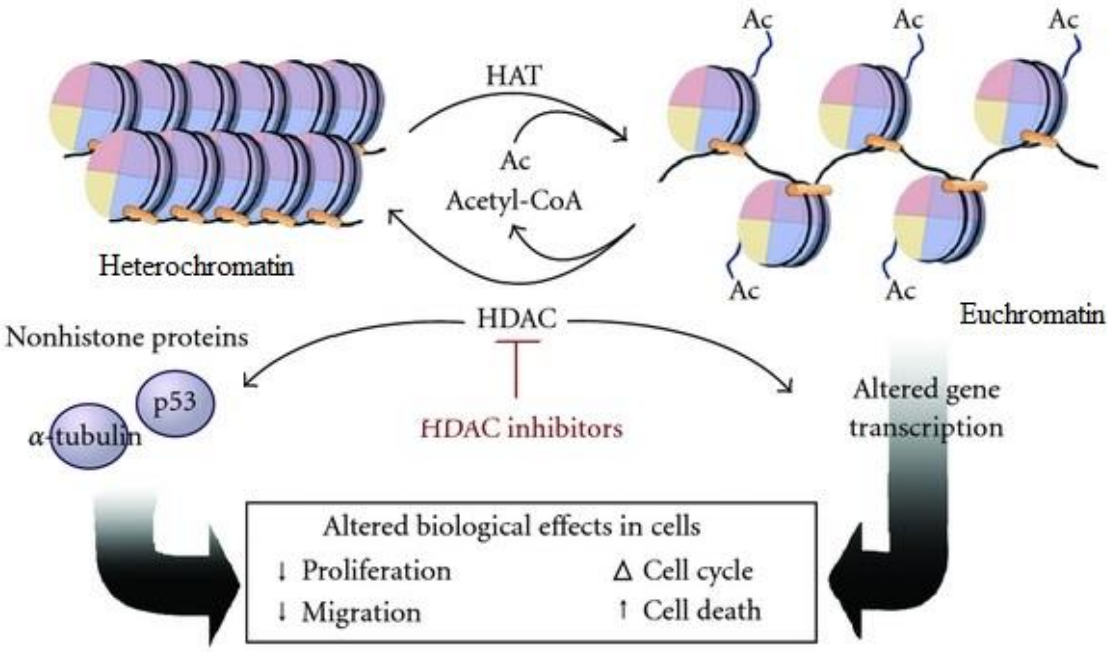

Figure 6 Histone acetylation and deacetylation modified after Rodd et al.[51]

Acetylation of the histones results in a loosened interaction with the DNA and the genes are accessible for transcription[46].

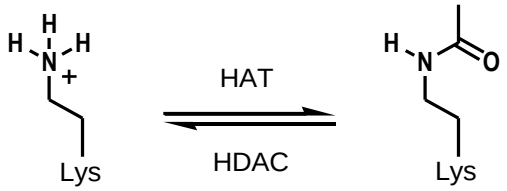

Figure 7 Conversion between the acetylated and non-acetylated state of lysine

The key role histone deacetylases play in transcriptional control is not only depending on their ability to deacetylate lysine residues (figure 7) in histone tails but also other proteins. Among these non-histone proteins are transcription factors, cytoskeletal proteins like α-tubulin or proteins like p53 and chaperones that are affected in their stability by their state of acetylation[53–55]. To date there are 18 known lysine deacetylases that are subdivided into four main classes. Class one Histone deacetylases are HDAC1-3 and HDAC8, class 2 consists of HDAC4-7, 9 and 10, class 3 histone deacetylases are also called sirtuins and consists of SIRT1-7 and class 4 only holds one enzyme, HDAC11[54]. Class 2 is subdivided

into two groups class 2a containing HDAC4, 5, 7, 9 and class 2b HDAC 6 and HDAC10. The criterion for this subdivision is the number of catalytic domains in the enzyme. Class 2a enzymes have one catalytic domain whereas class 2b enzymes have two catalytic domains[46]. The first classification can be the differentiation of the histone deacetylases by their catalytic mechanism. Class 1, 2 and 4 are zinc-dependent enzymes whereas the class 3 enzymes, the sirtuins are NAD^+-dependent. The zinc-dependent HDACs are the "classical" histone deacetylases and are subdivided into class 1 and class 2 by their similarity to different enzymes found in *Saccharomyces cerevisae*[46,56]. Class 4 does not fit into these classifications and contains only HDAC11[57].

Generally speaking it can be roughly stated that class 1 HDACs are ubiquitously expressed except for HDAC8 which is only expressed in small amounts. They are found exclusively in the nucleus as multi protein complexes (again with the exception of HDAC8) and take part in proliferation and survival of cells. However class 2 HDACs are expressed rather restrictedly which suggests an involvement in developmental processes and cellular differentiation. They are able to shuttle between the nucleus and the cytoplasm in response to certain cellular signals; they show tissue specific activity like deacetylation of tubulin and cortactin or chaperones. Class 4, HDAC11 seems to have a role in immune system activation and immune tolerance[46,57,58].

1.2.3 Structure of class 1 histone deacetylases

The histone deacetylases of class 1 have a common general structure. They have an α/β domain with a sandwich-like composition. Approximately half of the amino acids form secondary structures, the other half form loops between the secondary structure elements as well as the catalytic pocket. In the center of the enzyme there is an 8 β-sheet which is positioned between two layers of α-helices. A zinc ion (Zn^{2+}) is coordinated at the bottom of the catalytic pocket by two conserved aspartate residues as well as one histidine residue[59,60] (see figures 8 and 9).

The catalytic region resembles a 12 Angstrom long hydrophobic pocket with a catalytic zinc ion at its bottom. This was demonstrated in a crystal structure of an inactive mutant of the human HDAC8 and a p53 derived diacetylated substrate ((N-acetyl)Arg-His-Lys(ε-acetyl)-Lys (ε-acetyl)(*C*-amino-7-yl-methyl-4-coumarine)) (PDB 2V5X) as can be seen in figure 8. The crystal structure of this enzyme substrate complex confirmed the position and shape of the binding pocket that had been assumed according to several inhibitors[61]. However the crystal structure revealed more insights to the binding pocket. The carbonyl

oxygen of the acetyl residue of the p53 derived peptide coordinated towards the catalytic zinc ion. Throughout all class 1 and class 2 histone deacetylases there is a conserved aspartate (Asp 101). It is positioned on the rim of the catalytic pocket and interacts with the peptide backbone of the substrate. Positioning the substrate correctly and adhering it throughout the process of deacetylation is likely to be the function of the conserved aspartate[54,61].

The described general structure has been confirmed by more than 50 solved crystal structures of human class I HDACs. Recently first crystal structures of the parasitic *S. mansoni* HDAC8 (*sm*HDAC8) have been solved. They demonstrated high similarity to their human orthologues, especially to human HDAC8 (*h*HDAC8). Figure 9 shows the superposition of the *h*HDAC8 (PDB 1T69) and the *sm*HDAC8 (PDB 4BZ6) both co-crystalized with the inhibitor SAHA. They both have a characteristic α/β-fold of the catalytic domain and a long hydrophobic pocket with the zinc ion at the bottom. The main differences are in the loops not adjacent to the catalytic pocket. The amino acid constitution of the substrate binding pocket is also highly similar, but not identical, which opens the doors for structure-based drug design.

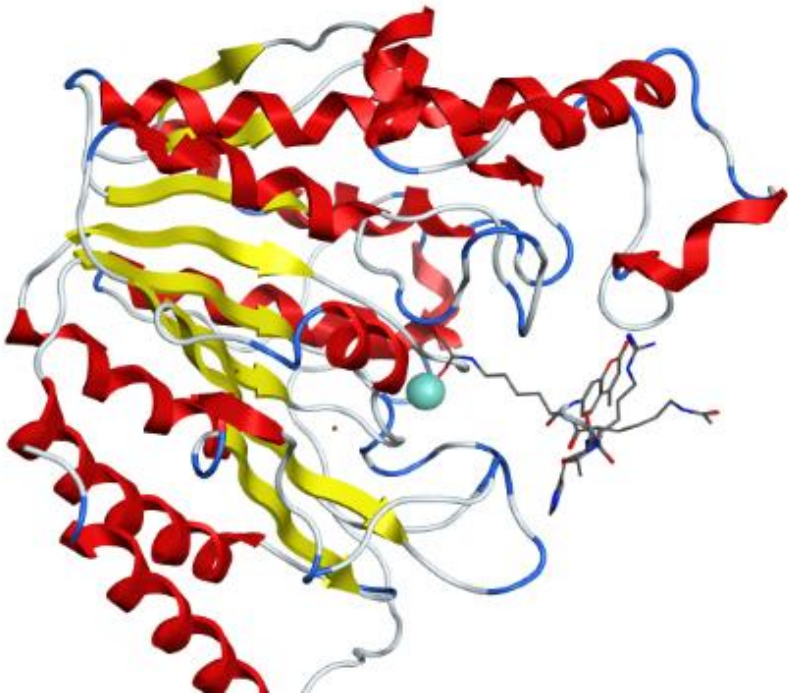

Figure 8 Crystal structure of an inactive Tyr306Phe mutant of the human HDAC8 co-crystalized with the artificial substrate ((N-acetyl)Arg-His-Lys(ε-acetyl)-Lys (ε-acetyl)(C-amino-7-yl-methyl-4-coumarine) (grey) (PDB 2V5X); the catalytic zinc ion is shown in turquoise at the bottom of the catalytic pocket. Modified after VANNINI ET AL[61]

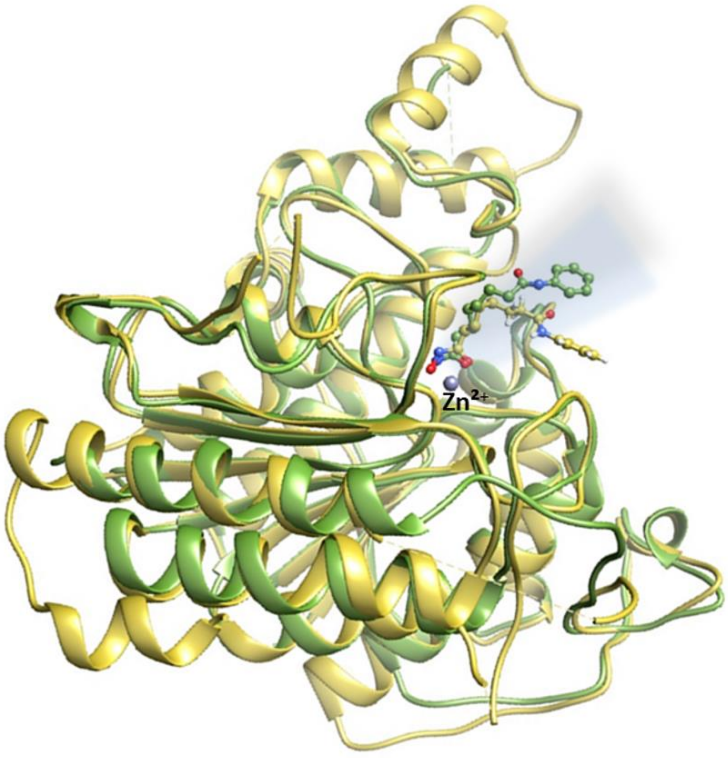

Figure 9 Superposition of the human HDAC8 (green) and the schistosome HDAC8 (yellow) each with the inhibitor SAHA; the catalytic pocket is marked in light blue.

1.2.4 Catalytic mechanism of class 1 histone deacetylases

There are several different theories about the catalytic mechanism of the histone deacetylases. The catalytic pocket contains two His-Asp dyads out of which both histidine residues are supposedly working as a general acid-base catalytic pair. This would indicate a simultaneous protonation of both histidine residues which was questioned theoretically and found to be rather unlikely after investigation[61,62]. As of today it is assumed that the deacetylation takes place as a result of a nucleophilic attack of an enzymatically activated water molecule on the carbonyl carbon of the ε-acetyl group of the acetylated lysine. A tetrahedral intermediate is formed. The origin of the proton which is necessary for this mechanism is not definitely proven but there are several mechanisms that are discussed. One hypothesis states that the proton is passed from His142 to the neighboring His143 and onto the nitrogen of the amide[12,62]. A different one suggests the proton originates from the Tyr306. This hypothesis would explain why a Tyr306Phe-mutant is catalytically inactive[61]. However there is no explanation of how the deprotonated Tyr306 anion is stabilized. It could also be possible that the Tyr306 has a different role in the catalytic mechanism. Tyr306 could possibly interact with the acetyl group via a hydrogen bridge bond between the Tyr306-OH group and the carbonyl oxygen of the acetyl residue. This would withdraw electron density from the C=O bond and therefore make the carbonyl carbon vulnerable to a nucleophilic attack[12]. Figure 10 shows a postulated mechanism of action of zinc dependent histone deacetylases.

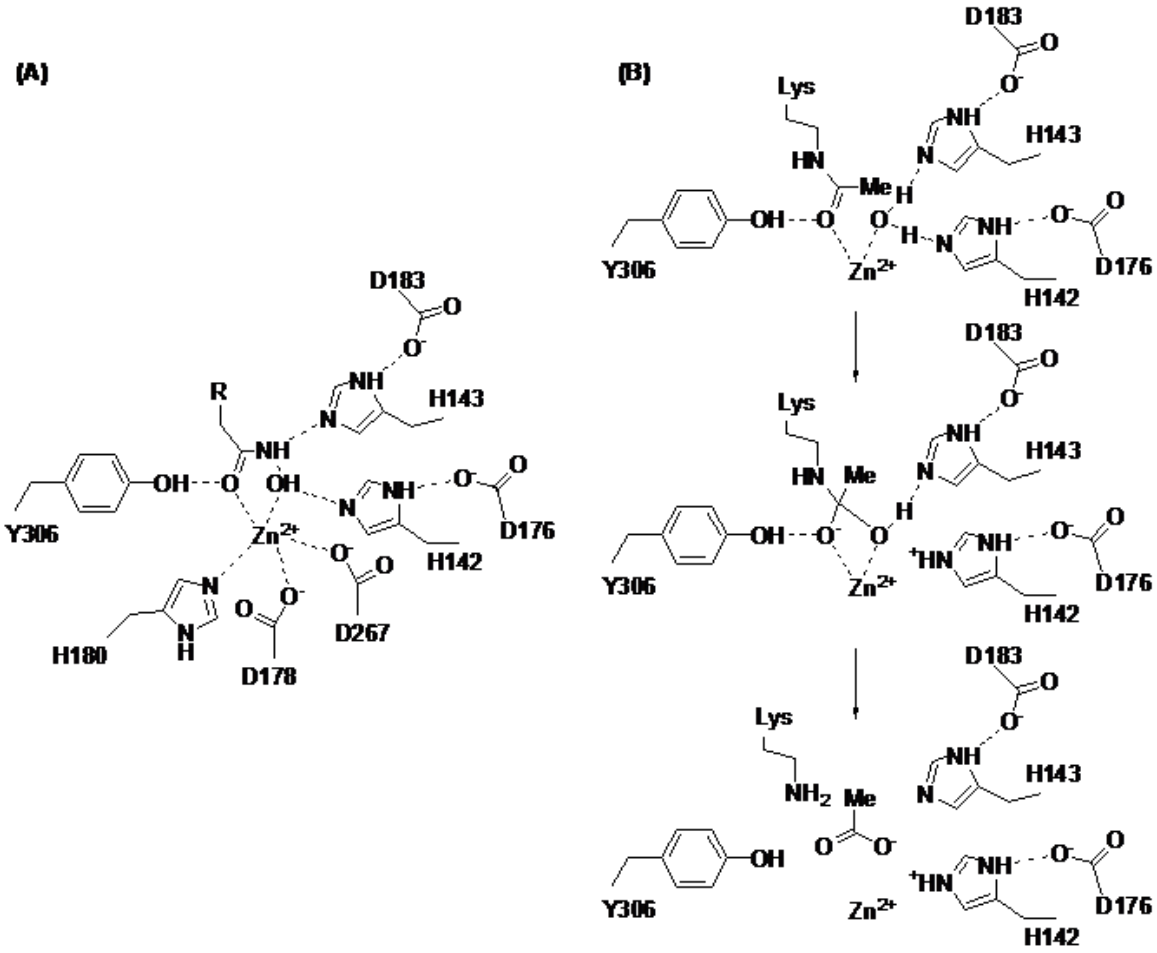

Figure 10 Postulated catalytic mechanism of histone deacetylases modified after SIPPL AND JUNG[12]

1.2.5 Class 1 histone deacetylases as anti-parasitic targets

During the complex transformations between the different life cycle stages the parasite undergoes major morphological and metabolic changes. This implies the necessity for tight control of gene transcription to govern these changes with epigenetic processes likely to play a crucial role[63]. The actors in these processes, and in particular the enzymes that modulate chromatin architecture via the addition or subtraction of histone posttranslational modifications are therefore potential targets for drug development. Of these the focus was on the class I zinc-dependent histone deacetylases. The human histone deacetylases are the best studied epigenetic targets[64]. Therefore it was possible to use a *piggy-back* approach to finding new lead structures for the development of anti-parasitic compounds. The advantage here is that the targets have been validated in other human diseases and that chemical starting points are available[63,65]. Today there are several inhibitors of human histone deacetylases, for example, Vorinostat® (SAHA) or Belinostat® (PXD101) which

are in use for different anti-cancer therapies[66,67]. These and many ohter HDAC inhibitors are being developed and tested against different parasitic diseases like leishmanias, malaria, bilharzias, toxoplasmosis and trypanosomiasis[63,68]. This also bares the possibility of a cross reactivity on the human enzyme homologues which is to be avoided to minimize unintended side effects.

Parasites also have a chromatin structure similar to the one of humans. There are different histones with their respective histone modifications. Histone deacetylating enzymes of parasites like *Plasmodium falciparum*, *Trypanosoma cruzi*, *Trypanosoma brucei*, *Schoistosoma mansoni* and *Leishmania major* have been identified and classified according to the classification of the human homologues[63].

Knowing of the importance of epigenetic modifications for the maintenance of a functioning transcription of genes those mechanisms are an interesting target to address in order to disturb that sensitive balance.

One of the promising anti-parasitic targets *sm*HDAC8 is expressed during all life cycle stages and the treatment of schistosomes with histone deacetylase inhibitors leads to an increase of acetylation of proteins which also result in mortality of the adult worms depending on the dose of the inhibitors[69]. The treatment of the juvenile stage of schistosomes, the schistosomula with the panHDAC inhibitor Trichostatin A (further referred to as TSA) confirms the efficacy of targeting the schistosome HDAC8[69]. It was demonstrated that the application of TSA hindered the metamorphosis from the larval stage (miracidia) to the sporocysts[70] (see figure 11).

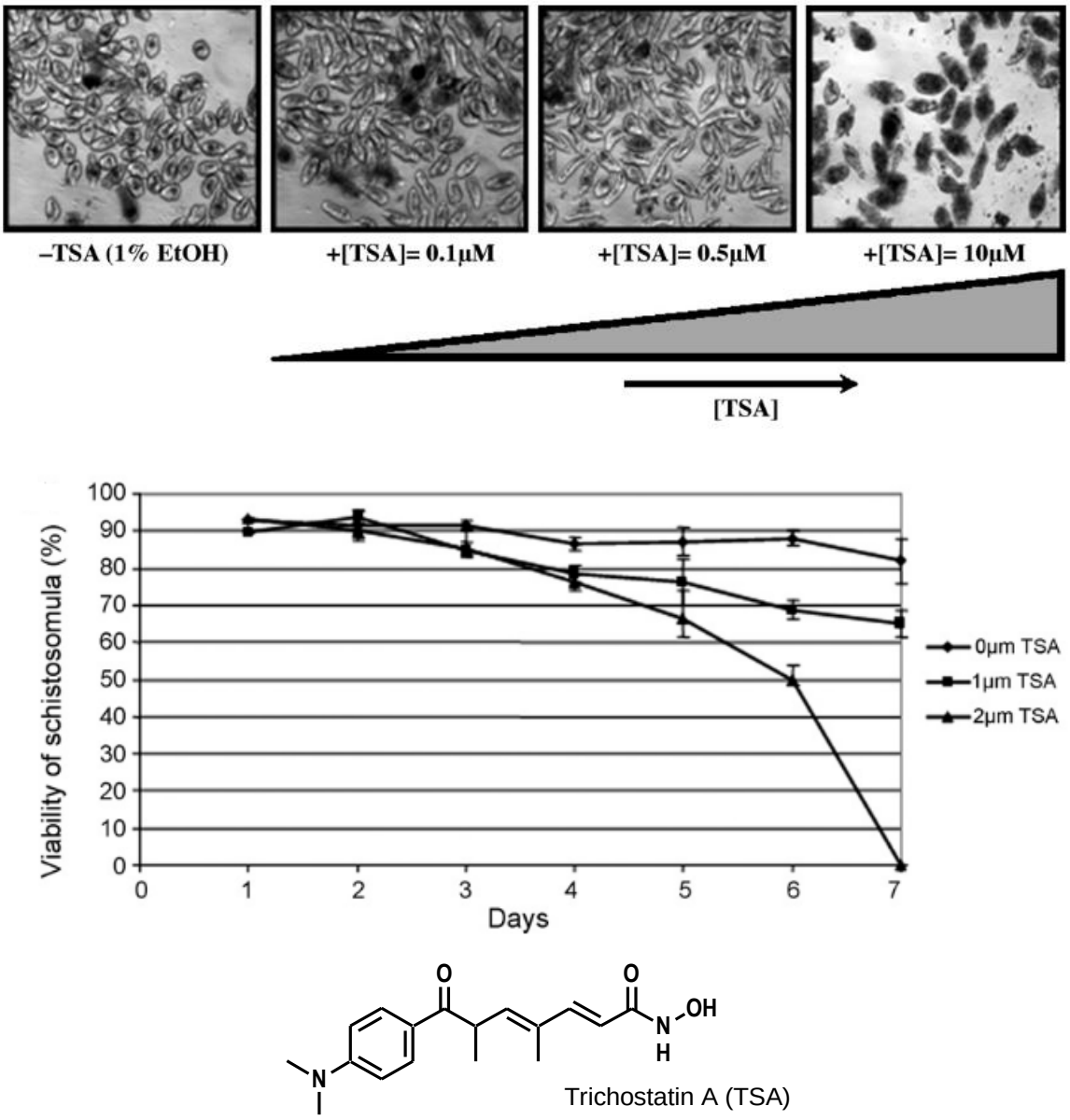

Figure 11 Viability of schistosomula in presence of different concentrations of Trichostain A modified after DUBOIS[69]

Trichostatin A treatment was found to induce a marked genome-wide change in the transcriptome profile including the downregulation of 20 out of 22 genes encoding proteins involved in protection against reactive oxygen species[68].

*Sm*HDAC8 was recently identified as a potential target for anti-parasitic therapy[5,71]. It is expressed at higher levels than other HDAC isoforms in all life-cycle stages of the parasite except for schistosomula while, in contrast, its human orthologue shows the lowest level of expression of the four class I HDACs[69]. *Sm*HDAC8 can therefore be assumed to have specific and vital functions in schistosomes and this was confirmed by transcript

knockdown using RNAi that led to a significant reduction in worm development and survival in infected mice[5] confirming its status as a valuable potential target. So far, only a few series of *sm*HDAC8 inhibitors have been reported and most were only moderately effective against the parasite or showed no effect[72–74]. For example, based on virtual screening and structure-guided optimization of a co-crystallized hit, a benzamido hydroxamic acid was reported as a *sm*HDAC8 inhibitor that is able to kill *S. mansoni* larvae in culture but it also inhibited human HDACs to some extent[73,75]. Therefore novel inhibitors of *sm*HDAC8 with improved properties are needed.

Virtual screening of several libraries of chemical compounds and subsequent enzymatic testing of the promising candidates resulted in several new hit structures. Out of 75 compounds that were purchased for testing 51 contained a hydroxamic acid moiety to address the catalytic zinc ion at the end of the catalytic tunnel of the enzyme. After the first pretests 26 compounds were identified to be active on the *sm*HDAC8 again there were 25 hydroxamic acids among them. The most promising candidates out of that set were analyzed further and IC_{50} values were determined. In the end this investigation resulted in a few small molecule hits which all shared one hydroxamic acid feature able to chelate the zinc ion in the target protein[76]. The screening hit **J1075** (see figure 12) which shows moderate anti-parasitic activity is a benzothiophene-based hydroxamic acid[71].

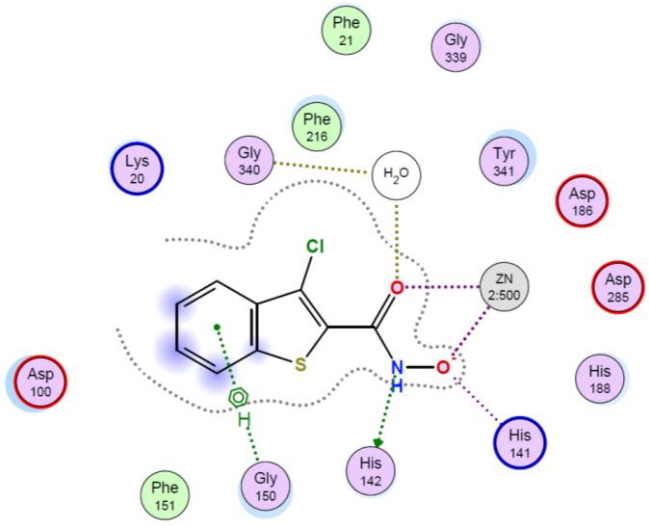

Figure 12 Interaction of the hit compound J1075 at smHDAC8 (PDB ID 4BZ9)

There are several other well-known inhibitors of human histone deacetylases showing anti-parasitic properties known (see figure 13). One of them is the before mentioned hydroxamic acid "SAHA" also known as Vorinostat® that is an approved drug in the use against cutaneous T-cell lymphoma and has activity against different carcinomas[77].

The fungal metabolite apicidin was discovered to exhibit anti-protozoal activity in the late 1990ies and parasites treated with it show hyperacetylation of histones. It shows activity against different parasites like *Trypanosoma cruci*, *Trypanosoma brucei*, *Leishmania major* and *Plasmodium* strains[78].

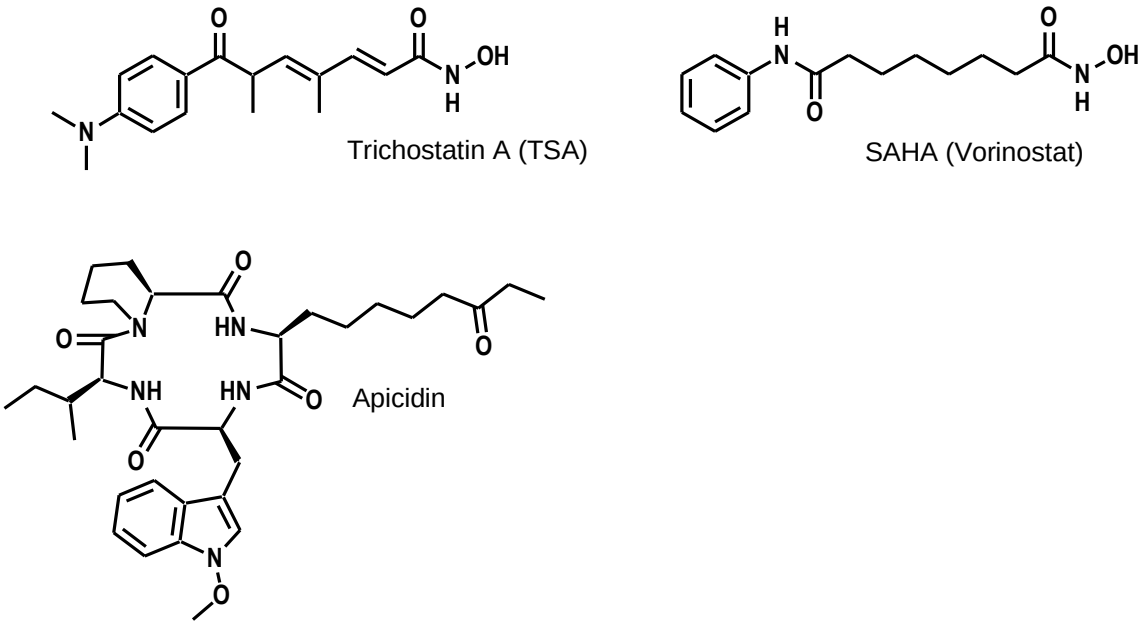

Figure 13 Examples of known histone deacetylase inhibitors with anti-parasitic activity

2 Concept of work

The work presented here was part of the EU FP7 A-ParaDDisE **(**Anti-Parasitic Drug Discovery in Epigenetics) collaborative project. In this project the compound **J1075** (3-chlorobenzothiophene-2-hydroxamic acid) was identified as a micromolar hit by virtual screening and was tested for inhibition of *sm*HDAC8[76] (see figure 14). The aim of this work was to synthesize **J1075**-derived hydroxamic acids (see figure 15) which were then to be tested towards their activity on *sm*HDAC8 and other parasitic targets. The fragment-like hit was modified in several positions. For instance, the heteroatom of the five-membered ring of the bicyclic scaffold was changed to form indene, indole, benzofuran, or benzothiophene scaffolds to examine its influence. Also the ring-open cinnamic acid analogue was synthesized to examine the influence of that flexible scaffold as opposed to the rather rigid bicyclic compounds. Moreover the bare scaffolds were synthesized with various substitutions of different size and polarity in different positions in order to examine the influence of the modified characteristics and geometry on the respective targets. Chemical optimization was guided by *in silico* studies as well as co crystallization of compounds with its target. The developed inhibitors were first tested *in vitro* against recombinant and human HDACs to determine their selectivity. Most promising compounds were then tested in phenotypic assay, toxicity tests and in early pharmacokinetic studies. This synergistic interplay of the different methodologies allowed an ongoing optimization of the synthesized compounds according to each new finding.

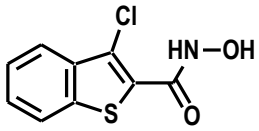

*Figure 14 Compound **J1075** IC_{50} on smHDAC8 4300 nM* [76]

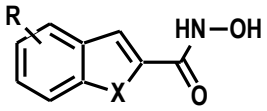

X: S, O, NH, CH_2 or ring-opened

Figure 15 Modifications derived from the starting molecule J1075

3 Synthetic work

Looking at **J1075** as the starting point for derivatization the hydroxamic acid warhead is a crucial feature of all following derivatives.

3.1 Synthesis of the hydroxamic acid warhead

For the synthesis of the hydroxamic acids the corresponding carboxylic acid was used in all cases (see figure 16).

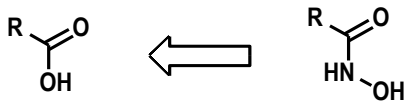

Figure 16 Retrosynthesis of a hydroxamic acid from a carboxylic acid.

There are several different synthetic options to obtain hydroxamic acids starting from their corresponding carboxylic acids. According to literature[79] hydroxamic acid can be obtained from a reaction of an activated carboxylic acid and hydroxylamine (mostly available as hydroxylamine hydrochloride) (see figure 17).

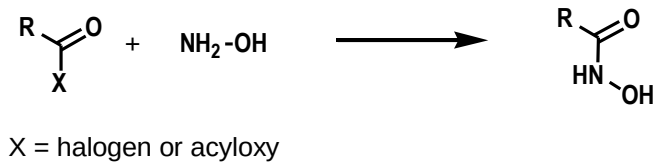

Figure 17 General scheme of an activated carboxylic acid with hydroxylamine to result in a hydroxamic acid modified after SCHWETLICK ET AL.[79]

A simple way to obtain a hydroxamic acid starting from a carboxylic acid is to activate the carboxylic acid and then let it react via nucleophilic substitution with hydroxylamine (see figure 19). There are several different ways of activating a carboxylic acid. It can be activated in situ as a carboxyl chloride using e.g. thionylchloride, phosphorous trichloride or phosphorous pentachlorid[80] (see figure 18).

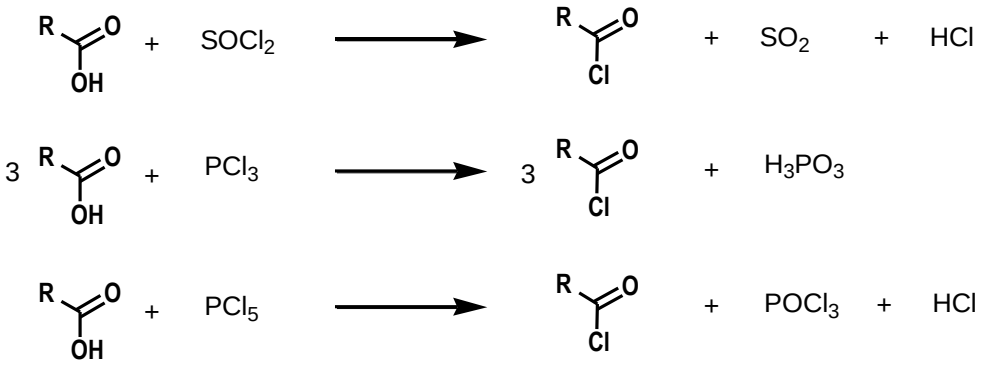

Figure 18 Reaction schemes of forming carboxyl chlorides modified after ADAMS ET AL.[80]

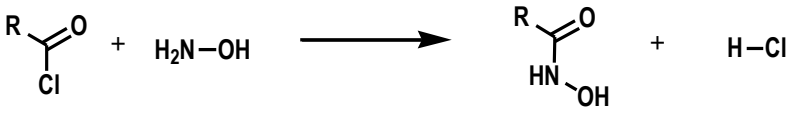

Figure 19 Scheme of follow up reaction forming a hydroxamic acid from a carbonyl chloride modified after BAUER AND EXNER[81]

For these procedures literature suggests yields up to 96%[80,81], however, the problem with these procedures lie within the purification of the resulting products. In case of optimized reaction conditions as well as quantities of the reacting partners which should result in an optimum of the desired products there is still the difficulty of separating the hydroxamic acid from the residual carboxylic acid due to their similar lipophilicity as depicted in figure 20.

Figure 20 Lipophilicity of a carboxylic acid (left hand side) in comparison to a hydroxamic acid (right hand side) (both "R" representing any sort of identical residue).

In order to obtain an above 90% purity of the final compound without high losses due to difficult purification it was useful to introduce a seemingly unnecessary reaction step. This

extra step however enables an easy chromatographic removal of the residual carboxylic acid from the reaction batch so that the above described problem of the difficult separation of a hydroxamic acid from its analogous carboxylic acid is being avoided. Ideally the protecting group of the hydroxamic acide would be lipophilic and fairly voluminous in order to create an intermediate molecule that is easily separable from as well the carboxylic acid in one step as well as the hydroxamic acid in the following step. It should also be available at low cost because it would be needed for the synthesis of every single compound and the cleavage of the protecting group should also be pursuable under mild conditions for the benefit of the stability of the rest of the molecule.

There are a few possible options for amines that can be used which are presented in figure 21 below.

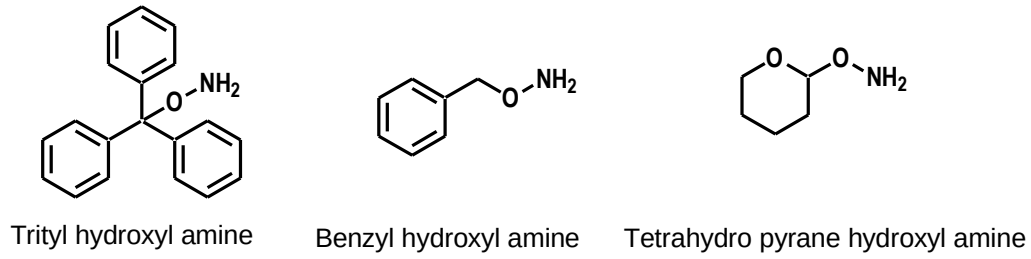

Figure 22 Examples of hydroxyl amines

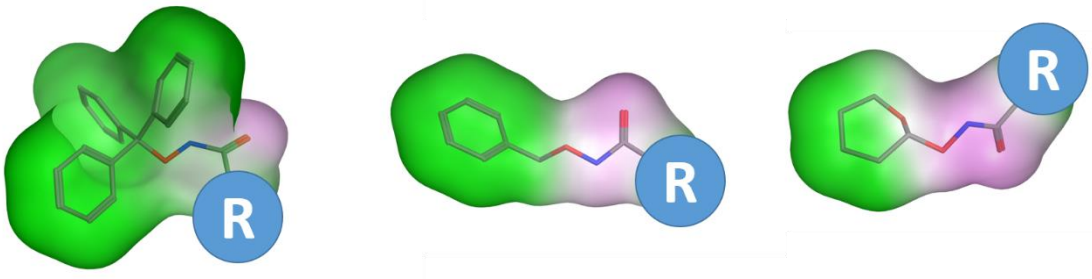

Figure 21 Surface properties of the above mentioned hydroxyl amines. Lipophilic areas marked in green and hydrophilic areas in magenta.

All of these three examples would create an intermediate that is voluminous and lipophilic in order to separate them from products or educts of the reaction batch.

All of the three examples of protection groups serve the expectation of high lipophilicity (see figure 22) in order to easily purify the reaction mixture from polar residues and is a second step from the residual protected hydroxamic acid.

It was further tested how to conduct the reaction of the carboxylic acid with the protected hydroxyl amine. In order to pursue the reaction under comparably mild conditions a coupling agent was used (see figure 23).

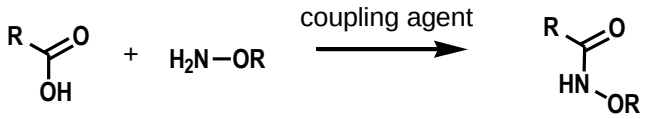

Figure 23 Scheme of coupling reaction of a carboxylic acid and a hydroxylamine modified after AL-WARHI ET AL. [82]

There are several different coupling agents available that were originally designed for peptide synthesis. There is the group of the carbodiimides (figure 24). It is probably the most broadly used group of coupling reagents. The first of such reagents, namely N,N'-dicyclohexyl-carbodiimide (DCC) was introduced for peptide synthesis in 1955[83]. There have been several other carbodiimide based structures that were introduced as coupling reagents[82]. The general structure can be described as a central carbodiimide with identical or different residues at both sides if the central element.

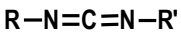

DCC: R = R'= cyclohexyl
DIC: R = R' = isopropyl
EDC: R= ethyl, R' = dimethylaminopropyl

Figure 24 Examples of carbodiimide based coupling agents: dicyclohexyl carbodiimide (DCC), diisopropyl carbodiimide (DIC), ethyl dimethylaminopropyl carbodiimide (EDC) modified after AL-WARHI ET AL. [82]

The reaction using DCC is typically carried out in dried dichloromethane or chloroform with the use of a base in order to deprotonate the acid which is to be coupled. The resulting dicyclohexane urea is not soluble in dichlormethane and therefore precipitates as the reaction proceeds[82,83]. The reaction mechanism is described in figure 25 below.

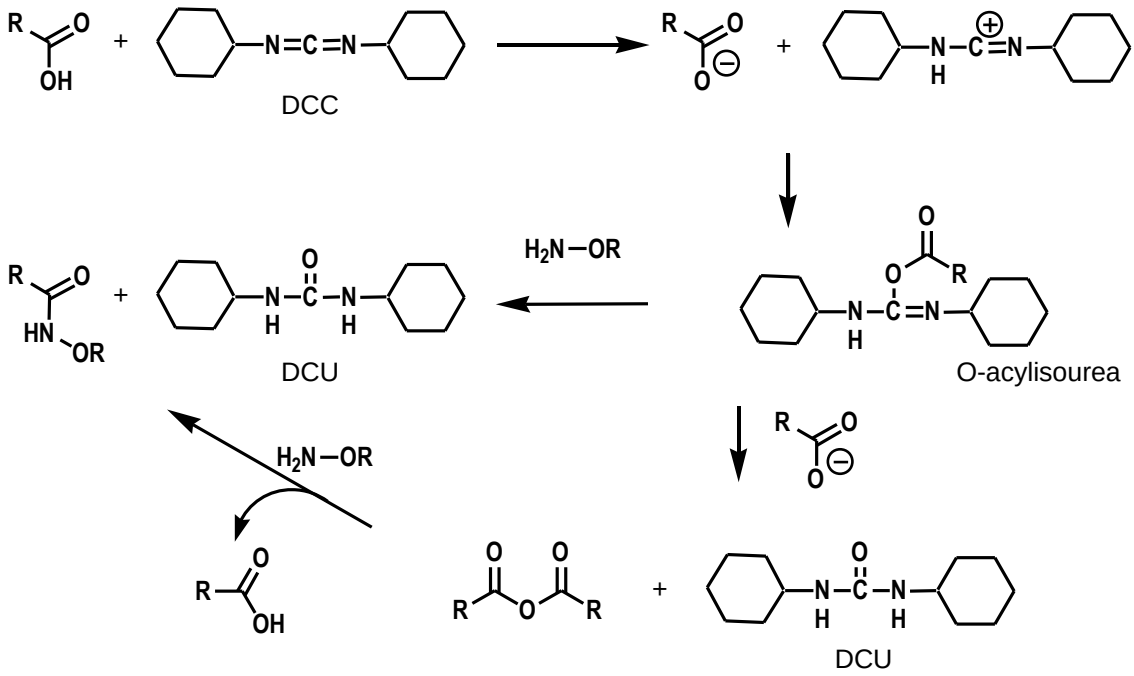

Figure 25 Reaction mechanism of N,N'-dicyclohexyl-carbodiimide (DCC) modified after SHEEHAN ET AL[83]

Another group of coupling reagents contains the phosphonium and aminium salt based coupling reagents. They also provide a relatively mild environment for the activation of the carboxylic acid. The reaction can for example be carried out in tetrahydrofuran as a solvent with a base added for deprotonation of the carboxylic acid. Diisopropyl ethylamine (DIPEA or Hünig base) is used oftentimes. There are some examples of benzotriazole / 7 – azabenzotriazole based coupling agents shown in the figure 26 below.

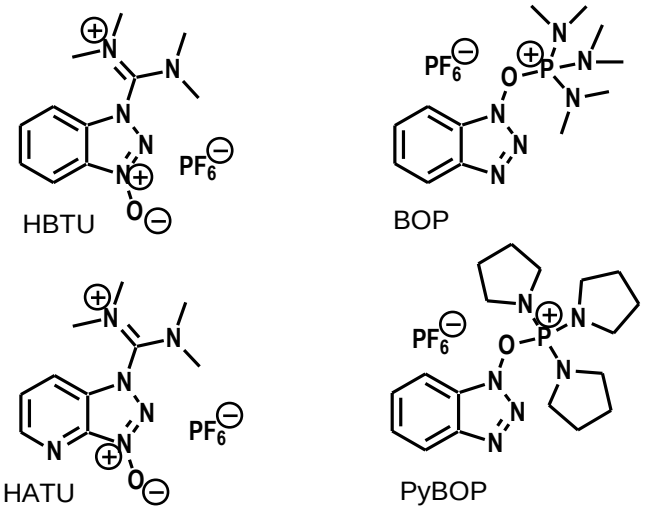

Figure 26 Different phosphonium salt based coupling reagents: top left O-(Benzotriazol-1-yl)-N,N,N',N'-tetramethyluronium hexafluorophosphate (HBTU), bottom left O-(7-Azabenzotriazol-1-yl)-N,N,N',N'-tetramethyluronium hexafluorophosphate (HATU), top right (Benzotriazol-1-yloxy)tris(dimethylamino)phosphonium hexafluorophosphate (BOP), bottom right (Benzotriazol-1-yloxy) tripyrrolidino phosphonium hexafluorophosphate (PyBOP)

The coupling agent PyBOP® ((Benzotriazol-1-yloxy) tripyrrolidino phosphonium hexafluorophosphate) was originally developed for peptide coupling reactions by CASTRO ET AL[84,85] in 1990. It was an advancement of (Benzotriazol-1-yloxy)tris(dimethylamino)phosphonium hexafluorophosphate (further referred to as BOP®) which is also an effective coupling reagent but has lost importance due to the formation of hexamethyl phosphoramide (further referred to as HMPA). HMPA is a polar but aprotic colorless liquid which is formed as a byproduct of the reaction and is a highly hazardous carcinogen. Using PyBOP® the formation of HMPA cannot take place because the dimethyl amino residues are replaced by pyrrolidino residues which leads to a less toxic byproduct[84,85]. The reaction mechanism of BOP® and PyBOP® also works through and activated ester of the carboxylic acid and either the phosphonium group or the benzotriazole residue. The coupling reaction mechanism is postulated as shown in the figure 27 below.

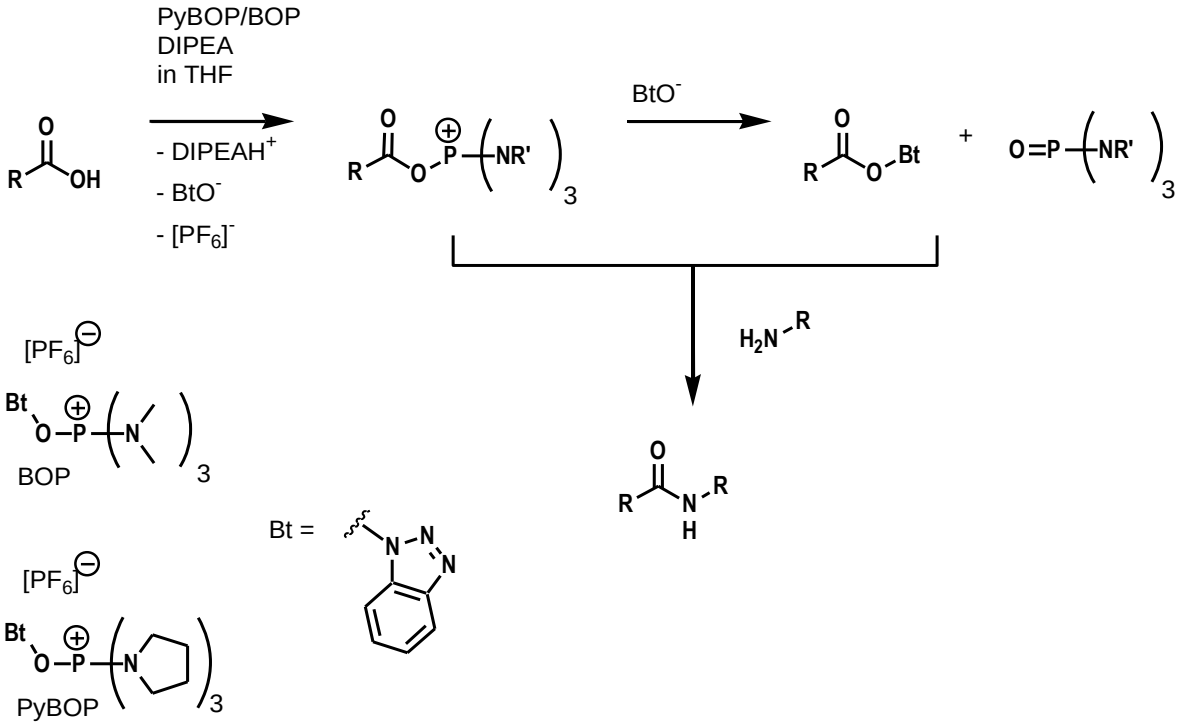

Figure 27 Reaction mechanism of BOP and PyBOP® modified after KIM et al.[86]

Minus a few exceptions all the hydroxamic acid derivatives described herein were obtained by using the respective carboxylic acids as starting materials following a procedure described by MISRA ET AL.[87] which involves the use of *O*-(tetrahydro-2*H*-pyran-2-yl) hydroxylamine and subsequent cleavage of the THP protecting group under acidic conditions (figure 28).

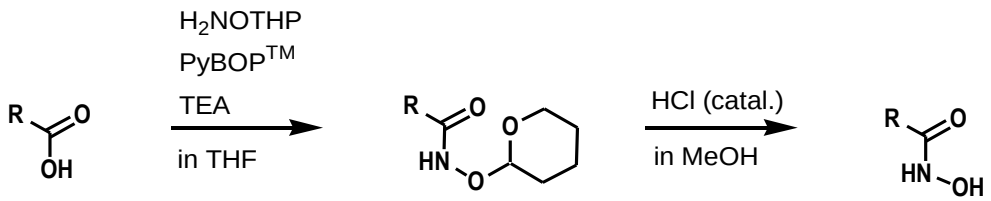

Figure 28 Scheme of the reaction steps transforming a carboxylic acid into a hydroxamic acid modified after MISRA ET AL.[87]

Out of the above described protected hydroxyl amide groups all three fulfilled the requirements for simple and sufficient purification and cost efficiency. However there was a different factor to be thought of, namely the cleavage of the protecting group from the

intermediate. An efficient and easy procedure for cleaving the protecting group was needed that could be conducted under mild conditions. Therefore, the benzyl-protected intermediate was not an option anymore because it cannot be cleaved with catalytic amounts of a suitable acid. It would need harsher conditions and possibly hydrolysis. For the other two options a cleavage under mild acetic conditions is possible.

The THP-protecting group was first cleaved off using para-toluenesulfonic acid (further referred to as pTSA) or hydrochloric acid. The efficiency of the cleavage reaction is similar between the hydrochloric acid and pTSA but the pTSA could be found in the final compound in traces and therefore lowered the purity of the sample. Therefore, hydrochloric acid is to be preferred over pTSA. For the trityl group formic acid was used as suggested by literature[88].

3.2 Synthesis of the carboxylic acid building blocks

3.2.1 Synthesis of the indene carboxylic acid

In 1960 ORTTMANN and TREIBS[89] published a synthesis route on which various olefins and aromatic compounds can be transformed into their corresponding carboxylic acids (see figure 29).

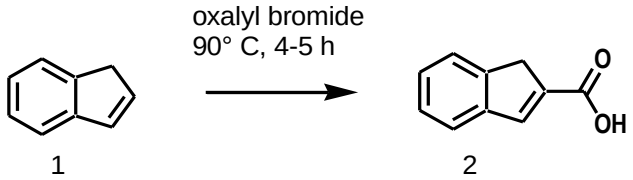

Figure 29 Synthesis of indene carboxylic acid as postulated by ORTTMANN AND TREIBS[89]

The aromatic compound is supposed to be transformed into the carboxylic acid when heated up over a period of time with oxalyl bromide[89,90]. The general procedure is described either solvent free or in solvents like diethyl ether, dioxane or carbon tetrachloride. Either the reagents are mixed together at the beginning or the oxalyl bromide is slowly dripped into a solution of the compound that is to be transformed into the carboxylic acid or vice versa. In case of the indene-2-carboxylic acid the reaction conditions are described as solvent free, mixing both reagents together right at the beginning and heating up the reaction to 90°C for 4-5 hours. Since in contrast to ORTTMANN and TREIBS, very small amounts of both reagents were used (1 mmol indene and 0.5 mmol of oxalyl bromide compared to 0.2 mol indene and 0.1 mol oxalyl bromide) at the first attempt a solvent (THF) was used simply to enlarge the volume of the reaction batch. Conducting the reaction in a solvent did not result in the formation of the desired product which could have been due to a lower temperature. At a second attempt the solvent free method as described by literature was used. The desired product was formed according to the reaction mechanism described in figure 30.

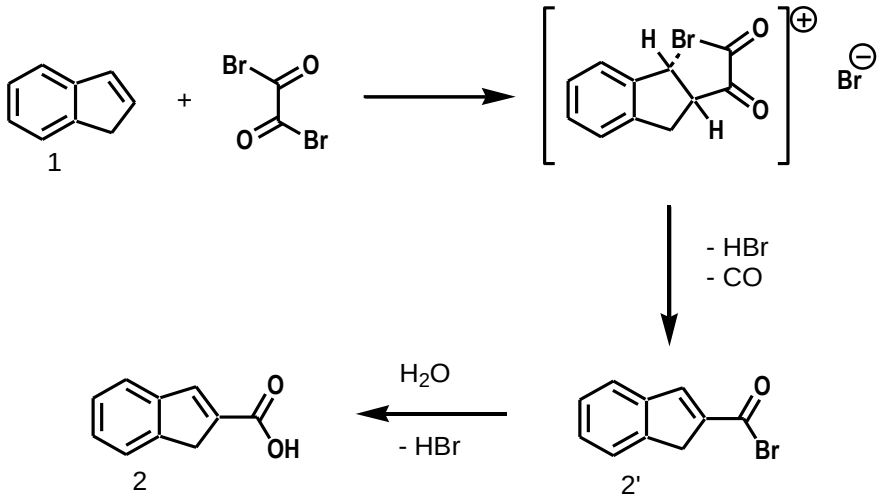

Figure 30 Reaction mechanism as postulated by ORTTMANN AND TREIBS [89]

The product **2** could be purified from the reaction mixture by dissolving the mixture in ethyl acetate and extracting it with a saturated potassium carbonate solution afterwards acetifying the aqueous phase with hydrochloric acid and extracting it with ethyl acetate again[89]. The yield was at 8.5 % which did not deliver a sufficient amount of product for further synthesis steps. Considering the proportionally high losses during purification processes a second batch was started following the same procedure with doubled amounts of both reactants which led to a yield that was more than tripled to 27 %. This presents a trend which could explain why the yield of 74 % described in literature for larger batches were not achieved.

Table 1 Structure obtained via carboxylation of indene

name	structure
2 (TB2s)	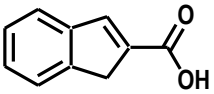

3.2.2 Indoles

ROSAUER ET AL.[91] suggested a novel synthesis route on which substituted anilines could be transformed into indole-2-carboxylic acids by first adding an iodine atom in ortho position to the amine and then, in a second step cyclisation with pyruvic acid[91]. (See figure 31).

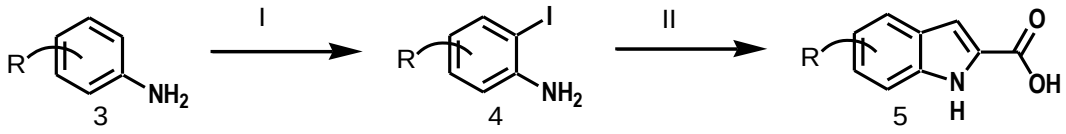

Figure 31 Proposed synthesis route for the formation of indoles. Reagents and conditions: (I) Ag_2SO_4, I_2, EtOH, rt 16h; (II) pyruvic acid, DABCO $Pd(OAc)_2$ DMF, 105°C, 4h

The catalyst silver sulfate was synthesized by precipitating it from silver nitrate with sulfuric acid. Mass spectrometry showed that the first intermediate was formed which would supposedly be the aniline with an iodine substituent in ortho position to the amine function **4**. Due to the iodine present in the reaction mixture it was not possible to observe the progress of the reaction by TLC. There was no information about purification procedures or methods in the ROSAUER ET AL. publication. Several methods like column chromatography and solvent extraction with different solvents did not lead to satisfying results. Neither the position of the iodine substituent nor the quantity of the yield could be verified. In a second attempt a direct conversion from the reaction mixture was tried by simply evaporating the solvent under reduced pressure and then adding the reagents and reactants for the second step of the reaction. DMSO and DMF as solvents and TEA and DABCO as tertiary amine bases were tried. At this step the same problems as with the first step arose; inability to observe the progress of the reaction by TLC due to the smudging of the iodine, thus no information given about the purification of the product. There were no traces to be found by mass spectrometry.

For **5b** the commercially available 5-methoxyindole-2-carboxylic acid was used. And considering newer docking studies the idea to add a lipophilic residue to the 5 membered ring seemed appealing. Based on the plain indole-2-carboxylic acid and its 5-methoxy derivative their *N*-methyl and *N*-ethyl derivatives were to be synthesized.

For the methyl derivatives a nucleophilic substitution using trimethyl silyl diazomethane was planned. This would firstly give the alkyl esters which would then be cleaved in an additional step. Several approaches using the indole-2-carboxylic acid as the reagent dissolved in methanol slowly dripping two equivalents of the etheric solution of trimethyl

silyl diazomethane into the reaction batch did not result in product formation. A homologous reaction using the 5-methoxy indole-2-carboxylic acid as the reagent also failed to deliver the desired product.

Since the *N*-alkylation using trimethyl silyl diazomethane did not lead to satisfying results a different approach for the *N*-alkylation was tried. According to literature many synthesis procedures are using alkyl iodides and a base as a catalyst for *N*-alkylation reactions.

For this procedure the indole-2-carboxylic acid is dissolved in acetone and the potassium hydroxide is suspended in the solution. The alkyl iodide which in this case was the ethyl iodide is slowly dripped into the mixture at 0°C. Once all of the ethyl iodide is added to the reaction batch, the mixture is slowly heated up to room temperature and then stirred for 18 hours at room temperature. As a result product formation could not be detected by mass spectroscopy.

In consideration of time and cost efficiency the indole carboxylic acids (**5a, 5b**) were purchased from commercial suppliers and then transformed into the analogous hydroxamic acids using the synthetic procedures described in 3.1.

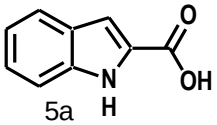

5a

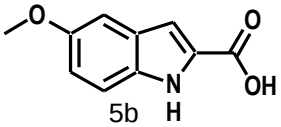

5b

3.2.3 Benzofuranes

The synthesis route for benzofurane was modified according to PAREKH ET AL.[92] and KUMARASWAMY ET AL.[93].

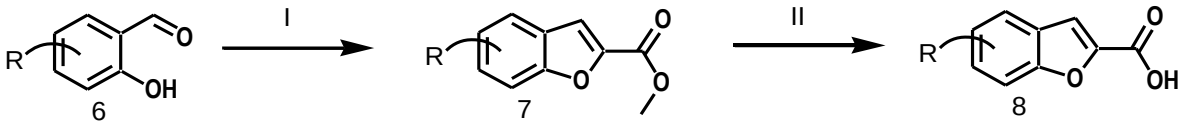

Figure 32 Synthesis of benzofurane derivatives. Reagents and conditions (modified after KUMARASWAMY et al. [93]): I) $BrCH_2CO_2Me$, K_2CO_3, CH_3CN, 6 h, 60 °C; II) NaOH, MeOH

The salicylaldehyde is to be dissolved in acetonitrile. Methyl bromoacetate and potassium carbonate are added. The mixture is then to be stirred at room temperature then heated to about 50-60°C for 30 min. This described reaction leads to the first intermediate product which is the methyl ester of the benzofurane-2-carboxylic acid, which is further hydrolyzed under alkaline conditions to result in the free carboxylic acid (figure 32).

This procedure worked fine for the unsubstituted salycaldehyde. Unfortunately it did not lead to sufficient results for substituted salycaldehydes. Neither an elevation of the reaction temperature nor the elongation of the reaction time resulted in satisfactory results. Traces of the desired product were found in mass spectrometry but the amounts were too little to separate them from the reaction batch. In order to obtain a small number of different benzofurane derivatives commercially available benzofurane carboxylic acids were transformed into the analogue hydroxamic acids following the procedure described in 3.1.

Table 2 Structure obtained via cyclisation reaction of salicaldehyde and methyl bromoacetate

name	structure
8a (TB3s)	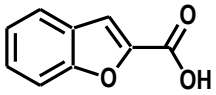
8b (TB41s)	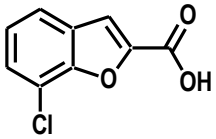
8c (TB42s)	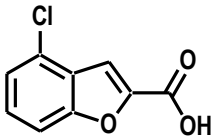

3.2.4 Benzothiophenes

The benzothiophene derivatives have been synthesized by utilizing a modified route described by CAI ET AL.[94] (figure 33).

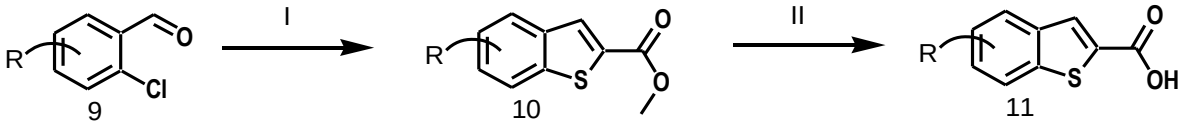

Figure 33 Synthesis route for the benzothiophene derivatives. Reagents and conditions: I) $HSCH_2CO_2Me$, K_2CO_3, DMF, 4 h, 60 °C; II) NaOH, MeOH

The 2-chloro benzaldehyde is dissolved in DMF with potassium carbonate as a solid phase base and the methyl thioglycolate. The reaction batch was heated to 60°C for four hours. The reaction then results in the intermediate methyl ester of the benzothiophene derivative (figure 33). When the reaction is completed the crude methyl ester is to be purified from the reactant and reagent remnants. So firstly the reaction batch is filtered to eliminate the solid potassium carbonate. The DMF was evaporated under reduced pressure and toluene was then added to drag out the residual solvent.

The reaction was performed with the 2-chloro benzaldehyde for the unsubstituted benzothiophene-2-carboxylic acid and with the 2,6-chloro benzaldehyde for the 4-chloro benzothiophene carboxylic acid. It was not possible to synthesize the unsubstituted benzothiophene derivative on this route possibly due to the missing of the second chloro substituent in ortho position to the aldehyde function which seems to have an additional activating effect.

In order to compare the simple unsubstituted benzothiophene derivative to the chloro substituted derivative as the indene, indole and benzofurane scaffold, the commercially available benzothiophene - 2 - carboxylic acid was used as a starting point for the synthesis of the hydroxamic acid.

Table 3 Structure obtained via cyclisation reaction of 2,6 dichloro benzaldehyde and methyl thiooglycolate

name	structure
11a (TB5s)	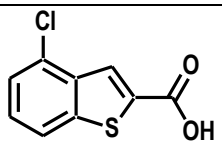

3.2.5 Cinnamic acids

A virtual screening carried out also resulted in a potent cinnamic acid derivative. Therefore, also this scaffold was further investigated. The rigid bicyclic benzothiophenes, indoles, benzofuranes, indenes and the flexible cinnamic acids show almost the same distance between the benzene residue and the zinc binding groups.

3.2.5.1 Classic KNOEVENAGEL condensation

For their synthesis a classic KNOEVENAGEL[79] condensation was used starting with a benzaldehyde and malonic acid which were dissolved in pyridine and 10 mol% piperidine as a catalyst (figure 34).

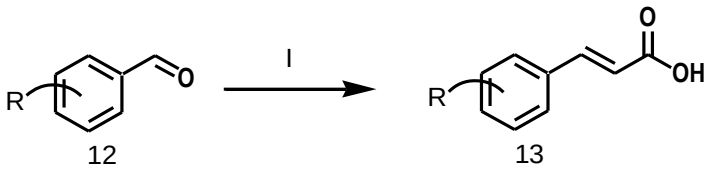

Figure 34 KNOEVENAGEL condensation. Reagents and conditions (modified after Schwetlick et al.[79]):

I) malonic acid, piperidine, pyridine

The general procedure had to be modified to simply increase the volume of the reaction batches. The reaction batches were in the millimolar range and, therefore, the relations of the solvent piperidine and the catalyst pyridine were adjusted due to the voluminous amounts of the respective benzaldehydes. In comparison the suggested equivalents in the literature the amount of the piperidine was approximately doubled and the piperidine was also slightly increased. For one mmol 600 µl of pyridine and 20 µl of piperidine were used instead of 270µl and 18 µl. The reaction was gently heated over a water bath until there was no more CO_2 evaporation observable, kept at that temperature for 30 – 180 minutes, then it was cooled to room temperature again and ice and concentrated hydrochloric acid were added. The product formation is postulated as shown in figure 35.

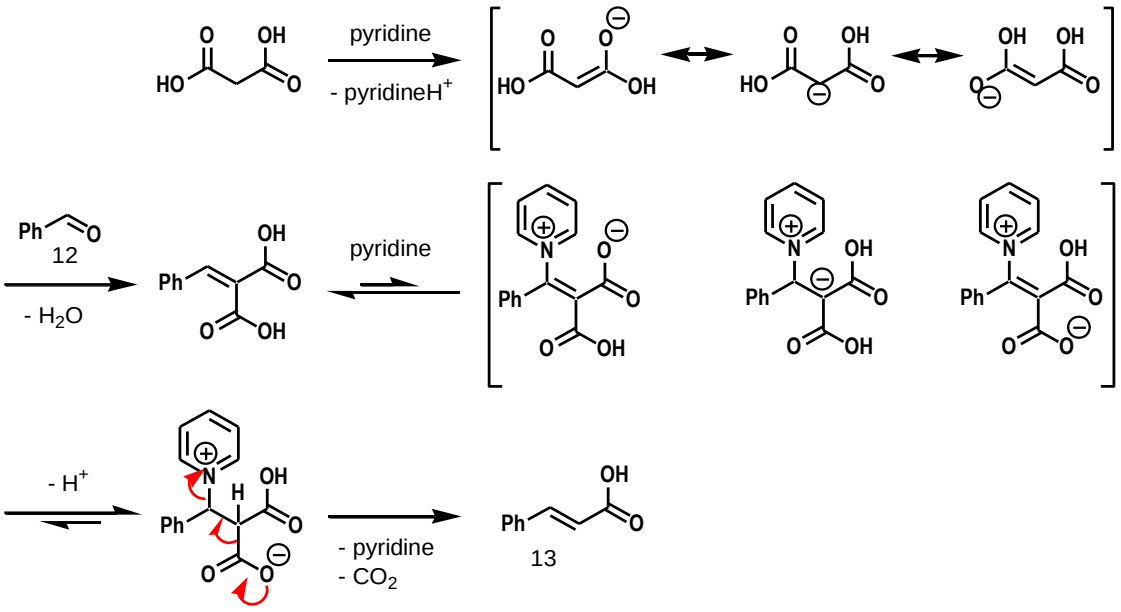

Figure 35 Reaction mechanism of the KNOEVENAGEL condensation postulated by BRÜCKNER[95]

Solid compounds were crystallized directly from the ice hydrochloric acid mixture at in the fridge overnight and liquid compounds were extracted from the reaction batch with diethyl ether. For the solid compounds an ether extraction of the residual aqueous phase after filtration of the solid compound was proposed to increase the yields. In this work this step has been resigned in most cases for the benefit of higher purities.

3.2.5.2 Microwave irradiation assisted KNOEVENAGEL condensation

According to PENG AND SONG[96] the KNOEVENAGEL condensation can also be conducted under microwave and ultrasound irradiation. In the procedure described the reaction is conducted between aromatic aldehydes and malonic acid just like the classical KNOEVENAGEL reaction. As for the catalytic base they use piperidine, potassium carbonate and water as the solvent. The reaction time then is reduced to 60 – 95 seconds under simultaneous microwave and ultrasound irradiation. They also investigated the differences in reaction time of microwave irradiation alone, sonication on its own, and conventional heating. The shortest reaction time was needed using both, microwave and sonication at once. But also using microwave irradiation reduced the reaction time to approximately 30 minutes in comparison to approximately 2.5 hours using only sonication and 7 hours using conventional refluxing. The yields for all methods were ranging between 79 % and 87 %.

Since the synthetic microwave available was not able to simultaneously sonicate the samples, the reactions were conducted under only microwave irradiation. Due to the longer reaction times and the noise pollution which is not negligible the method using only sonication did not prove to be a method of choice. However the reaction mechanism still stays similar to that one described in the chapter of the conventional KNOEVNAGEL reaction.

Table 4 Cinnamic acid derivatives obtained via conventional KNOEVENAGEL reaction

name	structure	name	structure
13a (TB7s)	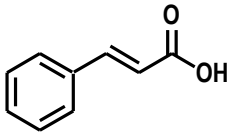	13b (TB8s)	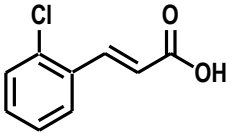
13c (TB9s)	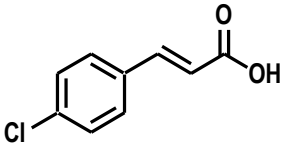	13d (TB10s)	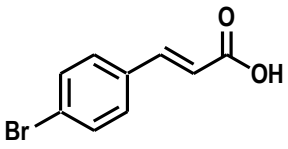
13e (TB11s)	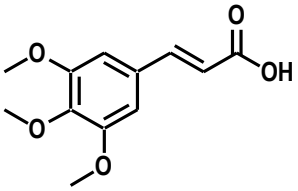	13f (TB12s)	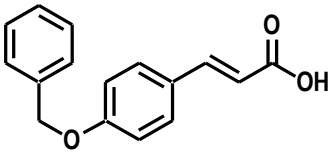
13g (TB14s)	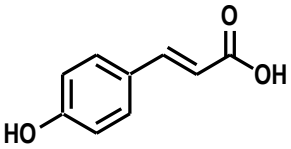	13h (TB15s)	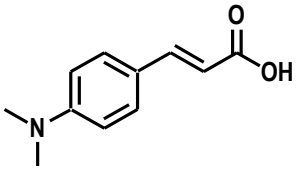
13i (TB16s)	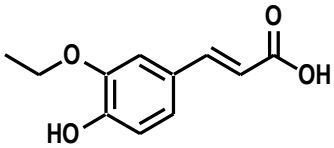	13j (TB27s)	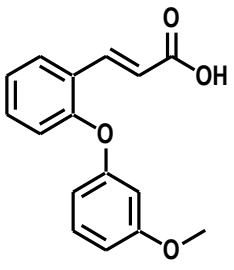

name	structure	name	structure
13k (TB31s)	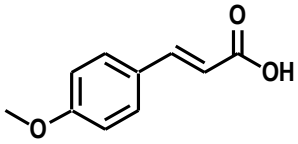	13l (TB32s)	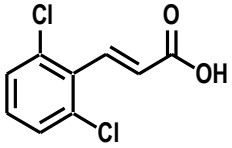
13m (TB33s)	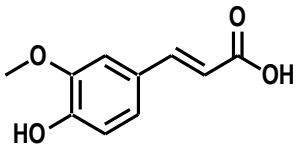	13n (TB38s)	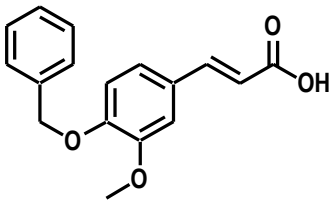
13o (TB51s)	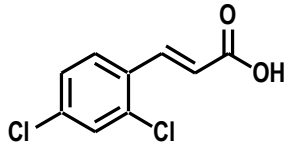	13p (TB53s)	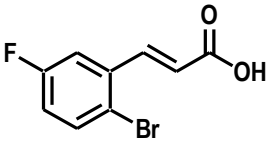
13q (TB54s)	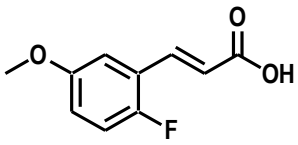	13r (TB55s)	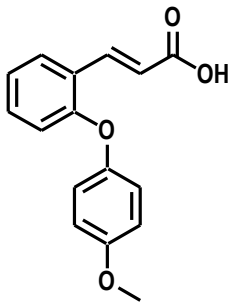
13t (TB56s)	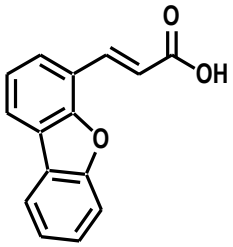	13u (TB57s)	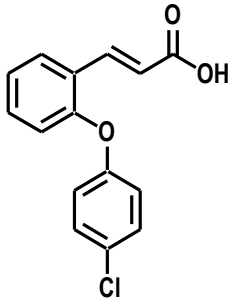
13v (TB58s)	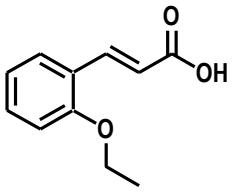	13w (TB59s)	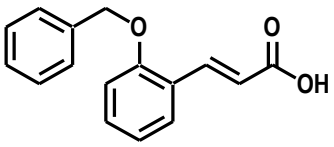
13x (TB61s)	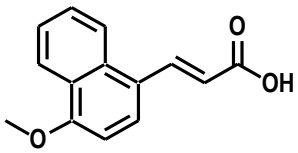	13y (TB62s)	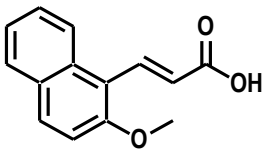

name	structure	name	structure
13z (TB63s)	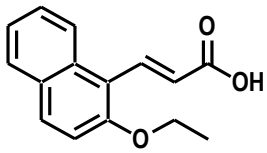	13za (TB64s)	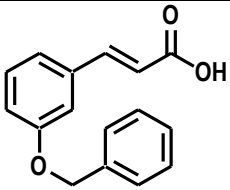
13zb (TB67s)	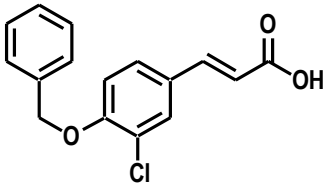	13zc (TB72s)	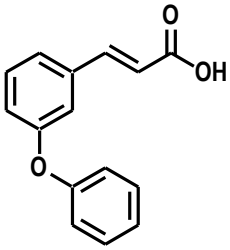
13zd (TB73s)	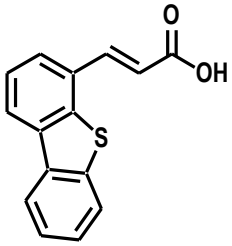	13ze (TB77s)	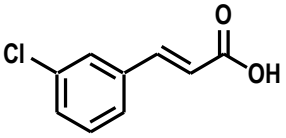
13zf (TB87s)	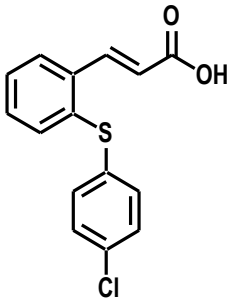	13zg (TB91s)	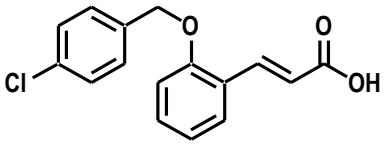
13zh (TB92s)	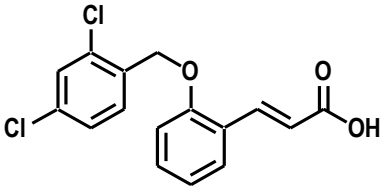	13zi (TB93s)	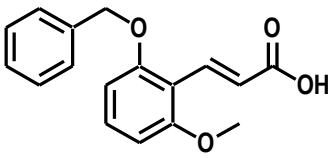
13zj (TB98s)	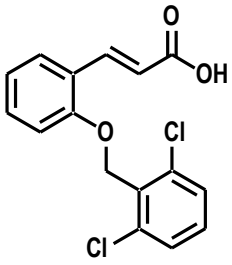	13zk (TB106s)	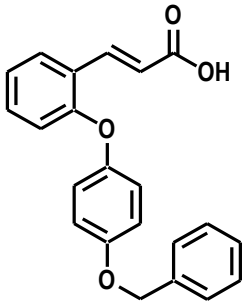

name	structure
13zl (TB107s)	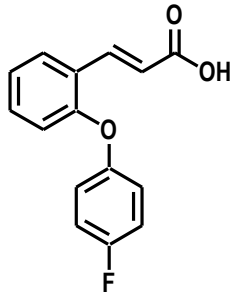

3.2.5.3 *HECK reaction*

A second approach to obtain cinnamic acid derivatives which does not limit the synthesis to the availability of aldehydes is the HECK reaction[97]. It is a palladium catalyzed coupling reaction which enables an olefination of aryl halides.

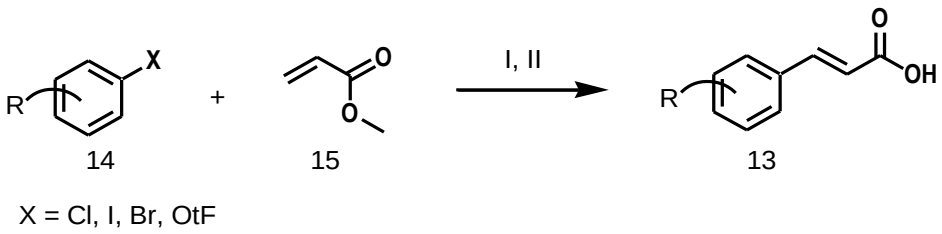

Figure 36 Scheme of synthesis of a cinnamic acid via HECK reaction: I) Pd(catalyst), base; II) alkaline cleavage of the methyl ester

The so called HECK reaction[97] (figure 36) is related to the SUZUKI-Reaction and was developed in 1972. It is a coupling reaction to form carbon-carbon bonds from an aryl halide and an olefin under the addition of a palladium complex as a catalyst. Typical HECK catalysts are for example tetrakis(triphenylphosphine)palladium(0), palladium chloride or palladium(II)acetate. The reaction also requires the addition of a base to neutralize the hydro halide acid which is formed during the coupling process[98].

Based on this reliable synthesis route it was possible to build a series of different cinnamic acid derivatives which was a good basis to further study the biological relevance of the different residues and their position.

3.2.6 N-alkylation of phenothiazine derivatives

The shape of the binding pocket of the *sm*HDAC8 suggests a ligand that has a narrower linker between the hydroxamic acid residue which coordinates the zinc ion at the bottom of the catalytic pocket and a bulkier residue to force the binding pocket into the wider conformation. Phe151 of the *sm*HDAC8 is able to take an inward facing conformation or flip away from the catalytic pocket which leaves room for bulkier residues. The *h*HDAC8 does not have that flexibility in the Phe152 which is in the same position. Therefore, ligands with bulkier residues are rather likely to fit into the catalytic pocket of the schistosome HDAC8 but rather unlikely to fit into the human analogous catalytic pocket. So using phenothiazines as the bulkier residue connected with a 4-methyl benzoic acid or a crotonic acid as the narrower substructure to fit the catalytic pocket was an idea to investigate.

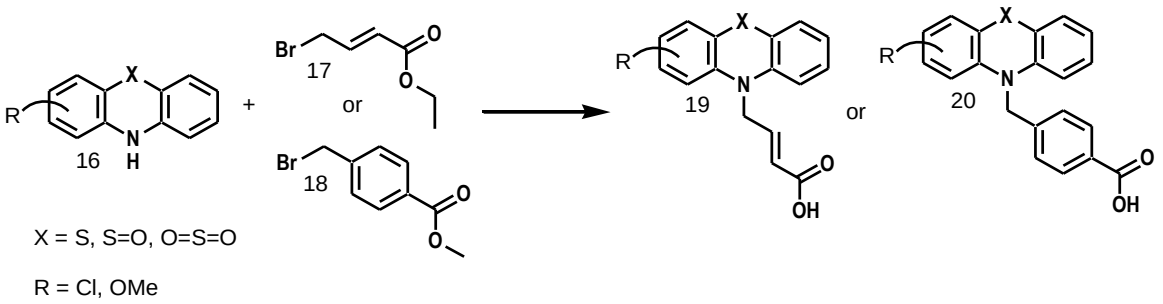

Figure 37 Scheme of the reactions for obtaining N-alkylated phenothiazines

According to FAN ET AL[99] the reaction can be conducted under microwave irradiation. Using DMF as solvent and KOH as an alkaline solid phase catalyst the reaction is carried out under microwave irradiation for less than 30 minutes (figure 37). After cooling the reaction batch it is mixed with water and then filtered to remove the insoluble materials. The filtrate is collected and acidified with hydrochloric acid whereupon the product precipitates. The product can be collected by filtration. Due to the very alkaline conditions the cleavage of the methyl or ethyl ester of the respective carboxylic acid also occurs in the same reaction step as the *N*-alkylation. In the publication of FAN ET AL[99] the procedure was described using an open vessel and a domestic microwave oven. They irradiated the reaction mixture at 375 W. The reaction time ranged from 2.5 minutes to 5.5 minutes. Out of safety reasons the procedure was modified. Instead of the domestic microwave oven and an open vessel a closed vessel was used in a microwave suitable for organic synthesis. This made it rather difficult to follow the exact procedure because the synthetic microwave

measures the pressure and temperature and adjusts the watt to maintain the conditions over the time of the reaction. The reaction was conducted at 150 °C over a period of 5.0 minutes. In addition there was the heating up phase and time to cool down the vessel after the reaction time was over. Added up the reaction including the waiting times took less than an hour which made it a very efficient and attractive procedure.

Beforehand several methods using an ice chilled phenothiazine solution with THF as a solvent, slowly adding DBU and then the ethyl-(4-bromo)chrotonate or respective methyl- (4-bromomethyl-) benzoate or refluxing a reaction mixture of the phenothiazine, Cs_2CO_3 and the ethyl-(4-bromo)chrotonate or respective methyl- (4-bromomethyl-) benzoate in DMF failed to deliver satisfying results.

Table 5 Structures of phenothiazine carboxylic acid derivatives obtained via N-alkylation of the respective phenothiazine

name	structure	name	structure
20a TB48s	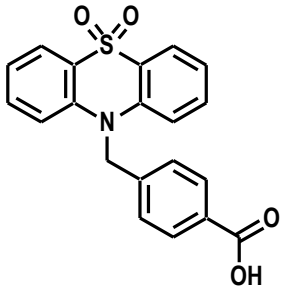	20b TB84s	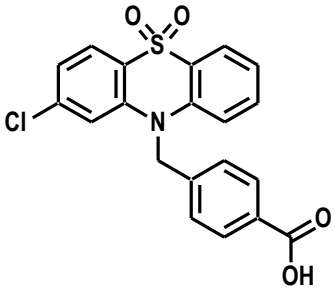
20c TB50s	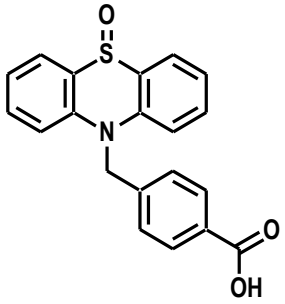	20d TB85s	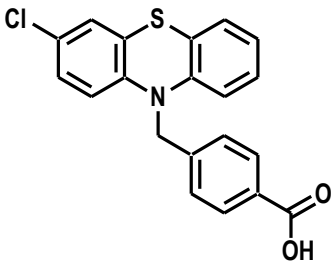
20e TB82s	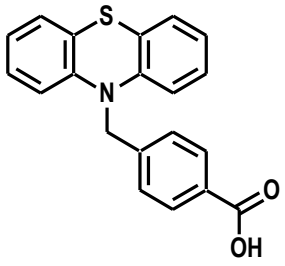	20f TB86s	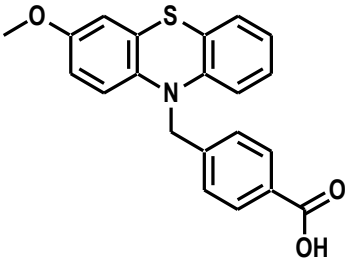

name	structure	name	structure
20g TB83s	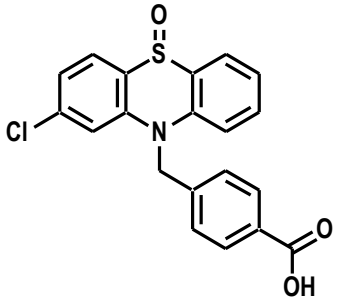	19a TB81s	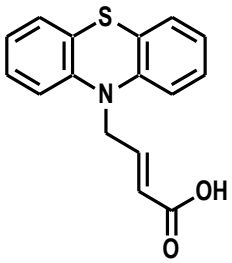

3.3 Summary of all synthesized hydroxamic acids assorted by structural similarity

All hydroxamic acids were transformed from the carboxylic acid using the procedure described in chapter 3.2 (see figure 38).

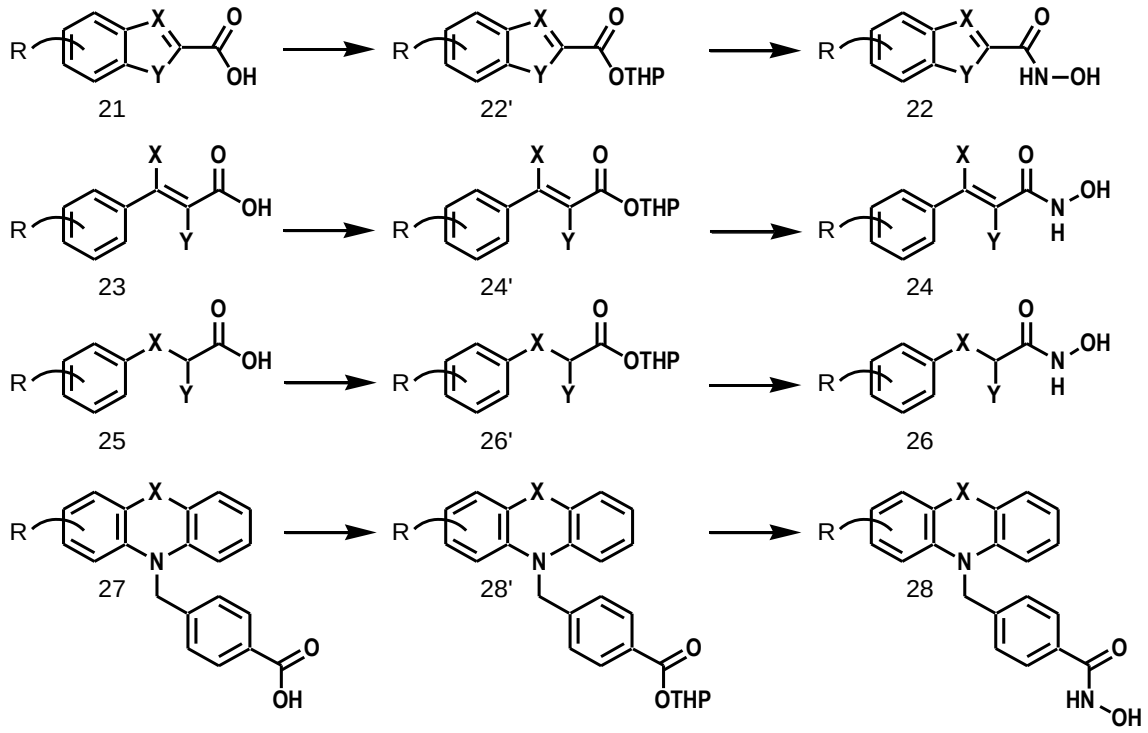

Figure 38 Reaction scheme of the transformation from the carboxylic acids to the hydroxamic acids

There are structures to be found here in the summary of the hydroxamic acids which were obtained from commercially available carboxylic acids or their respective methyl or ethyl esters. There are also some structures listed in the synthetic chapter above but which were not followed up on and which were not transformed into the respective hydroxamic acid. This was either due to a lack of sufficient amount of carboxylic acid derivative or because the substances were not promising anymore for the targets that were to be investigated in this work.

Table 6 Bicyclic derivatives (J1075 derived structures)

name	structure	Name	structure
22a (TB1)	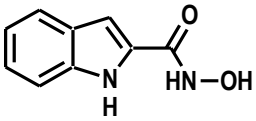	22b (TB13)	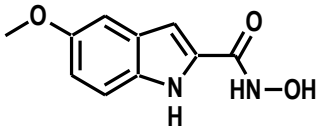
22c (TB74)	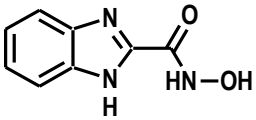	22d (TB2)	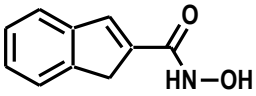
22e (TB3)	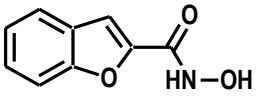	22f (TB42)	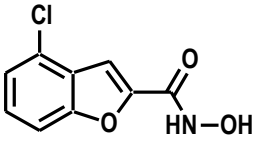
22g (TB45)	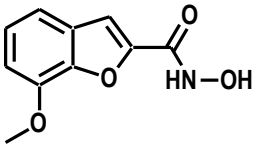	22h (TB46)	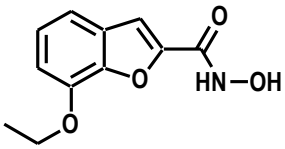
22i (TB4)	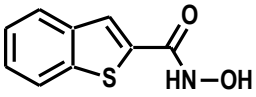	22j (TB5)	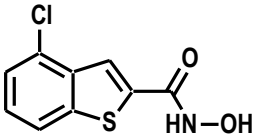

Table 7 Cinnamic acid derivatives

name	structure	name	structure
24a (TB7)	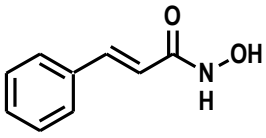	24b (TB8)	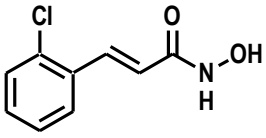
24c (TB77)	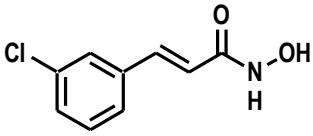	24d (TB9)	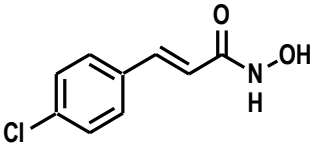
24e (TB32)	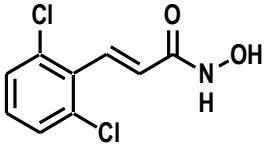	24f (TB51)	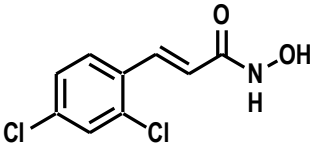
24g (TB10)	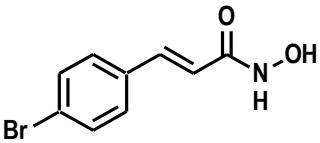	24h (TB76)	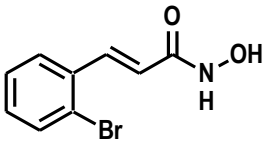

name	structure	name	structure
24i (TB53)	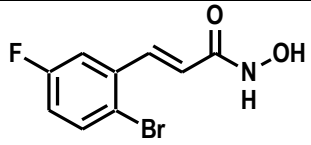	24j (TB54)	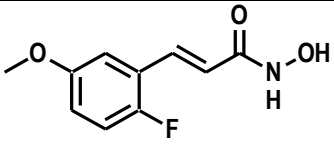
24k (TB15)	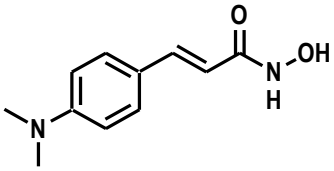	24l (TB14)	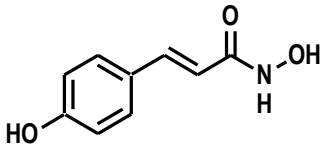
24m (TB33)	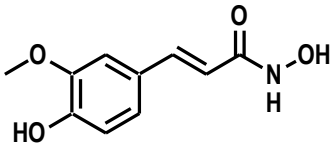	24n (TB16)	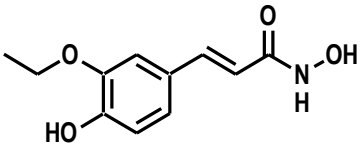
24o (TB31)	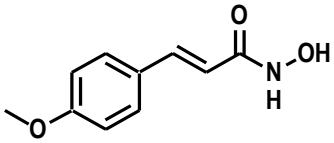	24p (TB44)	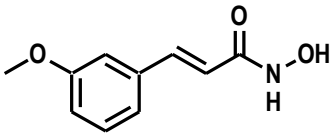
24q (TB43)	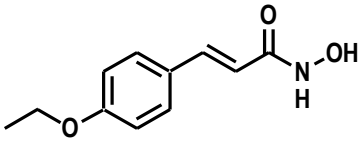	24r (TB58)	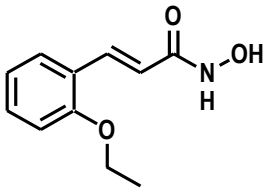
24s (TB11)	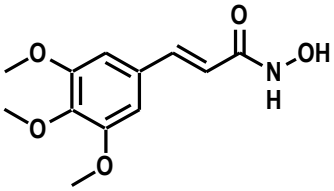	24t (TB57)	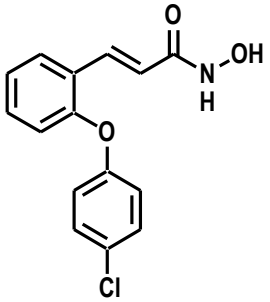
24u (TB55)	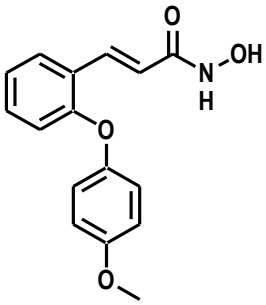	24v (TB27)	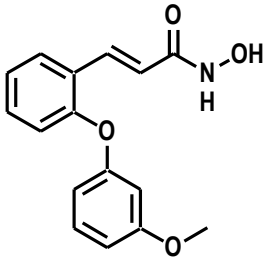

name	structure	name	structure
24w (TB72)	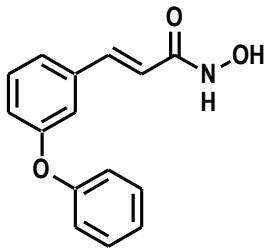	24x (TB87)	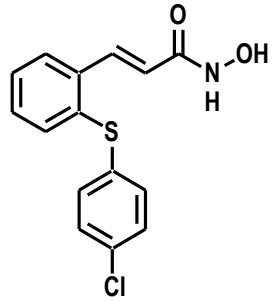
24y (TB59)	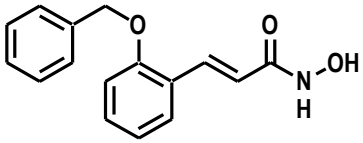	24z (TB64)	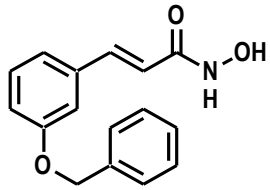
24za (TB12)	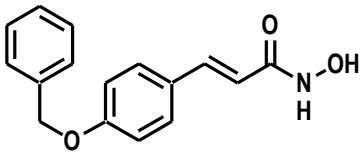	24zb (TB67)	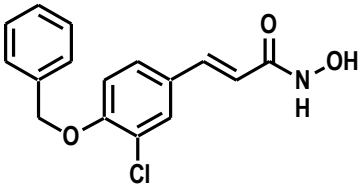
24zc (TB38)	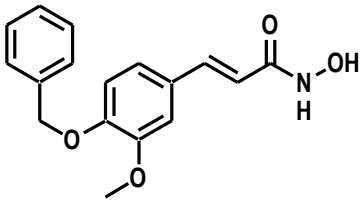	24zd (TB93)	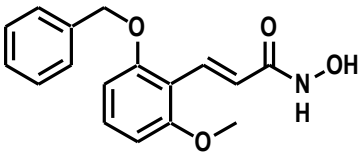
24ze (TB91)	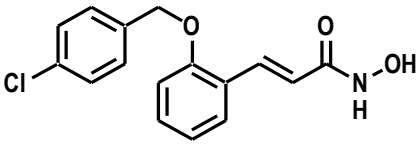	24zf (TB92)	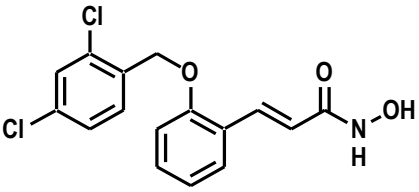
24zg (TB98)	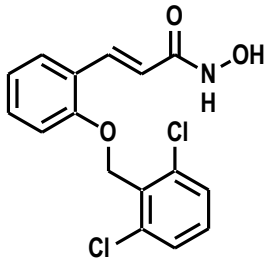	24zh (TB56)	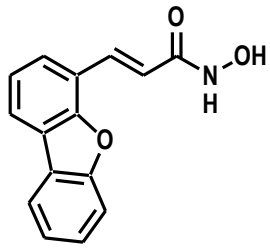
24zi (TB73)	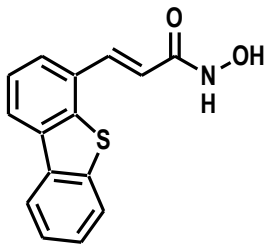	24zj (TB75)	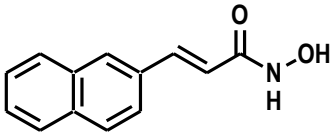

name	structure	name	structure
24zk (TB78)	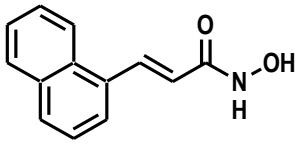		

Table 8 Miscellaneous other hydroxamic acids

name	structure	name	structure
24zl (TB37)	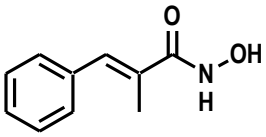	24zm (TB40)	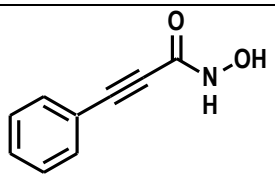
26a (TB89)	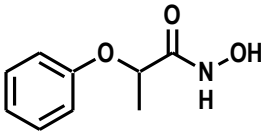	26b (TB88)	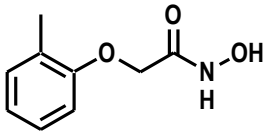
26c (TB96)	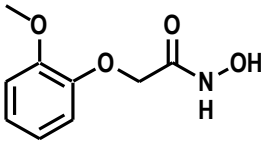	26d (TB79)	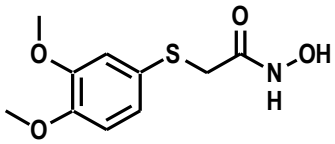
26e (TB94)	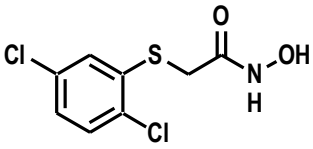	26f (TB103)	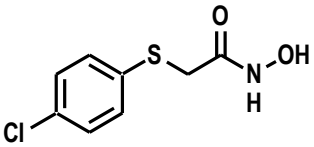
26g (TB104)	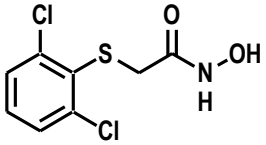	26h (TB105)	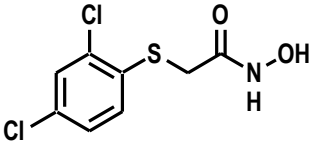
26i (TB90)	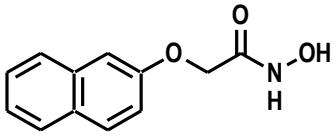	26j (TB97)	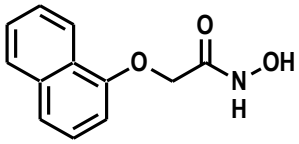

name	structure	name	structure
26k (TB80)	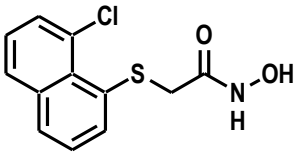	28a (TB83)	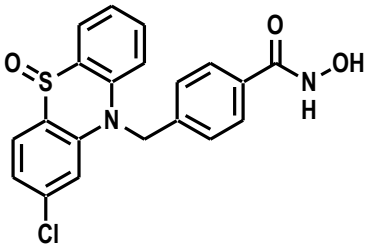

4 Results and Discussion

4.1 Schistosoma mansoni

4.1.1 Comparison of the assay systems ZMAL, ZMTFAL and Flour de Lys®[100]

The herein utilized assay systems have been developed for class I and class II histone deacetylases described by HILDMANN ET AL[101]. The general scheme is illustrated in the figure below. The substrate consists of an acetylated lysine (LYS-NHAc) linked to a variable residue (R) and a fluorophore (AMC). In a first step of the assay the artificial substrate is deacetylated by the histone deacetylase. In a second step the endopeptidase trypsin is added which then cleaves the fluorophore from the lysine metabolite. The free fluorophore now has different spectroscopic properties than in the linked state like it was in the original substrate and the first metabolite. The residual acetylated substrate cannot be cleaved by the endopeptidase trypsin (see figure 39).

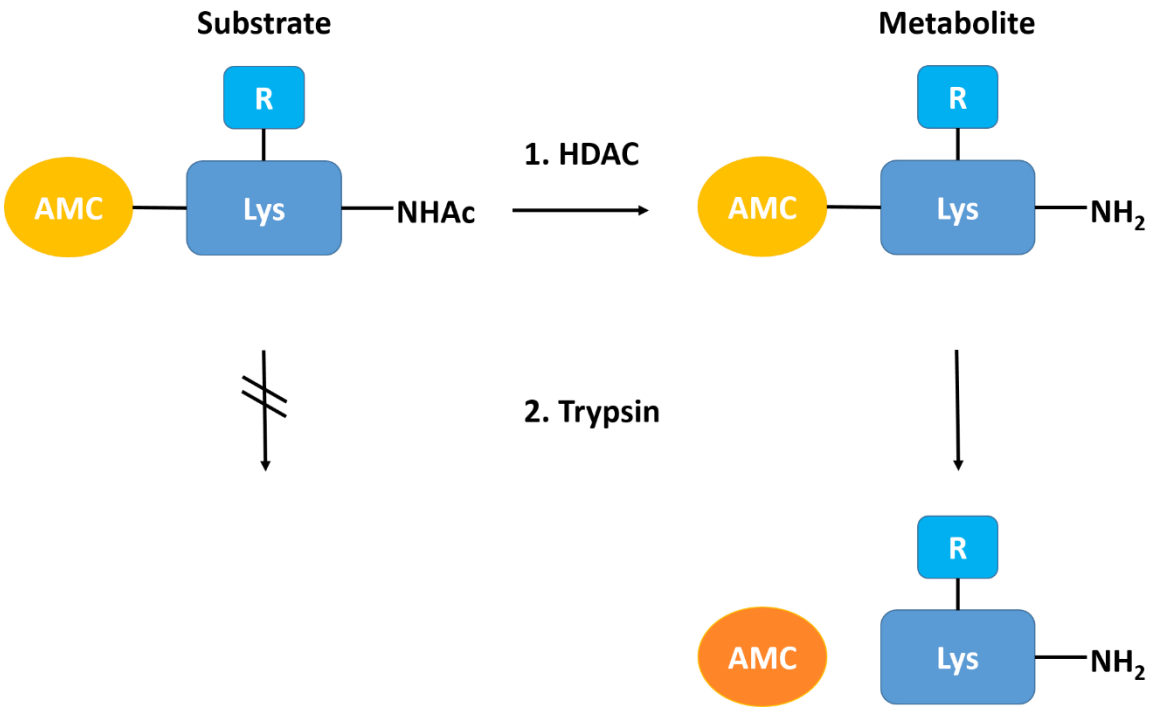

Figure 39 General reaction scheme of HDAC8 assays modified after TRAPP[100]

In previous works different *in vitro* assay systems for testing the effects of substances on histone deacetylases were developed and evaluated towards their suitability and robustness[100,102]. In case of Fluor de Lys® the substrate consists of an aliphatic side chain

with a terminal acetylated amino acid. The substrate also contains a fluorophore which changes its fluorescent wave length after enzymatic cleavage from the substrate by trypsin. The difference in wave length can be measured and the activity of the enzyme can be determined. ZMAL (*(S)*-[5-acetyl amino-1-(4methyl-2-oxo-*2H*-chromene-7-ylcarbamoyl) pentyl] carbaminic acid benzyl ester) also is an acetylated substrate and like Fluor de Lys® also imitates the acetylated lysine side chain which is a substrate of the histone deacetylase (reaction scheme shown in figure 40).

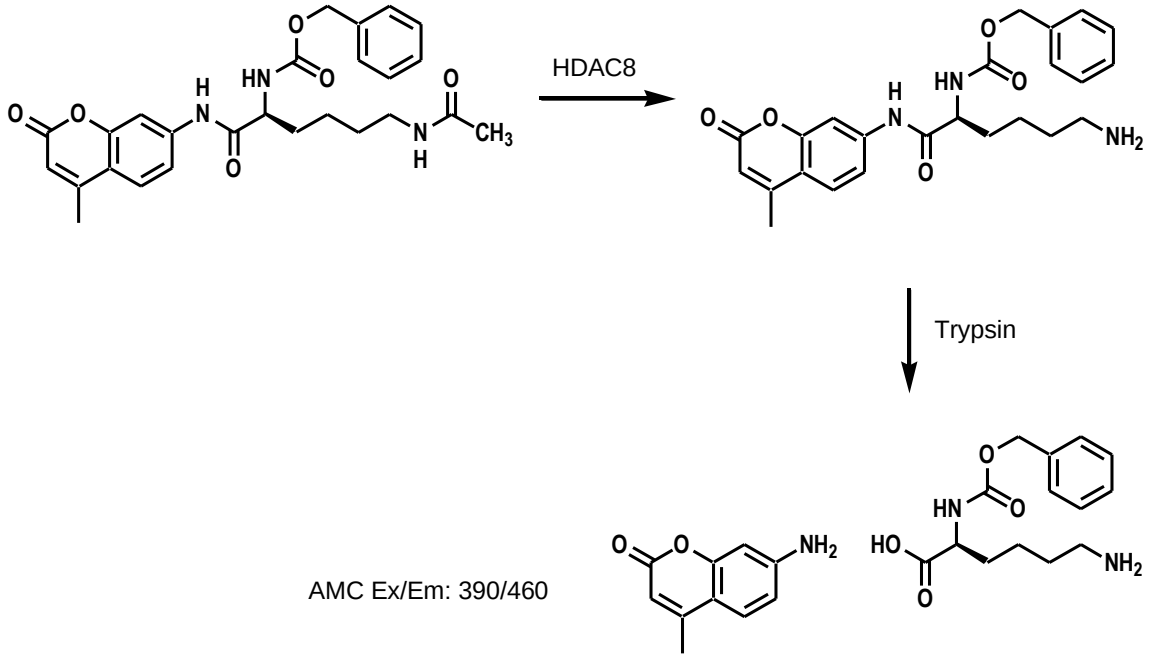

Figure 40 Reaction scheme for the histone deacetylase assay with the substrate ZMAL

This assay is low in cost but unfortunately the HDAC8 does not cleave the acetyl residue of the ZMAL substrate too well[103]. In comparison Fluor de Lys® is a better substrate to measure the inhibitory effects of different substances on HDAC8. Due to practical reasons the assay was used only for the human and schistosome histone deacetylase 8 in order to obtain reliable and reproducible results. For the inhibitory effects of the substances on the human isoforms HDAC1 and HDAC6 the less expensive ZMAL assay was used. The assay delivery reliable results for these subtypes and the results are an orientation for the comparison of the different inhibitors among each other. Another assay system for HDAC8 is based on the artificial substrate ZMTFAL. The substrate is similar to the one of the ZMAL assay. ZMTFAL (*(S)*-[5-trifuoracetyl amino-1-(4methyl-2-oxo-*2H*-chromene-7-

ylcarbamoyl) pentyl] carbaminic acid benzyl ester) is an artificial substrate that also is recognized and cleaved by the human and schistosome HDAC8. It carries a trifluor acetylated lysine instead of the acetylated lysine of the ZMAL substrate. Some of the substances were tested in all three assay systems for comparison of the methodologies. (Structures shown in figure 41)

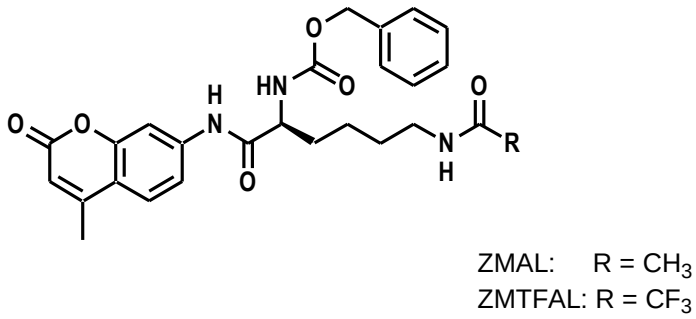

Figure 41 Structures of ZMAL and ZMTFAL

All of the substances were first tested in pretests against the target enzyme, *sm*HDAC8. Those substances that had good inhibitory properties in the pretests were further investigated; the IC_{50} values and the selectivity between the different subtypes of the histone deacetylases were determined. In the following chapters the results on the different enzymes will be presented and discussed.

Table 9 Fluor de Lys® results of the bicyclic compounds tested for their effect on the schistosome HDAC8. IC_{50} values presented in µM or nM as declared in the table. Results of pretests are presented in % inhibition of the enzyme at the declared concentration. If the prestests showed low percentages of inhibition despite high concentrations of the compound or low dose dependance the IC_{50} value was not determined (n.d.). When there is no standard deviation n = 1, if a standard deviation is indcated n = 3.

name	structure	pretest	IC_{50}
indene derivative			
22d (TB2)	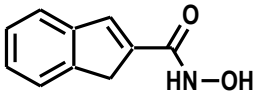	10µM: 98 %	n.d.
indole / benzimidazole derivatives			
22a (TB1)	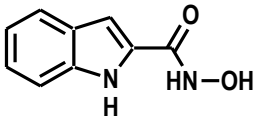		4.90 ± 1.1 µM
22b (TB13)	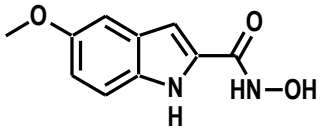		1.8 ± 0.8 µM
22c (TB74)	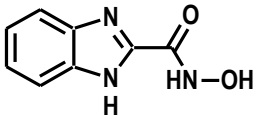	5 µM: 0 % 0.5 µM: 0 % .	n.d.
benzofurane derivatives			
22e (TB3)	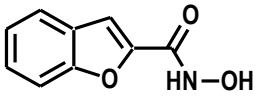		240 ± 50 nM
22f (TB42)	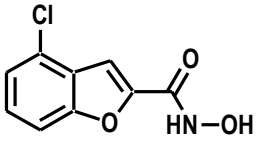		780 ± 40 nM
22g (TB45)	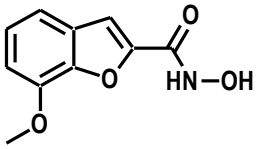		2.1 ± 0.5 µM

name	structure	pretest	IC_{50}
benzothiophene derivatives			
22i (TB4)	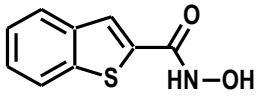		630 ± 100 nM
22j (TB5)	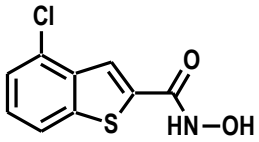		250 ± 20 nM

This table sums up the results of the bicyclic compounds tested in the Fluor de Lys® assay for the *sm*HDAC8. The first compound **22d** (TB2), the indene hydroxamic acid was found to be weakly active. In comparison the unsubstituted indole derivative **22a** (TB1) has an IC_{50} value in the lower micromolar range. The 5-methoxy substituted indole hydroxamic acid **22b** (TB13) shows an improved IC_{50} value of just under half of the value its unsubstituted homologue. The introduction of a second nitrogen atom into the five-membered ring (benzimidazole derivative **22c** (TB74)) resulted in a complete loss of inhibitory effects on the *sm*HDAC8. Looking at **22e** (TB3) and **22i** (TB4), the unsubstituted benzofurane and the unsubstituted benzothiophene the IC_{50} values are in the nanomolar range. A 4-chloro substitution of the benzothiophene derivative **22j** (TB5) shows an improvement of the IC_{50} value by about 300 nM whereas the same 4-chloro substitution in the benzofurane derivative increases the IC_{50} value by about 500 nM. None of the substitutions (chloro-, methoxy-, ethoxy-) in position 7 of the benzofurane was able to bring a significant improvement of the IC_{50} value.

Table 10 Fluor de Lys® results of the cinnamic acid compounds with smaller residues tested for their effect on the schistosome HDAC8. IC_{50} values presented in µM or nM as declared in the table. Results of pretests are presented in % inhibition of the enzyme at the declared concentration. If the prestests showed low percentages of inhibition despite high concentrations of the compound or low dose dependance the IC_{50} value was not determined (n.d.). When there is no standard deviation n = 1, if a standard deviation is indcated n = 3.

name	structure	pretest	IC_{50}
cinnamic acid derivatives (smaller residues)			
24a (TB7)	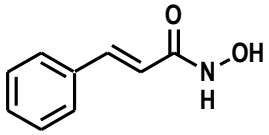	5 µM: 80 % 0.5 µM: 50 %	130 ± 20 nM
24b (TB8)	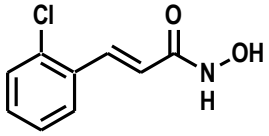		60 ± 20 nM
24c (TB77)	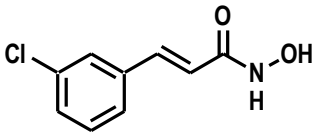	5 µM: 78 % 0.5 µM: 43 %	n.d.
24d (TB9)	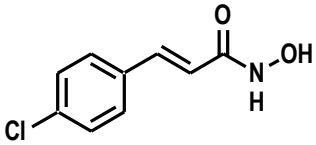		800 ± 110 nM
24e (TB32)	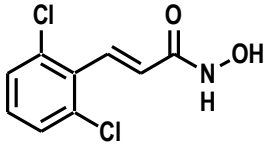		210 ± 30 nM
24f (TB51)	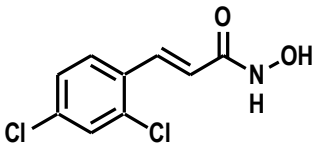	0.5 µM: 50 %	n.d.
24g (TB10)	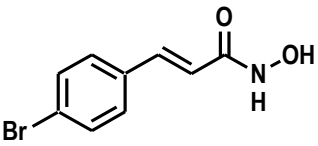		240 ± 50 nM

name	structure	pretest	IC_{50}
24i (TB53)	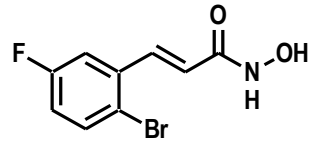	0.5 µM: 60 %	500 ± 150 nM
24j (TB54)	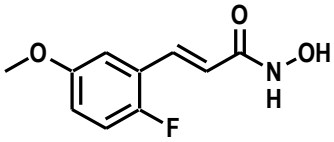	0.5 µM: 45 %	840 ± 200 nM
24k (TB15)	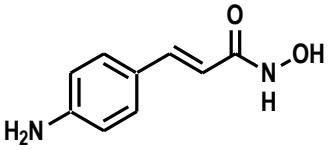	100 µM 50 % 10 µM 84 %	n.d.
24l (TB14)	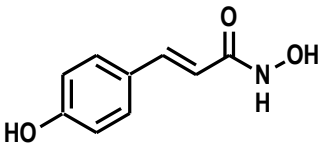		60 ± 30 nM
24m (TB33)	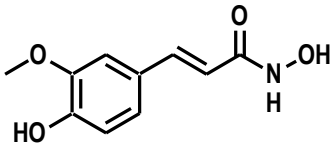	0.5 µM: 53 %	n.d.
24n (TB16)	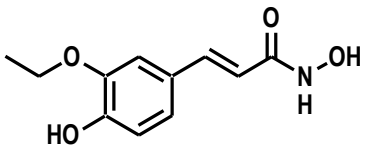		660 ± 170 nM
24o (TB31)	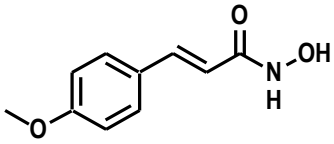	0.5 µM: 57 %	n.d.
24p (TB44)	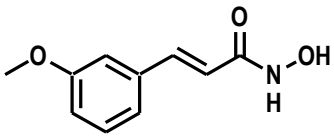	0.5 µM: 45 %	n.d.
24q (TB43)	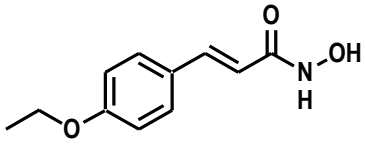	0.5 µM: 60 %	n.d.

name	structure	pretest	IC_{50}
24r (TB58)	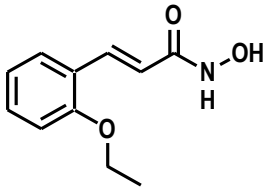	0.5 µM: 53 %	n.d.
24s (TB11)	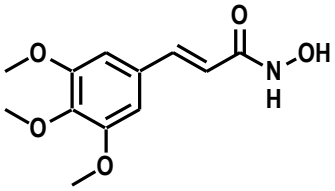		620 ± 140 nM

For the cinnamic acid compounds the results are rather heterogenic. The unsubstituted compound **24a** (TB7) has an IC_{50} value of around 130 nM. An ortho-chloro substitution **24b** (TB8) resulted in an improvement of the IC_{50} value to about half of the value of the unsubstituted compound. Moving the chloro substituent to the meta- or para-position resulted in significant increase of the IC_{50} value. The introduction of a second chloro substituent to the ortho-chloro compound to the second ortho position **24e** (TB32) resulted in an increase of the IC_{50}-value to approximately 200 nM and the compound with the ortho- , para-bichloro substitution pattern **24f** (TB51) again resulted in a significant loss of the inhibitory effects on the *sm*HDAC8. Exchanging the chloro substituent to a bromo substituent **24g** (TB10) resulted in a significant improvement for the both para substituted compounds which could possibly be based on the increase in size and lipophilicity of a brome instead of a chlorine atom. Neither the combination of an ortho-bromine and a meta-fluorine atom **24i** (TB53) nor an ortho-fluorine together with a meta-methoxy residue **24j** (TB54) showed good results. A para-amino function did also show little positive effect on the inhibitory effects of the cinnamic hydroxamate. Interestingly the para-hydroxy cinnamic acid derivative **24l** (TB14) shows an IC_{50} value of around 60 nM. Adding an additional ethoxy- or methoxy-substituent in meta-position causes a loss of inhibitory activity on the *sm*HDAC8. All together there was no improvement that could be achieved by all modifications that were tried out for the para-hydroxy derivative **24l** (TB14). Single or multiple methoxy- or ethoxy-substituted cinnamic acid derivatives (**24o**-**24s**) did not show improved smHDAC8 inhibitory activity in comparison to the unsubstituted cinnamic acid derivative.

Table 11 Fluor de Lys® results of the cinnamic acid compounds with bulkier phenyloxy- or phenylthio- residues tested for their effect on the schistosome HDAC8. IC_{50} values presented in µM or nM as declared in the table. Results of pretests are presented in % inhibition of the enzyme at the declared concentration. If the prestests showed low percentages of inhibition despite high concentrations of the compound or low dose dependance the IC_{50} value was not determined (n.d.). When there is no standard deviation n = 1, if a standard deviation is indcated n = 3.

name	structure	pretest	IC_{50}
cinnamic acid derivatives (phenyloxy- or phenylthioether residues)			
24t (TB57)	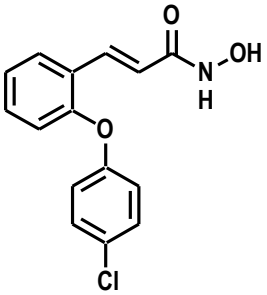		220 ± 10 nM
24u (TB55)	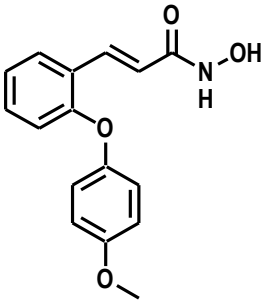		90 ± 20 nM
24v (TB27)	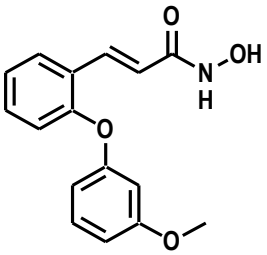		250 ± 30 nM
24w (TB72)	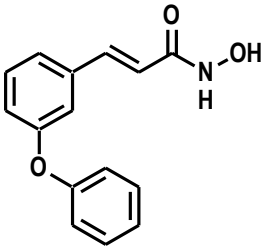	5 µM: 80 % 0.5 µM: 44 %	n.d.

name	structure	pretest	IC_{50}
24x (TB87)	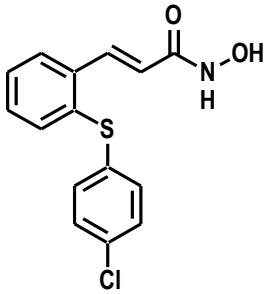		180 ± 30 nM

Knowing that the binding pocket of the schistosome enzyme can take a Phe151-flipped out conformation leaving a broader area at the entry of the binding pocket it seemed attractive to create compounds that have a bulkier residue pointing sideways from the zinc binding group for the molecule to take a shape which resembles an “L”. For the phenyl ether and respective phenyl thioether residues it can generally be said that the ortho-position is favorable in comparison to the meta-position whereas a para-position for this kind of residues was not synthesized due to the straight “I-shaped” geometry the molecule would take.

Table 12 Fluor de Lys® results of the cinnamic acid compounds with bulkier benzyloxy residues tested for their effect on the schistosome HDAC8. IC_{50} values presented in µM or nM as declared in the table. Results of pretests are presented in % inhibition of the enzyme at the declared concentration. If the prestests showed low percentages of inhibition despite high concentrations of the compound or low dose dependance the IC_{50} value was not determined (n.d.). When there is no standard deviation n = 1, if a standard deviation is indcated n = 3.

name	structure	pretest	IC_{50}
cinnamic acid derivatives (benzyloxy residues)			
24y (TB59)	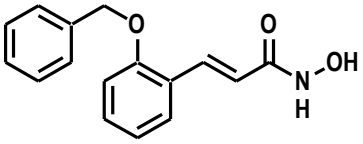	0.5 µM: 56%	n.d.
24z (TB64)	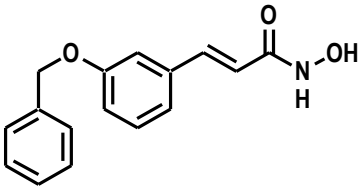	5 µM: 74 % 0.5 µM: 36 %	n.d.

name	structure	pretest	IC_{50}
24za (TB12)	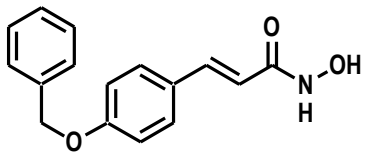		250 ± 40 nM
24zb (TB67)	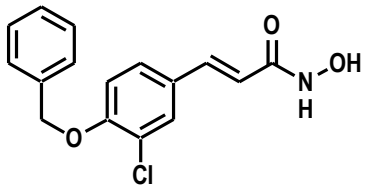	0.5 µM: 33 %	3.3 ± 1.6 µM
24zc (TB38)	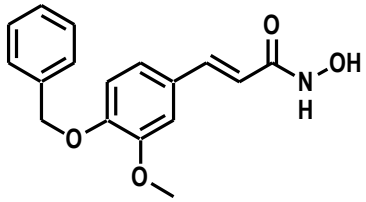		500 ± 70 nM
24zd (TB93)	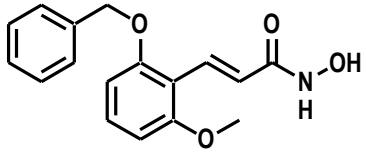	5 µM: 99 % 0.5 µM: 77 %	130 ± 20 nM
24ze (TB91)	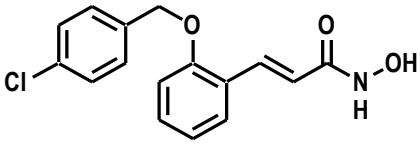	5 µM: 84 % 0.5 µM: 53 %	720 ± 10 nM
24zf (TB92)	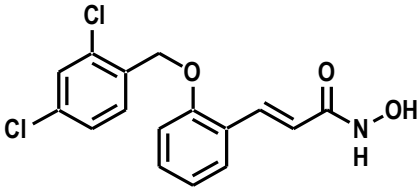	5 µM: 87 % 0.5 µM: 52 %	520 ± 80 nM
24zg (TB98)	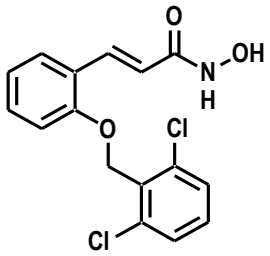		440 ± 40 nM

For the cinnamic acids with benzyloxy residues it can be generally said that the activity on the *sm*HDAC8 depends on the position of the benzyloxy residue and other possible residues. Out of the three possible positions (ortho-, meta- or para-) the meta-position is the

one which makes the least effective compound. The compound **24z** (TB64) showed an inhibition of approximately 36 % at 0.5 µM. Compounds with benzyloxy residues in both other positions showed better results. Interestingly the unsubstituted para-benzyloxy cinnamic acid derivative **24za** (TB12) shows best results with an IC_{50} value of approximately 250 nM. However none of the other para-benzyloxy compounds shows better or equal results. The 3-methoxy, 4-phenyloxy cinnamic acid derivative **24zc** (TB38) shows slightly better results than the 3-chloro, 4-phenyloxy derivative **24zb** (TB67). The unsubstituted ortho-benzyloxy derivative **24y** (TB59) shows an inhibitory activity of about 56 % at a concentration of 0.5 µM. Substitutions on the second ring bring slight improvement (in case of **24zg** (TB98), the [(2,6- dichloro)-benzyloxy] cinnamic acid derivative) in comparison to the unsubstituted derivative (IC_{50} value of approximately 440 nM). However the other two substituted phenoxy moieties show equal results compared to **24y** (TB59). Compound **24zd** (TB93), the 6 - methoxy, 2 - benzyloxy derivative has the lowest IC_{50} value of approximately 130 nM.

Table 13 Fluor de Lys® results of the cinnamic acid compounds with annulated ring systems tested for their effect on the schistosome HDAC8. IC_{50} values presented in µM or nM as declared in the table. Results of pretests are presented in % inhibition of the enzyme at the declared concentration. If the prestests showed low percentages of inhibition despite high concentrations of the compound or low dose dependance the IC_{50} value was not determined (n.d.). When there is no standard deviation n = 1, if a standard deviation is indcated n = 3.

name	structure	pretest	IC_{50}
cinnamic acid derivatives (annulated aromatic rings)			
24zh (TB56)	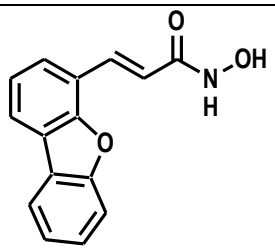	0.5 µM: 49 %	n.d.
24zi (TB73)	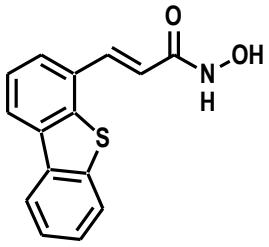	5 µM: 78 % 0.5 µM: 33 %	n.d.

name	structure	pretest	IC_{50}
24zj (TB75)	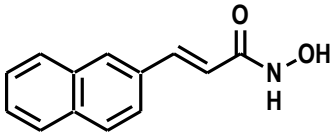	5 µM: 78 % 0.5 µM: 40 %	n.d.
24zk (TB78)	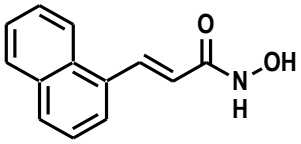	5 µM: 93 % 0.5 µM: 61 %	n.d.

For the cinnamic acid derivatives with annulated rings it can be said that unfortunately none of them performed very well as for inhibition of *sm*HDAC8. Not for all of the compounds IC_{50} values were determined and for those that were tested only pretests were performed. Looking at the results of the pretests IC_{50} values can be estimated only roughly. Compound **24zh** (TB56) the dibenzo furane derivative shows approximately 50 % of inhibition at a concentration of 0.5 µM whereas its sulfur homologue **24zi** (TB73) only shows about 30 % inhibition at the same concentration. Comparing the naphtyl-derivatives there is a slight preference for the 1-napthyl derivative **24zj** (TB75) in comparison to the 2-naphtyl derivative **24zk** (TB78).

Table 14 Fluor de Lys® results of the miscellaneous small molecule hydroxamic acids tested for their effect on the schistosome HDAC8. IC_{50} values presented in µM as declared in the table. Results of pretests are presented in % inhibition of the enzyme at the declared concentration. If the prestests showed low percentages of inhibition despite high concentrations of the compound or low dose dependance the IC_{50} value was not determined (n.d.). When there is no standard deviation n = 1, if a standard deviation is indcated n = 3.

name	structure	pretest	IC_{50}
miscellaneous structures			
24zl (TB37)	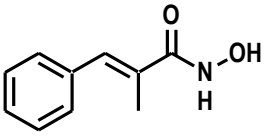	0.5 µM: 53%	n.d.
24zm (TB40)	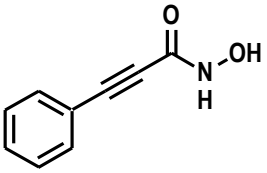	0.5 µM: 2.8%	n.d.
26e (TB94)	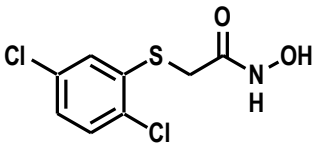		1.3 ± 0.3 µM

After investigating the inhibitory capability of various hydroxamic acid based compounds on the *sm*HDAC8 it was interesting to see the effects of a modified linker connecting the hydroxamic acid warhead to the rest of the molecule. The compound **24zl** (TB37) contains a methyl residue at the α-position the cinnamic acid linker, however the results did not inspire to further investigate alike structures. The pretest results shows an inhibition of just over 50 % at 0.5 µM in comparison the unsubstituted cinnamic acid derivative has an IC_{50} value of approximately 130 nM. Also **24zm** (TB40), the cinnamic acid homologue with the linker containing a triple bond instead of the double bond characteristic for the cinnamic acids shows almost no activity in the assay for evaluating the inhibitory potential on the *sm*HDAC8. Most of the ether- and thioether- linker structures were not tested for their effects on this target. The IC_{50} value for the thioether-linker compound **26e** (TB94) was determined at 1.3 µM which is not promising enough for a further investigation of this structural trait.

4.1.2 Crystal structures

Crystal structures of promising inhibitors with smHDAC8 were solved by DR. T. B. SHAIK, DR. M. MAREK and DR. C. ROMIER from the Département de Biologie Structurale Intégrative, Institut de Génétique et Biologie Moléculaire et Cellulaire (IGBMC), Université de Strasbourg, CNRS, INSERM, 67404 Illkirch Cedex (France).

The crystal structures deliver important structure information which were used as input for computational studies and structure-guided chemical optimization. For the visualization and analysis of the crystal structures program MOE[104] was used.

4.1.2.1 Ligand interaction plots

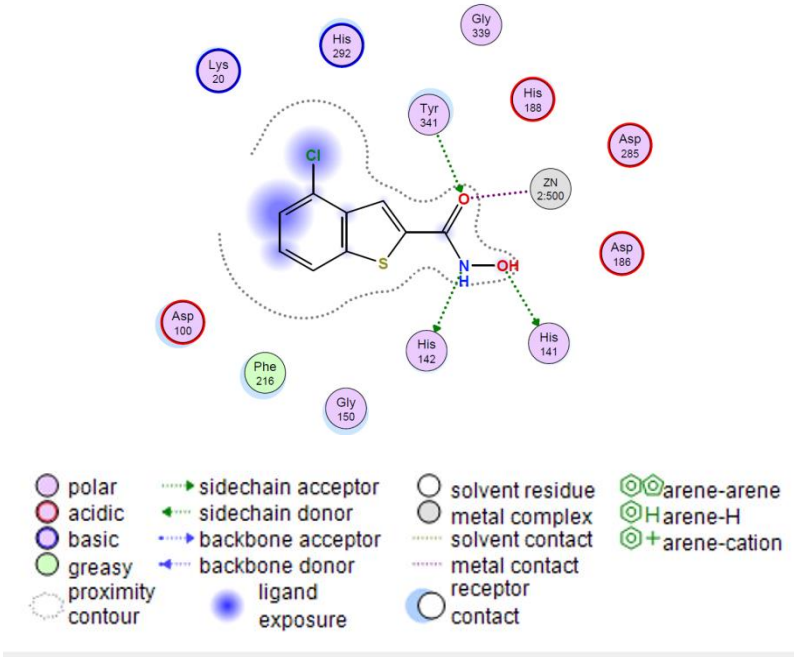

Figure 42 Ligand plot of the interactions between the compound 22j (TB5) and the smHDAC8 (PDB ID 6GX3) created with MOE. Interaction types given in the legend.

Figure 44 shows the ligand interaction plot of **22j** (TB5) in the binding pocket of the target enzyme *sm*HDAC8 derived from the solved crystal structure (PDB ID 6GX3). It clearly shows the interactions of the hydroxamate warhead of the ligand with the catalytic zinc ion of the binding pocket. The two oxygen atoms chelate the positively charged zinc ion in a bidentate fashion. Additionally the nitrogen and the oxygen interact with His142 and His141 by H-bonds as well as the other carbonyl oxygen is interacting with Tyr341 by an H-bond. Phe216 interacts with C7 of the ligand via arene-H interaction. The chlorine in position four and the backside (C5 and C6) of the ligand do not show direct interactions to the binding pocket but might be responsible for the orientation of the ligand in the narrow

binding pocket. Out of the group of the bicyclic compounds most structures resemble the above shown compound **22j** (TB5). The interactions are very similar and the measured IC_{50}-values are in the medium three digit nanomolar range. The weak inhibitory potential of **22a** (TB1) and **22b** (TB13), the indole derivatives as well as **22c** (TB74) the benzimidazole derivative providing one respective two nitrogen heteroatoms on the five-membered ring with IC_{50}-values in the lower micromolar range respective with no effect on the enzyme could be due to their higher polarity which prevents them from entering the hydrophobic entrance of the binding pocket.

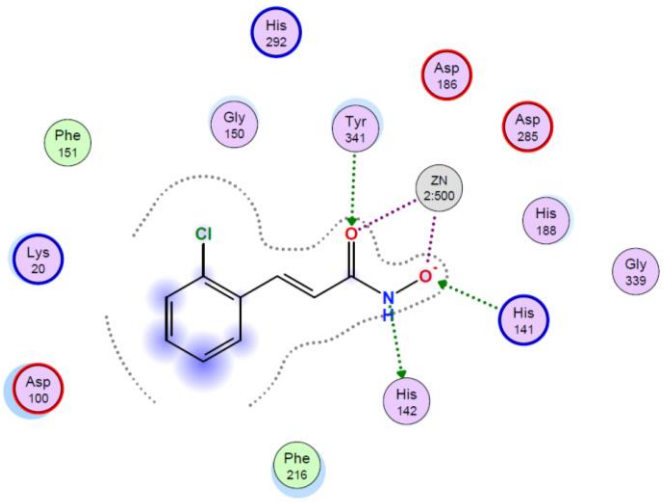

Figure 43 Ligand plot of the interactions between the compound 24b (TB8) and smHDAC8 (PDB ID 6GXA) created with MOE

The above-shown ligand plot (figure 45) depicts the ligand-enzyme interactions of **24b** (TB8) and s*m*HDAC8 as derived from the solved crystal structure (PDB ID 6GXA). Here, just like before at the example of **22j** (TB5) the hydroxamate chelates the catalytic zinc ion in a bidentate fashion utilizing both oxygen atoms. The carbonyl oxygen also interacts with Tyr341 via H-bond as well as both His141 and His142 form H-bonds to the second oxygen of the hydroxamate. The flexible linker of the cinnamic acid fits the narrow catalytic tunnel and also allows the aromatic ring at the hind side of the cinnamic acid to freely pick an orientation which is most comfortable for the respective moiety. In case of **24b** (TB8) there is a chlorine residue in position 2 of the aromatic ring which is oriented towards Lys20 but however is exposed with no specific interactions. That side of the catalytic pocked in which

the chloro residue is oriented does however have a lipophilic surface which will be discussed later.

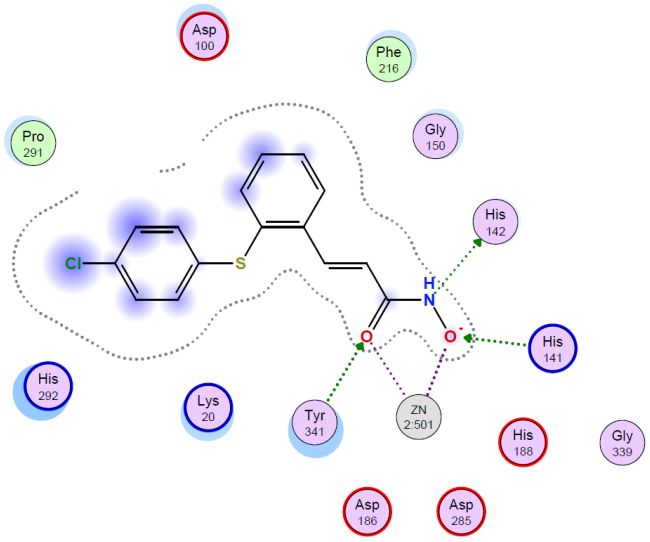

Figure 44 Ligand plot of the interactions between the compound 22x (TB87) and the smHDAC87 (PDB ID 6GXU) created with MOE

In figure 46 the interactions between **24x** (TB87) and the enzyme *sm*HDAC8 are depicted as observed in the solved crystal structure (PDB ID 6GXU). As well as in the other ligand plots before the hydroxamate equally chelates the catalytic zinc ion. Here, the binding is also stabilized via H-bonds connecting from the neighboring amino acids. The interaction pattern delivers no explanation for the differences in IC_{50} values between the different compounds of the subgroup of the phenyloxy- or phenylthioehter substituted cinnamic acids. All of the compounds of this subgroup are ortho substituted minus the exception of compound **24w** (TB72). Assuming that a weak H-bond between the sulfur or oxygen of the respective ether connection and the amino acid Lys20 might be formed the lower inhibitory potential on the enzyme of the meta substituted compound **24w** (TB72) is explainable.

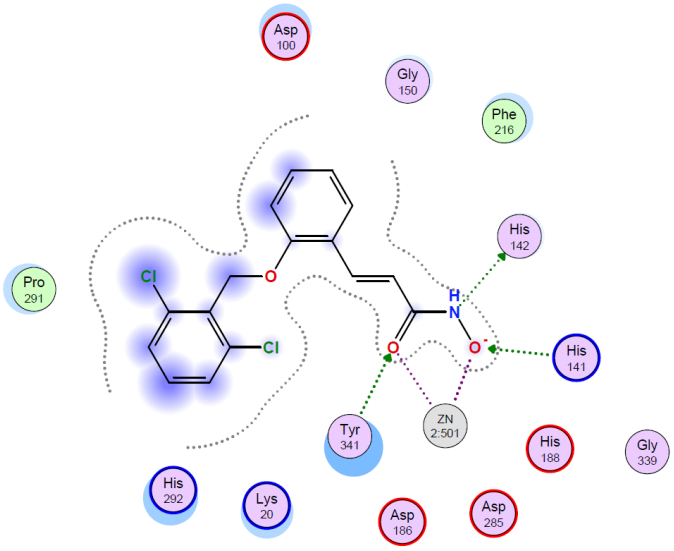

Figure 45 Ligand plot of the interactions between the compound 24zg (TB98) and the smHDAC8 (PDB ID 6GXW) created with MOE

Like in the other ligand plots, the hydroxamate warhead of **24zg** (TB98) chelates the zinc ion at the bottom of the catalytic pocket in a bidentate fashion (figure 47). The cinnamic acid linker provides the distance between the chelating warhead and the spacious aromatic moiety at the opposite side of the compound.

In this case there are no further specific interactions visible between compound **24zg** (TB98) and the *sm*HDAC8 based on the solved crystal structure (PDB ID 6GXW). Therefore it seems obvious why this compound showed lower inhibition of the *sm*HDAC8 than for example **24x** (TB87) which does show an additional specific interaction.

4.1.2.2 3-D visualization

The other option that was used here was a 3-D visualization and visual evaluation of the crystal structures especially the binding pocket with each respective inhibitor.

Comparing the different available crystal structures of the *sm*HDAC8 co-crystallized with different inhibitors altered conformations of the binding pockets are reported depending on the respective inhibitor[5].

The *sm*HDAC8 has a phenylalanine at the entrance of the catalytic pocket (Phe151) which is able to take either the flipped in or the flipped out conformation. This conformational flexibility is a trait which cannot be found in the human homologous enzyme and therefore is one possibility to address in order to gain selectivity.

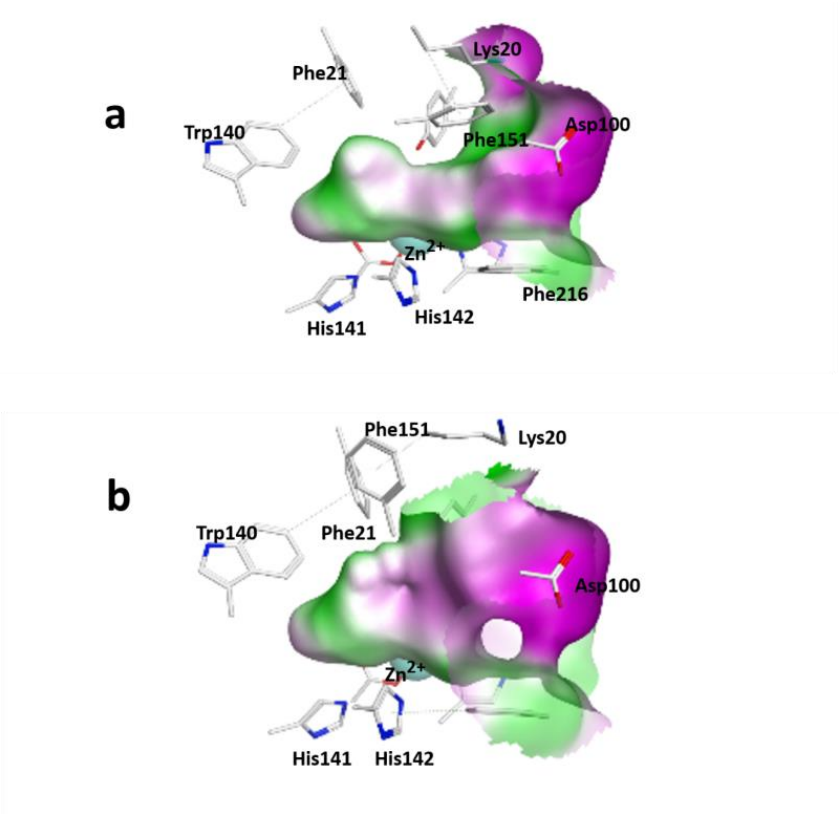

Figure 46 Binding pocket of smHADC8. Hydrophilic surface shown in magenta and lipophilic surface shown in green. The upper picture, a shows the size and shape of the pocket with the phenylalanine 151 taking the "flipped-in" conformation and b shows the size and shape of the pocket with phenylalanine 151 taking the "flipped-out" conformation.

In the above shown figure 48 the binding pocket of *sm*HDAC8 is shown. The pocket surface is described by the hydrophilic (magenta) and lipophilic (green) properties. Both, **a** and **b** are extracted from the crystal structure of *sm*HDAC8 co-crystalized with the inhibitor **22k** (TB5, PDB ID 6GX3).

The most outstanding difference between the two is the great difference in size of the same pocket of the same enzyme by just the conformational change of one amino acid residue namely Phe151. In picture **a** it takes the "flipped-in" conformation while in **b** it takes the "flipped-out" conformation. Interestingly these two states are extracted from two different chains of one *sm*HDAC8 tetramer in which two of the monomers show a conformation with Phe151 pointing inward, narrowing the catalytic canal and the other two showing the opposite conformation with Phe151 pointing away from the catalytic canal leaving room for larger inhibitors. So Phe151 is serving as a kind of gatekeeper.

The enzyme was co-crystalized with the inhibitor **22k** (TB5), a fragment-like molecule which leaves room for conformational changes of the binding pocket. Interestingly, in the

tetrameric crystal structure form the binding pocket and inhibitor take different conformation. This demonstrates the flexibility of the *sm*HDAC8 binding pocket which makes it possible to adjust to different shapes of ligands. Knowing that the human HDAC8 has not been reported to perform such transformation (previously discussed in the introduction) it is a trait that can be exploited in order to aim for selective compounds which cannot fit the narrow opening of the human enzyme's catalytic pocket but are able to modify the schistosome binding pocket to their spatial requirements.

In general, the binding pocket of the *sm*HDAC8 can not only take one or another strictly defined conformation but rather can adjust the conformation of amino acid residues according to the ligand which interacts with the binding pocket.

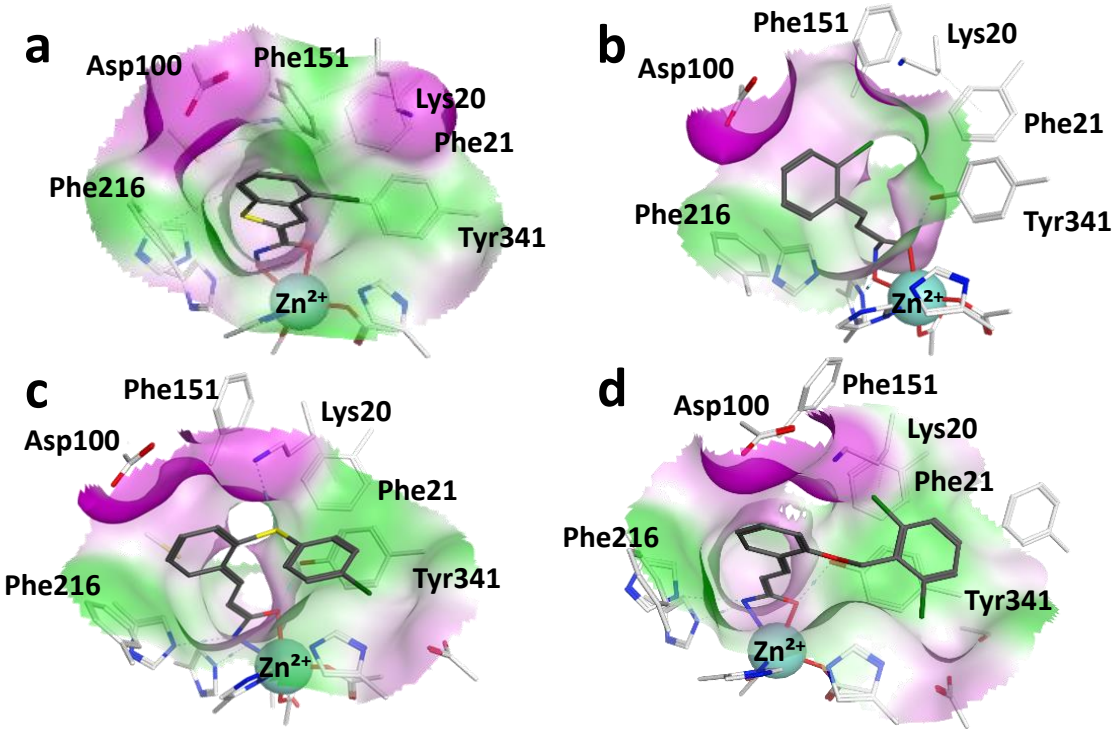

Figure 47 Binding pocket of smHDAC8 with the inhibitors A: 22j (TB5), B: 24b (TB8), C: 24x (TB87), D: 24zg (TB98). Surface of the binding pocket is colored by lipophilicity: magenta – hydrophilic, green – lipophilic. Protein amino acid residues (white carbons) and ligands (grey carbons) are depicted in stick representation. Oxygen atoms are colored red, nitrogen – blue, sulfur – yellow, chlorine – green. The catalytic zinc ion is shown as a turquoise ball. Hydrogen bonds are displayed as dashed pale blue lines, while the bonds between the hydroxamic acid moiety and the zinc ion (threshold 2.5 Å) are displayed as solid lines.

In picture **a** the ligand **22j** (TB5), a 4-chloro benzothiophene derivative chelates the zinc ion with the hydroxamate moiety in position 2 of the benzothiophene. The 6-membered ring of the molecule shows π-π interaction with Phe216 while the chloro-residue is pointing

towards the lipophilic region formed by Phe21 and Tyr341. The flexible "gatekeeper" Phe151 takes the "flipped-out" conformation leaving a larger opening to the catalytic canal. Meanwhile Lys20 is also pointing away from the active site not participating in any specific interactions.

Picture **b** shows the *sm*HDAC8 co-crystalized with the inhibitor **24b** (TB8), a 2-chloro cinnamic acid derivative. Here, the hydroxamate warhead also chelates the catalytic zinc ion in favourable bidentate form. The flexible linker of the cinnamic acid allows the aromatic ring to take a position in which the chloro residue is pointing towards the lipophilic area formed by Phe21 and Tyr341 and the opposite side of the aromatic ring pointing towards the lipophilic area around Phe216. Phe151, the "gatekeeper" is in the "flipped-out" conformation leaving room for larger residues and Lys20 is oriented somewhat parallel to the catalytic canal. Since Lys20 is not interacting with the compound, it could as well take a conformation pointing away from the catalytic tunnel. This demonstrates the high flexibility of the amino acid residues at the rim of the binding pocket.

In **c** there is the same enzyme co-crystalized with **24x** (TB87). This compound is a bit more spatially demanding. It is a cinnamic acid compound with a 4-chloro phenyl thioether in position 2. Its hydroxamate coordinates the zinc ion as in case of the other hydroxamtes. Similar to the compound **22k** (TB8) in picture **b** carbon C5 and C6 of the aromatic ring of the cinnamic acid are oriented towards the lipophilic area made up by Phe216. The "gatekeeper" Phe151 is again taking the "flipped-out" conformation due to the ligand's spatial needs. In this case Lys20 is located close to the sulfur of the thioether substructure of **24x** (TB87). Even if thioethers are generally not observed as strong hydrogen bond acceptors there might be a weak electrostatic interaction between the sulfur and the protonated Lys20. The 4-chloro phenyl moiety is oriented towards the outside of the pocket yet situated in the lipophilic surface area made up by Phe21 and Tyr341.

Picture **d** shows the visualization of the binding pocket of *sm*HDAC8 co-crystalized with compound **24zg** (TB98), a cinnamic acid with a 2,6-chloro benzyloxy residue in position 2. The cinnamic acid portion of the ligand molecule is oriented in the catalytic pocket similar to the before described compound **24x** (TB87). Also Phe151 and Lys20, the two most flexible amino acid residues of the binding pocket are taking a similar position to the before described enzyme-ligand complexes. In the case of **24zg** (TB98) there is no specific interaction with Lys20. Although the ε-amino function of the lysine could just as well form an H-bond to the ether oxygen as it did to the thioether sulfur of **24x** (TB87), there is no

evidence of such. This does correlate with the IC_{50} values of these two compounds though which is approximately 440 nM for **24zg** (TB98) and approximately 180 nM for **24x** (TB87). The additional carbon atom between the cinnamic acid aromatic ring and the second aromatic ring forces the first ring to lean closer to the lipophilic surface area of Phe216 for the 2,6-chloro benzyloxy moiety still to be able to address the lipophilic area of Phe21 and Tyr341. This simply brings a greater distance between the Lys20 and the ether oxygen of the ligand so that there is no H-bond formed between the two.

4.1.3 Phenotypic testing

A selection of synthesized compounds have also been tested for their effects in a phenotypic assay (*ex vivo*). A few different aspects were investigated. Namely the effect of a compound on the viability of the adult parasites as well as their pairing behavior and also the effect of the compound on the viability of the juvenile stage of the schistosomes, the so called schistosomula.

Taking a closer look at the impairment of the parasitic viability is obvious whereas the pairing behavior of the adult parasites does not seem crucially important at first sight. Knowing that the female can lay eggs when paired with a male parasite and considering that many sickness causing effects of bilharzias disease is based on the immune systems reaction to the constant irritation of different tissues by the parasite's eggs, the paring behavior becomes an important parameter to investigate.

4.1.3.1 Testing of the effects on S. mansoni schistosomula

The compounds were analyzed towards their toxicity on juvenile *S. mansoni*, so called schistosomula. An Alamar-Blue based viability assay system was used for this evaluation. The compounds were tested at a concentration of 10 µM initially and selected compounds were tested again at 20 µM in order to determine possible dose dependency. The testing was carried out in triplicates on two biological replicates each. Praziquantel, the standard therapy for schistosomiasis and the selective HDAC8-inhibitor **PCI-34051** (IC_{50} on *sm*HDAC8 400 nM)[74] were used as a reference here. Results are listed in table 15 below.

Table 15 Viability of schistosomula treated with either 10 µM or 20 µM of the respective compound (n.d. – not determined).

Compounds	10 µM		20 µM	
	% viability	± SEM	% viability	± SEM
praziquantel	92	8	89	6
PCI-34051	71	1	62	4
22c (TB74)	92.9	4.0	n.d	n.d
24h (TB76)	77.0	0.4	n.d	n.d
24w (TB72)	92.1	1.8	n.d	n.d
24x (TB87)	24.6	4.4	2.5	1.8
24zd (TB93)	84.3	5.6	n.d	n.d
24ze (TB91)	69.7	0.1	39.8	6.3
24zf (TB92)	68.4	1.8	18.1	5.7
24zg (TB98)	53.0	4.0	11.4	1.7
24zj (TB75)	73.4	2.6	58.0	7.2
24zk (TB78)	73.5	0.5	51.8	9.1
26c (TB96)	94.4	3.3	n.d	n.d
26d (TB79)	89.8	2.4	n.d	n.d
26e (TB94)	80.7	2.5	n.d	n.d
26j (TB97)	86.5	3.1	n.d.	n.d.
26k (TB80)	81.8	0.3	n.d	n.d
28a (TB83)	93.3	11.6	n.d	n.d

Both references, praziquantel and **PCI-34051** do not show high toxicity against the schistosomula in this assay. For praziquantel it was known beforehand that it has low effects on the juvenile stage of *S. mansoni*[105]. For **PCI-34051** there is an approximate decrease in viability of 30 % at 10 µM but only an additional 10 % decrease at the doubled concentration.

Out of the tested substances **24x** (TB87) and **24zg** (TB98) show the best results. Not only do they show the greatest reduction of viable schistosomula at a concentration of 10 µM but also show definite dose-dependency. These two compounds that performed best in this assay were investigated further. Their IC_{50} values were determined using the same Alamar Blue® based assay with 6.5 µM for **24x** (TB87) and 11.8 µM for **24zg** (TB98) (figure 50).

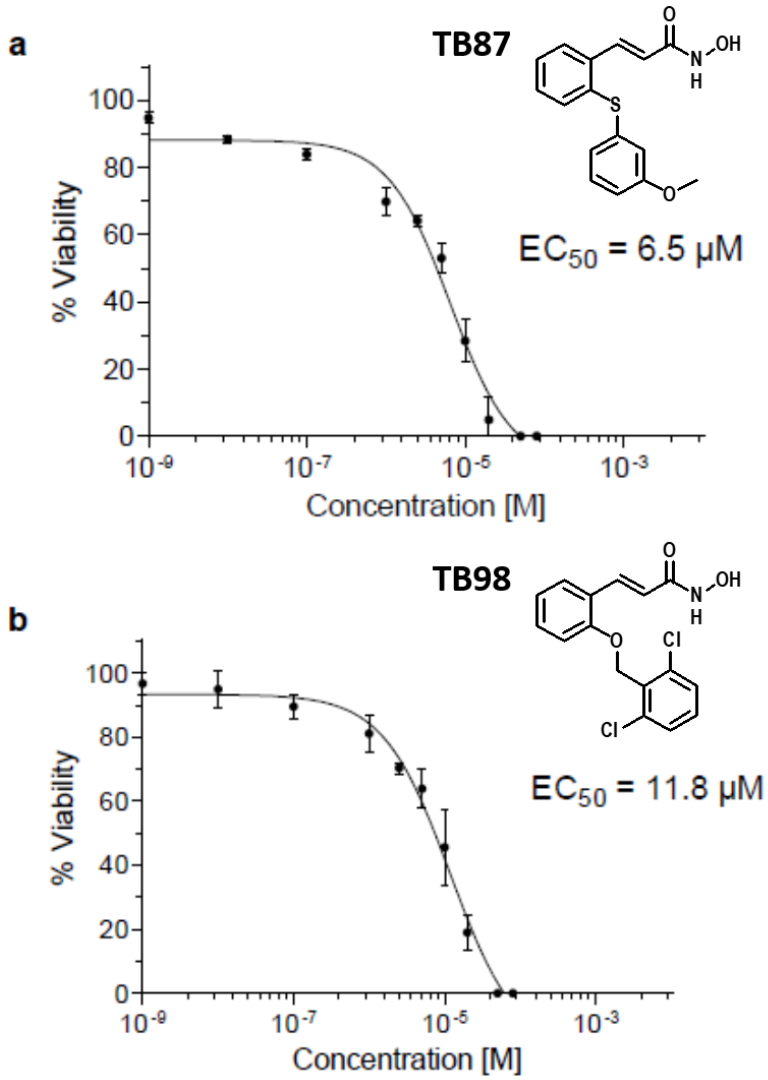

Figure 48 IC_{50} values of 24x (TB87) and 24zg (TB98) (provided by the working group of Raymond J. Pierce, University of Lille, CNRS, Inserm),

4.1.3.2 Pairing behavior

As mentioned in the introduction the adult schistosome worms pair up in couples; the shorter male embracing a longer female. Paired up like this the female lays several hundreds of eggs daily which leads to inflammatory and immuno reactions which lead to a series of symptoms[2,7,8]. Therefore the pairing behavior is also an interesting feature to observe in terms of disease and symptom control.

Two of the substances, **22j** (TB5), the 4-chloro benzothiophene derivative and **24b** (TB8), the 2-chloro cinnamic acid derivative have been tested for their influence on the adult parasite's viability. Also the compound **22b** (TB8) was tested for its behavior on the pairing behavior of adult schistosomes. Results are presented in figures 51 and 52 below.

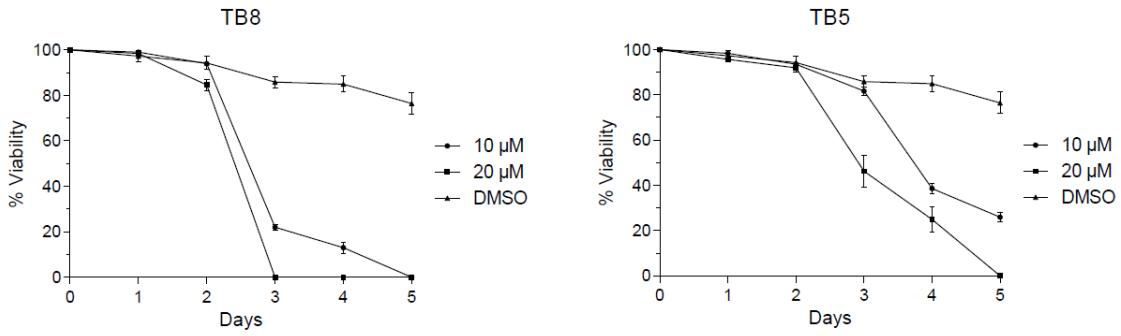

Figure 49 Results of adult schistosomes viability incubated with different concentrations of the respective compound over time.

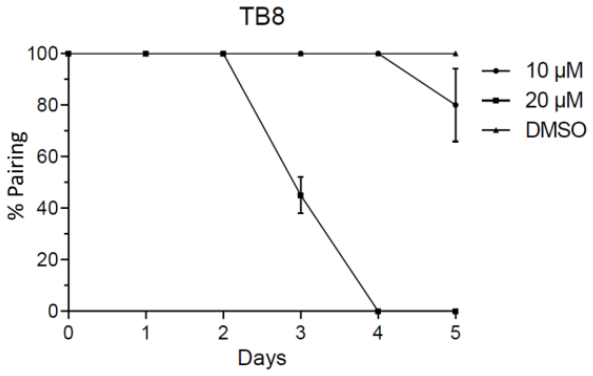

Figure 50 Results of the adult parasites' pairing behavior after treatment of different concentrations of the compound 24b (TB8) over time.

4.1.4 Selectivity between human HDAC isoforms

Although the human enzymes are not the desired target it is still important to know the compounds' effects on each of the human isoforms. The selectivity between the different HDAC isoforms helps to evaluate the possible side effects of a compound which could be used as a model substance for future drugs. Therefore, most of the compounds were also tested on the human zinc dependent histone deacetylases that are most expressed (*h*HDAC1, *h*HDAC6) or most similar to *sm*HDAC8 (*h*HDAC8). The compounds were tested in a ZMAL assay for the human isoforms and are presented in comparison to the results of the Fluor de Lys® assay results of the *sm*HDAC8 results. The both assay systems are described in chapter 4.1.1.

Table 16 Comparison of the results of the bicyclic compounds on the human HDAC isoforms 1, 6 and 8 and the schistosome HDAC8. The results are either presented as IC_{50} values or percent inhibition of the respective enzymes.

name	*h*HDAC1	*h*HDAC6	*h*HDAC8	*sm*HDAC8
indene derivative				
22d (TB2)	100 µM: 93.1% 10 µM: 81.4%	n.d.	100 µM 100.1% 10 µM 99.9%	100 µM: 99.8% 10 µM: 98.4%
indole / benzimidazole derivatives				
22a (TB1)	100 µM: 25 % 10 µM: 3.1%	n.d.	610 ± 80 nM	4.90 ± 1.1 µM
22b (TB13)	n.d.	n.d.	5 µM: 83.4% 0.5 µM: 43.7%	1.8 ± 0.8 µM
22c (TB74)	n.d.	n.d.	5 µM: 0 %	5 µM: 0 %
benzofuran derivatives				
22g (TB45)	n.d.	n.d.	640 ± 100 nM	2.1 ± 0.5 µM
22h (TB46)	n.d.	n.d.	380 ± 90 nM	n.d.
benzothiophene derivatives				
22i (TB4)	3.6 ± 0.4 µM	260 ± 50 nM	300 ± 100 nM	630 ± 100nM

name	*h*HDAC1	*h*HDAC6	*h*HDAC8	*sm*HDAC8
22j (TB5)	36 ± 0.4 µM	540 ± 100 nM	70 ± 20 nM	250 ± 20 nM

For **22d** (TB2), the indene derivative, the results on all of the three enzymes that were tested, do not greatly differ, however, it needs to be mentioned that the concentrations that were used are very high. For the indole derivatives **22a** (TB1) and **22b** (TB13) the results on the human HDAC8 are slightly better than the effects on the schistosome HDAC8. The unsubstituted indole derivative has an IC_{50} value on the human HDAC8 in the nanomolar range whereas the result on the schistosome enzyme is in the lower micromolar range. Both benzofuran derivatives **22g** (TB45) and **22h** (TB46) show good inhibitory activity on the human HDAC8, both with IC_{50} values in the nanomolar range. **22h** (TB45) was also tested on the schistosome enzyme, where the results are in the lower micromolar range. Both benzothiophenes, the unsubstituted **22i** (TB4) and the 4-chloro derivative **22j** (TB5) were tested on all of the different isoforms that are discussed here. Both have IC_{50} values in the nanomolar range for the schistosome enzyme. In comparison the results for the *h*HDAC1 are in the lower micromolar range for **22i** (TB4) and over 35 µM for **22j** (TB5). For the human HDAC6 and HDAC8 both compounds have IC_{50} values in the nanomolar range for **22i** (TB4) there is a preference for the both human enzymes and for **22j** (TB5) there is a preference for the *h*HDAC8.

Table 17 Comparison of the results of the cinnamic acid compounds with smaller residues on the human HDAC isoforms 1, 6 and 8 and the smHDAC8. The results are either presented as IC_{50} values or percent inhibition of the respective enzymes.

name	*h*HDAC1	*h*HDAC6	*h*HDAC8	*sm*HDAC8
cinnamic acid derivatives (smaller residues)				
24a (TB7)	n.d.	n.d.	5 µM: 83 % 0.5 µM: 44 %	130 ± 20 nM
24b (TB8)	2.2 ± 0.2 µM	100 ± 10 nM	54 ± 9 nM	60 ± 20 nM
24c (TB77)	n.d.	n.d.	5 µM: 82.8% 0.5 µM: 42.5%	5 µM: 78 % 0.5 µM: 43 %
24e (TB32)	9.1 ± 0.9 µM	140 ± 10 nM	175 ± 46 nM	210 ± 30 nM

name	*h*HDAC1	*h*HDAC6	*h*HDAC8	*sm*HDAC8
24f (TB51)	n.d.	0.7 ± 0.23 µM	330 ± 40 nM	0.5 µM: 50 %
24i (TB53)	n.d.	0.9 ± 0.1 µM	240 ± 30 nM	0.5 µM: 60 %
24j (TB54)	n.d.	0.9 ± 0.1 µM	1.1 ± 0.3 µM	0.5 µM: 45 %
24l (TB14)	1.5 ± 0.2 µM	33 ± 5 nM	194 ± 39 nM	60 ± 30 nM

The unsubstituted cinnamic acid derivative, **24a** (TB7) was tested for its effect on the human HDAC8 where pretests showed that the IC_{50} value could be expected roughly around 0.5 µM. The results for the meta-chloro cinnamic acid derivative **24c** (TB77) are very similar to those of **24a** (TB7). For the ortho-chloro derivative **24b** (TB8) there is a whole different picture. The compound is almost equally active on both the human and the *sm*HDAC8 with IC_{50} values around 50 nM. The compound also inhibits the human HDAC6 in very low concentrations (IC_{50} value around 100 nM). Only the inhibition of the human HDAC1 requires concentrations in the lower micromolar range which is a pattern that can be observed for most of the compounds that were tested here. The 2,6-bichloro substituted cinnamic acid derivative has an IC_{50}-value around 10 µM for the human HDAC1 and around 100 – 200 nM for all other tested enzymes. The compounds **24f** (TB51), **24i** (TB53) and **24j** (TB54) all have IC50 values around 1 µM for the human HDAC6 and around 300 nanomlar (**24f** (TB51) and **24i** (TB53)) or just over 1 µM (**24j** (TB54)). The para hydroxy cinnamic acid was tested to be very active on the human HDAC6 with an IC_{50} value of roughly 33 nM. The results for the human HDAC8 is approximately 200 nM and for the schistosome enzyme about 60 nM, whereas the IC_{50} value for the human HDAC1 is in the lower micromolar range.

Table 18 Comparison of the results of the cinnamic acid compounds with phenyloxy- or phenylthioether residues on the human HDAC isoforms 1, 6 and 8 and the schistosome HDAC8. The results are either presented as IC_{50} values or percent inhibition of the respective enzymes.

name	*h*HDAC1	*h*HDAC6	*h*HDAC8	*sm*HDAC8
cinnamic acid derivatives (phenyloxy- or phenylthioether residues)				
24t (TB57)	13.4 ± 2.4 µM	11.4 ± 2.5 µM	150 ± 30 nM	220 ± 10 nM

name	*h*HDAC1	*h*HDAC6	*h*HDAC8	*sm*HDAC8
24u (TB55)	11.5 ± 2.1 µM	6.1 ± 0.5 µM	80 ± 10 nM	90 ± 20 nM
24v (TB27)	n.d.	n.d.	60 ± 10 nM	250 ± 30 nM
name	*h*HDAC1	*h*HDAC6	*h*HDAC8	*sm*HDAC8
24w (TB72)	n.d.	0.30 ± 0.1 µM	3.1 ± 1.1 µM	5 µM: 80 % 0.5 µM: 44 %
24x (TB87)	20µM: 84 % 2µM: 35 %	20µM: 96 % 2µM: 65 %	180 ± 40 nM	180 ± 30 nM

The results of the phenyloxy- and phenylthioether substituted cinnamic acid derivatives are presented in table 18. Compounds **24t** (TB57) and **24u** (TB55) which only differ in the para substitution of the second aromatic ring one being a methoxy- and the other a chloro substitution. Both need concentrations in the micromolar range for the inhibition of human HDAC1 and HDAC6 and then they are approximately equally active on the both human and schistosome HDAC8 (IC_{50} values in the nanomolar range). Compound **24v** (TB27) is much more active on the human HDAC8 than the schistosome enzyme. And **24x** (TB87) has the same inhibitory pattern as the before described compounds **24t** (TB57) and **24u** (TB55); very high concentrations needed for the both human HDAC1 and HDAC6 and equally active on the human and schistosome HDAC8 in the nanomolar range.

Table 19 Comparison of the results of the cinnamic acid compounds with benzyloxy residues on the human HDAC isoforms 1, 6 and 8 and the schistosome HDAC8. The results are either presented as IC_{50} values or percent inhibition of the respective enzymes.

name	*h*HDAC1	*h*HDAC6	*h*HDAC8	*sm*HDAC8
cinnamic acid derivatives (benzyloxy residues)				
24z (TB64)	1.39 ± 0.18 µM	1.46 ± 0.12 µM	5 µM: 75 % 0.5 µM: 14 %	0.5 µM: 36 %
24za (TB12)	750 ± 30 nM	210 ± 30 nM	1.2 ± 0.1 µM	250 ± 40 nM
24zb (TB67)	n.d.	300 ± 50 nM	3.1 ± 1.1 µM	0.5 µM: 33 %

name	*h*HDAC1	*h*HDAC6	*h*HDAC8	*sm*HDAC8
24zc (TB38)	n.d.	680 ± 170 nM	2.1 ± 0.6 µM	490 ± 70 nM
24zd (TB93)	20 ± 4.3 µM	4.2 ± 0.7 µM	130 ± 10 nM	130 ± 20 nM
24zg (TB98)	20 ± 2.2 µM	6.1 ± 0.7 µM	470 ± 90 nM	440 ± 40 nM

Among the benzyloxy- substituted cinnamic acid derivatives there are the compounds **24z** (TB64), **24za** (TB12), **24zb** (TB67) and **24zc** (TB38) which interestingly need higher concentrations for the inhibition of the human HDAC8 compared to the schistosome enzyme. **24zd** (TB93) and **24zg** (TB98) follow the same pattern which was described before, with higher concentrations needed for the human HDAC1 and HDAC6 and lower concentrations for the human and schistosome HDAC8.

Table 20 Comparison of the results of the compounds with miscellaneous structures on the human HDAC isoforms 1, 6 and 8 and the schistosome HDAC8. The results are either presented as IC_{50} values or percent inhibition of the respective enzymes.

name	*h*HDAC1	*h*HDAC6	*h*HDAC8	*sm*HDAC8
miscellaneous strucures				
26e (TB94)	1.0 ± 0.2 µM	3.1 ± 0.9 µM	420 ± 50 nM	1.3 ± 0.3 µM
24zj (TB75)	n.d.	n.d.	5 µM: 78 % 0.5 µM: 43 %	n.d.
28a (TB83)	n.d.	n.d.	5 µM: 74 % 0.5 µM: 31 %	n.d.

The derivative **26e** (TB94) was tested to be most active on the human HDAC8 with an IC_{50} value of approximately 400 nM whereas the IC_{50} values for all other tested enzymes are in the lower micromolar range. For **24zj** (TB75) and **28a** (TB83) there are only pretest results for the human HDAC8, so there are no conclusions to be drawn from those.

The compounds were tested towards their activity on the human HDAC isoforms in comparison to their activity on the schistosome target enzyme. All of the compounds were designed to inhibit a zinc dependent histone deacetylase therefore it does not seem

surprising that they all are active on all of the tested enzymes to some extent. However, the goal was to create a compound which is able to discriminate against the human HDAC isoforms but which is active on *sm*HDAC8. For the herein tested compounds there was no compound that fulfilled this ideal, however many compounds showed good selectivity for *sm*HDAC8 compared to human HDAC1 and HDAC6. In contrast no selectivity was observed for *sm*HDAC8 compared to the human HDAC8.

4.1.5 Pharmacokinetic studies

Among the synthesized inhibitors two compounds (**24zh** (TB56) and **24x** (TB87)) were selected as first candidates for testing their pharmacokinetic effects. **24x** (TB87) was selected since it showed promising activity in the S. mansoni phenotypic assay and **24zh** (TB56) was selected since it was active against Trypanosoma cruzi (detailed in vitro results in Chaper 4.2).The testing was carried out by JOHAN SCHULZ (Kancera and Adlego, Sweden).

The mice were administered 50 mg/kg of the respective compound, two mice per os (p.o.) and two mice intra venous (i.v.). Blood samples were collected after 15 or 30, 60 and 180 minutes as well as a urine sample at the end of the time. The samples were analyzed towards their concentration of the respective compound and the results are presented in table 21 below.

Table 21 Plasma concentrations of mice which were administered 50 mg/kg of the respective compound p.o. versus i.v.

mouse ID	administration	time (min)	conc (µM)	mouse ID	administration	time (min)	conc (µM)
126	24zh (TB56) 50 mg/kg p.o.	30	1.97	130	24x (TB87) 50 mg/kg p.o.	30	2.30
		60	1.55			60	n.d.
		180	0.18			180	0.025
127	24zh (TB56) 50 mg/kg p.o.	30	6.3	131	24x (TB87) 50 mg/kg p.o.	30	3.28
		60	2.89			60	n.d.
		180	0.25			180	0.073
128	24zh (TB56) 50 mg/kg i.v.	15	81.5	132	24x (TB87) 50 mg/kg i.v.	15	93.5
		60	45.0			60	12.8
		180	0.90			180	0.23
129	24zh (TB56) 50 mg/kg i.v.	15	57.0	133	24x (TB87) 50 mg/kg i.v.	15	65.5
		60	27.9			60	2.78
		180	0.86			180	0.021

As shown in figures 53 and 54 the concentrations of each compound is highest at the first measuring point after 15 minutes after i.v. administration. The p.o. administration shows lower blood plasma concentrations in the range of 2-3 µM at the first measuring point after 30 minutes past administration. The plasma concentrations drop quickly and after three hours the concentrations are well below 1 µM.

The results show that the p.o. administration of **24x** (TB87) is not able to reach plasma concentrations above the EC_{50} value of the inhibitor (6.5 µM in the Alamar-blue assay) whereas the i.v. administration gave plasma concentrations above the EC_{50} value only at the first data points. Overall the pharmacokinetic properties of the hit compounds have to be improved before testing the smHDAC8 *in vivo*. Similar results were obtained for **24zh**/TB56.

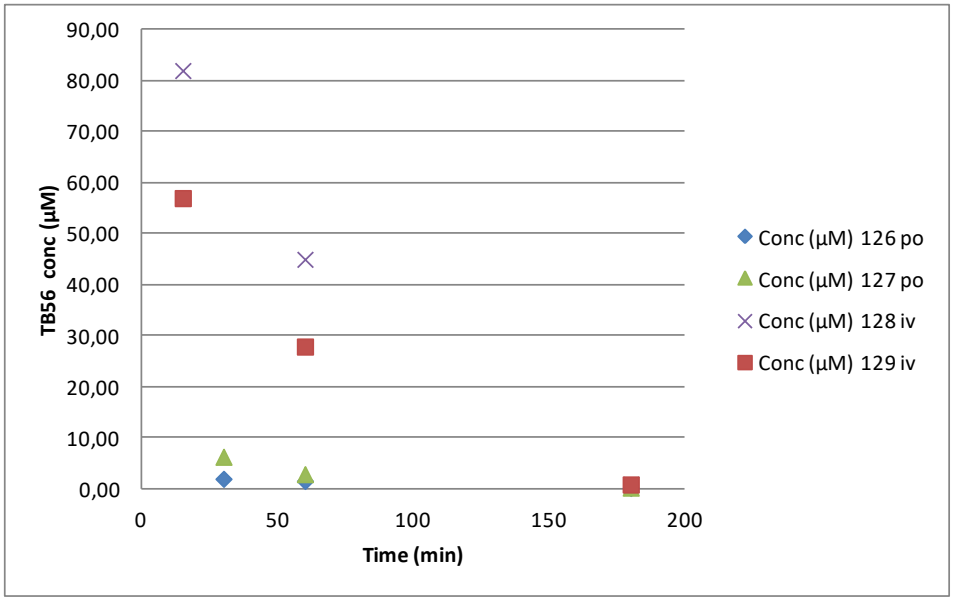

Figure 51 Compound 24zh (TB56) concentration vs time in mouse plasma samples after administration of 50 mg/kg 24zh (TB56) p.o. (mouse 126 and 127) or i.v. (mouse 128 and 129).

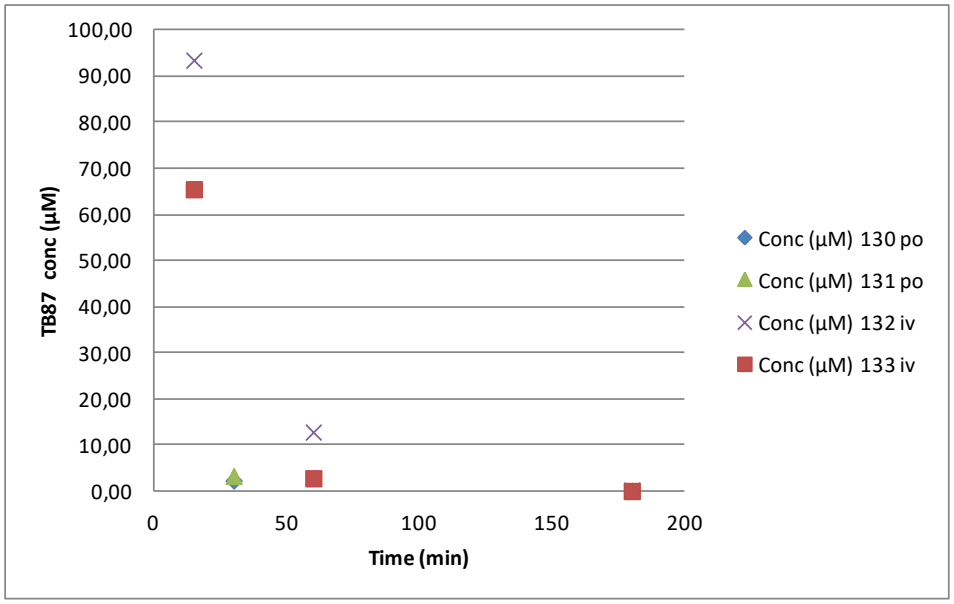

Figure 52 Compound 24x (TB87) concentration vs time in mouse plasma samples after administration of 50 mg/kg 24x (TB87) p.o. (mouse 130 and 131) or i.v. (mouse 132 and 133).

4.2 *Trypanosoma cuzi* / *Tc*DAC2

Another target of the current project was the parasite *T. cruzi*. This parasite expressed four different histone deacetylases named *tc*DAC1-4. Knock-out studies have shown the crucial effect of *tc*DAC1 and 2 for the parasite development. Knock-out of *tc*DAC2 on one allele shows parasites with slow proliferation and knock-out on two alleles produces unviable parasites[106,107].

All developed compounds were tested in a ZMTFAL assay (principle described in chapter 4.1.1) against recombinant *tc*DAC2 and the results are presented in the table below.

Table 22 Results of compounds tested on TcDAC2 in a ZMTFAL assay. Results highlighted in red shows no inhibition, those highlighted in yellow have IC_{50}-values lower than 5 µM, those in green less than 1 µM. Pretests are presented in % inhibition at the declared concentrations, IC_{50} values in the declared unit.

name	*tc*DAC2 pretest	*tc*DAC2 IC_{50}-value	name	*tc*DAC2 pretest	*tc*DAC2 IC_{50}-value
22a (TB1)	833 µM: 69 % 400 µM: 59 % 100 µM: 24 %	n.d.	24i (TB53)	16.67 µM: 87% 4.17 µM: 73 %	6.1 ± 0.44 µM
22d (TB2)	50 µM: 116 % 10 µM: 95 % 1µM: 48 %	0.89 ± 0.08µM	24j (TB54)	16.67 µM: 77% 4.17 µM: 55 %	5.61 ± 2.78 µM
22i (TB4)	50 µM: 110 % 10 µM: 55 % 1µM: 43 %	1.16 ± 0.13µM	24r (TB58)	16.67 µM: 54% 4.17 µM: 19 %	n.d.
22j (TB5)	16.67 µM: 2 % 4.17 µM: 10 %	n.d.	24t (TB57)	16.67 µM: 57% 4.17 µM: 29 %	n.d.
22h (TB46)	16.67 µM: 27 % 4.17 µM: 26 %	n.d.	24u (TB55)	16.67 µM: 73% 4.17 µM: 53 %	n.d.
22c (TB74)	25µM: -18 % 5µM: 2 %	n.d.	24v (TB27)	16.67 µM: 19% 4.17 µM: -10%	n.d.
24f (TB51)	16.67 µM: 88 % 4.17 µM: 75 %	4.1 ± 0.36 µM	24w (TB72)	25µM: 89 % 5µM: 82 %	n.d.
24h (TB76)	25µM: 82 % 5µM: 68 %	3.5 ± 0.6 µM	24x (TB87)	25µM: 9.3 % 5µM: 50.4 %	n.d.

name	*Tc*DAC2 pretest	*Tc*DAC2 IC_{50}-value	name	*Tc*DAC2 pretest	*Tc*DAC2 IC_{50}-value
24y (TB59)	16.67 µM: 56 % 4.17 µM: 29%	n.d.	24zi (TB73)	25µM: 76 % 5µM: 59 %	2.6 ± 0.5 µM
24z (TB64)	25µM: 94 % 5µM: 76	1.0 ± 0.3 µM	24zj (TB75)	25µM: 93 % 5µM: 63 %	0.82 ± 0.11 µM
24zb (TB67)	n.d.	0.73 ± 0.09 µM	24zk (TB78)	25µM: 91 % 5µM: 79 %	1.26 ± 0.12 µM
24zc (TB38)	n.d.	4.2 ± 1.3 µM	26a (TB89)	25µM: -0.5 % 5µM: 5.2 %	n.d.
24zd (TB93)	25µM: 33 % 5µM: 12 %	n.d.	26c (TB96)	25µM: -32 % 5µM: -23 %	n.d.
24ze (TB91)	25µM: 46 % 5µM: 15 %	n.d.	26d (TB79)	25µM: 45 % 5µM: 43 %	n.d.
24zf (TB92)	25µM: 51 % 5µM: 34 %	n.d.	26e (TB94)	25µM: 83 % 5µM: 65 %	3.3 ± 0.6 µM
24zg (TB98)	25µM: 69 % 5µM: 61 %	n.d.	26k (TB80)	25µM: 76 % 5µM: 50 %	4.9 ± 1.7 µM
24zh (TB56)	16.67 µM: 88 % 4.17 µM: 74 %	1.15 ± 0.22 µM			

In table 22 above the results of the *tc*DAC2 testing are presented. Results highlighted in yellow are those that have an IC_{50} value lower than 5 µM, those in green lower than 1 µM. Those substances that performed best on this target are **22d** (TB2), a fragment like bicyclic compound, an unsubstituted indene derivative, **24z** (TB64), the meta-benzyloxy cinnamic acid derivative, **24zb** (TB67) a meta-chloro para-benzyloxy cinnamic acid derivative and **24zj** (TB75), the annulated cinnamic acid derivative. Those results which are highlighted in yellow are also diverse in their structures. However **24zk** (TB78) is also an annulated cinnamic acid derivative like **24zj** (TB75). Compound **22i** (TB4), an unsubstituted bicyclic (benzothiophene) derivative is also a small, fragment-like compound just as **22d** (TB2) which was mentioned before. The two compounds **24zh** (TB56) and **24zi** (TB73) are analogues of each other, **24zh** (TB56) is a dibenzofuran and **24zi** (TB73) is the sulfur

analogue, a dibenzothiophene derivative. In addition **26e** (TB94) which is a 2,5-dichloro(phenylthio)acetic acid derivative showed good inhibition.

So far there is no crystal structure available for *tc*DAC2 however there is a homology model (see figure 55) developed by Dr. Melesina (AG Sippl) which reveals that the binding pocket of *tc*DAC2 is most similar to that one of *sm*HDAC8[108]. This could be an explanation why the substances that were originally designed as inhibitors of the smHDAC8 are also effective against *tc*DAC2.

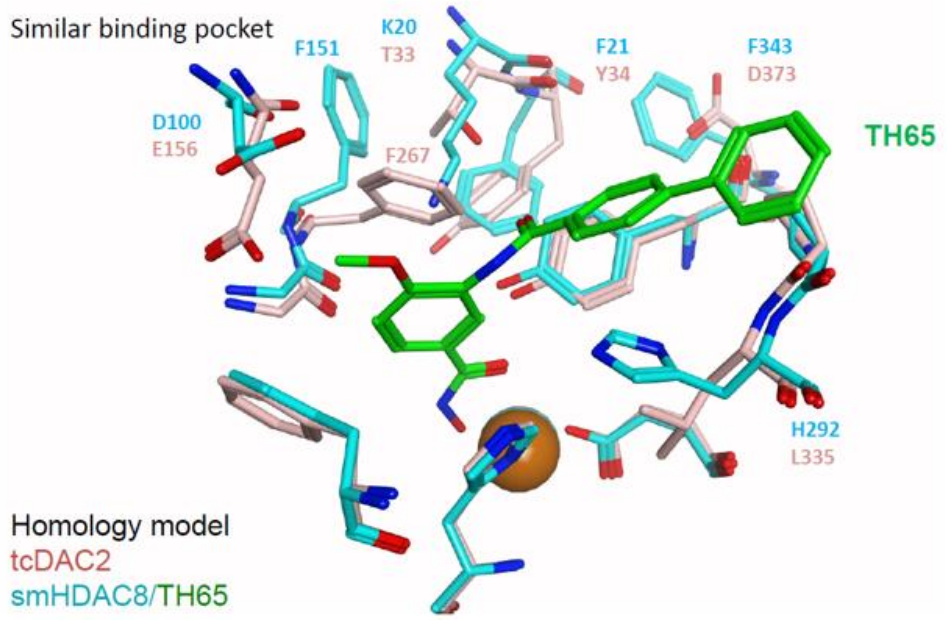

Figure 53 Homology model of tcDAC2 binding pocket in superposition with the crystal structure of smHDAC8 co-crystalized with the compound TH65[73,76,108].

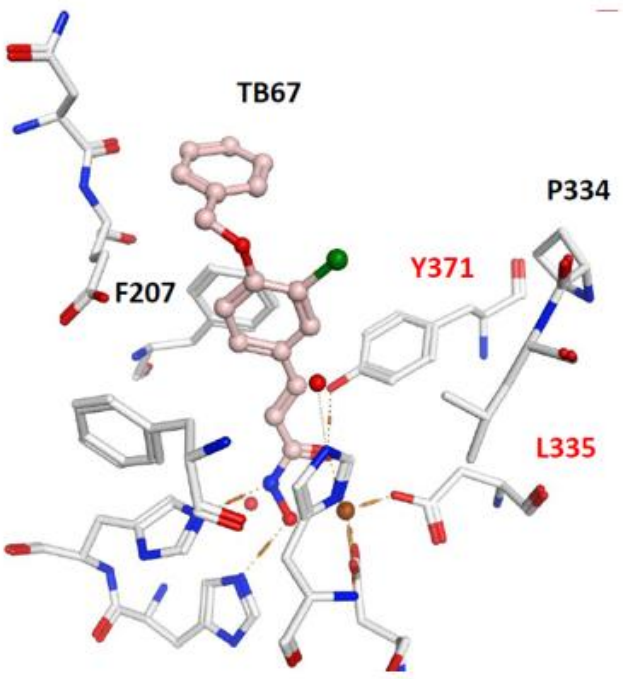

Figure 54 Docking solution of 24zb (TB67) in the binding pocket of TcDAC2[108].

Due to the high structural similarity, *sm*HDAC8 was used as template, here shown with the cocrystallized inhibitior TH65. In figure 56 we can see that the inhibitor **24zb** (TB67) which was one of the better performing compounds in the *tc*DAC2 assay testing is adopting a linear conformation. These are important information for future structural optimization of *tc*DAC2 inhibitors.

4.3 *T.cruzi* phenotypic data

4.3.1 Activity over amastigote and trypomastigotes forms of T. cruzi

To determine the activity of the selected compounds towards *T. cruzi* amastigotes and trypomastigotes a β-galactosidase based assay was performed. The β-galactosidase transfected Tulahuen strain of *T.cruzi* was used to infect L929 cells. For the infection of the cells they were exposed to the 10-fold number of β-galactosidase transfected Tulahuen trypomastigotes for two hours then the cells were incubated at 37°C for two days in order for the infection to develop. Afterwards the infected cells were incubated with different concentrations of the respective compound for four days. The toxicity of the compounds towards the L929 cells was determined in an Alamar Blue® assay[109]. Benznidazole was used as a reference drug in this assay. The results are presented in table 23 below.

Table 23 [a]Inhibition of amastigotes and trypomastigotes growth under the action of the different concentrations of compound; [b]Compound concentration that inhibits 50% of the growth of the amastigotes and trypomastigotes; [c]Compound concentration that inhibits 50% of the L929 cell viability; [d]IC_{50} cell/IC_{50} parasite. IC_{50} values were calculated by linear interpolation. [¥]This concentration promotes 100% of death of L929 cells.

name	concentration (μM)	activity (%)[a]	IC_{50}[b] (μM)	Toxicity[c] (μM)	selectivity index[d]
24f (TB51)	80 40 20 10 5	L929 cell death[¥] 96 84 67 12	8.4	40	4.8
24i (TB53)	80 40 20 10 5	L929 cell death[¥] 98 85 35 15	13	20	1.5
24j (TB54)	80 40 20 10	77 81 39 0	25.2	40	1.6
24t (TB57)	80 40 20 10	93 93 91 0	15.5	125	8.1
24u (TB55)	80 40 20 10 5	92 93 70 28 0	15.2	84.4	5.6
24y (TB59)	80 40 20	82 55 0	38.2	132.2	3.5
24zb (TB67)	10 5	L929 cell death[¥] 42	> 5	< 10	< 2

name	concentration (µM)	activity (%)[1]	IC_{50}[2] (µM)	toxicity[3] (µM)	selectivity index[4]
24zh (TB56)	80 40 20 10 5	76 86 87 83 9	7.8	40	5.1
24zi (TB73)	40 20 10 5	L929 cell death[¥] 84 67 37	7.2	30	4.2
Benz-nidazole	3.81	-	3.81	2,381	625

Looking at the results presented in table 23 it can be observed that all of the compounds show some sort of activity against trypomastigotes and amastigotes of the Tulahuen strain of *T.cruzi*. The compound **24y** (TB59) has an IC_{50} value of close to 40 µM which could be considered inactive. The other nine compounds have IC_{50} values in a lower micromolar range. The compound **24zb** (TB67) shows toxicity towards the L929 cells at a concentration of 10µM. Out of the tested compounds six (**24f** (TB51), **24i** (TB53), **24j** (TB54), **24y** (TB59), **24zb** (TB67) and **24zi** (TB73)) are poorly selective with a selectivity index (SI) of < 5. Among those compounds that were tested there are also three that showed moderate selectivity (SI between 5 and 20). Compounds **24u** (TB55) and **24zh** (TB56) both have a selectivity index of just over five and **24t** (TB57) just over eight.

Looking at the IC_{50} values the herein tested compounds are in the lower two digit or even single digit micromolar range just like the reference drug benznidazole. However comparing the results focusing on the selectivity the superiority of benznidazole comes to show. Benznidazole has a selectivity index in this assay setting of 625 whereas the best substance out of the tested batch reaches an SI value of just over eight. Literature suggests substances with a selectivity index greater than 50 for in vivo testing and further investigation[65,109].

4.4 Plasmodium falciparum

The compounds were further tested on two different strains of *P.falciparum* one being Dd2 and the other one 3D7. The two strains differ in their resistance to a certain standard anti-malaria medication *P.facliparum* Dd2 is resistant to chloroquine whereas *P.falciparum* 3D7 is chloroquine sensitive. The compounds were tested in a *P.falciparum* in vitro growth inhibition with chloroquine as a reference[110,111]. Results were provided by the groups of JAMAL KHALIFE, Lille, France and KATHY ANDREWS, Queensland, Australia. Since no recombinant HDAC from *P. falciparum* is available in vitro testing was not possible.

Table 24 Results of P.falciparum testing. Prestests were conducted at 10 µM in triplicate wells; IC_{50} value determination was performed in n = 2-4.

name	*P.falciparum* Dd2 IC_{50} µM	*P.falciparum* 3D7 IC_{50} µM	name	*P.falciparum* Dd2 IC_{50} µM	*P.falciparum* 3D7 IC_{50} µM
22i (TB4)	13.57 ± 0.78	0.85 ± 0.02	24j (TB54)	n.d.	10 µM: 89 ± 5 %
22j (TB5)	16.7 ± 4.06	5.66 ± 1.25	24k (TB15)	9.15 ± 4.59	5.49 ± 0.189
24a (TB7)	9.3 ± 3.9	2.07 ± 0.59	24n (TB16)	4.07 ± 1.4	2.78 ±0.399
24b (TB8)	2.47 ± 0.4	1.31 ± 0.18	24o (TB31)	16.75 ± 4.88	10 µM: 93 ± 1 %
24d (TB9)	4.03 ± 1.1	2.67 ± 0.28	24r (TB58)	n.d.	10 µM: 76 ± 10 %
24f (TB51)	n.d.	10 µM: 101 ± 4 %	24s (TB11)	10 µM: -12.9 ± 7.5 %	10 µM: 23 ± 16%
24g (TB10)	6.67 ± 0.75	1.48 ± 0.057	24t (TB57)	n.d.	10 µM: 96 ± 1 %
24h (TB76)	2.9 ± 0.56	n.d.	24u (TB55)	n.d.	10 µM: 96 %
24i (TB53)	n.d.	10 µM: 95 ± 4 %	24v (TB27)	3.43 ± 1.33	1.64 ± 0.17

name	*P.falciparum* Dd2 IC_{50} in µM	*P.falciparum* 3D7 IC_{50} in µM	name	*P.falciparum* Dd2 IC_{50} in µM	*P.falciparum* 3D7 IC_{50} in µM
24w (TB72)	14.57 ± 0.81	n.d.	24zi (TB73)	1.3 ± 0.27	n.d.
24x (TB87)	6.3 ± 2.66	n.d.	24zj (TB75)	6.77 ± 1.11	n.d.
24y (TB59)	n.d.	10 µM: 95 ± 1%	24zk (TB78)	4.85 ± 2.08	n.d.
24za (TB12)	2.93 ± 1.63	1.55 ± 0.10	26c (TB96)	28.17 ± 3.4	n.d.
24zb (TB67)	n.d.	10 µM: 99 ± 1%	26d (TB79)	22.53 ± 12	n.d.
24zd (TB93)	5.9 ± 3.97	n.d.	26e (TB94)	2.57 ± 0.35	n.d.
24ze (TB91)	2.33 ± 0.59	n.d.	26k (TB80)	7.1 ± 2.2	n.d.
24zf (TB92)	3.4 ± 0.79	n.d.	28a (TB83)	0.73 ± 0.23	n.d.
24zh (TB56)	n.d.	0.99 ± 0.61			

The compounds with IC_{50} values lower than 1 µM are highlighted in green, those between 1 and 2 µM are highlighted in yellow. The substances **24b** (TB8) and **24za** (TB12) have IC_{50} values between 1 and 2 µM on the chloroquine sensitive strain *P.falciparum* 3D7 and **22j** (TB4) and **24zh** (TB56) have values of less than 1 µM. There is quite a structural variety between the different compounds that performed better at this assay. The compounds **24zi** (TB73) and **28a** (TB83) are the ones that performed best on the chloroquine resistant strain *P.falciparum* Dd2 which are again structurally different from each other and from the other compounds which performed best on the other strain. However **24zh** (TB56) and **24zi** (TB73) are analogues of each other. **24zh** (TB56) is a dibenzofurane derivative and **24zi** (TB73) is the sulfur analogue, a dibenzothiophene derivative. Interestingly the both

substances perform well in the growth inhibition assay but on different strains. Compound **24zh** (TB56) performs well on the chloroquine resistant strain and **24zi** (TB73) performs well on the chloroquine sensitive strain. Knowing that the compounds which are designed as inhibitors of zinc dependent deacetylases, can inhibit both, the chloroquine resistant and sensitive strains of *P.falciparum* indicates that the compounds most likely have a different mechanism of action than chloroquine. From the inhibitor structures it is likely that the inhibit one of the plasmodial HDAC. In the literature *Pf*HDAC1 is discussed as putative target of hydroxamic acid derivatives[63,110–112]. This would then explain the results that were obtained here. Further cellular tests, e.g. measuring the hyperacetylation level of plasmodial histones, have to be carried out to confirm this hypothesis.

4.5 Toxicity assays

In order to determine general toxicity or *"off-target"*- effects against human cells the compounds were tested for their effects on different human cell lines as well as bacteria and yeast cells. This data was provided by FRANK ERDMANN, Institute of Pharmacy, Martin-Luther-University, Halle, Germany. For estimation the general toxicity of the compounds the human cell line HEK293 was used.

4.5.1 Toxicity assay against human cell lines

The compounds were tested in an Alamar Blue® viability assay system which determines the metabolic activity of cells. The assay principle is explained in detail in chapter 4.1.1. The different cells were incubated with the respective compound solutions at a concentration of 50 µM for 45 hours. Then the metabolic activity was determined via fluorescence measuring in comparison to standard solutions.

Table 25 Results of HEK293 human epitheliak kidney cells viability testing. The compounds were tested in singles where there is no standard deviation given or triplicates when there is a standard deviation. Entries are highlighted in red in case there is a viability of less than 10 % of the cells, those highlighted in yellow show a viability of less than 30 % but more than 10 %.

compound	HEK 293 % viability at 50 µM	compound	HEK293 % viability at 50 µM	compound	HEK293 % viability at 50 µM
22a (TB1)	n.d.	24d (TB9)	110 ± 1.1	24q (TB43)	93 ± 3.1
22b (TB13)	104 ± 2.2	24e (TB32)	79 ± 2.3	24r (TB58)	75 ± 3.2
22c (TB74)	86 ± 0	24f (TB51)	79 ± 1.1	24s (TB11)	103 ± 1.4
22d (TB2)	n.d.	24g (TB10)	110 ± 1.3	24t (TB57)	72 ± 0.8
22e (TB3)	n.d.	24h (TB76)	86 ± 1	24u (TB55)	75 ± 3.3
22f (TB42)	64 ± 5.7	24i (TB53)	78 ± 2.2	24v (TB27)	90 ± ± 1.7
22g (TB45)	12 ± 1.9	24j (TB54)	80 ± 0.4	24w (TB72)	77 ± 2
22h (TB46)	38 ± 4.7	24k (TB15)	107 ± 1.1	24x (TB87)	64 ± 3
22i (TB4)	n.d.	24l (TB14)	n.d.	24y (TB59)	77 ± 1.2
22j (TB5)	90 ± 1.4	24m (TB33)	111 ± 6.5	24z (TB64)	n.d.
24a (TB7)	100 ± 1.5	24n (TB16)	100 ± 2.7	24za (TB12)	113 ± 2.3
24b (TB8)	97 ± 4.0	24o (TB31)	89 ± 2.4	24zb (TB67)	81 ± 1.9
24c (TB77)	n.d.	24p (TB44)	94 ± 3.0	24zc (TB38)	85 ± 5.6

compound	HEK 293 % viability at 50 µM	compound	HEK293 % viability at 50 µM	compound	HEK293 % viability at 50 µM
24zd (TB93)	78 ± 1	24zk (TB78)	80 ± 3	26e(TB94)	75 ± 9
24ze (TB91)	80 ± 3	24zp (TB37)	86 ±3.7	26i (TB90)	n.d.
24zf (TB92)	79 ± 2	24zq (TB40)	97 ± 3.3	26j (TB97)	n.d.
24zg (TB98)	n.d.	26a (TB89)	93 ± 2	26k (TB80)	85 ± 6
24zh (TB56)	81 ± 0.3	26b (TB88)	n.d.	26g (TB104)	n.d.
24zi (TB73)	87 ± 2	26c (TB96)	87 ± 6	28a (TB83)	97 ± 5
24zj (TB75)	79 ± 2	26d (TB79)	101 ± 2		

For the HEK293 cells there is only one compound which reduces the viability of the cells to below 30 %. Looking at the structure of **22g** (TB45) there is no explanation for this phenomenon. The compound **22g** (TB45) differs in only one methylene group to compound **22h** (TB46). Also **22f** (TB42) is structurally related but neither of the other two compound show such a great impact on the human epithelial kidney cells used in this assay.

5 Summary and Outlook

5.1 Summary

This work was part of the FP7 project A-ParaDDisE which aimed to identify new therapeutic options for neglected tropical diseases including malaria, trypanosomiasis and schistosomiasis. Having the infrastructure of this A-ParaDDisE project allowed to obtain results quickly and adjust the direction to focus on. It also combined the advantages of different research disciplines such as chemical synthesis and characterization of small molecules, crystallographic studies, computational studies, biological assay development and even pharmacokinetic studies which are difficult to gather otherwise at academia.

The starting point of this work was the screening hit **J1075** which showed dose dependent mortality in schistosomes and inhibition of the *sm*HDAC8 in the lower micromolar range. The goal was to find new molecules that would inhibit the identified target of *Schistosoma mansoni* (*sm*HDAC8) with no or minimal off-target effects and also the identification of targets for the other three parasitic diseases and the respective molecules that would inhibit those (ideally also without off-target effects).

Throughout this work many small molecule hydroxamic acids were synthesized and characterized. The synthesis was at first focused on structures that are related to the hit **J1075** but as work proceeded synthetic aims changed depending on the incoming results of biological assay results and computational studies.

Within this work a series of small molecule hydroxamic acids were synthesized and characterized and additionally a small series phenothiazine derivatives have been synthesized to the stage of a carboxylic acid that were not transformed into hydroxamic acids. Synthetic routes were altered and optimized in order to obtain sufficient amounts of the desired product within the least amount of time at sufficient purities.

Out of these compounds most were tested towards their inhibitory activity on the *sm*HDAC8. Almost all of them showed some activity, some even in the sub-micromolar range.

Throughout this work a total of four compounds, **22j** (TB5), **24b** (TB8), **24x** (TB87) and **24zg** (TB98) could be cocrystallized with the *sm*HDAC8 and the crystal structured were resolved to give closer insights to the interactions between the respective inhibitor and the target protein. This in combination with computational studies built a solid base for the further direction of synthesis. The crystal structures of the four ligand-enzyme complexes

also served as a good base for structure-activity-relationship evaluations of the other compounds that were tested in enzymatic assays but were not co-crystalized with the enzyme.

Furthermore 17 of the compounds were tested against schistosomula *ex vivo* and evaluated towards their effect on the schistosomula viability. Two compounds, **24x** (TB87) and **24zg** (TB98) were identified to have good and dose dependent impacts on the viability of the schistosomula.

Since the pairing is an important feature in the lifecycle and reproductive ability of the schistosomes two compounds were also tested towards their ability to inhibit the pairing behavior of the male and female parasites. Parasite pairs treated compounds, **22k** (TB5) and **24b** (TB8) showed dose and time dependent unpairing which causes the loss of ability to lay eggs which themselves cause some of the disease's symptoms and of course which eventually result in a new generation of parasites. Therefore the unpairing is also a desired effect.

Moreover two of the compounds, **24zh** (TB56) and **24x** (TB87) were tested in pharmacokinetic mouse studies. This gave insight to the compounds' distribution in the organism and also revealed that the chosen compounds were not immediately toxic for the mice (tested at 50 mg/kg).

Most of the compounds were also tested towards their effects on the main human histone deacetylases, *h*HDAC1, *h*HDAC6 and *h*HDAC8 to estimate possible off-target effects. The results of these assays lead to the conclusion that most of the compounds with a good inhibitory potency on the schistosome target do not affect the human to an extreme extent.

In order to clarify the general toxicity of the compounds, they were evaluated in Alamar Blue® assays towards their effects on the viability of different human cell lines. The great majority of the compounds did not affect the viability of the HEK 293 cells at a concentration of 50 µM.

Since the project did not only focus on the one parasitic disease the compounds were also tested for their effects on other parasites.

For *T. cruzi* a possible target (*tc*DAC2) has been identified via knock-out studies. The *tc*DAC2 has proven to be an essential target to address in order to inhibit cell differentiation growth and viability. Out of the compounds a number of 33 were tested towards their effects against *tc*DAC2. Among those 33 tested compounds nine were identified with IC_{50} values

of around 1µM and out of those nine there are three in the sub-micromolar range. Also ten substances were tested for their effects on trypomastigotes and amastigotes infected L929 cells. Herein nine of the substances were found to be active and also six of them slightly and three of them even moderately selective towards the parasites over the host cells.

For *Plasmodium falciparum* the compounds were tested in a full parasite assay on two different strains, one *P.f.* Dd2 being chloroquine resistant and *P.f.* 3D7 being chloroquine sensitive. The results from these assays show a rather diverse situation. However, some of the compounds proved to have good inhibitory effects one strain and some on the other. This at least leads to the conclusion that the postulated target *Pf*HDAC1 might be an attractive target to kill the parasite.

In order to rule out general toxicity the compounds were also tested for their toxicity towards *E.coli* bacteria and *S. cerevisiae* yeast cells (data not shown; see appendix for details). The tested compound showed no effect on either bacteria or yeast cells. This is another indication that the *sm*HDAC8 inhibitors do not show general toxicity.

5.2 Outlook

The knowledge of this work can be applied for further synthesis and characterization of new small molecules as epigenetic modulators. The solved crystal structures in combination with the results from computational studies can be used for specific and directed design and synthesis of new inhibitors. The TB-series of small molecule hydroxamic acids has proven to be a good starting point for addressing *tc*DAC2 as a potential target in tackling trypanosomiasis. Also this work delivers a few good starting points in addressing malaria from an epigenetic point of view.

6 Experimental part

6.1 Materials and Methods

6.1.1 Chemicals

The chemicals were purchased from *Carbolution Chemicals St. Ingbert*, *abcr GmbH Karlsruhe* or *Sigma Aldrich Darmstadt.* All chemicals that are not explicitly mentioned were taken from the chemical issuing counter of the Pharmaceutical Faculty of the Martin-Luther-University Halle Wittenberg.

6.1.2 Treatment of the Solvents

All of the solvents that were used have been dried according to protocols from literature[79].

Chloroform	Refluxing over phosphorus pentoxide for at least 2 h and afterwards distilling
Diethylether	Pre-drying over potassium hydroxide, drying over molecular sieve 4 Å
Dimethylformamide	Fractionated distillation after addition of toluene and water
Heptane	Refluxing over potassium hydroxide for 1 h and distilling afterwards
Methanol	Storing over metallic magnesia flakes for several hours, afterwards refluxing for two hours and finally distilling
Pyridine	Storing over potassium hydroxide for 1 week afterwards distillation through a fractionating column
Tetrahydrofurane	Refluxing over metallic sodium until a dark blue coloring of the indicator benzophenone stays constant, subsequently distillation
Toluene	Refluxing over metallic sodium until a dark blue coloring of the indicator benzophenone stays constant, subsequently distillation

6.1.3 Chromatography

Thin layer chromatography:

The thin layer chromatography (further referred to as TLC) was used to observe the progress of a reaction, to estimate purity of reaction products and final compounds as well as characterization by determining the R_f-values and the chromatographical characteristics of the compounds. For the TLC silica gel 60 F_{254} aluminum sheets 5x7.5 cm and TLC silica gel 60 F_{254} aluminum sheets 20x20 cm that were cut to size of the manufacturer *Merck KgaA* have been used. The substance had been dissolved in an adequate solvent or was taken directly from the reaction mixture and applied to the TLC aluminum sheet with a glass capillary. The TLC sheet is placed into a TLC chamber which is saturated with the mobile phase and developed.

The following mobile phases (MP) were used:

MP 1: chloroform / methanol; 80/20

MP 2: chloroform / methanol; 90/10

MP 3: chloroform

MP 4: chloroform / methanol; 80/20, 0.25 % trimethylamine

MP 4: chloroform / methanol; 80/20, 0.25 % formic acid

Detection methods

The detection of the TLC sheets via UV light at the wave length 254 nm (short wave UV light) or 366 nm (long wave UV light) was used in all cases. The method is based on the deletion of fluorescence of the silica sheet or on a substance's own fluorescence.

Secondly sheets with an expected THP-protected intermediate of a hydroxamic acid or a hydroxamic acid were dipped in a 3 % $FeCl_3$ solution and in case of the expected THP-protected intermediate heated up to approximately 70 °C to give a reddish purple or bluish purple stain of the substances.

Column chromatography:

Silica gel 60 (0.063 – 0.200 mm) from the manufacturer *Merck KgaA* was used as a stationary phase. As mobile phases, either chloroform with a methanol gradient and an addition of 0.25 % formic acid was used or the column was pre conditioned with chloroform and 0.5 % triethyl amine which in this case has also been the mobile phase. The

columns were dry packed with a silica gel/substance ratio of 10 – 30:1. For the detection of the substances in the different fractions TLC was used.

MPLC:

The MPLC (*medium pressure liquid chromatography*) was utilized for a more thorough purification of compounds that after the first column chromatography had purities of less than 95 %. As a stationary phase silica gel 60 (0,040 - 0,063 mm) from the manufacturer *Merck* was used. The filling of the columns was performed with the aid of a *Cartriger C-670*. The elution solvent was mixed and pumped through the column via two pumps (both *Pump Module C-601)* and the *Pump Manager C-615*. The fractions were collected by a *FractionCollector C-660*. All equipment mentioned above was acquired from the manufacturer *Büchi*. The eluent was also Chloroform with 0.25 % formic acid and a methanol gradient. For the detection of the product a *UV-Monitor C-630* was used as well as TLC.

HPLC:

The determination of the purities was performed by HPLC. The HPLC consists of an XTerra RP18 column (3.5 µm 3.9 x 100 mm) form the manufacturer *Waters (Milford, MA, USA)* two LC-10AD pump, a SPD-M10A VP PDA detector, and a SIL-HT auto sampler all from the manufacturer *Shimadzu (Kyoto, Japan).* The mobile phase was in all cases a gradient of methanol/water (starting at 95 % water going to 5 % water). The water is mixed with 0.1 % TFA.

6.1.4 NMR-Spectroscopy

The recording of the ^{1}H-NMR - spectra was performed with the *Gemini 2000* from the manufacturer *Varian*. The spectra were recorded at 400 MHz. The solvent that was used for the recording of the spectra is Hexadeuterodimethyl sulfoxide, also known as DMSO-d_6.The solvent was coevally used as the internal standard for the spectra.

The chemical shift δ is expressed in ppm and is set at the axis of symmetry of the separate peaks. In case of a multiplet the range of the chemical shift is indicated. The signals of ^{1}H-NMR spectra are specified in the following manner: (multiplicity, coupling constant J in Hz, number of protons, assigned proton(s)).

The following abbreviations were used for the multiplicities: s (singlet), d (doublet), t (triplet), dd (doublet of doublet), m (multiplet).

6.1.5 Mass spectrometry

6.1.5.1 Electron spray mass spectrometry (ESI-MS)

The samples were dissolved in an eligible solvent and injected via a pump Harvard Apparatus 22 (20 µl min^{-1}). The ionization is performed via electron spray technique at 5 kV in positive and negative mode. The spectra were recorded by the Finnigan LCQ-Classic mass spectrometer of the manufacturer Thermo Electron (Egelsbach, Germany). It has a heatable capillary (220 °C) and a flow rate of 20 µl/min.

6.1.5.2 High resolution mass spectrometry (HR-MS)

For proof of identity of the final compounds they were characterized by high resolution mass spectrometry. The samples were dissolved in a mixture of chloroform and methanol (variable mixture of the two solvents) and ionized via a Proxeon-Nano-ESI-source of the manufacturer Thermo Fisher Scientific (Bremen, Germany) at 1.3 kV. The spectra were recorded by the LTQ-Orbitrap-XL-mass spectrometer of the manufacturer Thermo Fisher Scientific (Bremen, Germany).

6.2 Computer based studies

6.2.1 Docking

The docking was performed as described in literature[52]: The resolved crystal structure of *sm*HDAC8 with 13c (chain B), *h*HDAC8 (PDB ID: 2V5X), *h*DAC6 (PDB ID: 5EDU), and *h*HDAC1 (PDB ID: 4BKX) were downloaded from the Protein Data Bank (PDB; www.rcsb.org)[113]. Protein preparation was done using Schrödinger's Protein Preparation Wizard[114] by adding hydrogen atoms, assigning protonation states, and minimizing the protein. Ligands were prepared in MOE[104] from smiles in neutral form. The ligands were subsequently prepared for docking using the LigPrep tool[115] as implemented in Schrödinger's software and energy minimized using the OPLS force field. Conformers of the prepared ligands were calculated with ConfGen using the default settings (Fast) and allowing minimization of the output conformations. Molecular docking was performed using the program Glide[116] in the Standard Precision mode. In *sm*HDAC8 and *h*HDAC8, two conserved water molecules were included in the protein models, corresponding to HOH 2061 and 2152 in the *h*HDAC8 X-ray structure (PDB ID: 2V5X).

6.3 Synthesis of the structures

6.3.1 Synthesis of indene carboxylic acid 2 (TB2s)

1 eq indene is mixed together with 0.5 eq and stirred 90 °C on an oil bath. After the reaction time of five hours the batch is cooled to room temperature, dissolved in ethyl acetate and extracted with an aqueous saturated potassium carbonate solution three times. The aqueous phases are combined, acidified with concentrated hydrochloric acid and extracted with ethyl acetate. The solvent is evaporated under reduced pressure to result in a white powder.

2 (TB2S) 1*H*-indene-2-carboxylic acid

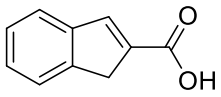

Appearance:	white powder
Yield:	27 %
Mw:	160.05 g/mol
m/z:	159.15 [M-H^+]

^{1}H NMR (400 MHz, DMSO-d6) δ 12.45 (s, 1H, COO**H**), 7.68 (s, 1H, H3), 7.59 (dd, *J* = 5.2, 3.4 Hz, 1H, H4), 7.56 – 7.52 (m, 1H, H5), 7.36 – 7.32 (m, 2H, H6, H7), 3.63 (d, *J* = 1.6 Hz, 2H, H1, H1')

6.3.2 General procedure for the benzofurane derivatives

1 mmol of the respective salicylaldehyde was dissolved in acetonitrile. One equivalent methyl bromoacetate and K_2CO_3 were added. The mixture was stirred at room temperature at first, then heated to 50°C for 30 minutes. The solvent was evaporated under reduced pressure and the crude product was re-dissolved in EtOAc and then washed with brine three times. The resulting methyl ester was dissolved in equal amounts of MeOH and H_2O with a catalytic amount of K_2CO_3. This mixture was stirred at room temperature overnight, the reaction batch was acidified using HCl and extracted with ethyl acetate. The solvent was evaporated under reduced pressure.

6.3.3 General procedure for the benzothiophene derivative

1 mmol 2,6-di-chlorobenzaldehyde was dissolved in DMF with 1 equivalent methyl thioglycolate and 1 equivalent K_2CO_3. The batch was heated at 60°C for 4-5 h. The mixture was filtered to eliminate the solid K_2CO_3 and the solvent was evaporated under reduced pressure. Toluene was added and evaporated three times to extract residual DMF. The mixture was re-dissolved in $CHCl_3$ and extracted with brine three times, the organic phases were combined and evaporated. The mixture was re-dissolved in MeOH, a catalytic amount of NaOH (1M) was added and the batch was stirred at RT for 16 h. The sol- vent was

evaporated under reduced pressure and the mixture re-dissolved in $CHCl_3$ and extracted with a 1m sodium carbonate solution three times. The aqueous phases are combined and concentrated, HCl was added until the solution reached pH 1–2, and then the solution was extracted with $CHCl_3$ three times. The organic phases were combined and evaporated under reduced pressure.

6.3.4 General procedure for the cinnamic acid derivatives

1.5 mmol of the respective aldehyde and 1.8 mmol of malonic acid were dis- solved in 600 mL pyridine and 20 mL piperidine. The mixture was heated in a water bath to ~80°C and stirred for 4 h. After that, ice and concentrated HCl were added. In most cases, a pale precipitate was formed and the reaction mixture was left in the refrigerator overnight for complete crystallization. The obtained carboxylic acids were filtered under suction and dried under reduced pressure.

General procedure of the *N*-alkylation of phenothiazine derivatives: 2 mmol of the respective phenothiazine derivative was dissolved in dried DMF one equivalent of either ethyl-(4-bromo) chrotonate or methyl- (4-bromomethyl-) benzoate and one equivalent of solid KOH were added. The reaction was conducted in a microwave oven suitable for organic synthesis in a closed vessel at 150°C for 5 minutes. After cooling down the reaction batch was mixed with water and filtrated. The aqueous phase was acidified and filtrated again. The precipitate is the carboxylic acid derivative which was used for further synthesis.

The following carboxylic acids were purified via column chromatography (purity controlled by thin layer chromatography only). The structures were either analyzed by mass spectrometry (ESI-MS) (m/z always refers to the isotope of highest abundance) and thin layer chromatography and then were used for direct transformation into further derivatives or they were directly used for further transformation without analysis.

name	structure	ESI-MS m / z
8a (TB3s) 1-benzofuran-2-carboxylic acid	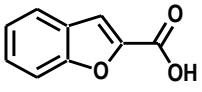	161.88 [$M+H^+$]
8b (TB41s) 7-chloro-1-benzofuran-2-carboxylic acid	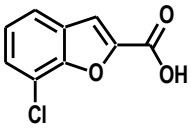	195.39 [$M-H^+$]

name	structure	ESI-MS m / z
8c (TB42s) 4-chloro-1-benzofuran-2-carboxylic acid	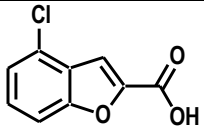	195.40 [M-H$^+$]
11a (TB5s) 4-chloro-1-benzothiophene-2-carboxylic acid	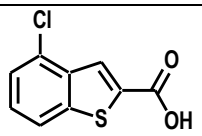	210.98 [M-H$^+$]
13a (TB7s) (2*E*)-3-phenylprop-2-enoic acid	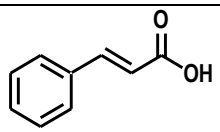	147.10 [M-H$^+$]
13b (TB8s) (2*E*)-3-(2-chlorophenyl)prop-2-enoic acid	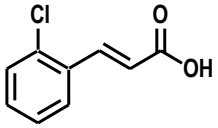	181.11 [M-H$^+$]
13c (TB9s) (2*E*)-3-(4-chlorophenyl)prop-2-enoic acid	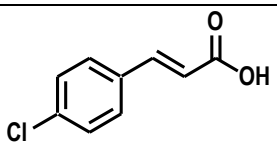	181.08 [M-H$^+$]
13d (TB10s) (2*E*)-3-(4-bromophenyl)prop-2-enoic acid	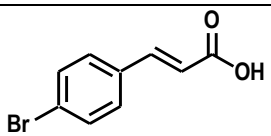	227.05 [M-H$^+$]
13e (TB11s) (2*E*)-3-(3,4,5-trimethoxyphenyl)prop-2-enoic acid	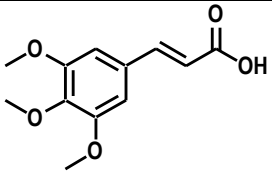	237.12 [M-H$^+$]
13f (TB12s) (2*E*)-3-[4-(benzyloxy)phenyl]prop-2-enoic acid	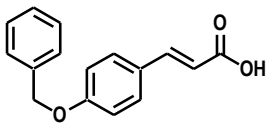	253.18 [M-H$^+$]
13g (TB14s) (2*E*)-3-(4-hydroxyphenyl)prop-2-enoic acid	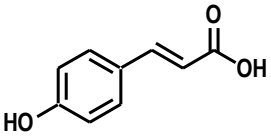	n.d.
13h (TB15s) (2*E*)-3-[4-(dimethylamino)phenyl]prop-2-enoic acid	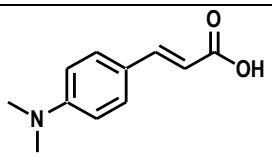	192.06 [M+H$^+$]
13i (TB16s) (2*E*)-3-(3-ethoxy-4-hydroxyphenyl)prop-2-enoic acid	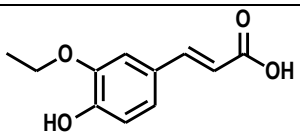	207.18 [M-H$^+$]

name	structure	ESI-MS m / z
13j (TB27s) (2*E*)-3-[2-(3-methoxyphenoxy)phenyl]prop-2-enoic acid	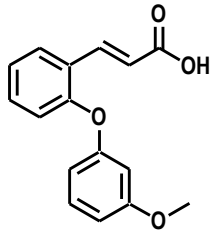	269.19 [M-H$^+$]
13k (TB31s) (2*E*)-3-[4-methoxyphenyl]prop-2-enoic acid	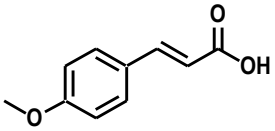	178.92 [M+H$^+$]
13l (TB32s) (2*E*)-3-(2,6-dichlorophenyl)prop-2-enoic acid	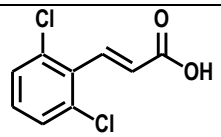	215.15 [M-H$^+$]
13m (TB33s) (2*E*)-3-(3-methoxy-4-hydroxyphenyl)prop-2-enoic acid	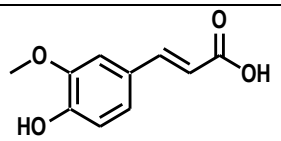	193.14 [M-H$^+$]
13n (TB38s) (2*E*)-3-[4-(benzyloxy)-3-methoxyphenyl]prop-2-enoic acid	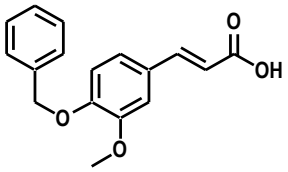	n.d.
13o (TB51s) (2*E*)-3-(2,4-dichlorophenyl)prop-2-enoic acid	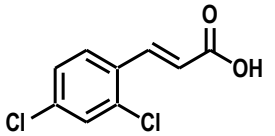	215.48 [M-H$^+$]
13p (TB53s) (2*E*)-3-(2-bromo-5-fluorophenyl)prop-2-enoic acid	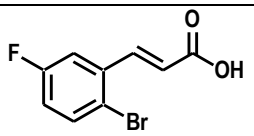	243.27 [M-H$^+$]
13q (TB54s) (2*E*)-3-(2-fluoro-5-methoxyphenyl)prop-2-enoic acid	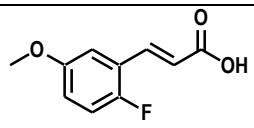	195.40 [M-H$^+$]
13r (TB55s) (2*E*)-3-[2-(4-methoxyphenoxy)phenyl]prop-2-enoic acid	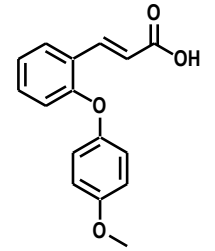	269.25 [M-H$^+$]

name	structure	ESI-MS m / z
13s (TB56s) (2*E*)-3-(dibenzo[*b*,*d*]furan-4-yl)prop-2-enoic acid	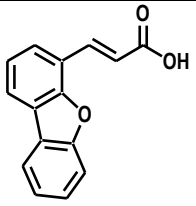	237.16 [M-H$^+$]
13u (TB57s) (2*E*)-3-[2-(4-chlorophenoxy)phenyl]prop-2-enoic acid	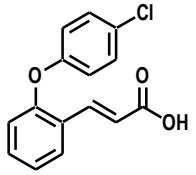	273.17 [M-H$^+$]
13v (TB58s) (2*E*)-3-(2-ethoxyphenyl)prop-2-enoic acid	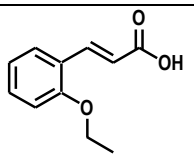	191.23 [M-H$^+$]
13w (TB59s) (2*E*)-3-[2-(benzyloxy)phenyl]prop-2-enoic acid	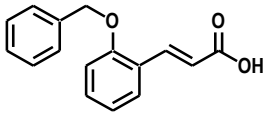	n.d.
13x (TB61s) (2*E*)-3-(4-methoxynaphthalen-1-yl)prop-2-enoic acid	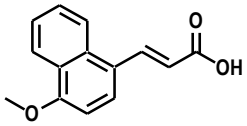	227.23 [M-H$^+$]
13y (TB62s) (2*E*)-3-(2-methoxynaphthalen-1-yl)prop-2-enoic acid	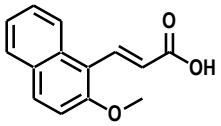	227.60 [M-H$^+$]
13z (TB63s) (2*E*)-3-(2-ethoxynaphthalen-1-yl)prop-2-enoic acid	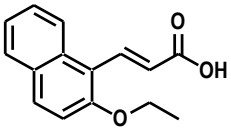	241.22 [M-H$^+$]
13za (TB64s) (2*E*)-3-[3-(benzyloxy)phenyl]prop-2-enoic acid	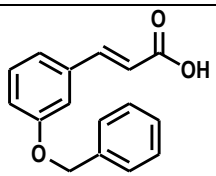	253.22 [M-H$^+$]
13zb (TB67s) (2*E*)-3-[4-(benzyloxy)-3-chlorophenyl]prop-2-enoic acid	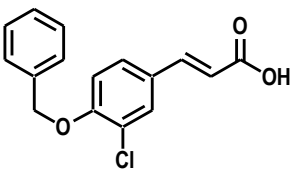	287.17 [M-H$^+$]

name	structure	ESI-MS m / z
13zc (TB72s) (2*E*)-3-(3-phenoxyphenyl)prop-2-enoic acid	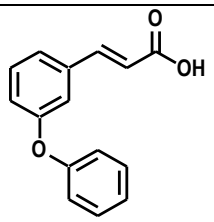	239.25 [M-H$^+$]
13zd (TB73s) (2*E*)-3-(dibenzo[*b*,*d*]thiophene-4-yl)prop-2-enoic acid	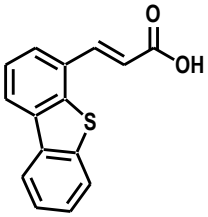	253.55 [M-H$^+$]
13ze (TB77s) (2*E*)-3-(3-chlorophenyl)prop-2-enoic acid	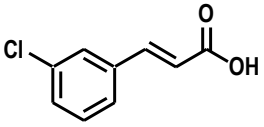	181.31 [M-H$^+$]
13zf (TB87s) (2*E*)-3-{2-[(4-chlorophenyl)sulfanyl]phenyl}prop-2-enoic acid	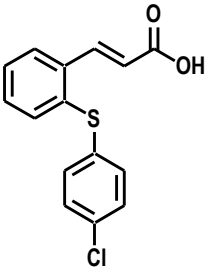	289.16 [M-H$^+$]
13zg (TB91s) (2*E*)-3-{2-[(4-chlorophenyl)methoxy]phenyl}prop-2-enoic acid	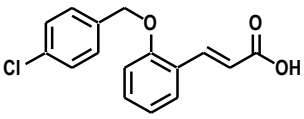	287.15 [M-H$^+$]
13zh (TB92s) (2*E*)-3-{2-[(2,4-dichlorophenyl)methoxy]phenyl}prop-2-enoic acid	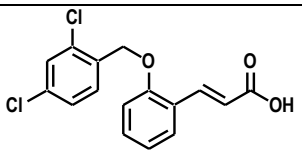	321.15 [M-H$^+$]
13zi (TB93s) (2*E*)-3-[2-(benzyloxy)-6-methoxyphenyl]prop-2-enoic acid	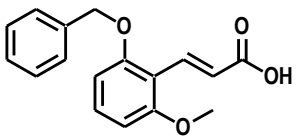	283.21 [M-H$^+$]
13zj (TB98s) (2*E*)-3-{2-[(2,6-dichlorophenyl)methoxy]phenyl}prop-2-enoic acid	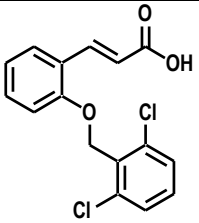	321.56 [M-H$^+$]

name	structure	ESI-MS m / z
13zk (TB106s) (2*E*)-3-{2-[4-(benzyloxy)phenoxy]phenyl}prop-2-enoic acid	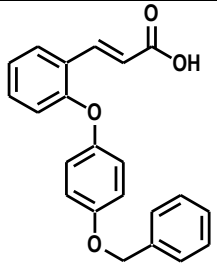	n.d.
13zl (TB107s) (2*E*)-3-[2-(4-fluorophenoxy)phenyl]prop-2-enoic acid	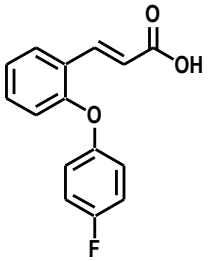	n.d.
20a (TB48s) 4-[(5,5-dioxo-5λ^6-phenothiazin-10(5*H*)-yl)methyl]benzoic acid	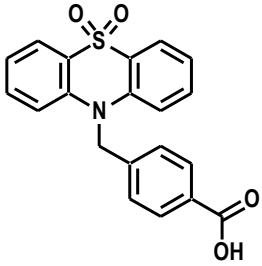	364.33 [M-H$^+$]
20b (TB84s) 4-[(2-chloro-5,5-dioxo-5λ^6-phenothiazin-10(5*H*)-yl)methyl]benzoic acid	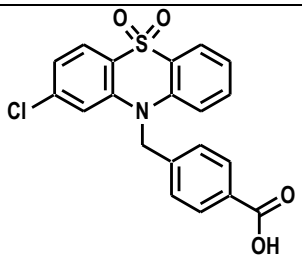	398.42 [M-H$^+$]
20c (TB50s) 4-[(5-oxo-5λ^4-phenothiazin-10(5*H*)-yl)methyl]benzoic acid	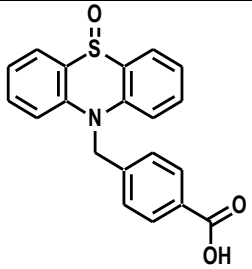	348.48 [M-H$^+$]
20d (TB85s) 4-[(5-oxo-5λ^4-phenothiazin-10(5*H*)-yl)methyl]benzoic acid	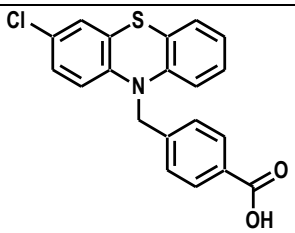	366.42 [M-H$^+$]

name	structure	ESI-MS m / z
20e (TB82s) 4-[(10*H*-phenothiazin-10-yl)methyl]benzoic acid	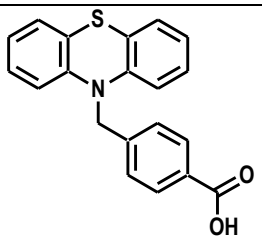	333.39 [M+H$^+$]
20f (TB86s) 4-[(3-methoxy-10*H*-phenothiazin-10-yl)methyl]benzoic acid	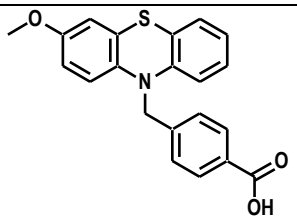	362.35 [M-H$^+$]
(TB83s) 4-[(2-chloro-5-oxo-5λ^4-phenothiazin-10(5*H*)-yl)methyl]benzoic acid	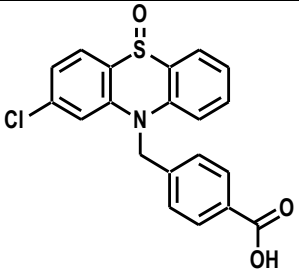	382.14 [M-H$^+$]
19a (TB81s) (2*E*)-4-(10*H*-phenothiazin-10-yl)but-2-enoic acid	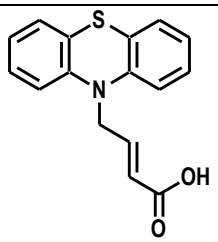	282.52 [M-H$^+$]

6.3.5 General procedure for the formation of the THP-protected intermediate

The carboxylic acids were dissolved in dry THF and 1.2 equivalent of PyBOP®, 1.5 equivalents of *O*-(tetrahydro-*2H*-pyran-2-yl)hydroxylamine and 2.5 equivalents of *N,N*-diisopropylethylamine (DIPEA) were added. The reaction mixture was stirred at room temperature and the progression of the reaction was observed by TLC. The THP-protected intermediate was purified by column chromatography; the mobile phase being $CHCl_3$ with 0.25% triethylamine (TEA) and the stationary phase being silica (previously washed with the mobile phase).

The THP-protected intermediates were characterized by mass spectrometry (m/z always refers to the isotope with the highest abundance) or used directly without characterization for the last synthetic step.

name	structure	ESI-MS m / z
22a' (TB1THP) *N*-[(oxan-2-yl)oxy]-1*H*-indole-2-carboxamide	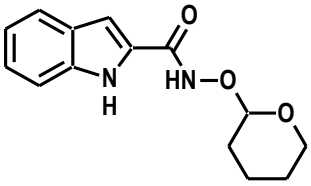	259.24 [M-H$^+$]
22b' (TB13THP) 5-methoxy-*N*-[(oxan-2-yl)oxy]-1*H*-indole-2-carboxamide	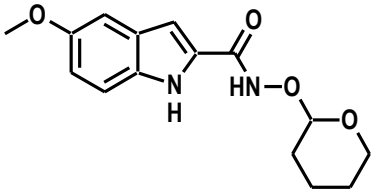	289.27 [M-H$^+$]
22c' (TB74THP) *N*-[(oxan-2-yl)oxy]-1*H*-benzimidazole-2-carboxamide	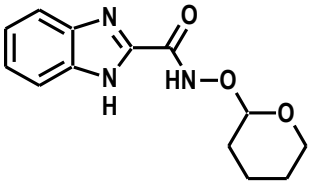	n.d.
22d' (TB2THP) *N*-[(oxan-2-yl)oxy]-1*H*-indene-2-carboxamide	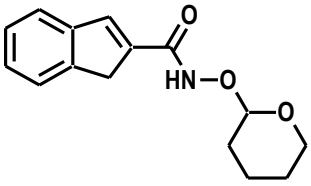	n.d.
22e' (TB3THP) *N*-[(oxan-2-yl)oxy]-1-benzofuran-2-carboxamide	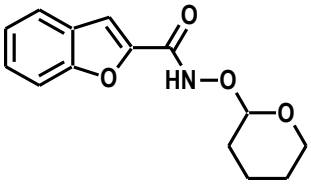	n.d.
22f' (TB42THP) 4-chloro-*N*-[(oxan-2-yl)oxy]-1-benzofuran-2-carboxamide	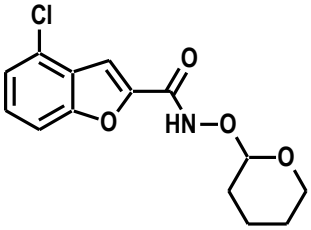	294.21 [M-H$^+$]
22g' (TB45THP) 7-methoxy-*N*-[(oxan-2-yl)oxy]-1-benzofuran-2-carboxamide	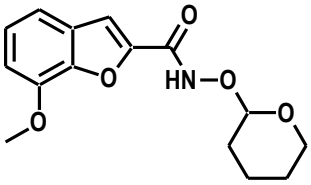	290.28 [M-H$^+$]

name	structure	ESI-MS m / z
22h' (TB46THP) 7-ethoxy-*N*-[(oxan-2-yl)oxy]-1-benzofuran-2-carboxamide	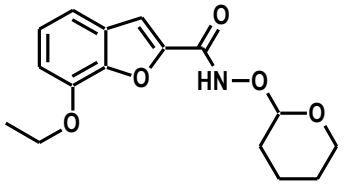	304.22 [M+H$^+$]
22i' (TB4THP) *N*-[(oxan-2-yl)oxy]-1-benzothiophene-2-carboxamide	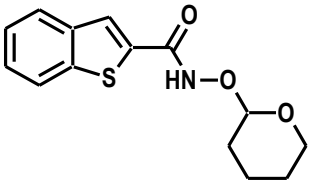	276.22 [M-H$^+$]
22j' (TB5THP) 4-chloro-*N*-[(oxan-2-yl)oxy]-1-benzothiophene-2-carboxamide	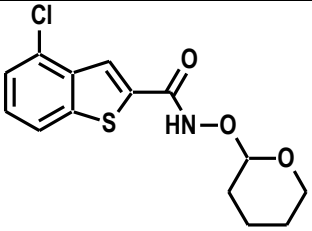	310.25 [M-H$^+$]
24a' (TB7THP) (2*E*)-*N*-[(oxan-2-yl)oxy]-3-phenylprop-2-enamide	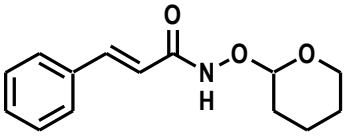	246.24 [M-H$^+$]
24b' (TB8THP) (2*E*)-3-(2-chlorophenyl)-*N*-[(oxan-2-yl)oxy]prop-2-enamide	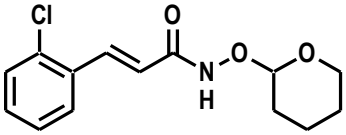	n.d.
24c' (TB77THP) (2*E*)-3-(3-chlorophenyl)-*N*-[(oxan-2-yl)oxy]prop-2-enamide	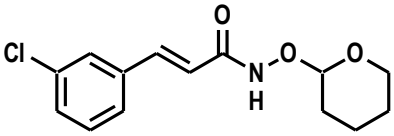	280.23 [M-H$^+$]
24d' (TB9THP) (2*E*)-3-(4-chlorophenyl)-*N*-[(oxan-2-yl)oxy]prop-2-enamide	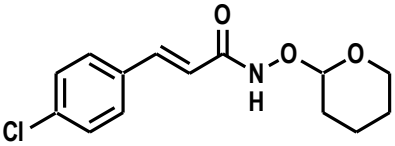	280.17 [M-H$^+$]
24e' (TB32THP) (2*E*)-3-(2,6-dichlorophenyl)-*N*-[(oxan-2-yl)oxy]prop-2-enamide	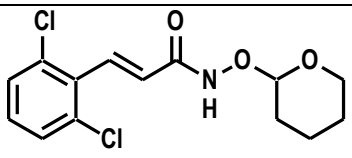	n.d.

name	structure	ESI-MS m / z
24f' (TB51THP) (2*E*)-3-(2,4-dichlorophenyl)-*N*-[(oxan-2-yl)oxy]prop-2-enamide	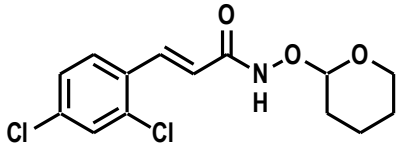	340.15 [M-H$^+$]
24g' (TB10THP) (2*E*)-3-(4-bromophenyl)-*N*-[(oxan-2-yl)oxy]prop-2-enamide	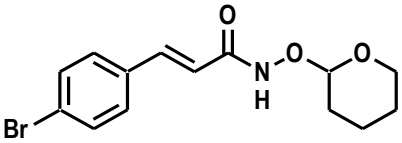	325,14 [M-H$^+$]
24h' (TB76THP) (2*E*)-3-(2-bromophenyl)-*N*-[(oxan-2-yl)oxy]prop-2-enamide	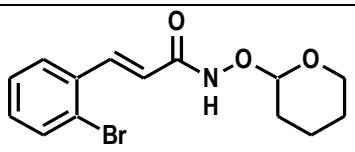	324.44 [M-H$^+$]
24i' (TB53THP) (2*E*)-3-(2-bromo-5-fluorophenyl)-*N*-[(oxan-2-yl)oxy]prop-2-enamide	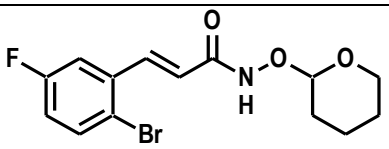	342.29 [M-H$^+$]
24j' (TB54TP) (2*E*)-3-(2-fluoro-5-methoxyphenyl)-*N*-[(oxan-2-yl)oxy]prop-2-enamide	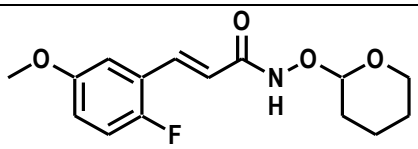	n.d.
24k' (TB15THP) (2*E*)-3-[4-(dimethylamino)phenyl]-*N*-[(oxan-2-yl)oxy]prop-2-enamide	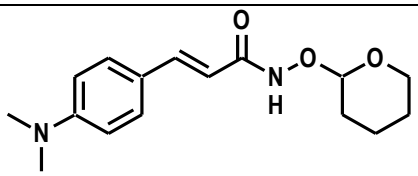	289.19 [M-H$^+$]
24l' (TB14THP) (2*E*)-3-(4-hydroxyphenyl)-*N*-[(oxan-2-yl)oxy]prop-2-enamide	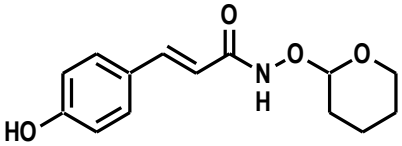	262.18 [M-H$^+$]
24m' (TB33THP) (2*E*)-3-(3-methoxy-4-hydroxyphenyl)-*N*-[(oxan-2-yl)oxy]prop-2-enamide	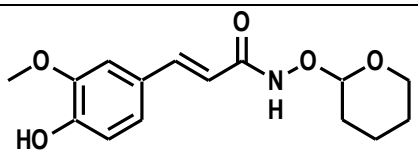	292.24 [M-H$^+$].
24n' (TB16THP) (2*E*)-3-(3-ethoxy-4-hydroxyphenyl)-*N*-[(oxan-2-yl)oxy]prop-2-enamide	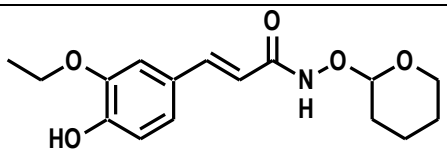	306.21 [M-H$^+$]
24o' (TB31THP) (2*E*)-3-(4-methoxyphenyl)-*N*-[(oxan-2-yl)oxy]prop-2-enamide	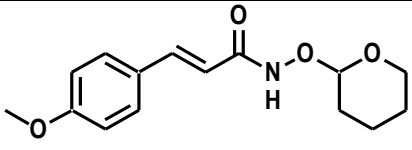	276.19 [M-H$^+$]

name	structure	ESI-MS m / z
24p' (TB44THP) (2*E*)-3-(3-methoxyphenyl)-*N*-[(oxan-2-yl)oxy]prop-2-enamide	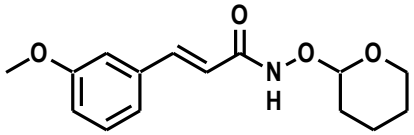	n.d.
24q' (TB43THP) (2*E*)-3-(4-ethoxyphenyl)-*N*-[(oxan-2-yl)oxy]prop-2-enamide	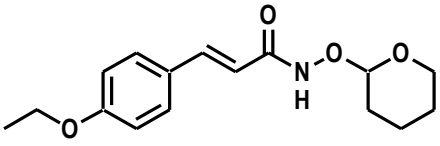	291.14 [M-H$^+$]
24r' (TB58THP) (2*E*)-3-(2-ethoxyphenyl)-*N*-[(oxan-2-yl)oxy]prop-2-enamide	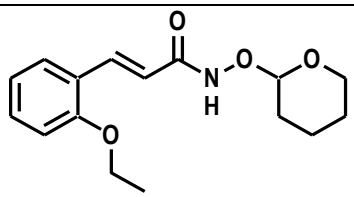	290.78 [M-H$^+$]
24s' (TB11THP) (2*E*)-*N*-[(oxan-2-yl)oxy]-3-(3,4,5-trimethoxyphenyl)prop-2-enamide	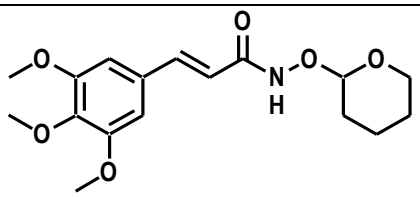	291.14 [M-H$^+$]
24t' (TB57THP) (2*E*)-3-[2-(4-chloroxyphenoxy)phenyl]-*N*-[(oxan-2-yl)oxy]prop-2-enamide	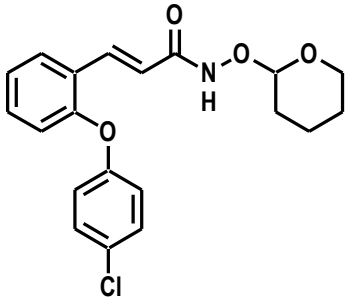	372.29 [M-H$^+$]
24u' (TB55THP) (2*E*)-3-[2-(4-methoxyphenoxy)phenyl]-*N*-[(oxan-2-yl)oxy]prop-2-enamide	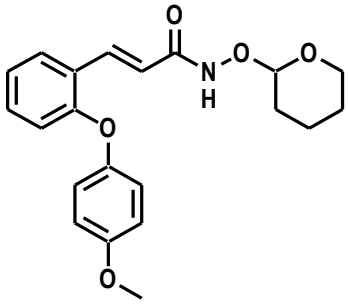	368.25 [M-H$^+$]
24v' (TB27THP) (2*E*)-3-[2-(3-methoxyphenoxy)phenyl]-*N*-[(oxan-2-yl)oxy]prop-2-enamide	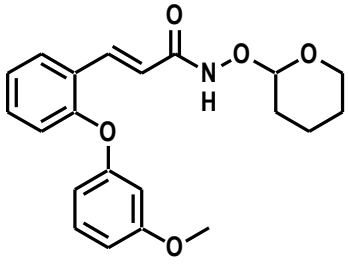	368.22 [M-H$^+$]

name	structure	ESI-MS m / z
24w' (TB72THP) (2*E*)-*N*-[(oxan-2-yl)oxy]-3-(3-phenoxyphenyl)prop-2-enamide	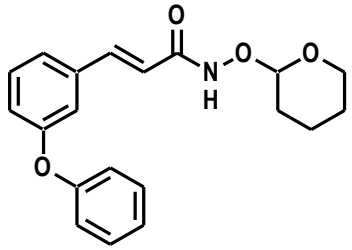	338.31 [M-H$^+$]
24x' (TB87THP) (2*E*)-3-{2-[(4-chlorophenyl)sulfanyl]phenyl}-*N*-[(oxan-2-yl)oxy]prop-2-enamide	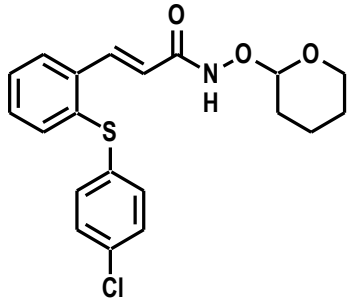	388.17 [M-H$^+$]
24y' (TB59THP) (2*E*)-3-[2-(benzyloxy)phenyl]-*N*-[(oxan-2-yl)oxy]prop-2-enamide	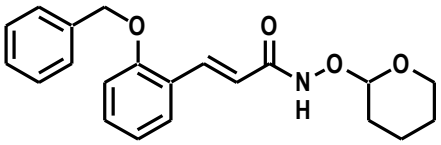	352.30 [M-H$^+$]
24z' (TB64THP) (2*E*)-3-[3-(benzyloxy)phenyl]-*N*-[(oxan-2-yl)oxy]prop-2-enamide	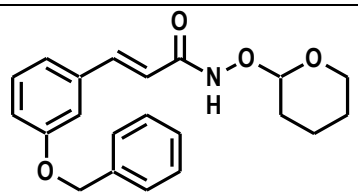	352.30 [M-H$^+$]
24za' (TB12THP) (2*E*)-3-[4-(benzyloxy)phenyl]-*N*-[(oxan-2-yl)oxy]prop-2-enamide	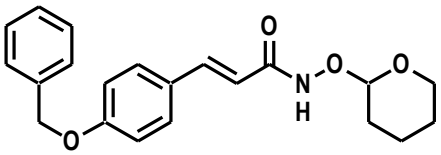	352.21 [M-H$^+$]
24zb' (TB67THP) (2*E*)-3-[4-(benzyloxy)-3-chlorophenyl]-*N*-[(oxan-2-yl)oxy]prop-2-enamide	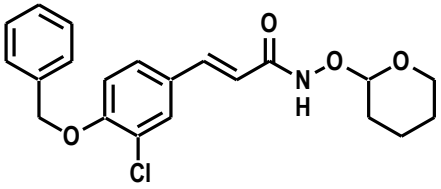	386.16 [M-H$^+$]
24zc' (TB38THP) (2*E*)-3-[4-(benzyloxy)-3-methoxyphenyl]-*N*-[(oxan-2-yl)oxy]prop-2-enamide	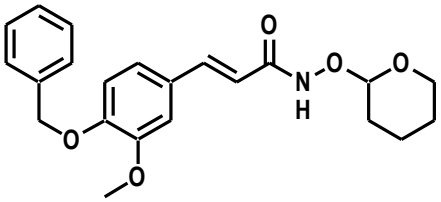	382.19 [M-H$^+$]

name	structure	ESI-MS m / z
24zd‘ (TB93THP) (2*E*)-3-[2-(benzyloxy)-6-methoxyphenyl]-*N*-[(oxan-2-yl)oxy]prop-2-enamide	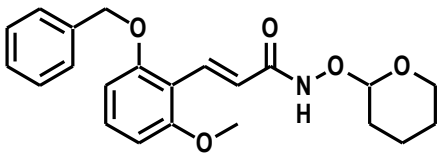	n.d.
24ze’ (TB91THP) (2*E*)-3-{2-[(4-chlorophenyl)methoxy]phenyl}-*N*-[(oxan-2-yl)oxy]prop-2-enamide	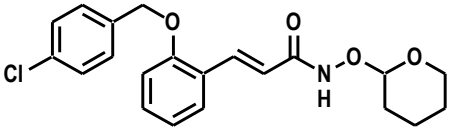	386.22 [M-H$^+$]
24zf’ (TB92THP) (2*E*)-3-{2-[(2,4-dichlorophenyl)methoxy]phenyl}-*N*-[(oxan-2-yl)oxy]prop-2-enamide	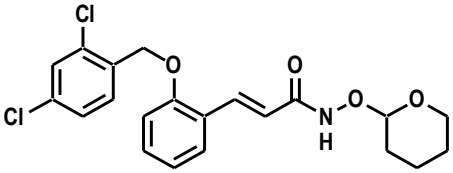	420.13 [M-H$^+$]
24zg‘ (TB98THP) (2*E*)-3-{2-[(2,6-dichlorophenyl)methoxy]phenyl}-*N*-[(oxan-2-yl)oxy]prop-2-enamide	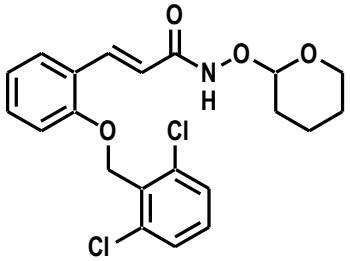	420.28 [M-H$^+$]
24zh’ (TB56THP) (2*E*)-3-(dibenzo[*b*,*d*]furan-4-yl)-*N*-[(oxan-2-yl)oxy]prop-2-enamide	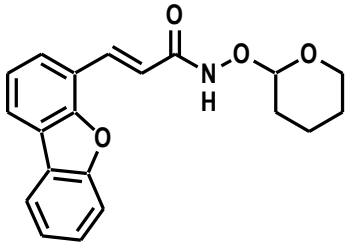	336.17 [M-H$^+$]
24zi’ (TB73THP) (2*E*)-3-(dibenzo[*b*,*d*]thiophen-4-yl)-*N*-[(oxan-2-yl)oxy]prop-2-enamide	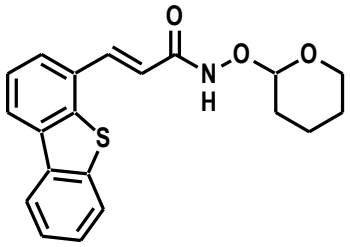	n.d.
24zj’ (TB75THP) (2*E*)-3-(naphthalen-2-yl)-*N*-[(oxan-2-yl)oxy]prop-2-enamide	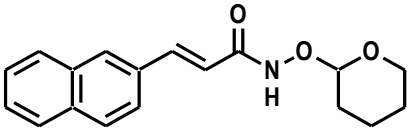	296.55 [M-H$^+$]

name	structure	ESI-MS m / z
24zk‘ (TB78THP) (2*E*)-3-(naphthalen-1-yl)-*N*-[(oxan-2-yl)oxy]prop-2-enamide	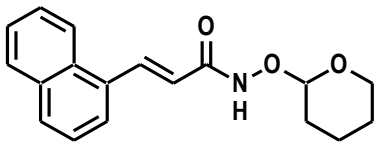	296.54 [M-H$^+$]
24zl’ (TB37THP) (2*E*)-2-methyl-*N*-[(oxan-2-yl)oxy]-3-phenylprop-2-enamide	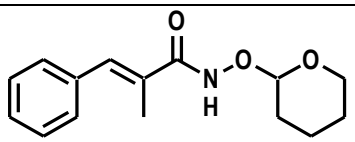	260.21 [M-H$^+$]
24zm’ (TB40THP) *N*-[(oxan-2-yl)oxy]-3-phenylprop-2-ynamide	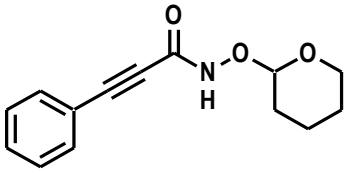	n.d.
26a’ (TB89THP) *N*-[(oxan-2-yl)oxy]-2-phenoxypropanamide	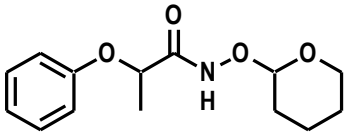	264.21 [M-H$^+$]
26b’ (TB88THP) 2-(2-methylphenoxy)-*N*-[(oxan-2-yl)oxy]acetamide	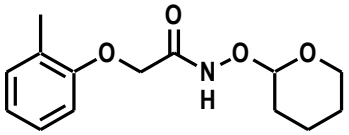	264.21 [M-H$^+$].
26c’ (TB96THP) 2-(2-methoxyphenoxy)-*N*-[(oxan-2-yl)oxy]acetamide	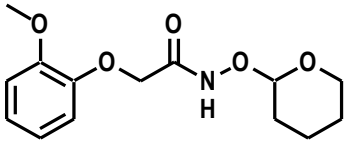	280.25 [M-H$^+$]
26d’ (TB79THP) 2-[(3,4-dimethoxyphenyl)sulfanyl]-*N*-[(oxan-2-yl)oxy]acetamide	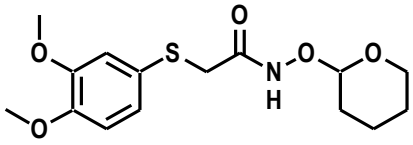	226.11 [M-H$^+$]
26e’ (TB94THP) 2-[(2,5-dichlorophenyl)sulfanyl]-*N*-[(oxan-2-yl)oxy]acetamide	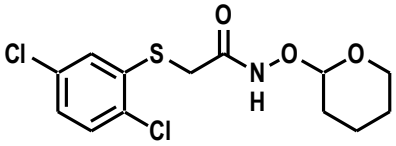	358.00 [M+Na$^+$]
26f‘ (TB103THP) 2-[(4-chlorophenyl)sulfanyl]-*N*-[(oxan-2-yl)oxy]acetamide	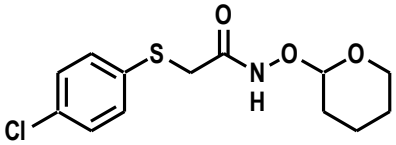	n.d.

name	structure	ESI-MS m / z
26g‘ (TB104THP) 2-[(2,6-dichlorophenyl)sulfanyl]-*N*-[(oxan-2-yl)oxy]acetamide	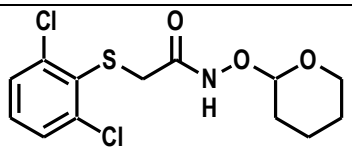	n.d.
26h’ (TB105THP) 2-[(2,4-dichlorophenyl)sulfanyl]-*N*-[(oxan-2-yl)oxy]acetamide	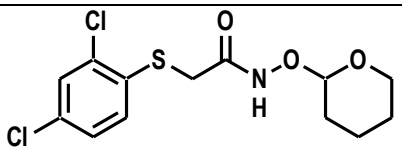	n.d.
26i’ (TB90THP) 2-[(naphthalen-2-yl)oxy]-*N*-[(oxan-2-yl)oxy]acetamide	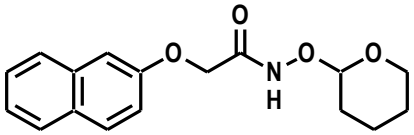	300.25 [M-H$^+$]
26j‘ (TB97THP) 2-[(naphthalen-1-yl)oxy]-*N*-[(oxan-2-yl)oxy]acetamide	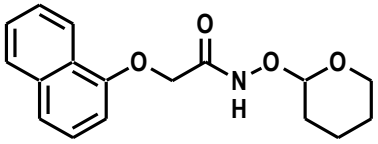	n.d.
26k‘ (TB80THP) 2-[(8-chloronaphthalen-1-yl)sulfanyl]-*N*-[(oxan-2-yl)oxy]acetamide	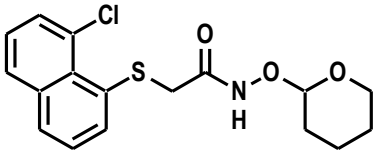	350.58 [M-H$^+$]
28a’ (TB83THP) 4-[(2-chloro-5-oxo-5λ^4-phenothiazin-10(5*H*)-yl)methyl] *N*-[(oxan-2-yl)oxy]acetamide	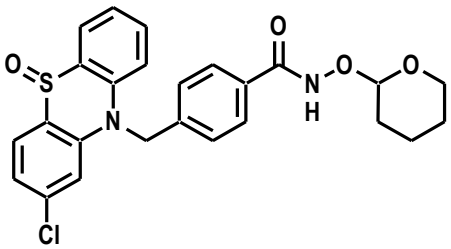	481.31 [M-H$^+$]

6.3.6 Cleavage of tetrahydropyrane protecting group

For the last synthetic step of all compounds the THP-protecting group is cleaved off. Therefore the THP-protected intermediate of each compound is dissolved in either THF (cleavage method 1) or methanol (cleaving method 2) and a catalytic amount of hydrochloric acid is added. The reaction mixture is stirred at room temperature. The reaction is observed by TLC. After the reaction is completed the solvent is evaporated under reduced pressure and the product is purified chromatographically.

22a (TB1) *N*-hydroxy-1*H*-indole-2-carboxamide

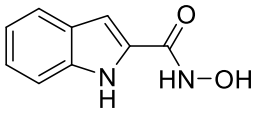

Appearance: white powder

Yield: 77 %

Mw: 176.17 g/mol

ESI-MS: 175.20 [M-H^+]

HPLC: rt 7.31 min (99.16 %)

^{1}H NMR (400 MHz, DMSO-d6) δ 11.60 (s, 1H, NH), 11.21 (s, 1H, NHOH), 9.09 (s, 1H, NHOH), 7.58 (d, *J* = 7.8 Hz, 1H, H4), 7.41 (d, *J* = 8.2 Hz, 1H, H7), 7.16 (t, *J* = 7.7 Hz, 1H, H6), 7.02 (t, *J* = 7.57 Hz, 1H, H5), 6.98 (s, 1H, H3).

22b (TB13) *N*-hydroxy-5-methoxy-1*H*-indole-2-carboxamide

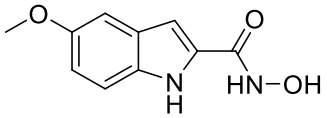

Appearance: off white powder

Yield: 52 %

Mw: 206.20 g/mol

ESI-MS: 205.17 [M-H^+], 207.02 [M+H^+]

HR-MS: 207.0766 [M+H^+]

HPLC: rt 8.57 min (99.40 %)

^{1}H NMR (400 MHz, DMSO-d6) δ 11.44 (s, 1H, NH), 11.15 (s, 1H, NHOH), 9.05 (s, 1H, NHOH), 7.30 (d, *J* = 8.9 Hz, 1H, H7), 7.05 (d, *J* = 2.1 Hz, 1H, H4), 6.90 (s, 1H, H4), 6.82 (dd, *J* = 8.9, 2.3 Hz, 1H, H6), 3.75 (s, 3H, C**H**$_3$).

22c (TB74) *N*-hydroxy-1*H*-benzimidazole-2-carboxamide

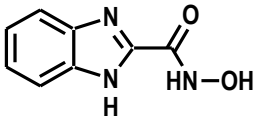

Appearance: pale powder

Yield: 59 %

Mw: 177.1602 g/mol

ESI-MS: 176.36 [M-H^+]

HR-MS: 178.0612 [M+H^+]

HPLC: 3.770 min (98.31 %)

^{1}H NMR (400 MHz, DMSO-d6) δ 13.25 (s, 1H, N**H**OH), 11.75 (s, 1H, NHO**H**), 9.31 (s, 1H, N**H**OH), 7.70 (d, *J* = 7.0 Hz, 1H, H4/H7), 7.53 (d, *J* = 6.7 Hz, 1H, H4/H7), 7.36 – 7.20 (m, 2H, H5, H6).

22d (TB2) *N*-hydroxy-1*H*-indene-2-carboxamide

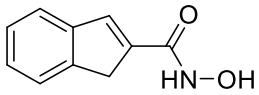

Appearance: white powder

Yield: 8.6 %

Mw: 175.18 g/mol

ESI-MS: 174.20 [M-H^+]; 176.28 [M+H^+]

HPLC: rt 12.48 min (99.51 %)

^{1}H NMR (400 MHz, DMSO-d6) δ 10.92 (s, 1H, NHOH), 8.95 (s, 1H, NHOH), 7.50 (m, 2H, H3, H4), 7.48 (m, 1H, H5), 7.33 – 7.26 (m, 2H, H7, H6), 3.63 (s, 2H, C**H**$_2$)

22e (TB3) *N*-hydroxy-1-benzofuran-2-carboxamide

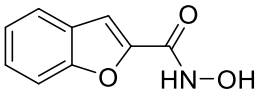

Appearance: white powder

Yield: 23 %

Mw: 177.16 g/mol

ESI-MS: 176.17 [M-H^+]; 178.00 [M+H^+]

HPLC: rt 8.72 min (99.75 %)

^{1}H NMR (400 MHz, DMSO-d6) δ 11.49 (s, 1H, NHOH), 9.26 (s, 1H, NHOH), 7.76 (d, *J* = 8.2 Hz, 1H, H4), 7.64 (d, *J* = 7.8 Hz, 1H, H7), 7.54 – 7.39 (m, 2H, H3, H6), 7.35 – 7.29 (m, *J* = 7.3 Hz, 1H; H5).

22f (TB42) 4-chloro-*N*-hydroxy-1-benzofuran-2-carboxamide

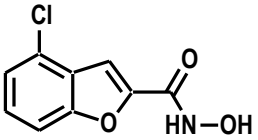

Appearance: pale powder

Yield: 19 %

Mw: 211.6016 g/mol

ESI-MS: 210.51 [M-H^+]

HR-MS: 212.0110 [M+H^+]

HPLC: 8.848 min (99.4 %)

^{1}H NMR (400 MHz, DMSO-d6) δ 11.29 (s, 1H, NHO**H**), 9.32 (s, 1H, N**H**OH), 7.59 – 7.43 (m, 5H, H2-H6).

22g (TB45) *N*-hydroxy-7-methoxy-1-benzofuran-2-carboxamide

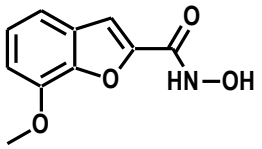

Appearance: light grey powder

Yield: 63 %

Mw: 207.1828 g/mol

ESI-MS: 206.33 [M-H^+]

HR-MS: 208.0606 [M+H^+]

HPLC: 7.642 min (98.23 %)

^{1}H NMR (400 MHz, DMSO-d6) δ 11.47 (s, 1H, NHO**H**), 9.24 (s, 1H, N**H**OH), 7.45 (s, 1H, H3), 7.29 (d, *J* = 7.6 Hz, 1H, H4), 7.23 (t, *J* = 7.8 Hz, 1H, H5), 7.05 (d, *J* = 7.7 Hz, 1H, H6), 3.96 (s, 3H, CH_3).

22h (TB46) *N*-hydroxy-7-ethoxy-1-benzofuran-2-carboxamide

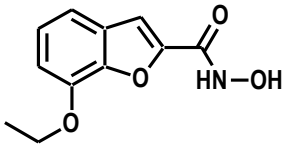

Appearance: pale pink powder

Yield: 41 %

Mw: 221.2094 g/mol

ESI-MS: 220.29 [M-H^+]

HR-MS: n.d.

HPLC: 8.722 min (97.79 %)

^{1}H NMR (400 MHz, DMSO-d6) δ 11.46 (s, 1H, NHO**H**), 9.24 (s, 1H, N**H**OH), 7.44 (s, 1H, H3), 7.28 (d, *J* = 7.0 Hz, 1H, H4), 7.21 (t, *J* = 7.8 Hz, 1H, H5), 7.03 (d, *J* = 7.1 Hz, 1H, H6), 4.26 (q, *J* = 7.0 Hz, 2H, CH_2), 1.42 (t, *J* = 7.0 Hz, 3H, CH_3).

22i (TB4) *N*-hydroxy-1-benzothiophene-2-carboxamide

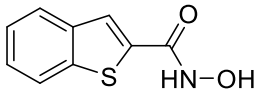

Appearance: white powder

Yield: 89 %

Mw: 193.22 g/mol

ESI-MS: 192.20 [M-H^+]

HPLC: 8.44 min (99.77 %)

^{1}H NMR (400 MHz, DMSO-d6) δ 11.46 (s, 1H, NHOH), 9.25 (s, 1H, NHOH), 8.02 (d, *J* = 7.2 Hz, 1H, H7), 7.92 (m, 2H), 7.49 – 7.40 (m, 2H).

22j (TB5) 4-chloro-*N*-hydroxy-1-benzothiophene-2-carboxamide

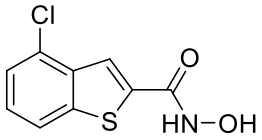

Appearance: pale pink /white powder

Yield: 7 %

Mw: 227.67 g/mol

ESI-MS: 226.22 [M-H$^+$]

HR-MS: 227.9884 [M+H$^+$]

HPLC: rt 12.12 min (99.15 %)

^{1}H NMR (400 MHz, DMSO-d6) δ 11.63 (s, 1H, NHOH), 9.34 (s, 1H, NHOH), 8.06 (s, 1H, H3), 8.03 (d, *J* = 7.8 Hz, 1H, H7), 7.54 (d, *J* = 7.3 Hz, 1H, H5), 7.49 – 7.44 (m, 1H, H6).

24a (TB7) (2*E*)-*N*-hydroxy-3-phenylprop-2-enamide

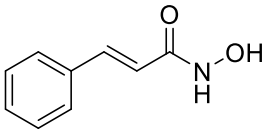

Appearance: white powder

Yield: 97%

Mw: 163.12 g/mol

ESI-MS: 162.17 [M-H$^+$]; 313.11[2M-H$^+$]

HR-MS: 164.0706 [M+H$^+$]

HPLC: rt 8.76 min (98.92 %)

^{1}H NMR (400 MHz, DMSO-d6) δ 10.74 (s, 1H, NHOH), 9.02 (s, 1H, NHOH), 7.56 (d, *J* = 6.8 Hz, 2H, H2, H6), 7.42 (m, 4H, Hβ, H3, H4, H5) 6.46 (d, *J* = 15.9 Hz, 1H, Hα).

24b (TB8) (2*E*)-3-(2-chlorophenyl)-*N*-hydroxyprop-2-enamide

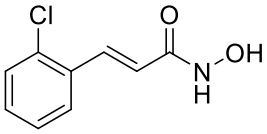

Appearance: white powder

Yield: 49 %

Mw: 197.62 g/mol

ESI-MS: 196.21 [M-H$^+$]

HR-MS: 198.0318 [M+H$^+$]

HPLC: rt 10.50 min (99.83 %)

^{1}H NMR (400 MHz, DMSO-d6) δ 10.85 (s, 1H, NHOH), 9.12 (s, 1H, NHOH), 7.74 (d, *J* = 15.6 Hz, 1H, Hβ), 7.74 – 7.68 (m, 1H, H6), 7.55 – 7.50 (m, 1H, H4), 7.43 – 7.37 (m, 1H, H5), 6.51 (d, *J* = 15.9 Hz, 1H, Hα).

24c (TB77) (2*E*)-3-(3-chlorophenyl)-*N*-hydroxyprop-2-enamide

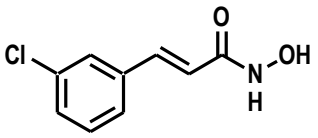

Appearance: off-white powder

Yield: 51 %

Mw: 197.6181 g/mol

ESI-MS: 196.23 [M-H^+]

HR-MS: 198.0315 [M+H^+]

HPLC: 8.004 min (97.81 %)

^{1}H NMR (400 MHz, DMSO-d6) δ 10.77 (s, 1H, N**H**OH), 9.09 (s, 1H, NHO**H**), 7.63 (s, 1H, H2), 7.53 (d, *J* = 3.5 Hz, 1H, H6), 7.48 – 7.36 (m, 3H, H4, H5, Hβ), 6.52 (d, *J* = 15.8 Hz, 1H, Hα).

24d (TB9) (2*E*)-3-(4-chlorophenyl)-*N*-hydroxyprop-2-enamide

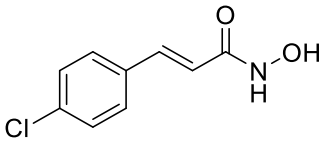

Appearance: pale pink powder

Yield: 55 %

Mw: 197.62 g/mol

ESI-MS: 196.18 [M-H^+]

HR-MS: 198.0318 [M+H^+]

HPLC: rt 10.96 min (98.65 %)

^{1}H NMR (400 MHz, DMSO-d6) δ 10.77 (s, 1H, NHOH), 9.05 (s, 1H, NHOH), 7.59 (d, *J* = 8.4 Hz, 2H, H2, H6), 7.52 – 7.40 (m, 3H, H3, H5, Hβ), 6.46 (d, *J* = 15.9 Hz, 1H, Hα).

24e (TB32) (2*E*)-3-(2,6-dichlorophenyl)-*N*-hydroxyprop-2-enamide

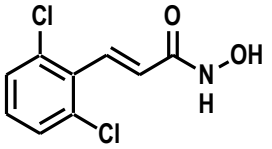

Appearance: pale powder

Yield: 65 %

Mw: 232.06 g/mol

ESI-MS: 230.14 [M-H^+]

HR-MS: 231.9927 [M+H^+]

HPLC: 9.759 min (98.835 %)

^{1}H NMR (400 MHz, DMSO-d6) δ 10.95 (s, 1H, NHO**H**), 9.17 (s, 1H, N**H**OH), 7.55 (d, *J* = 8.1 Hz, 2H, H3,H5), 7.49 (d, *J* = 16.1 Hz, 1H, Hβ), 7.41 – 7.35 (m, 1H, H4), 6.53 (d, *J* = 16.1 Hz, 1H, Hα).

24f (TB51) (2*E*)-3-(2,4-dichlorophenyl)-*N*-hydroxyprop-2-enamide

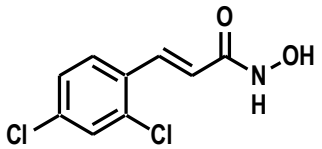

Appearance:	pale powder
Yield:	48 %
Mw:	232.0628 g/mol
ESI-MS:	230.17 [M-H$^+$]
HR-MS:	231.9928 [M+H$^+$]
HPLC:	10.161 min (99.41 %)

^{1}H NMR (400 MHz, DMSO-d6) δ 10.88 (s, 1H, NHO**H**), 9.16 (s, 1H, N**H**OH), 7.72 (d, *J* = 8.8 Hz, 1H, H6), 7.70 (d, *J* = 2.1 Hz, 1H, H3), 7.67 (d, *J* = 15.9 Hz, 1H, Hβ), 7.48 (dd, *J* = 8.4, 1.8 Hz, 1H, H5), 6.53 (d, *J* = 15.7 Hz, 1H, Hα).

24g (TB10) (2*E*)-3-(4-bromophenyl)-*N*-hydroxyprop-2-enamide

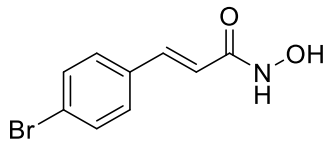

Appearance:	light pink powder
Yield:	49 %
Mw:	242.07 g/mol
ESI-MS:	242.2 [M-H$^+$]
HPLC:	rt 11.37 min (99.35 %)

^{1}H NMR (400 MHz, DMSO-d6) δ 10.77 (s, 1H, NHOH), 9.05 (s, 1H, NHOH), 7.61 (d, *J* = 8.4 Hz, 2H, H2, H6), 7.52 (d, *J* = 8.5 Hz, 2H, H3, H5), 7.43 (d, *J* = 15.8 Hz, 1H, Hβ), 6.47 (d, *J* = 15.9 Hz, 1H, Hα).

24h (TB76) (2*E*)-3-(2-bromophenyl)-*N*-hydroxyprop-2-enamid

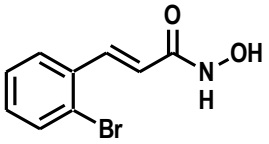

Appearance:	light tan powder
Yield:	58 %
Mw:	242.0694 g/mol
ESI-MS:	240.60 [M-H$^+$]
HR-MS:	241.9811[M+H$^+$]
HPLC:	8.419 min (99.48 %)

^{1}H NMR (400 MHz, DMSO-d6) δ 10.86 (s, 1H, NHO**H**), 9.12 (s, 1H, N**H**OH), 7.73 – 7.64 (m, *J* = 16.4 Hz, 3H, Hβ, H3, H6), 7.46 – 7.42 (m, *J* = 7.4 Hz, 1H, H5), 7.31 (dd, *J* = 10.9, 4.4 Hz, 1H, H4), 6.47 (d, *J* = 15.7 Hz, 1H, Hα).

24i (TB53) (2*E*)-3-(2-bromo-5-fluorophenyl)-*N*-hydroxyprop-2-enamide

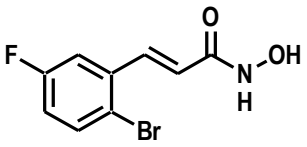

Appearance: off-white powder

Yield: 53 %

Mw: 260.0598 g/mol

ESI-MS: 258.29 [M-H$^+$]

HR-MS: n.d.

^{1}H NMR (400 MHz, DMSO-d6) δ 10.87 (s, 1H, NHO**H**), 9.16 (s, 1H, N**H**OH), 7.74 (dd, *J* = 8.9, 5.4 Hz, 1H, H6), 7.63 (d, *J* = 15.6 Hz, 1H, Hβ), 7.55 (dd, *J* = 9.8, 2.8 Hz, 1H, H3), 7.22 (td, *J* = 8.5, 3.0 Hz, 1H, H4), 6.52 (d, *J* = 15.7 Hz, 1H, Hα).

24j (TB54) (2*E*)-3-(2-fluoro-5-methoxyphenyl)-*N*-hydroxyprop-2-enamide

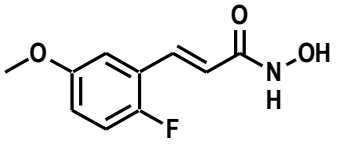

Appearance: pale tan powder

Yield: 56 %

Mw: 211.1897 g/mol

ESI-MS: 210.27 [M-H$^+$]

HR-MS: 212.0716 [M+H$^+$]

HPLC: 13.304 min (91.45 %)

^{1}H NMR (400 MHz, DMSO-d6) δ 10.82 (s, 1H, NHO**H**), 9.09 (s, 1H, N**H**OH), 7.47 (d, *J* = 16.0 Hz, 1H, Hβ), 7.23 – 7.14 (m, 2H, H3, H6), 6.97 (m, *J* = 8.9, 3.7 Hz, 1H, H4), 6.58 (d, *J* = 16.0 Hz, 1H, Hα), 3.77 (s, 3H, CH_3).

24k (TB15) (2*E*)-3-[4-(dimethylamino)phenyl]-*N*-hydroxyprop-2-enamide

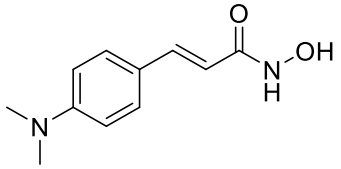

Appearance: pale red powder

Yield: 26 %

Mw: 206.24 g7mol

ESI-MS: 205.20 [M-H$^+$], 207.05 [M+H$^+$]

HPLC: 3.32 min (98.21 %)

^{1}H NMR (500 MHz, DMSO-d6) δ 10.51 (s, 1H, NHOH), 8.79 (s, 1H, NHOH), 7.38 (d, *J* = 8.5 Hz, 2H), 7.33 (d, *J* = 15.6 Hz, 1H, Hβ), 7.10 (d, *J* = 8.5 Hz, 2H, H3, H5), 6.73 (d, *J* = 8.8 Hz, 2H, H2, H6), 6.19 (d, *J* = 15.4 Hz, 1H, Hα), 2.95 (d, *J* = 3.1 Hz, 6H, CH_3, CH_3).

24l (TB14) (2*E*)-*N*-hydroxy-3-(4-hydroxyphenyl)prop-2-enamide

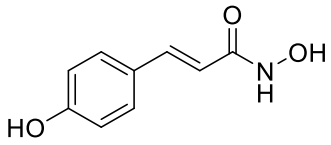

Appearance: light pink powder

Yield: 15.6 %

Mw: 179.17 g/mol

ESI-MS: 178.24 [M-H$^+$]

HPLC: rt: 6.80 min (90.23 %)

^{1}H NMR (500 MHz, DMSO-d6) δ 10.64 (d, *J* = 15.7 Hz, 1H, NHOH), 8.91 (s, 1H, NHOH), 7.37 (d, *J* = 8.6 Hz, 2H, H3, H5), 7.30 (d, *J* = 15.9 Hz, 1H, Hβ), 6.78 (d, *J* = 8.6 Hz, 2H, H2, H6), 6.24 (d, *J* = 15.6 Hz, 1H, Hα).

24m (TB33) (2*E*)-*N*-hydroxy-3-(4-hydroxy-3-methoxyphenyl)prop-2-enamide

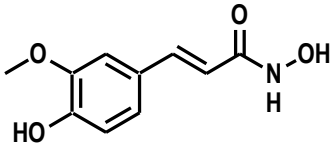

Appearance: light red powder

Yield: 49 %

Mw: 209.07 g/mol

ESI-MS: 208.22 [M-H$^+$]

HR-MS: 210.0763 [M+H$^+$]

HPLC: 5.613 min (96.71 %)

^{1}H NMR (400 MHz, DMSO-d6) δ 10.58 (s, 1H, NHO**H**), 9.40 (s, 1H, N**H**OH), 7.35 (d, *J* = 15.7 Hz, 1H, Hβ), 7.12 (s, 1H, H6), 6.99 (d, *J* = 8.1 Hz, 1H, H2), 6.78 (d, *J* = 8.1 Hz, 1H, H3), 6.27 (d, *J* = 15.7 Hz, 1H, Hα), 3.80 (s, 3H, CH_3).

24n (TB16) (2*E*)-3-(4-ethoxy-3-hydroxyphenyl)-*N*-hydroxyprop-2-enamide

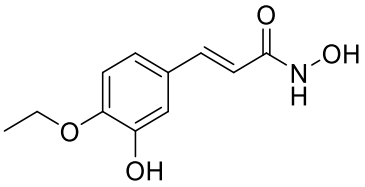

Appearance: pale red powder

Yield: 33 %

Mw: 223.23 g/mol

ESI-MS: 222.19 [M-H$^+$]

HR-MS: 224.0921 [M+H$^+$]

HPLC: 6.51 min (93.89 %)

^{1}H NMR (500 MHz, DMSO-d6) δ 10.57 (s, 1H, NHO**H**), 9.34 (s, 1H, N**H**OH), 7.33 (d, *J* = 15.8 Hz, 1H, Hβ), 7.09 (s, 1H, H2), 6.98 (d, *J* = 8.2 Hz, 1H, H6), 6.79 (d, *J* = 8.1 Hz, 1H, H5), 6.25 (t, *J* = 12.3 Hz, 1H, Hα), 4.09 – 4.01 (m, 2H, CH_2), 1.34 (t, *J* = 7.0 Hz, 3H, CH_3).

24o (TB31) (2*E*)-*N*-hydroxy-3-(4-methoxyphenyl)prop-2-enamide

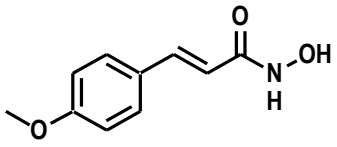

Appearance: light powder

Yield: 50 %

Mw: 193.20 g/mol

ESI-MS: 192.24 [M-H$^+$]

HR-MS: 194.0812 [M+H$^+$]

HPLC: 6.518 min (96.99 %)

^{1}H NMR (400 MHz, DMSO-d6) δ 10.64 (s, 1H, NHO**H**), 8.94 (s, 1H, N**H**OH), 7.50 (d, *J* = 8.4 Hz, 1H), 7.40 (d, *J* = 15.7 Hz, 1H, Hβ), 6.97 (d, *J* = 8.6 Hz, 1H), 6.31 (d, *J* = 15.8 Hz, 1H, Hα), 3.78 (s, 1H).

24p (TB44) (2*E*)-*N*-hydroxy-3-(3-methoxyphenyl)prop-2-enamide

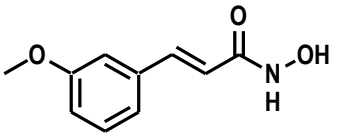

Appearance: pale powder

Yield: 37 %

Mw: 193.1993 g/mol

ESI-MS: 192.27 [M-H$^+$]

HR-MS: 194.0612 [M+H$^+$]

HPLC: 7.567 min (99.95 %)

^{1}H NMR (400 MHz, DMSO-d6) δ 10.73 (s, 1H, NHO**H**), 9.03 (s, 1H, N**H**OH), 7.43 (d, *J* = 15.8 Hz, 1H, Hβ), 7.32 (t, *J* = 7.9 Hz, 1H, H5), 7.13 (d, *J* = 7.9 Hz, 1H, H6), 7.11 (s, 1H, H2), 6.94 (dd, *J* = 8.2, 2.1 Hz, 1H, H4), 6.46 (d, *J* = 15.8 Hz, 1H, Hα), 3.78 (s, 3H, CH_3).

24q (TB43) (2*E*)-3-(4-ethoxyphenyl)-*N*-hydroxyprop-2-enamide

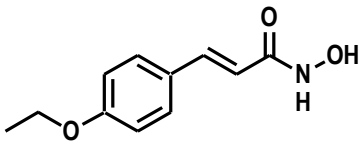

Appearance: pale powder

Yield: 35 %

Mw: 207.2259 g/mol

ESI-MS: 206.28 [M-H$^+$]

HR-MS: 208.0968 [M+H$^+$]

HPLC: 7.093 min (97.92 %)

^{1}H NMR (400 MHz, DMSO-d6) δ 10.63 (s, 1H, NHO**H**), 8.93 (s, 1H, N**H**OH), 7.48 (d, *J* = 8.5 Hz, 2H, H3, H5), 7.39 (d, *J* = 15.8 Hz, 1H, Hβ), 6.95 (d, *J* = 8.7 Hz, 2H, H2, H6), 6.30 (d, *J* = 15.6 Hz, 1H, Hα), 4.05 (q, *J* = 6.9 Hz, 2H, CH_2), 1.33 (t, *J* = 7.0 Hz, 3H, CH_3).

24r (TB58) (2*E*)-3-(2-ethoxyphenyl)-*N*-hydroxyprop-2-enamide

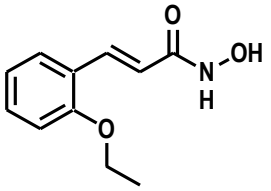

Appearance:	white powder
Yield:	35 %
Mw:	207.2259 g/mol
ESI-MS:	n.d.
HR-MS:	208.0971M+H$^+$]
HPLC:	8.554 min (91.98 %)

^{1}H NMR (400 MHz, DMSO-d6) δ 10.72 (s, 1H, NHO**H**), 8.96 (s, 1H, N**H**OH), 7.67 (d, *J* = 15.9 Hz, 1H, Hβ), 7.49 (d, *J* = 6.5 Hz, 1H, H6), 7.36 – 7.30 (m, 1H, H4), 7.05 (d, *J* = 7.9 Hz, 1H, H5), 6.96 (m, *J* = 7.5 Hz, 1H, H3), 6.51 (d, *J* = 15.9 Hz, 1H, Hα), 4.11 (q, *J* = 7.0 Hz, 2H, CH_2), 1.39 (t, *J* = 7.0 Hz, 3H, CH_3).

24s (TB11) (2*E*)-*N*-hydroxy-3-(3,4,5-trimethoxyphenyl)prop-2-enamide

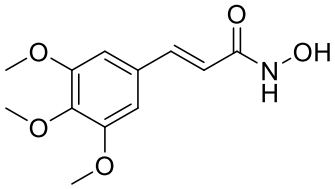

Appearance:	pale pink powder
Yield:	34.2 %
Mw:	253.25 g/mol
ESI-MS:	252.18 [M-H$^+$], 253.98 [M+H$^+$]
HR-MS:	276.0846 [M+Na$^+$]
HPLC:	rt 8.85 min (98.28 %)

^{1}H NMR (400 MHz, DMSO-d6) δ 10.66 (s, 1H, NHOH), 8.98 (s, 1H, NHOH), 7.40 (d, *J* = 15.9 Hz,1H, Hβ), 6.89 (s, 2H, H2, H6), 6.41 (d, *J* = 15.7 Hz, 1H, Hα), 3.81 (s, 6H, 2xC**H**$_3$), 3.68 (s, 3H, C**H**$_3$).

24t (TB57) (2*E*)-3-[2-(4-chlorophenoxy)phenyl]-*N*-hydroxyprop-2-enamide

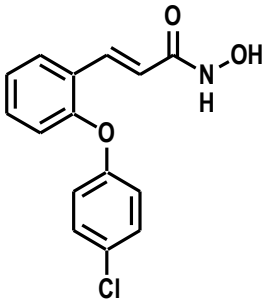

Appearance:	pale powder
Yield:	55 %
Mw:	289.71.34 g/mol
ESI-MS:	288.26 [M-H$^+$]
HR-MS:	290.0585 [M+H$^+$]

^{1}H NMR (400 MHz, DMSO-d6) δ 10.78 (s, 1H,NHO**H**), 9.02 (s, 1H, N**H**OH), 7.73 – 7.67 (m, 1H, H6), 7.58 (d, *J* = 15.9 Hz, 1H, Hβ), 7.46 – 7.37 (m, 3H, H6, H3', H5'), 7.25 (t, *J* = 7.3 Hz, 1H, H4), 7.01 – 6.95 (m, 3H, H5, H2', H6'), 6.55 (d, *J* = 15.9 Hz, 1H, Hα).

(2*E*)-*N*-hydroxy-3-[2-(4-methoxyphenoxy)phenyl]prop-2-enamide TB55

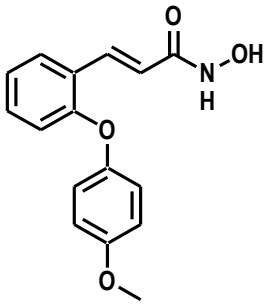

Appearance:	off-white powder
Yield:	57 %
Mw:	285.2946 g/mol
ESI-MS:	n.d.
HR-MS:	286.1086 [M+H$^+$]
HPLC:	X min (y %)

^{1}H NMR (400 MHz, DMSO-d6) δ 10.77 (s, 1H, NHO**H**), 9.01 (s, 1H, N**H**OH), 7.69 (d, *J* = 16.0 Hz, 1H, Hβ), 7.65 (d, *J* = 6.5 Hz, 1H, H6), 7.35 – 7.30 (m, 1H, H4), 7.14 (m, *J* = 7.6 Hz, 1H, H5), 7.01 – 6.94 (m, 4H, H2', H3', H5', H6'), 6.78 (d, *J* = 7.5 Hz, 1H, H3), 6.57 (d, *J* = 16.0 Hz, 1H, Hα), 3.75 (s, 3H, CH_3).

24v (TB27) (2*E*)-*N*-hydroxy-3-[2-(3-methoxyphenoxy)phenyl]prop-2-enamide

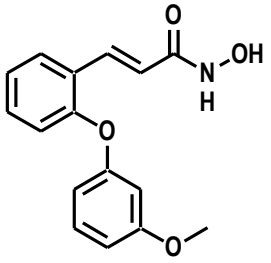

Appearance:	off-white powder
Yield:	32 %
Mw:	285.2946 g/mol
ESI-MS:	284.29 [M-H$^+$]
HR-MS:	286.1075 [M+H$^+$]
HPLC:	6.51 min (93.89 %)

^{1}H NMR (400 MHz, DMSO-d6) δ 10.77 (s, 1H, NHO**H**), 9.01 (s, 1H, N**H**OH), 7.69 (d, *J* = 7.7 Hz, 1H, H6), 7.61 (d, *J* = 15.9 Hz, 1H, Hβ), 7.39 (t, *J* = 7.8 Hz, 1H, H3, H4), 7.30 – 7.25 (m, 1H, H5), 7.22 (d, *J* = 7.4 Hz, 1H, H5'), 6.96 (d, *J* = 7.8 Hz, 1H), 6.72 (d, *J* = 8.4 Hz, 1H), 6.57 (s, 1H), 6.53 (s, 1H, H2'), 6.48 (d, *J* = 8.2 Hz, 1H), 3.74 (s, 3H, CH_3).

24w (TB72) (2*E*)-*N*-hydroxy-3-(3-phenoxyphenyl)prop-2-enamide

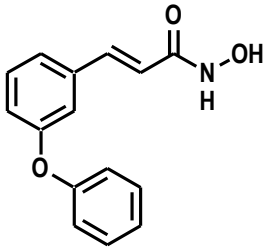

Appearance:	off-white powder
Yield:	39 %
Mw:	255.2687 g/mol
ESI-MS:	254.30 [M-H$^+$]
HR-MS:	256.0969 [M+H$^+$]
HPLC:	10.800 min (96.96 %)

^{1}H NMR (400 MHz, DMSO-d6) δ 10.72 (s, 1H, NHO**H**), 9.05 (s, 1H, N**H**OH), 7.47 – 7.36 (m, 4H, Hβ, H3', H4', H5'), 7.33 (d, *J* = 7.7 Hz, 1H, H6), 7.22 – 7.13 (m, 2H, H2, H5), 7.04 (dd, *J* = 8.6, 0.9 Hz, 2H, H2', H6'), 7.00 (dd, *J* = 8.0, 1.8 Hz, 1H, H4), 6.43 (d, *J* = 15.8 Hz, 1H, Hα).

24x (TB87) (2*E*)-3-{2-[(4-chlorophenyl)sulfanyl]phenyl}-*N*-hydroxyprop-2-enamide

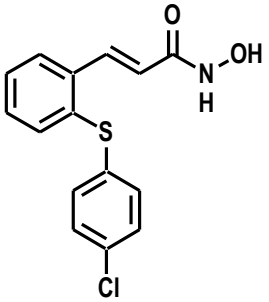

Appearance: pale powder

Yield: 28 %

Mw: 305.7800 g/mol

ESI-MS: 304.21x [M-H^+]

HR-MS: 306.0348 [M+H^+]

HPLC: 11.971 min (100.00 %)

^{1}H NMR (400 MHz, DMSO-d6) δ 10.79 (s, 1H, NHO**H**), 9.07 (s, 1H, N**H**OH), 7.88 (d, *J* = 15.7 Hz, 1H, Hβ), 7.72 (d, *J* = 7.6 Hz, 1H, H6), 7.51 – 7.44 (m, 1H, H5), 7.44 – 7.35 (m, 4H, H3, H4, H3', H5'), 7.20 – 7.14 (m, 2H, H2', H6'), 6.45 (d, *J* = 15.7 Hz, 1H, Hα).

24y (TB59) (2*E*)-3-[2-(benzyloxy)phenyl]-*N*-hydroxyprop-2-enamide

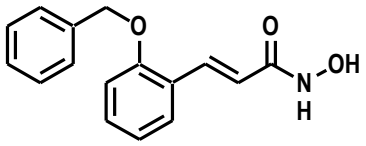

Appearance: light pink powder

Yield: 12 %

Mw: 269.2952 g/mol

ESI-MS: 268.20 [M-H^+]

HR-MS: 270.1128 [M+H^+]

HPLC: 8.615 min (99.07 %)

^{1}H NMR (400 MHz, DMSO-d6) δ 10.72 (s, 1H, NHO**H**), 8.96 (s, 1H, N**H**OH), 7.75 (d, *J* = 16.0 Hz, 1H, Hβ), 7.53 (d, *J* = 7.0 Hz, 1H, H6), 7.47 (d, *J* = 7.0 Hz, 2H, H2', H6'), 7.43 – 7.37 (m, 2H, H3', H5'), 7.37 – 7.29 (m, 2H, H4, H4'), 7.14 (d, *J* = 8.2 Hz, 1H, H3), 6.98 (t, *J* = 7.4 Hz, 1H, H5), 6.48 (d, *J* = 16.0 Hz, 1H, Hα), 5.21 (s, 2H, CH_2).

24z (TB64) (2*E*)-3-[3-(benzyloxy)phenyl]-*N*-hydroxyprop-2-enamide

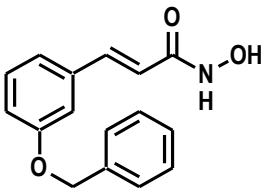

Appearance: light tan powder

Yield: 16 %

Mw: 269.2952 g/mol

HR-MS: 270.1126 [M+H^+]

HPLC: 11.233 min (99.912 %)

^{1}H NMR (500 MHz, DMSO-d6) δ 10.73 (s, 1H, NHO**H**), 9.02 (s, 1H, N**H**OH), 7.48 – 7.30 (m, 7H, Hβ, H5. H2', H3', H4', H5', H6'), 7.20 (m, 1H, H2), 7.14 (d, *J* = 7.5 Hz, 1H, H6), 7.02 (d, *J* = 8.1 Hz, 1H, H4), 6.46 (d, *J* = 15.8 Hz, 1H, Hα), 5.14 (s, 2H, C**H**$_2$).

24za (TB12) (2*E*)-3-[4-(benzyloxy)phenyl]-*N*-hydroxyprop-2-enamide

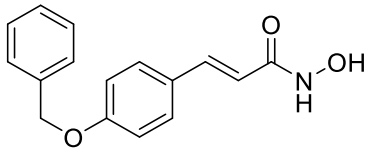

Appearance: pale pink powder

Yield: 15.6 %

Mw: 269.30 g/mol

ESI-MS: 268.17 [M-H^+], 270.07 [M+H^+]

HPLC: rt 13.10 min (97.53 %)

^{1}H NMR (400 MHz, DMSO-d6) δ 10.62 (s, 1H, NHOH), 8.94 (s, 1H, NHOH), 7.54 – 7.29 (m, *J* = 24.6, 17.1, 7.7 Hz, 8H, Hβ, H3, H5, H2', H3', H4', H5', H6'), 7.04 (d, *J* = 8.6 Hz, 2H, H2, H6), 6.31 (d, *J* = 15.9 Hz, 1H, Hα), 5.14 (s, 2H, C**H**$_2$).

24zb (TB67) (2*E*)-3-[4-(benzyloxy)-3-chlorophenyl]-*N*-hydroxyprop-2-enamide

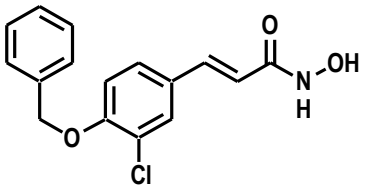

Appearance: pale tan powder

Yield: 38 %

Mw: 303.7400 g/mol

ESI-MS: 302.15 [M-H^+]

HR-MS: n.d.

HPLC: 11.945 min (100.00 %)

^{1}H NMR (400 MHz, DMSO-d6) δ 10.66 (s, 1H, NHO**H**), 9.00 (s, 1H, N**H**OH), 7.67 (d, *J* = 1.8 Hz, 1H, H2), 7.50 (dd, *J* = 8.6, 1.7 Hz, 1H, H6), 7.49 – 7.38 (m, 5H, Hβ, H2', H3', H5', H6'), 7.37 – 7.32 (m, 1H, H4'), 7.27 (d, *J* = 8.6 Hz, 1H, H5), 6.37 (d, *J* = 15.8 Hz, 1H, Hα), 5.25 (s, 2H, C**H**$_2$).

24zc (TB38) (2*E*)-3-[4-(benzyloxy)-3-methoxyphenyl]-*N*-hydroxyprop-2-enamide

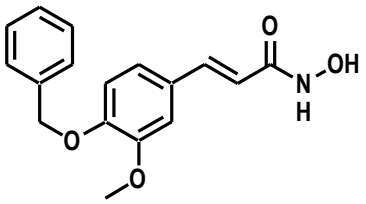

Appearance: off-white powder

Yield: 57 %

Mw: 299.12 g/mol

ESI-MS: 298.24 [M-H^+]

HR-MS: 300.1232 [M+H^+]

HPLC: 10.55 min (99.14 %)

^{1}H NMR (400 MHz, DMSO-d6) δ 10.62 (s, 1H, NHO**H**), 8.94 (s, 1H, N**H**OH), 7.46 – 7.31 (m, 6H, Hβ, 5Ar'H), 7.18 (s, 1H, H2), 7.09 (d, *J* = 8.7 Hz, 1H, H6), 7.06 (d, *J* = 8.3 Hz, 1H, H5), 6.34 (d, *J* = 15.7 Hz, 1H, Hα), 5.12 (s, 2H, CH_2), 3.81 (s, 3H, CH_3).

24zd (TB93) (2*E*)-3-[2-(benzyloxy)-6-methoxyphenyl]-*N*-hydroxyprop-2-enamide

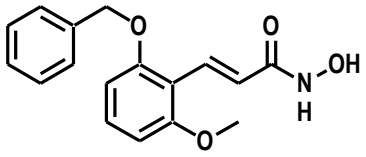

Appearance: off-white powder

Yield: 45 %

Mw: 299.3212 g/mol

ESI-MS: 298.25 [M-H$^+$]

HR-MS: 300.1230 [M+H$^+$]

HPLC: n.d.

^{1}H NMR (400 MHz, DMSO-d6) δ 10.72 (s, 1H, NHO**H**), 9.00 (s, 1H, N**H**OH), 7.71 (d, *J* = 16.1 Hz, 1H, Hβ), 7.45 (d, *J* = 6.8 Hz, 2H, H2', H6'), 7.41 – 7.31 (m, 3H, H6, H3', H5'), 7.11 (t, *J* = 6.7 Hz, 3H, H4, H5, H4'), 6.43 (d, *J* = 15.9 Hz, 1H, Hα), 4.96 (s, 2H, C**H$_2$**), 3.85 (s, 3H, C**H$_3$**).

24ze (TB91) (2*E*)-3-{2-[(4-chlorophenyl)methoxy]phenyl}-*N*-hydroxyprop-2-enamide

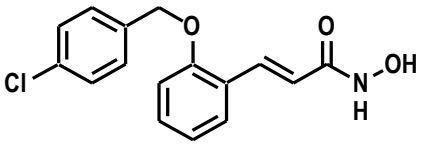

Appearance: pale powder

Yield: 55 %

Mw: 303.7400 g/mol

ESI-MS: 302.17 [M-H$^+$]

HR-MS: 304.0734 [M+H$^+$]

HPLC: 11.445 min (99.59 %)

^{1}H NMR (400 MHz, DMSO-d6) δ 10.72 (s, 1H, NHO**H**), 8.98 (s, 1H, N**H**OH), 7.73 (d, *J* = 16.0 Hz, 1H, Hβ), 7.53 (d, *J* = 6.9 Hz, 1H, H6), 7.51 – 7.44 (m, 4H, H2', H3', H5', H6'), 7.33 (t, *J* = 7.2 Hz, 1H, H5), 7.12 (d, *J* = 8.2 Hz, 1H, H3), 6.99 (t, *J* = 7.5 Hz, 1H, H4), 6.49 (d, *J* = 15.9 Hz, 1H, Hα), 5.21 (s, 2H, C**H$_2$**).

24zf (TB92) (2*E*)-3-{2-[(2,4-dichlorophenyl)methoxy]phenyl}-*N*-hydroxyprop-2-enamide

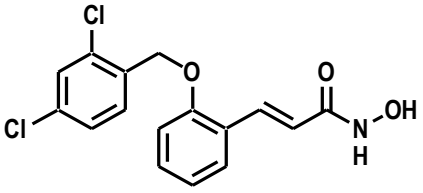

Appearance: light grey powder

Yield: 49 %

Mw: 338.1848 g/mol

ESI-MS: 336.12 [M-H$^+$]

HR-MS: 338.0347 [M+H$^+$]

HPLC: 12.794 min (98.03 %)

^{1}H NMR (400 MHz, DMSO-d6) δ 10.72 (s, 1H, NHO**H**), 8.98 (s, 1H, N**H**OH), 7.73 (d, *J* = 16.0 Hz, 1H, Hβ), 7.53 (d, *J* = 6.9 Hz, 1H, H6), 7.51 – 7.44 (m, 4H, H2', H3', H5', H6'), 7.33 (t, *J* = 7.2 Hz, 1H, H5), 7.12 (d, *J* = 8.2 Hz, 1H, H3), 6.99 (t, *J* = 7.5 Hz, 1H, H4), 6.49 (d, *J* = 15.9 Hz, 1H, Hα), 5.21 (s, 2H, C**H$_2$**).

24zg (TB98) (2*E*)-3-{2-[(2,6-dichlorophenyl)methoxy]phenyl}-*N*-hydroxyprop-2-enamide

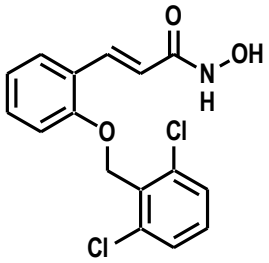

Appearance: pale red powder

Yield: 61 %

Mw: 338.1848 g/mol

ESI-MS: 338.46 [M+H$^+$]

HR-MS: 338.0340 [M+H$^+$]

HPLC: 11.678 min (97.69 %)

^{1}H NMR (400 MHz, DMSO-d6) δ 10.67 (s, 1H, NHO**H**), 8.93 (s, 1H, N**H**OH), 7.65 – 7.47 (m, 5H, Hβ, H6, H3', H4', H5'), 7.41 (dd, *J* = 12.0, 4.9 Hz, 1H, H4), 7.31 (d, *J* = 8.1 Hz, 1H, H3), 7.05 (t, *J* = 7.4 Hz, 1H, H5), 6.37 (d, *J* = 15.9 Hz, 1H, Hα), 5.30 (s, *J* = 11.7 Hz, 2H, C**H$_2$**).

24zh (TB56) (2*E*)-3-(dibenzo[*b*,*d*]furan-4-yl)-*N*-hydroxyprop-2-enamide

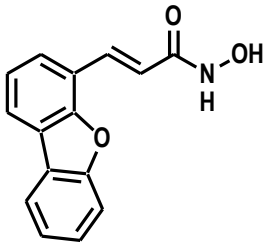

Appearance: pale pink powder

Yield: 26 %

Mw: 253.2528 g/mol

ESI-MS: 252.34 [M-H$^+$]

HR-MS: 254.0809 [M+H$^+$]

HPLC: 12.028 min (99.376 %)

^{1}H NMR (400 MHz, DMSO-d6) δ 10.97 (s, 1H, NHO**H**), 9.11 (s, 1H, N**H**OH), 8.22 – 8.16 (m, 2H), 7.81 – 7.70 (m, 3H), 7.59 (ddd, *J* = 8.4, 7.4, 1.3 Hz, 1H), 7.45 (dd, *J* = 10.8, 4.3 Hz, 2H), 7.02 (d, *J* = 15.9 Hz, 1H, Hα).

24zi (TB73) (2*E*)-3-(dibenzo[*b*,*d*]thiophen-4-yl)-*N*-hydroxyprop-2-enamide

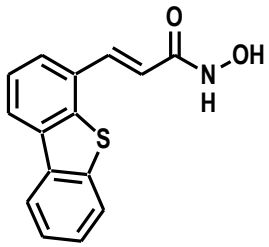

Appearance: off-white powder

Yield: 33 %

Mw: 269.3194 g/mol

ESI-MS: 268.51 [M-H$^+$]

HR-MS: 270.0582 [M+H$^+$]

HPLC: 12.303 min (99.59 %)

^{1}H NMR (400 MHz, DMSO-d6) δ 10.98 (s, 1H, NHO**H**), 9.15 (s, 1H, N**H**OH), 8.43 (d, *J* = 7.9 Hz, 2H, H1, H9), 8.13 – 8.07 (m, 1H, H6), 7.78 (d, *J* = 7.7 Hz, 1H3), 7.72 (d, *J* = 15.8 Hz, 1H, Hβ), 7.63 – 7.54 (m, 3H, H2, H7, H8), 6.74 (d, *J* = 15.9 Hz, 1H, Hα).

24zj (TB75) (2*E*)-*N*-hydroxy-3-(naphthalen-2-yl)prop-2-enamide

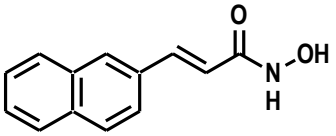

Appearance:	off-white powder
Yield:	62 %
Mw:	213.2320 g/mol
ESI-MS:	212.28 [M-H$^+$]
HR-MS:	214.0864 [M+H$^+$]
HPLC:	10.475 min (99.38 %)

^{1}H NMR (400 MHz, DMSO-d6) δ 10.80 (s, 1H, NHO**H**), 9.07 (s, 1H, N**H**OH), 8.07 (s, 1H, H1), 7.97 – 7.89 (m, 3H, H5, H6, H8), 7.71 (d, *J* = 8.7 Hz, 1H, H3), 7.62 (d, *J* = 15.8 Hz, 1H, Hβ), 7.54 (m, *J* = 6.3, 3.1 Hz, 2H, H4, H7), 6.60 (d, *J* = 15.8 Hz, 1H, Hα).

24zk (TB78) (2*E*)-*N*-hydroxy-3-(naphthalen-1-yl)prop-2-enamide

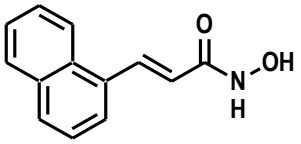

Appearance:	off-white powder
Yield:	52 %
Mw:	213.2320 g/mol
ESI-MS:	n.d.
HR-MS:	214.0862 [M+H$^+$]
HPLC:	10.153 min (99.52 %)

^{1}H NMR (400 MHz, DMSO-d6) δ 10.87 (s, 1H, N**H**OH), 9.10 (s, 1H, NHO**H**), 8.22 (d, *J* = 16.5 Hz, 1H, Hβ), 8.19 (d, *J* = 9.1 Hz, 1H, H8), 8.01 – 7.94 (m, 2H, H4, H5), 7.76 (d, *J* = 7.2 Hz, 1H, H2), 7.65 – 7.52 (m, 3H, H3, H6, H7), 6.55 (d, *J* = 15.6 Hz, 1H, Hα).

24zl (TB37) (2*E*)-*N*-hydroxy-2-methyl-3-phenylprop-2-enamide

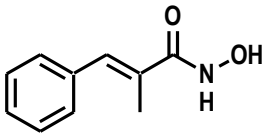

Appearance:	pale powder
Yield:	66 %
Mw:	177.20 g/mol
ESI-MS:	176.34 [M-H$^+$]
HR-MS:	178.0862 [M+H$^+$]
HPLC:	2.773 min (99.702 %)

^{1}H NMR (400 MHz, DMSO-d6) δ 10.81 (s, 1H, NHO**H**), 8.84 (s, 1H, N**H**OH), 7.41 (dt, *J* = 4.3, 1.7 Hz, 2H, H3, H5), 7.38 (dd, *J* = 5.5, 2.9 Hz, 2H, H2, H6), 7.31 (ddd, *J* = 6.0, 3.6, 1.7 Hz, 1H, H4), 7.12 (s, 1H, Hβ), 1.98 (d, *J* = 1.5 Hz, 3H, CH_3).

24zm (TB40) *N*-hydroxy-3-phenylprop-2-ynamide

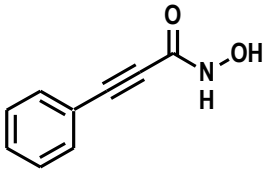

Appearance:	pale powder
Yield:	34 %
Mw:	161.20 g/mol
ESI-MS:	160.24 [M-H$^+$]
HR-MS:	162.0551 [M+H$^+$]
HPLC:	6.451 min (97.84 %)

^{1}H NMR (400 MHz, DMSO-d6) δ 11.29 (s, 1H, NHO**H**), 9.32 (s, 1H, N**H**OH), 7.59 – 7.43 (m, 5H, H2-H6).

26a (TB89) *N*-hydroxy-2-phenoxypropanamide

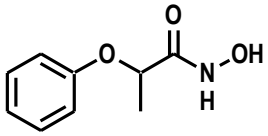

Appearance:	off-white powder
Yield:	70 %
Mw:	181.1886 g/mol
ESI-MS:	180.10 [M-H$^+$]
HR-MS:	204.0630[M+Na$^+$]
HPLC:	8.218 min (99.56 %)

^{1}H NMR (400 MHz, DMSO-d6) δ 10.81 (s, 1H, NHO**H**), 8.90 (s, 1H, N**H**OH), 7.31 – 7.25 (m, 2H, H3, H5), 6.97 – 6.88 (m, 3H, H2, H4, H6), 4.65 (q, *J* = 6.6 Hz, 1H, Hα), 1.43 (d, *J* = 6.6 Hz, 3H, C**H$_3$**).

26b (TB88) *N*-hydroxy-2-(2-methylphenoxy)acetamide

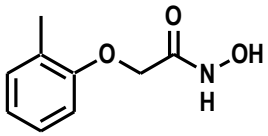

Appearance:	off-white powder
Yield:	y %
Mw:	181.1886 g/mol
ESI-MS:	180.10 [M-H$^+$]
HR-MS:	182.0810 [M+H$^+$]
HPLC:	5.433 min (98.99 %)

^{1}H NMR (400 MHz, DMSO-d6) δ 10.72 (s, 1H, NHO**H**), 8.96 (s, 1H, N**H**OH), 7.18 – 7.09 (m, *J* = 7.6 Hz, 2H, H3, H5), 6.90 – 6.80 (m, 2H, H4, H6), 4.46 (s, 2H, C**H$_2$**), 2.20 (s, 3H, C**H$_3$**).

26c (TB96) *N*-hydroxy-2-(2-methoxyphenoxy)acetamide

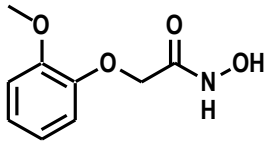

Appearance:	pale powder
Yield:	51 %
Mw:	197.1880 g/mol
ESI-MS:	n.d.
HR-MS:	198.0763 [M+H$^+$]
HPLC:	4.882 min (95.81 %)

^{1}H NMR (400 MHz, DMSO-d6) δ 10.70 (s, 1H, NHO**H**), 8.96 (s, 1H, N**H**OH), 6.97 (dd, *J* = 12.7, 4.7 Hz, 1H), 6.93 (d, *J* = 7.3 Hz, 2H), 6.89 – 6.83 (m, 1H), 4.40 (s, 2H, C**H$_2$**), 3.77 (s, 3H, C**H$_3$**).

26d (TB79) 2-[(3,4-dimethoxyphenyl)sulfanyl]-*N*-hydroxyacetamide

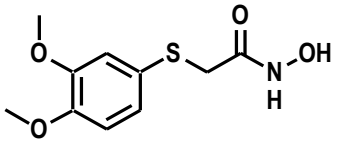

Appearance:	pale powder
Yield:	56 %
Mw:	243.2806 g/mol
ESI-MS:	242.13 [M-H$^+$]
HR-MS:	244.0638 [M+H$^+$]
HPLC:	5.488 min (97.09 %)

^{1}H NMR (400 MHz, DMSO-d6) δ 10.58 (s, 1H, NHO**H**), 8.94 (s, 1H, N**H**OH), 7.02 (d, *J* = 2.0 Hz, 1H, H6), 6.94 (d, *J* = 2.1 Hz, 1H, H5), 6.91 (s, 1H, H2), 3.75 (s, *J* = 2.6 Hz, 3H, C3-O-C**H$_3$**), 3.73 (s, 3H, C4-O-C**H$_3$**), 3.42 (s, 2H, C**H$_2$**).

26e (TB94) 2-[(2,5-dichlorophenyl)sulfanyl]-*N*-hydroxyacetamide

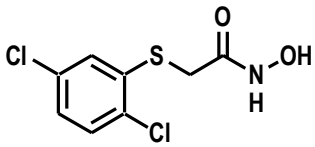

Appearance:	pale powder
Yield:	63 %
Mw:	252.1181 g/mol
ESI-MS:	249.98 [M-H$^+$]
HR-MS:	251.9649 [M+H$^+$]
HPLC:	8.028 min (98.88 %)

^{1}H NMR (400 MHz, DMSO-d6) δ 10.78 (s, 1H, NHO**H**), 9.07 (s, 1H, N**H**OH), 7.52 (d, *J* = 2.4 Hz, 1H, H6), 7.47 (d, *J* = 8.5 Hz, 1H, H3), 7.26 (dd, *J* = 8.5, 2.4 Hz, 1H, H4), 3.70 (s, 2H, C**H$_2$**).

26f (TB103) 2-[(4-chlorophenyl)sulfanyl]-*N*-hydroxyacetamide

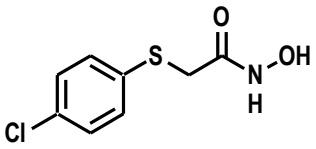

Appearance: white powder

Yield: 31%

Mw: 216.9964 g/mol

ESI-MS: n.d.

HR-MS: n.d.

HPLC: 6.585min (95.37 %)

^{1}H NMR (400 MHz, DMSO-d6) δ 10.69 (s, 1H), 8.99 (s, 1H), 7.43 – 7.34 (m, 4H), 3.54 (s, 2H).

26g (TB104) 2-[(2,6-dichlorophenyl)sulfanyl]-*N*-hydroxyacetamide

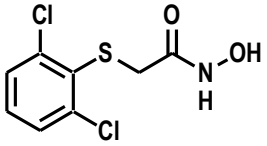

Appearance: white powder

Yield: 17 %

Mw: 252.1181 g/mol

ESI-MS: 250.21 [M-H$^+$]

HR-MS: n.d.

HPLC: 7.348 min (98.85 %)

^{1}H NMR (400 MHz, DMSO-d6) δ 10.79 (s, 1H), 9.27 (s, 1H), 7.58 (d, *J* = 2.5 Hz, 1H), 7.38 (dd, *J* = 8.9, 2.5 Hz, 1H), 7.09 (d, *J* = 8.9 Hz, 1H), 4.56 (s, 2H).

26h (TB105) 2-(2,4-dichlorophenoxy)-*N*-hydroxyacetamide

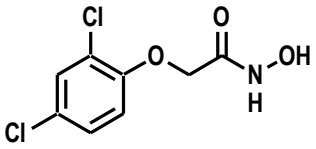

Appearance: white powder

Yield: 46 %

Mw: 236.0515 g/mol

ESI-MS: n.d.

HR-MS: n.d.

HPLC: 7.406 min (92.456%)

^{1}H NMR (400 MHz, DMSO-d6) δ 10.69 (s, 1H), 8.99 (s, 1H), 7.43 – 7.34 (m, 4H), 3.54 (s, 2H).

26i (TB90) *N*-hydroxy-2-[(naphthalen-2-yl)oxy]acetamid

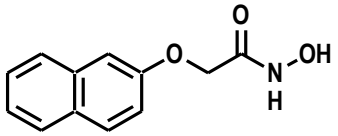

Appearance:	pale powder
Yield:	67 %
Mw:	217.2207 g/mol
ESI-MS:	n.d.
HR-MS:	240.0631[M+Na^+]
HPLC:	8.228 min (97.388 %)

^{1}H NMR (400 MHz, DMSO-d6) δ 10.90 (s, 1H, NHO**H**), 8.99 (s, 1H, N**H**OH), 7.84 (dd, *J* = 8.4, 3.1 Hz, 2H, H4, H5), 7.78 (d, *J* = 8.1 Hz, 1H, H8), 7.46 (dd, *J* = 11.1, 4.0 Hz, 1H, H7), 7.36 (dd, 1H, H6), 7.30 (d, *J* = 2.3 Hz, 1H, H1), 7.24 (dd, *J* = 8.9, 2.5 Hz, 1H, H3), 4.59 (s, 2H, C**H_2**).

26j (TB9) 7*N*-hydroxy-2-[(naphthalen-1-yl)oxy]acetamide

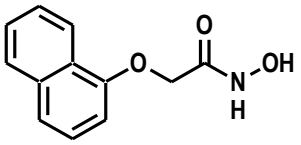

Appearance:	grey powder
Yield:	43 %
Mw:	217.2207 g/mol
ESI-MS:	216.34 [M-H^+]
HR-MS:	218.0813 [M+H^+]
HPLC:	8.303 min (97.71 %)

^{1}H NMR (400 MHz, DMSO-d6) δ 10.92 (s, 1H, NHO**H**), 9.02 (s, 1H, N**H**OH), 8.33 (d, *J* = 7.5 Hz, 1H, H8), 7.89 – 7.86 (m, 1H, H4), 7.56 – 7.48 (m, 3H, H5, H6, H7), 7.41 (t, *J* = 8.0 Hz, 1H, H3), 6.92 (d, *J* = 7.6 Hz, 1H, H2), 4.66 (s, 2H, C**H_2**).

26k (TB80) 2-[(8-chloronaphthalen-1-yl)sulfanyl]-*N*-hydroxyacetamide

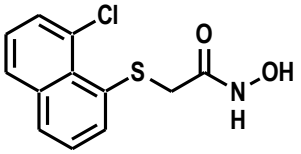

Appearance:	pale powder
Yield:	33 %
Mw:	267.7320 g/mol
ESI-MS:	266.29 [M-H^+]
HR-MS:	268.0194[M+H^+]
HPLC:	10.166 min (96.83 %)

^{1}H NMR (400 MHz, DMSO-d6) δ 10.76 (s, 1H, NHO**H**), 9.01 (s, 1H, N**H**OH), 7.92 (dd, *J* = 8.1, 0.9 Hz, 1H, H5), 7.80 (d, *J* = 7.5 Hz, 1H, H3), 7.64 (dd, *J* = 7.5, 1.2 Hz, 1H, H7), 7.58 (d, *J* = 6.9 Hz, 1H, H2), 7.47 (dt, *J* = 7.8, 2.7 Hz, 2H, H3, H6), 3.63 (s, 2H, C**H_2**).

28a (TB83) 4-[(2-chloro-5-oxo-5λ^4-phenothiazin-10(5*H*)-yl)methyl]-*N*-hydroxybenzamide

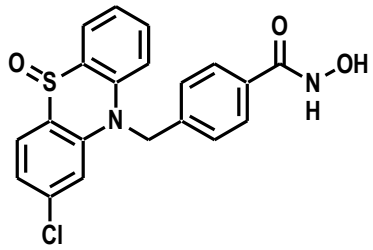

Appearance: pale blue powder

Yield: 37 %

Mw: 398.8635 g/mol

ESI-MS: 397.05 [M-H$^+$]

HR-MS: 399.0563[M+H$^+$]

HPLC: 9.910 min (97.95 %)

^{1}H NMR (400 MHz, DMSO-d6) δ 11.15 (s, 1H, NHO**H**), 9.00 (s, 1H, N**H**OH), 8.07 (d, *J* = 8.3 Hz, 1H, H4'), 8.03 (dd, *J* = 7.7, 1.6 Hz, 1H, H6'), 7.69 (d, *J* = 8.4 Hz, 2H, H2, H6), 7.63 (ddd, *J* = 8.7, 7.2, 1.6 Hz, 1H, H7'), 7.41 (d, *J* = 1.6 Hz, 1H, H1'), 7.38 (d, *J* = 8.6 Hz, 1H, H9'), 7.36 – 7.31 (m, *J* = 11.0, 6.3, 1.3 Hz, 2H, H3', H8'), 7.21 (d, *J* = 8.3 Hz, 2H, H3, H5), 5.81 – 5.68 (m, 2H, C**H$_2$**).

6.4 Biological assays

6.4.1 Pharmacokinetic studies (Kancera/Adlego)

Preparation of dose solutions for Stage 1 PK study of **24zh** (TB56) and **24x** (TB87)

Test compound concentration: 5 mg/ml

Dosing p.o.: one dose 50 mg/kg

Dosing i.v.: one dose 50 mg/kg

Final formulation: 7% DMSO, and 35% w/v HPβCD in Dubelcco's Phosphate buffered saline (DPBS), pH 6-8.

Storage: room temperature.

Solutions necessary to prepare the dosing solution

DMSO

50% w/v solution of HPβCD in distilled water

Dubelcco's Phosphate buffered saline (DPBS)

HCl and NaOH solutions for pH corrections if needed

Preparation of 50% w/v solution of HPβCD in distilled water

(2-hydroxypropyl)-β-cyclodextrin from Sigma-Aldrich (332607-100G; Lot # BCBN8227V) was used. Test preparing the 50% HPβCD solution well before making the formulation.

For the preparation e.g. a bit more than 10 ml of a 50% (w/v) HPβCD solution:

10 g of HPβCD were weighed into a glass beaker.

10 ml of distilled water was added, then the beaker was installed on a slow moving shaking table for 2-4 hours. Very slowly the powder becomes wet and eventually dissolves. After all powder has dissolved and the mixture looks homogenous it is sonicated and transferred to a Falcon tube.

The solution was stored at room temperature.

Formulation for **24zh** (TB56) and **24x** (TB87) (5 mg/ml; 7% DMSO, 35% HPbCD in DPBS, pH ca 7). The compound was weighed into a glass vial and dissolved in DMSO (7 % of the final volume).

An appropriate volume of 50% HPβCD solution was added to end up with 35% HPβCD in the calculated final volume. The mixture was again sonicated for 15 minutes.

An appropriate volume of DPBS was added to achieve the calculated final volume and the mixture was again sonicated for 10-20 minutes.

The solution was filtrated with a sterile filter (0.2 µm) into a sterile tube it is stable at least over night at room temperature.

The compound TB56 has been subjected to an initial in-vitro evaluation study followed by a Stage 1 PK study using the dose 50 mg/kg **24zh** (TB56) both p.o. and i.v.

The in-vitro evaluation study was performed at Kancera and consists of the following steps:

QC of compound (Identity, Purity and Chemical Stability).

Determination of the kinetic solubility of the compound in buffer.

Development of an MRM method.

Testing of a small number of standard formulations.

The Stage 1 PK study consists of the following steps:

Preparation of dose solution for the in-vivo experiments (Kancera).

Administration of compound to mice (Adlego)

2 male mice intravenously (i.v.); blood sampling at 15, 60 and 180 min.

2 male mice orally by gavage (p.o.); blood sampling at 30, 60 and 180 min.

Following the last blood sample the animals are euthanized and urine is collected from the bladder.

The health status of the mice is documented at sampling times.

Bioanalysis of plasma samples by LC-MS/MS (Kancera).

6.4.2 Toxicity assay on HEK293

For the toxicity assay the compounds have been tested on HEK293 cells. HEK293 is an epithelial kidney cell line that is immortalized by an adenovirus[117]. The toxicity of the compounds was tested in an alamarBlue® assay *(Trek Diagnostic Systems, Inc)*. The assay works with resazurin which is a blue dye that is sensitive to reduction and is converted into the red and fluorescent resorufin in living cells[118–122].

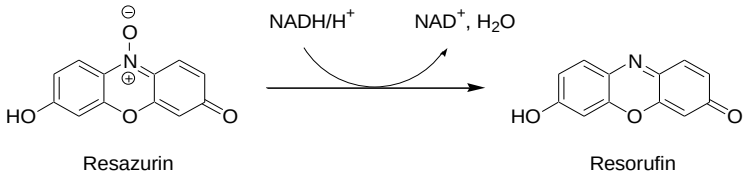

Figure 55 Scheme of the conversion of resazurin into resorufin

A solution of the compound was added to a 200 µl off cell suspension (approximately 10^5 cells) and was incubated for 24 h at 37 °C. Then the alamarBlue® solution was added and the batch was incubated for another 24 h. A control of cell suspension and DMSO and the indicator solution as well as a blanc control of just DMSO and indicator solution were treated the same way. Then the fluorescence was measured. Since the fluorescence is proportional to the amount of viable cells the percentages of the viable cells compared to the untreated controls could be estimated.

Values greater than 100 % could be explained by either division of the cells and therefore simply a greater number of cells or a formation of more mitochondria in the cells without a change in the number of the cells themselves.

7 Bibliography

1. Colley, D. G., Bustinduy, A. L., Secor, W. E. & King, C. H. Human schistosomiasis. *Lancet (London, England)* **383**, 2253–64 (2014).

2. Deribew, K. & Petros, B. Efficacy of praziquantel for the treatment of schistosomiasis in Ethiopia. *Int. J. Med. Med. Sci.* **5**, 131–139 (2013).

3. Gray, D. J. & Ross, A. G. Diagnosis and management of schistosomiasis Early manifestations. *Br. Med. Journaledicinal J.* 1–12 (2011). doi:10.1136/bmj.d2651

4. Cabezas-Cruz, A. Epigenetic control of gene function in schistosomes: a source of therapeutic targets? *Front. Genet.* **5**, 1–12 (2014).

5. Marek, M. *et al.* Structural basis for the inhibition of histone deacetylase 8 (HDAC8), a key epigenetic player in the blood fluke Schistosoma mansoni. *PLoS Pathog.* **9**, e1003645 (2013).

6. Ross, A. G. *et al.* Schistosomiasis. *N. Engl. J. Med.* **346**, 1212–1220 (2002).

7. G. Burchard, S. Ehrhardt, M. Grobusch, T. Junghanss, T. Löscher, E. Reisinger, J. Richter, A. Stich, H. Sudeck, D. G. für T. und I. G. Leitlinie : Diagnostik und Therapie der Schistosomiasis (Bilharziose). 1–36 (2013).

8. Fenwick, A. *et al.* The Schistosomiasis Control Initiative (SCI): rationale, development and implementation from 2002-2008. *Parasitology* **136**, 1719–30 (2009).

9. Kumar, V. & Gryseels, B. Use of praziquantel against schistosomiasis : a review of current status. *Int. J. Antimicrob. Agents* **4**, 313–320 (2000).

10. Danso-Appiah, A. & De Vlas, S. J. Interpreting low praziquantel cure rates of Schistosoma mansoni infections in Senegal. *Trends Parasitol.* **18**, 125–129 (2002).

11. Ismail, M. *et al.* Resistance to praziquantel: direct evidence from Schistosoma mansoni isolated from Egyptian villagers. *Am. J. Trop. Med. Hyg.* **60**, 932–5 (1999).

12. Garske, A. L. & Denu, J. M. New Frontiersin Epigenetic Modifications. in *Epigenetic Targets in Drug Discovery* (eds. Sippl, P. D. W. & Jung, P. D. M.) 1–17 (Wiley-VCH, 2009).

13. Arrowsmith, C. H., Bountra, C., Fish, P. V, Lee, K. & Schapira, M. Epigenetic protein families: a new frontier for drug discovery. *Nat. Rev. Drug Discov.* **11**, 384–

400 (2012).

14. Kornberg, R. D. & Lorch, Y. Twenty-five years of the nucleosome, fundamental particle of the eukaryote chromosome. *Cell* **98**, 285–94 (1999).

15. Cheung, W. L., Briggs, S. D. & Allis, C. D. Acetylation and chromosomal functions. *Curr. Opin. Cell Biol.* **12**, 326–33 (2000).

16. Witter, D. J. *et al.* Benzo[b]thiophene-based histone deacetylase inhibitors. *Bioorg. Med. Chem. Lett.* **17**, 4562–7 (2007).

17. Huang, L. Targeting histone deacetylases for the treatment of cancer and inflammatory diseases. *J. Cell. Physiol.* **209**, 611–6 (2006).

18. Romier, C., Wurtz, J.-M., Renaud, J.-P. & Cavarelli, J. Structural Biology of Epigenetic Targets. in *Epigenetic Targets in Drug Discovery* (eds. Sippl, W. & Jung, M.) 23–56 (Wiley-VCH, 2009).

19. Coura, J. R. & Borges-Pereira, J. Chagas disease: 100 years after its discovery. A systemic review. *Acta Trop.* **115**, 5–13 (2010).

20. Rassi, A., Rassi, A. & Marcondes de Rezende, J. American Trypanosomiasis (Chagas Disease). *Infectious Disease Clinics of North America* **26**, 275–291 (2012).

21. Brum-Soares, L. *et al.* High seroconversion rates in Trypanosoma cruzi chronic infection treated with benznidazole in people under 16 years in Guatemala. *Rev. Soc. Bras. Med. Trop.* **49**, 721–727 (2016).

22. Murcia, L. *et al.* Risk Factors and Primary Prevention of Congenital Chagas Disease in a Nonendemic Country. *Clin. Infect. Dis.* **56**, 496–502 (2013).

23. Fabbro, D. L. *et al.* Trypanocide Treatment of Women Infected with Trypanosoma cruzi and Its Effect on Preventing Congenital Chagas. *PLoS Negl. Trop. Dis.* **8**, e3312 (2014).

24. Schmunis, G. A. & Yadon, Z. E. Chagas disease: A Latin American health problem becoming a world health problem. *Acta Trop.* **115**, 14–21 (2010).

25. Sáez-Alquezar, A., Albajar-Viñas, P., Guimarães, A. V. & Corrêa, J. A. Quality Control in Screening for Infectious Diseases at Blood Banks. Rationale and Methodology. *Ejifcc* **26**, 278–85 (2015).

26. Mueller, I., Zimmerman, P. A. & Reeder, J. C. Plasmodium malariae and

Plasmodium ovale--the "bashful" malaria parasites. *Trends Parasitol.* **23**, 278–83 (2007).

27. Collins, W. E. Plasmodium knowlesi: A Malaria Parasite of Monkeys and Humans. *Annu. Rev. Entomol.* **57**, 107–121 (2012).

28. Nadjm, B. & Behrens, R. H. Malaria: An Update for Physicians. *Infect. Dis. Clin. North Am.* **26**, 243–259 (2012).

29. WHO | World malaria report 2018. *WHO* (2018).

30. Crutcher, J. M. & Hoffman, S. L. *Malaria*. *Medical Microbiology* (University of Texas Medical Branch at Galveston, 1996).

31. Bartoloni, A. & Zammarchi, L. CLINICAL ASPECTS OF UNCOMPLICATED AND SEVERE MALARIA. *Mediterr. J. Hematol. Infect. Dis.* **4**, 2012026 (2012).

32. WHO Fact sheet Malaria. Available at: https://www.who.int/en/news-room/fact-sheets/detail/malaria. (Accessed: 9th December 2018)

33. Tickell-Painter, M., Maayan, N., Saunders, R., Pace, C. & Sinclair, D. Mefloquine for preventing malaria during travel to endemic areas. *Cochrane database Syst. Rev.* **10**, CD006491 (2017).

34. Mylonas, I. Antibiotic chemotherapy during pregnancy and lactation period: aspects for consideration. *Arch. Gynecol. Obstet.* **283**, 7–18 (2011).

35. Griffiths AJF, Miller JH, Suzuki DT, et al. *An Introduction to Genetic Anlysis*. (2000).

36. Bird, A. Perceptions of epigenetics. *Nat. 2007 4477143* (2007).

37. Bennett, M. R. *et al.* Metabolic gene regulation in a dynamically changing environment. *Nature* **454**, 1119–22 (2008).

38. Turner, B. M. Environmental sensing by chromatin: An epigenetic contribution to evolutionary change. *FEBS Lett.* **585**, 2032–2040 (2011).

39. Yoo, C. B. & Jones, P. A. Epigenetic therapy of cancer: past, present and future. *Nat. Rev. Drug Discov.* **5**, 37–50 (2006).

40. Turner, B. M. The adjustable nucleosome: an epigenetic signaling module. *Trends Genet.* **28**, 436–444 (2012).

41. Klose, R. J. & Bird, A. P. Genomic DNA methylation: the mark and its mediators. *Trends Biochem. Sci.* **31**, 89–97 (2006).

42. Bernstein, B. E. *et al.* A Bivalent Chromatin Structure Marks Key Developmental Genes in Embryonic Stem Cells. *Cell* **125**, 315–326 (2006).

43. Azuara, V. *et al.* Chromatin signatures of pluripotent cell lines. *Nat. Cell Biol.* **8**, 532–538 (2006).

44. Smeenk, G. & Mailand, N. Writers, readers, and erasers of histone ubiquitylation in DNA double-strand break repair. *Front. Genet.* **7**, 1–14 (2016).

45. Berger, S. L., Kouzarides, T., Shiekhattar, R. & Shilatifard, A. An operational definition of epigenetics. *Genes Dev.* **23**, 781–3 (2009).

46. RUIJTER, A. J. M. de, GENNIP, A. H. van, CARON, H. N., KEMP, S. & KUILENBURG, A. B. P. van. Histone deacetylases (HDACs): characterization of the classical HDAC family. *Biochem. J.* **370**, 737–749 (2003).

47. Woodcock, C. L., Skoultchi, A. I. & Fan, Y. Role of linker histone in chromatin structure and function: H1 stoichiometry and nucleosome repeat length. *Chromosom. Res.* **14**, 17–25 (2006).

48. Szerlong, H. J. & Hansen, J. C. Nucleosome distribution and linker DNA: connecting nuclear function to dynamic chromatin structure. *Biochem. Cell Biol.* **89**, 24–34 (2011).

49. Pieterman, C. R. C. *et al.* Thoracic and duodenopancreatic neuroendocrine tumors in multiple endocrine neoplasia type 1: Natural history and function of menin in tumorigenesis. *Endocr. Relat. Cancer* **21**, (2014).

50. Falkenberg, K. J. & Johnstone, R. W. Histone deacetylases and their inhibitors in cancer, neurological diseases and immune disorders. *Nat. Rev. Drug Discov.* **13**, 673–691 (2014).

51. Rodd, A. L., Ververis, K. & Karagiannis, T. C. Current and Emerging Therapeutics for Cutaneous T-Cell Lymphoma: Histone Deacetylase Inhibitors. *Lymphoma* **2012**, 1–10 (2012).

52. Bayer, T. *et al.* Synthesis, Crystallization Studies, and in vitro Characterization of Cinnamic Acid Derivatives as SmHDAC8 Inhibitors for the Treatment of

Schistosomiasis. *ChemMedChem* **13**, 1517–1529 (2018).

53. Olson, D. E. *et al.* An Unbiased Approach To Identify Endogenous Substrates of 'Histone' Deacetylase 8. *ACS Chem. Biol.* **18**, (2014).

54. Sippl, W. & Jung, M. *Epigenetic Targets in Drug Discovery*. (WILEY-VCH Verlag, 2009).

55. Glozak, M. A., Sengupta, N., Zhang, X. & Seto, E. Acetylation and deacetylation of non-histone proteins. *Gene* **363**, 15–23 (2005).

56. Bjerling, P. & Silverstein, R. Functional divergence between histone deacetylases in fission yeast by distinct cellular localization and in vivo specificity. *... Cell. Biol.* **22**, 2170–81 (2002).

57. Villagra, A., Sotomayor, E. M. & Seto, E. Histone deacetylases and the immunological network: Implications in cancer and inflammation. *Oncogene* **29**, 157–173 (2010).

58. BUGGY, J. J. *et al.* Cloning and characterization of a novel human histone deacetylase, HDAC8. *Biochem. J.* **350**, 199–205 (2000).

59. Vannini, A. *et al.* Crystal structure of a eukaryotic zinc-dependent histone deacetylase, human HDAC8, complexed with a hydroxamic acid inhibitor. *Proc. Natl. Acad. Sci.* **101**, 15064–15069 (2004).

60. Somoza, J. R. *et al.* Structural snapshots of human HDAC8 provide insights into the class I histone deacetylases. *Structure* **12**, 1325–1334 (2004).

61. Vannini, A. *et al.* Substrate binding to histone deacetylases as shown by the crystal structure of the HDAC8–substrate complex. *EMBO Rep.* **8**, 879–884 (2007).

62. Vanommeslaeghe, K., Proft, F. De, Loverix, S., Tourwé, D. & Geerlings, P. Theoretical study revealing the functioning of a novel combination of catalytic motifs in histone deacetylase. *Bioorg. Med. Chem.* **13**, 3987–3992 (2005).

63. Andrews, K. T., Haque, A. & Jones, M. K. HDAC inhibitors in parasitic diseases. *Immunol. Cell Biol.* **90**, 66–77 (2012).

64. Lombardi, P. M., Cole, K. E., Dowling, D. P. & Christianson, D. W. Structure, mechanism, and inhibition of histone deacetylases and related metalloenzymes. *Curr. Opin. Struct. Biol.* **21**, 735–43 (2011).

65. Nwaka, S. & Hudson, A. Innovative lead discovery strategies for tropical diseases. *Nat. Rev. Drug Discov.* **5**, 941–955 (2006).

66. Niegisch, G. *et al.* Changes in histone deacetylase (HDAC) expression patterns and activity of HDAC inhibitors in urothelial cancers. *Urol. Oncol.* **31**, 1770–9 (2013).

67. Plumb, J. A. *et al.* Pharmacodynamic response and inhibition of growth of human tumor xenografts by the novel histone deacetylase inhibitor PXD101. *Mol. Cancer Ther.* **2**, 721–8 (2003).

68. Pierce, R. J., Dubois-Abdesselem, F., Lancelot, J., Andrade, L. & Oliveira, G. Targeting schistosome histone modifying enzymes for drug development. *Curr. Pharm. Des.* **18**, 3567–78 (2012).

69. Dubois, F. *et al.* Histone deacetylase inhibitors induce apoptosis, histone hyperacetylation and up-regulation of gene transcription in Schistosoma mansoni. *Mol. Biochem. Parasitol.* **168**, 7–15 (2009).

70. Azzi, A., Cosseau, C. & Grunau, C. Schistosoma mansoni: Developmental arrest of miracidia treated with histone deacetylase inhibitors. *Exp. Parasitol.* **121**, 288–291 (2009).

71. Kannan, S. *et al.* Discovery of inhibitors of Schistosoma mansoni HDAC8 by combining homology modeling, virtual screening, and in vitro validation. *J. Chem. Inf. Model.* **54**, 3005–19 (2014).

72. Ballante, F., Reddy, D. R., Zhou, N. J. & Marshall, G. R. Structural insights of SmKDAC8 inhibitors: Targeting Schistosoma epigenetics through a combined structure-based 3D QSAR, in vitro and synthesis strategy. *Bioorganic Med. Chem.* **25**, 2105–2132 (2017).

73. Heimburg, T. *et al.* Structure-Based Design and Synthesis of Novel Inhibitors Targeting HDAC8 from Schistosoma mansoni for the Treatment of Schistosomiasis. *J. Med. Chem.* **59**, 2423–2435 (2016).

74. Stolfa, D. A. *et al.* Molecular basis for the antiparasitic activity of a mercaptoacetamide derivative that inhibits histone deacetylase 8 (HDAC8) from the human pathogen schistosoma mansoni. *J. Mol. Biol.* **426**, (2014).

75. Stenzel, K. *et al.* Isophthalic Acid-Based HDAC Inhibitors as Potent Inhibitors of HDAC8 from *Schistosoma mansoni*. *Arch. Pharm. (Weinheim).* **350**, 1700096

(2017).

76. Kannan, S. *et al.* Discovery of Inhibitors of Schistosoma mansoni HDAC8 by Combining Homology Modeling, Virtual Screening, and in Vitro Validation. *J. Chem. Inf. Model.* (2014). doi:10.1021/ci5004653

77. Marks, P. A. & Breslow, R. Dimethyl sulfoxide to vorinostat: development of this histone deacetylase inhibitor as an anticancer drug. *Nat. Biotechnol.* **25**, 84–90 (2007).

78. Cannova, C. *et al.* Apicidin: A novel antiprotozoal agent that inhibits parasite histone deacetylase. *Proc. Natl. Acad. Sci.* **93**, 13143–13147 (2002).

79. Schwetlick, K. *et al. Organikum*. (Wiley-VCH, 2009).

80. Adams, R., Clarke, H. T., Conant, J. B. & Kamm, O. *Organic syntheses.* (J. Wiley & Sons).

81. Bauer, L. & Exner, O. Die Chemie der Hydroxamsäuren undN-Hydroxyimide. *Angew. Chemie* **86**, 419–428 (1974).

82. Al-Warhi, T. I., Al-Hazimi, H. M. A. & El-Faham, A. Recent development in peptide coupling reagents. *J. Saudi Chem. Soc.* **16**, 97–116 (2012).

83. Sheehan, J. C. & Hess, G. P. A New Method of Forming Peptide Bonds. *J. Am. Chem. Soc.* **77**, 1067–1068 (1955).

84. Castro, B., Oormoy, J. R. & Selve, G. E. C. Reactifs de couplage peptidique IV - l'Hexafluorophosphate de benzotriazolyl N-oxytridimethylamino phosphonium. *Tetrahedron Lett.* 1219–1222 (1975).

85. Coste, J., Le-Nguyen, D. & Castro, B. PyBOP®: A New Peptide Coupling Reagent Devoid of Toxic By-Product. *Tetrahedron Lett.* **31**, 205–208

86. Kim, M. H. & Patel, D. V. " BOP " as a reagent for mild and efficient preparation of esters. *Tetrahedron Lett.* **35**, 5603–5606 (1994).

87. Misra, R. N. *et al.* CYCLIC ARYL HYDBOXAMIC ACIDS : SYNTHESIS AND INHIBITION OF J-LIPOXYGENASE. *Bioorg. Med. Chem. Lett.* **1**, 295–298 (1991).

88. Kocienski, P. J. *Protecting groups*. (Georg Thieme, 2004).

89. Treibs, W. & Orttmann, H. Über Carbobromierung, III. Carbobromierung einiger Olefine und benzoider sowie nicht benzoider Aromaten. *Chem. Ber.* **93**, 545–551 (1960).

90. Varnavas, A. *et al.* Anthranilic acid based CCK1 antagonists: the 2-indole moiety may represent a 'needle' according to the recent homonymous concept. *Eur. J. Med. Chem.* **39**, 85–97 (2004).

91. Rosauer, K. G. *et al.* Novel 3,4-Dihydroquinolin-2(1H)-one inhibitors of human glycogen phosphorylase a. *Bioorg. Med. Chem. Lett.* **13**, 4385–4388 (2003).

92. Parekh, S. *et al.* Synthesis of some novel benzofuran-2-yl(4,5-dihyro-3,5-substituted diphenylpyrazol-1-yl) methanones and studies on the antiproliferative effects and reversal of multidrug resistance of human MDR1-gene transfected mouse lymphoma cells in vitro. *Eur. J. Med. Chem.* **46**, 1942–8 (2011).

93. Kumaraswamy, G., Ramakrishna, G., Raju, R. & Padmaja, M. An expedient synthesis of enantioenriched substituted (2-benzofuryl)arylcarbinols via tandem Rap–Stoermer and asymmetric transfer hydrogenation reactions. *Tetrahedron* **66**, 9814–9818 (2010).

94. Cai, J. *et al.* Design, synthesis, and in vitro antiproliferative activity of novel Dasatinib derivatives. *Bioorg. Med. Chem. Lett.* **22**, 806–10 (2012).

95. Brückner, R. *Reaktionsmechanismen*. (Springer Spektrum, 2004).

96. Peng, Y. & Song, G. Combined microwave and ultrasound accelerated Knoevenagel–Doebner reaction in aqueous media: a green route to 3-aryl acrylic acids. *Green Chem.* **5**, 704–706 (2003).

97. Heck, R. F. & Nolley, J. P. Palladium-catalyzed vinylic hydrogen substitution reactions with aryl, benzyl, and styryl halides. *J. Org. Chem.* **37**, 2320–2322 (1972).

98. Heck, R. F. Palladium-catalyzed reactions of organic halides with olefins. *Acc. Chem. Res.* **12**, 146 (1979).

99. Fan, X., You, J., Jiao, T., Tan, G. & Yu, X. Rapid N-Alkylation of Carbazole, Phenothiazlne and Acridone Under Microwave Irradiation. *Org. Prep. Proced. Int.* **32**, 284–287 (2000).

100. Trapp, J. Neue Testsysteme und Hemmstoffe für NAD + -abhängige

Histondesacetylasen. (2007).

101. Hildmann, C. *et al.* Substrate and inhibitor specificity of class 1 and class 2 histone deacetylases. *J. Biotechnol.* **124**, 258–270 (2006).

102. Heltweg, B., Trapp, J. & Jung, M. In vitro assays for the determination of histone deacetylase activity. *Methods* **36**, 332–7 (2005).

103. Wegener, D., Hildmann, C., Riester, D. & Schwienhorst, A. Improved fluorogenic histone deacetylase assay for high-throughput-screening applications. *Anal. Biochem.* **321**, 202–208 (2003).

104. Molecular Operating environment (MOE), 2014.09; Chemical Computing Group Inc.,1010 Sherbrook St. West, Suite # 910, Montreal, QC H3A 2R7, Canada, 2014.

105. Panic, G., Flores, D., Ingram-sieber, K. & Keiser, J. Fluorescence / luminescence-based markers for the assessment of Schistosoma mansoni schistosomula drug assays. *Parasit. Vectors* 1–12 (2015). doi:10.1186/s13071-015-1233-3

106. Godoy, L. Identification of novel PTMs in T. cruzi histones. *Intern. A-ParaDDisE Data*

107. Picchi, G. F. A. *et al.* Post-translational Modifications of Trypanosoma cruzi Canonical and Variant Histones. *J. Proteome Res.* **16**, 1167–1179 (2017).

108. A-ParaDDisE Final meeting DRAFT minutes v1b.

109. Romanha, A. J. *et al.* In vitro and in vivo experimental models for drug screening and development for Chagas disease. *Mem. Inst. Oswaldo Cruz* **105**, 233–238 (2010).

110. Andrews, K. T. *et al.* Potent antimalarial activity of histone deacetylase inhibitor analogues. *Antimicrob. Agents Chemother.* **52**, 1454–61 (2008).

111. Chua, M. J. *et al.* Effect of clinically approved HDAC inhibitors on Plasmodium, Leishmania and Schistosoma parasite growth. *Int. J. Parasitol. Drugs drug Resist.* **7**, 42–50 (2017).

112. Engel, J. A. *et al.* Profiling the anti-protozoal activity of anti-cancer HDAC inhibitors against Plasmodium and Trypanosoma parasites. *Int. J. Parasitol. Drugs Drug Resist.* **5**, 117–126 (2015).

113. Berman, H. M. *et al.* The Protein Data Bank. *Nucleic Acid Res.* **28**, 235–242 (2000).

114. Schrödinger Release 2014-2: Schrödinger Suite 2014-2 Protein Preparation Wizard; Epik version 2.8, Schrödinger, LLC, New York, NY, 2014; Impact version 6.3, Schrödinger, LLC, New York, NY, 2014; Prime version 3.6, Schrödinger, LLC, New York, NY, 2014.

115. Schrödinger Release 2014-2: LigPrep, Schrödinger, LLC, New York, NY, 2014.

116. Small-Molecule Drug Discovery Suite 2014-2: Glide, version 9.8, Schrödinger, LLC, New York, NY, 2014. Small-Molecule Drug Discovery Suite 2014-2: Glide, version 9.8, Schrödinger, LLC, New York, NY, 2014o Title.

117. Graham, F. L., Smiley, J., Russell, W. C. & Nairn, R. Characteristics of a human cell line transformed by DNA from human adenovirus type 5. *J. Gen. Virol.* **36**, 59–74 (1977).

118. Twigg, R. S. Oxidation-Reduction Aspects of Resazurin. *Nature* **155**, 401/402 (1945).

119. Larson, E. M., Doughman, D. J., Gregerson, D. S. & Obritsch, W. F. A new, simple, nonradioactive, nontoxic in vitro assay to monitor corneal endothelial cell viability. *Invest. Ophthalmol. Vis. Sci.* **38**, 1929–33 (1997).

120. Shiloh, M., Ruan, J. & Nathan, C. Evaluation of bacterial survival and phagocyte function with a fluorescence-based microplate assay. *Infect. Immun.* **65**, 3193–3198 (1997).

121. Bopp, S. K. & Lettieri, T. Comparison of four different colorimetric and fluorometric cytotoxicity assays in a zebrafish liver cell line. *BMC Pharmacol.* **8**, 8 (2008).

122. Wei, G.-X., Campagna, A. N. & Bobek, L. A. Effect of MUC7 peptides on the growth of bacteria and on Streptococcus mutans biofilm. *J. Antimicrob. Chemother.* **57**, 1100–9 (2006).

123. CDC - Schistosomiasis - Biology. Available at: https://www.cdc.gov/parasites/schistosomiasis/biology.html. (Accessed: 9th December 2018)

124. Cantey, P. T. *et al.* The United States Trypanosoma cruzi Infection Study: evidence for vector-borne transmission of the parasite that causes Chagas disease among United States blood donors. *Transfusion* **52**, 1922–1930 (2012).

125. Prevention, C.-C. for D. C. and. CDC - Malaria - About Malaria - Biology. (2018).

8 Appendix

8.1 Copies of relevant spectra

22a (TB1)

HPLC

<Chromatogram>

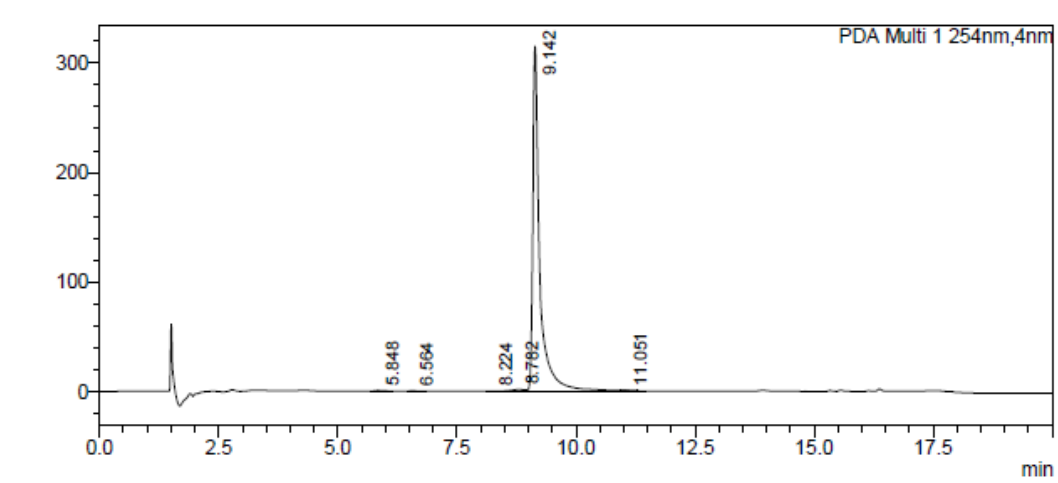

<Peak Table>

PDA Ch1 254nm

Peak#	Ret. Time	Area%	Area	Height
1	5.848	0.134	4347	367
2	6.564	0.057	1833	241
3	8.224	0.045	1447	78
4	8.782	0.701	22662	1186
5	9.142	99.018	3200671	315052
6	11.051	0.045	1456	197
Total		100.000	3232416	317120

^{1}H-NMR

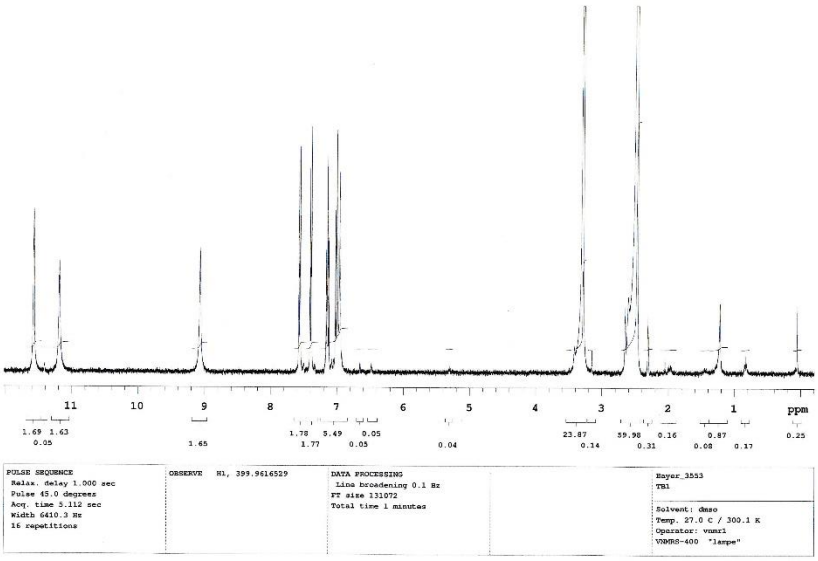

22b (TB13)

HPLC

<Chromatogram>

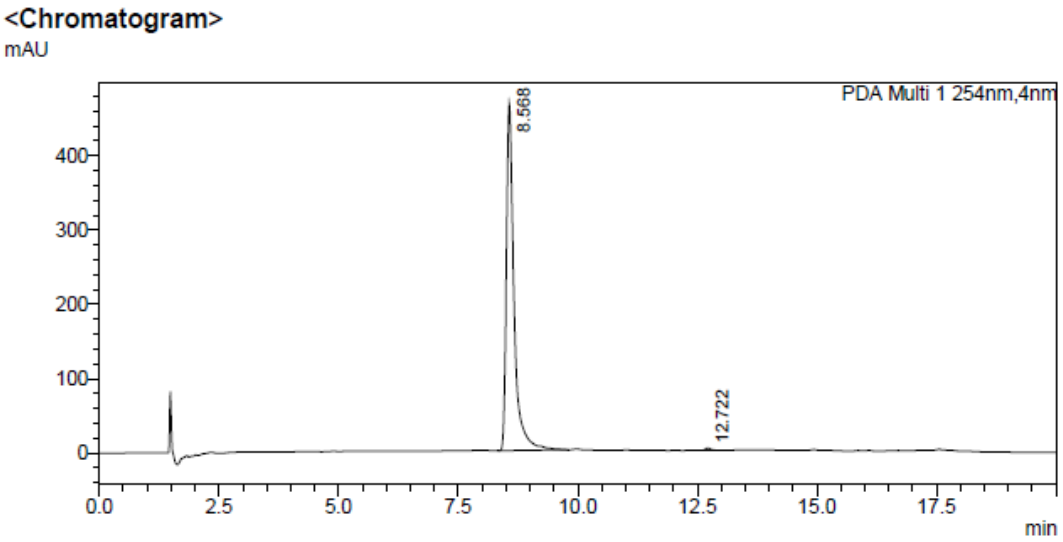

<Peak Table>

PDA Ch1 254nm

Peak#	Ret. Time	Area%	Area	Height
1	8.568	99.403	5190758	467036
2	12.722	0.597	31155	3502
Total		100.000	5221913	470538

^{1}H-NMR

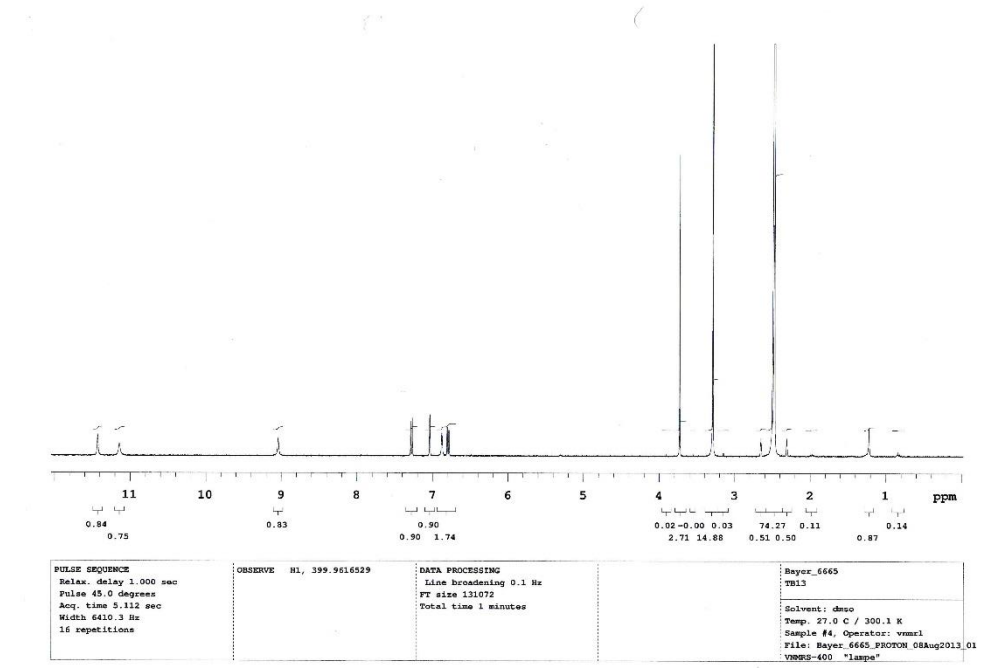

22c (TB74)

HPLC

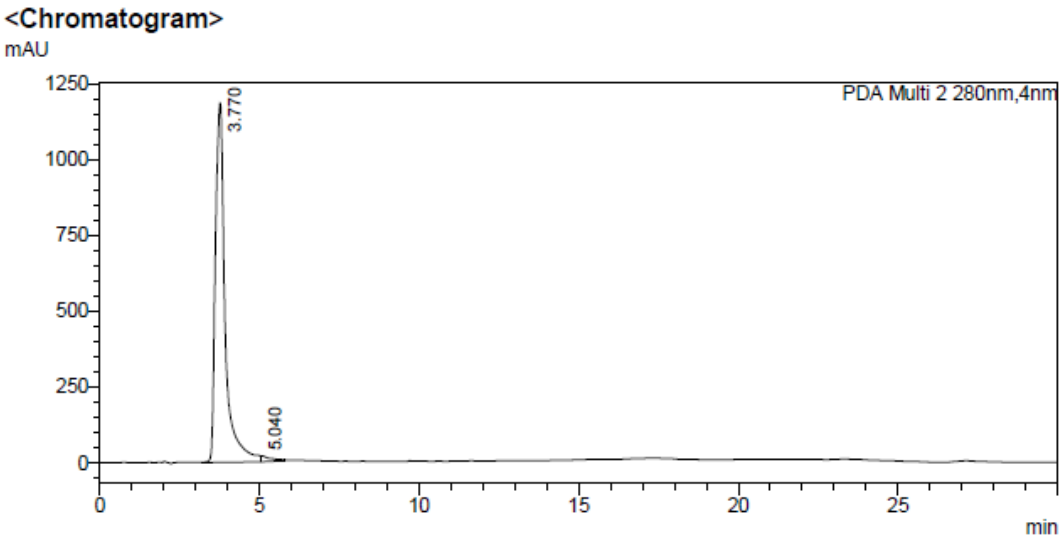

<Peak Table>

PDA Ch2 280nm

Peak#	Ret. Time	Area%	Area	Height
1	3.770	98.313	25102180	1185251
2	5.040	1.687	430729	19449
Total		100.000	25532909	1204701

^{1}H-NMR

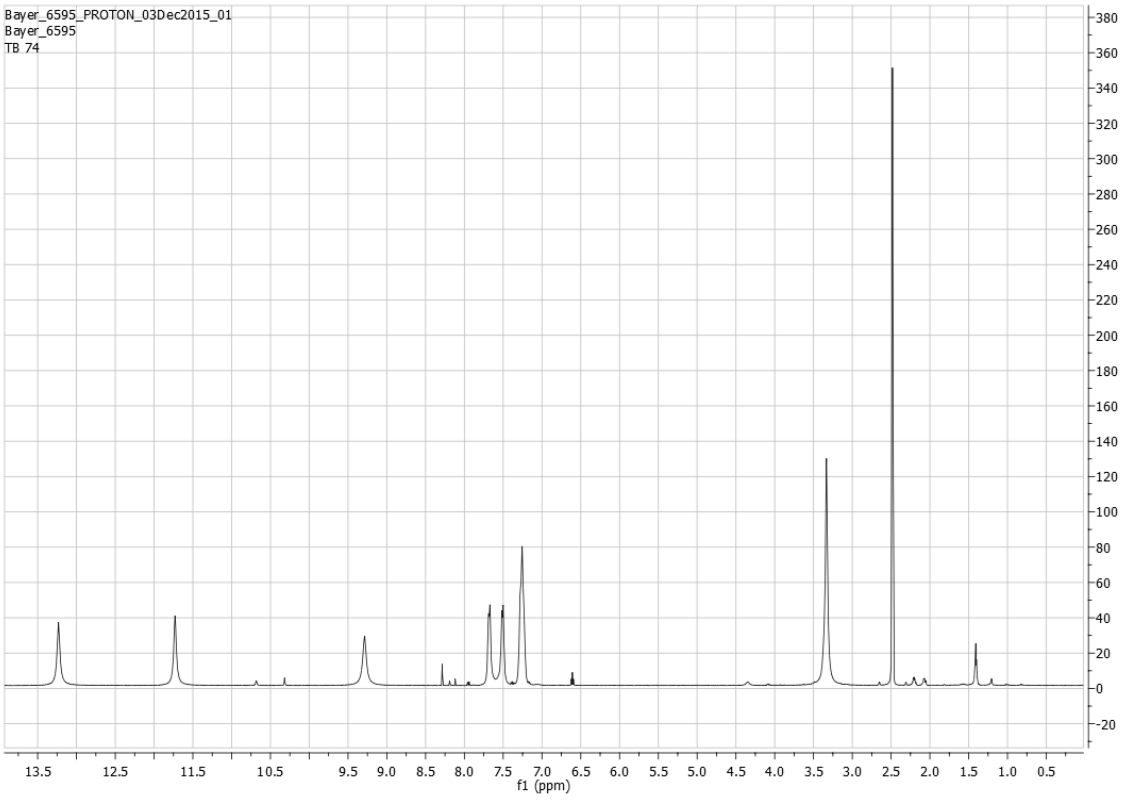

22d (TB2)

HPLC

<Chromatogram>

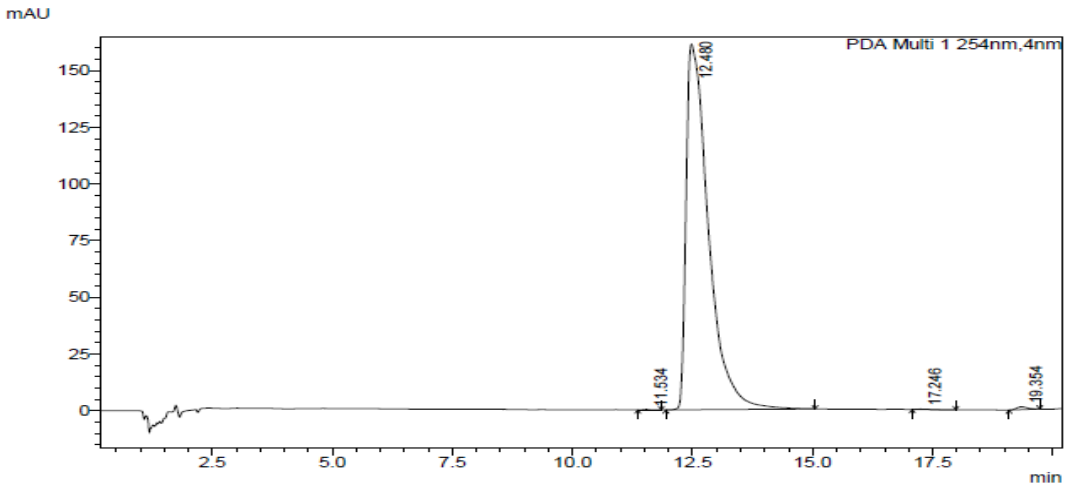

<Peak Table>

PDA Ch1 254nm

Peak#	Ret. Time	Area%	Area	Height
1	11.534	0.045	2375	208
2	12.480	99.512	5211725	161341
3	17.246	0.082	4278	221
4	19.354	0.361	18915	1255
Total		100.000	5237293	163026

^{1}H-NMR

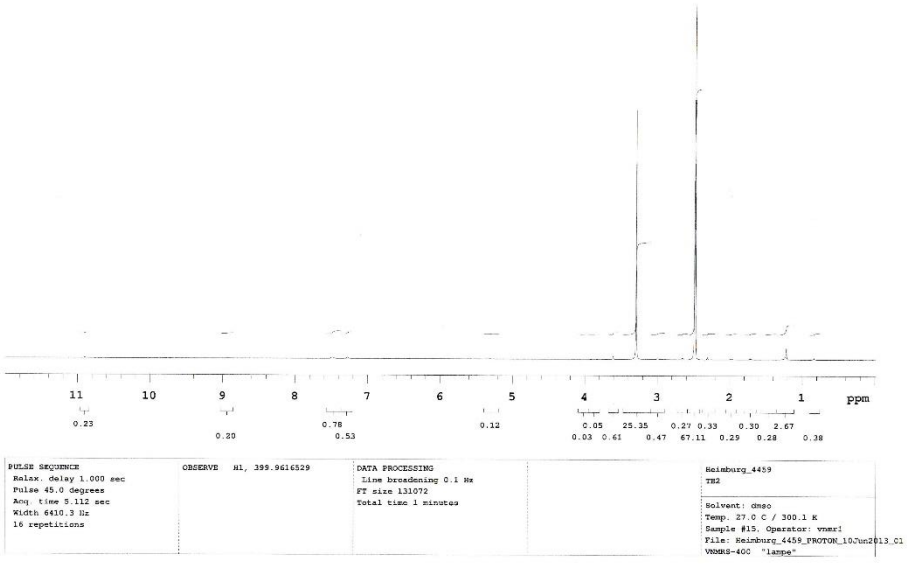

22e (TB3)

HPLC

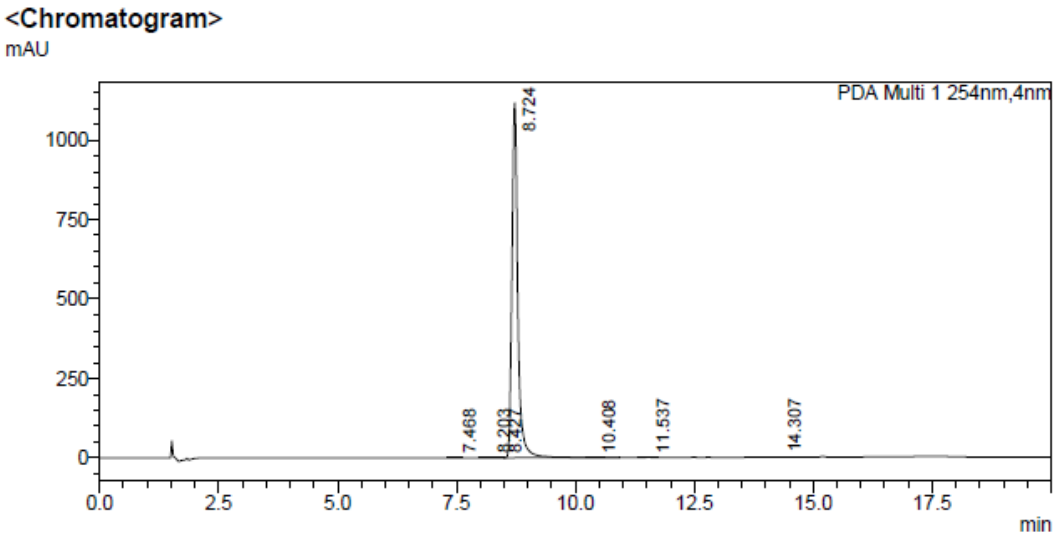

<Peak Table>

PDA Ch1 254nm

Peak#	Ret. Time	Area%	Area	Height
1	7.468	0.011	1054	133
2	8.203	0.045	4311	357
3	8.427	0.028	2729	266
4	8.724	99.748	9611160	1117827
5	10.408	0.019	1851	172
6	11.537	0.095	9186	1267
7	14.307	0.054	5189	483
Total		100.000	9635480	1120505

^{1}H-NMR

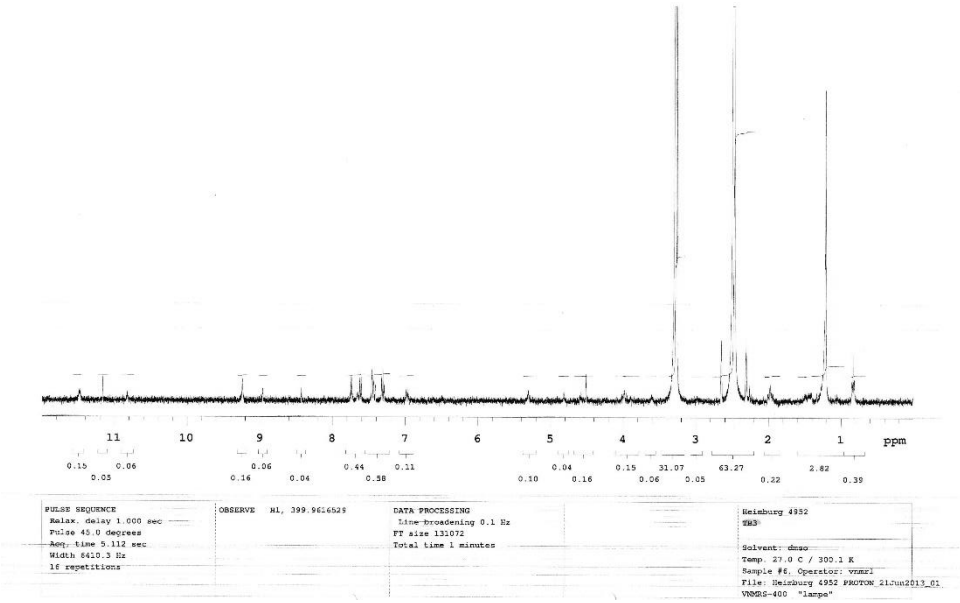

22f (TB42)

HPLC

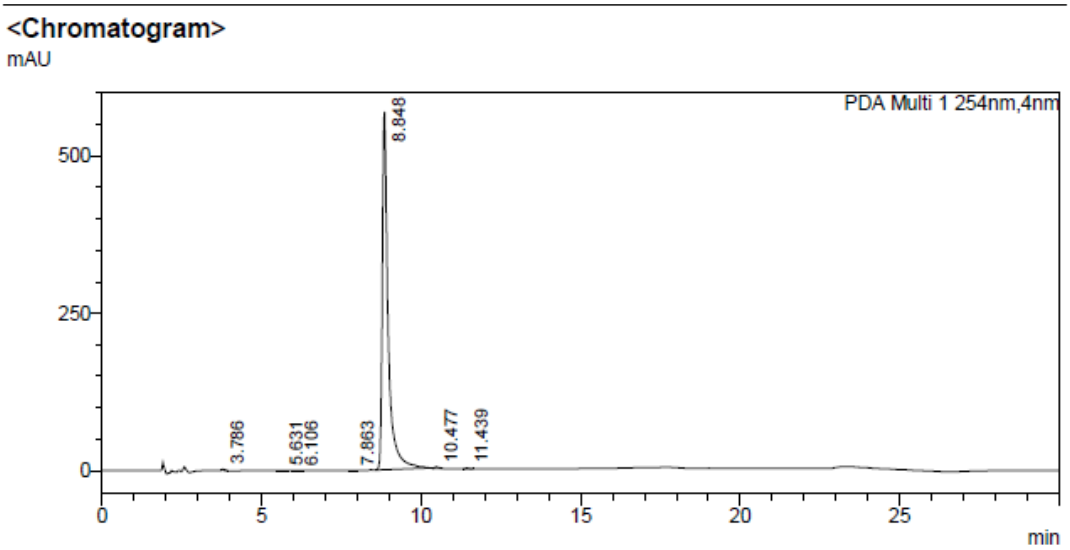

<Peak Table>

PDA Ch1 254nm

Peak#	Ret. Time	Area%	Area	Height
1	3.786	0.135	9860	1629
2	5.631	0.032	2330	243
3	6.106	0.027	1943	172
4	7.863	0.008	604	73
5	8.848	99.457	7278047	566617
6	10.477	0.223	16344	2116
7	11.439	0.118	8654	1385
Total		100.000	7317781	572234

^{1}H-NMR

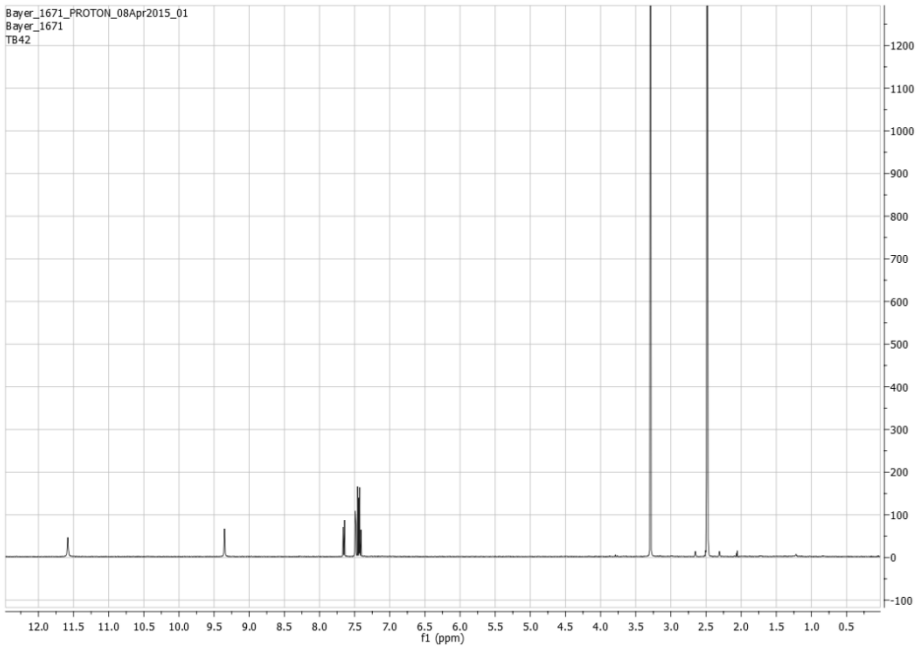

22g (TB45)

HPLC

<Chromatogram>

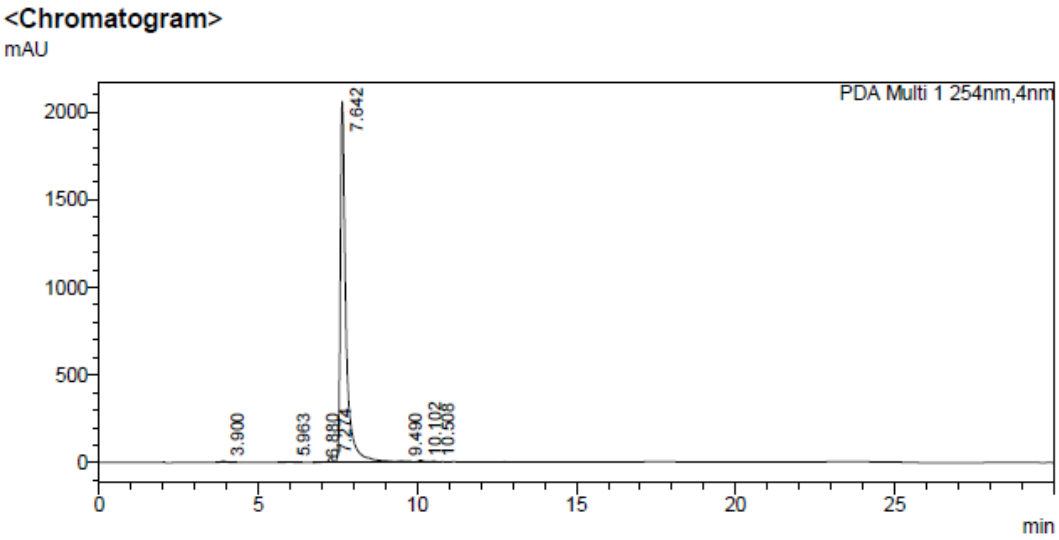

<Peak Table>

PDA Ch1 254nm

Peak#	Ret. Time	Area%	Area	Height
1	3.900	0.326	84527	8284
2	5.963	0.105	27199	2693
3	6.880	0.006	1550	192
4	7.274	0.839	217450	29181
5	7.642	98.229	25446738	2050454
6	9.490	0.086	22199	2252
7	10.102	0.318	82324	8854
8	10.508	0.091	23570	3842
Total		100.000	25905556	2105753

^{1}H-NMR

-

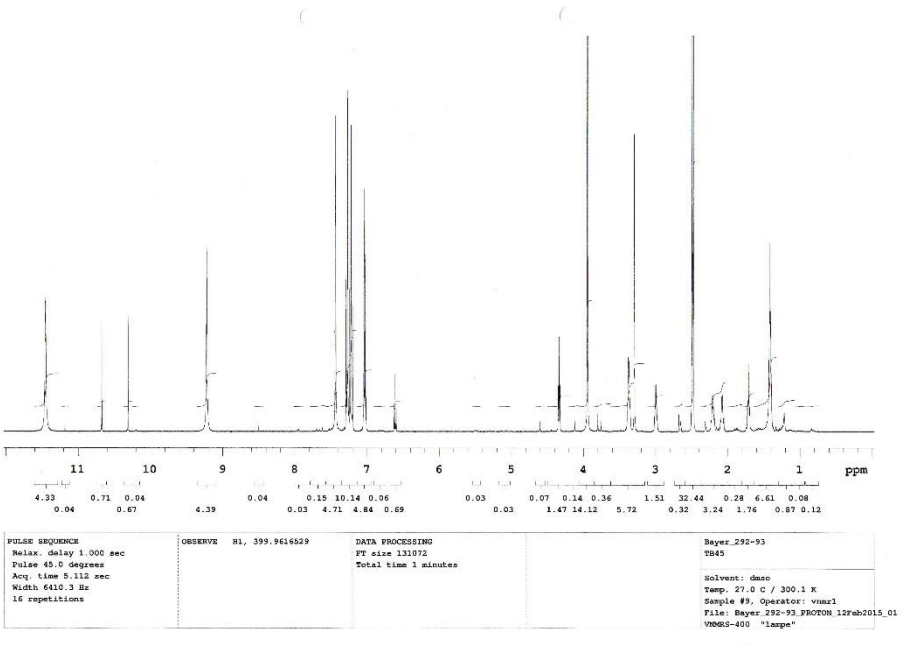

22h (TB46)

HPLC

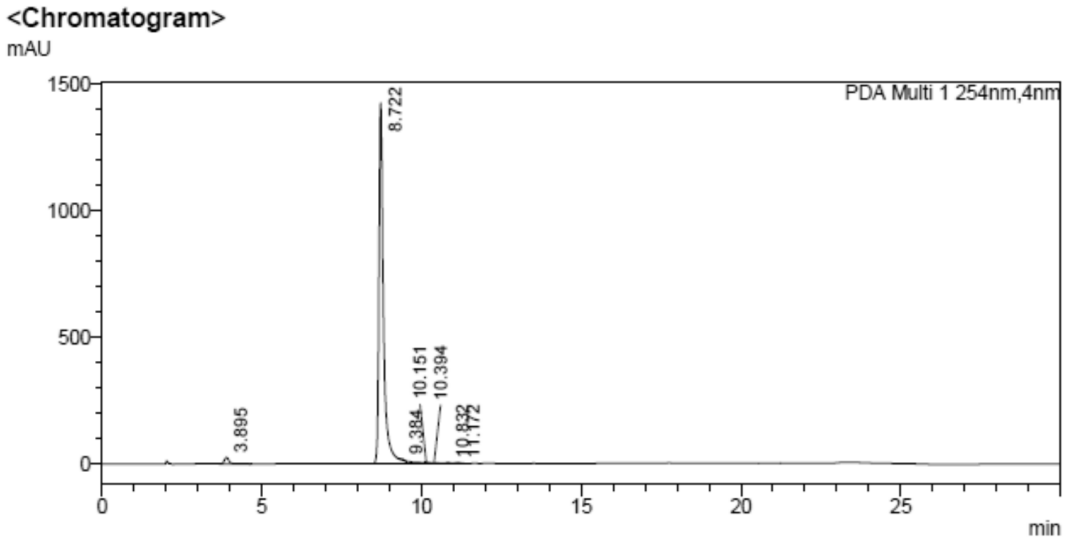

<Peak Table>

PDA Ch1 254nm

Peak#	Ret. Time	Area%	Area	Height
1	3.895	1.744	257946	25290
2	8.722	97.787	14464763	1426228
3	9.384	0.070	10307	2145
4	10.151	0.014	2005	306
5	10.394	0.028	4114	704
6	10.832	0.182	26934	3145
7	11.172	0.176	26037	2906
Total		100.000	14792106	1460724

^{1}H-NMR

-

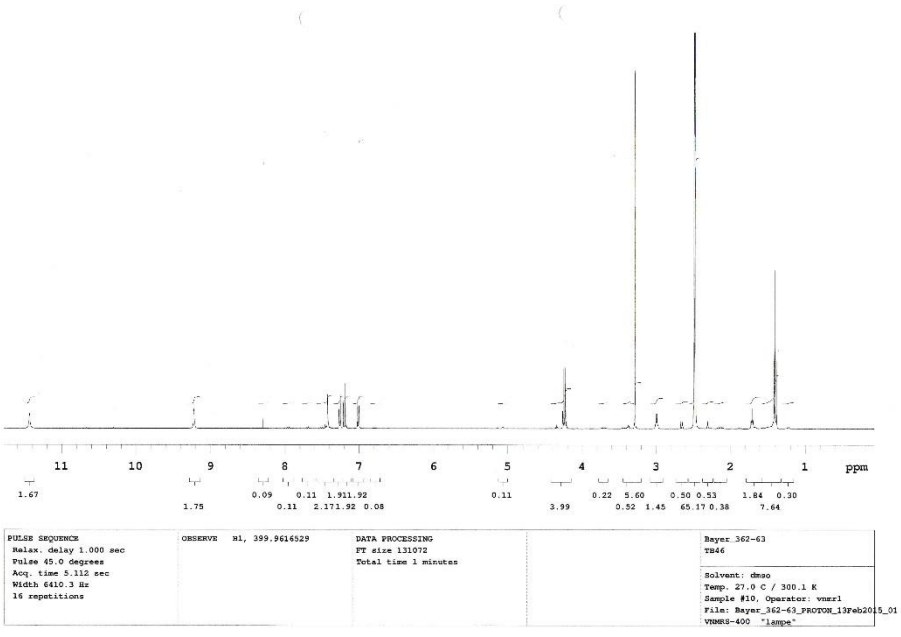

22i (TB4)

HPLC

<Chromatogram>

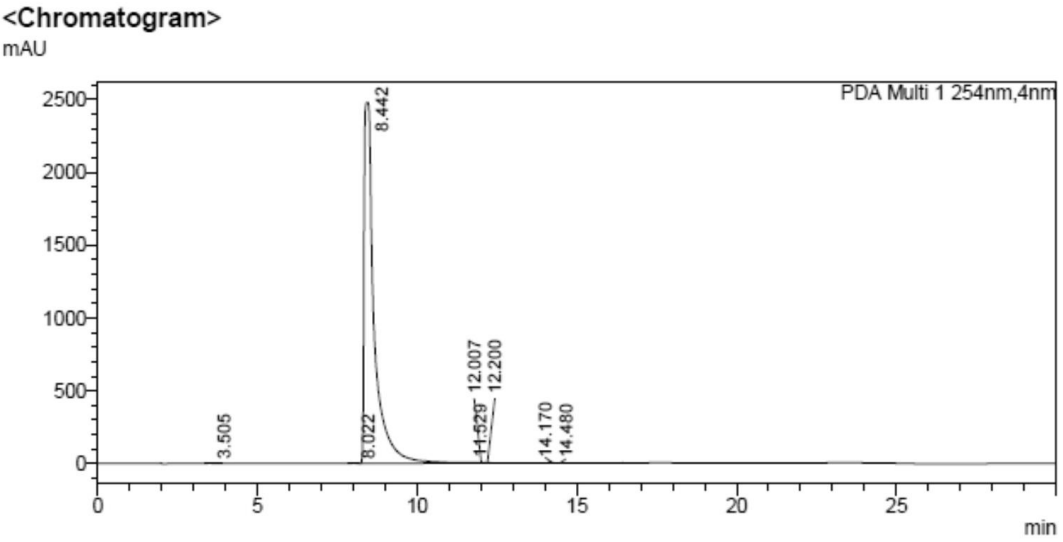

<Peak Table>

PDA Ch1 254nm

Peak#	Ret. Time	Area%	Area	Height
1	3.505	0.037	20410	2240
2	8.022	0.023	12443	1728
3	8.442	99.771	54947838	2478570
4	11.529	0.015	8268	1031
5	12.007	0.002	1280	206
6	12.200	0.020	11202	1614
7	14.170	0.125	68966	11747
8	14.480	0.006	3405	306
Total		100.000	55073812	2497441

^{1}H-NMR

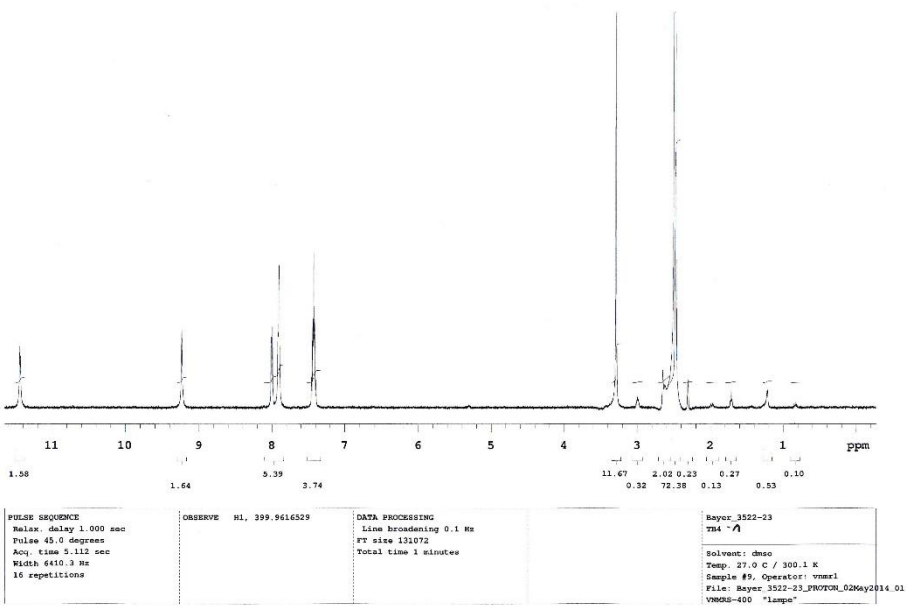

22j (TB5)

HPLC

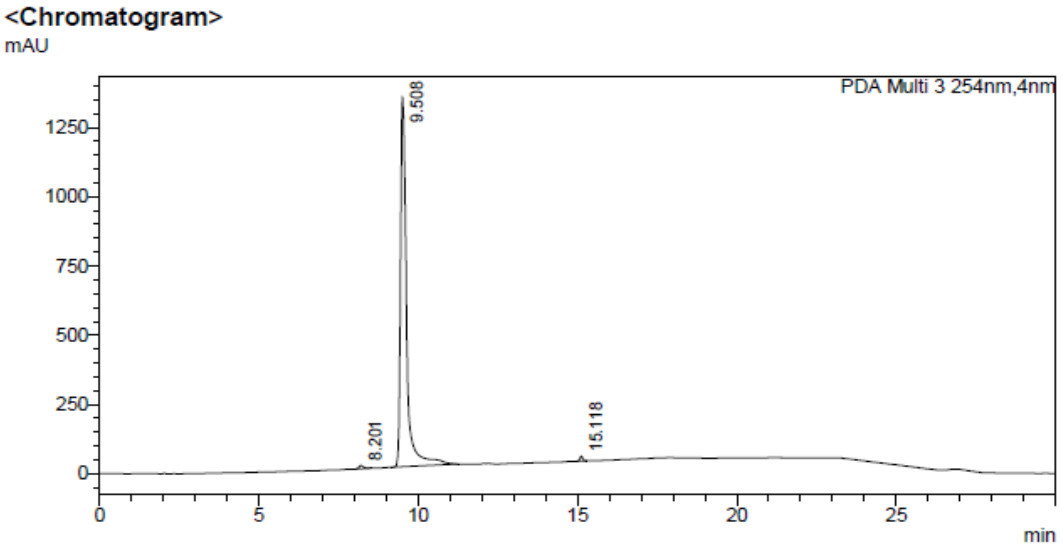

<Peak Table>

PDA Ch3 254nm

Peak#	Ret. Time	Area%
1	8.201	0.653
2	9.508	98.710
3	15.118	0.637
Total		100.000

^{1}H-NMR

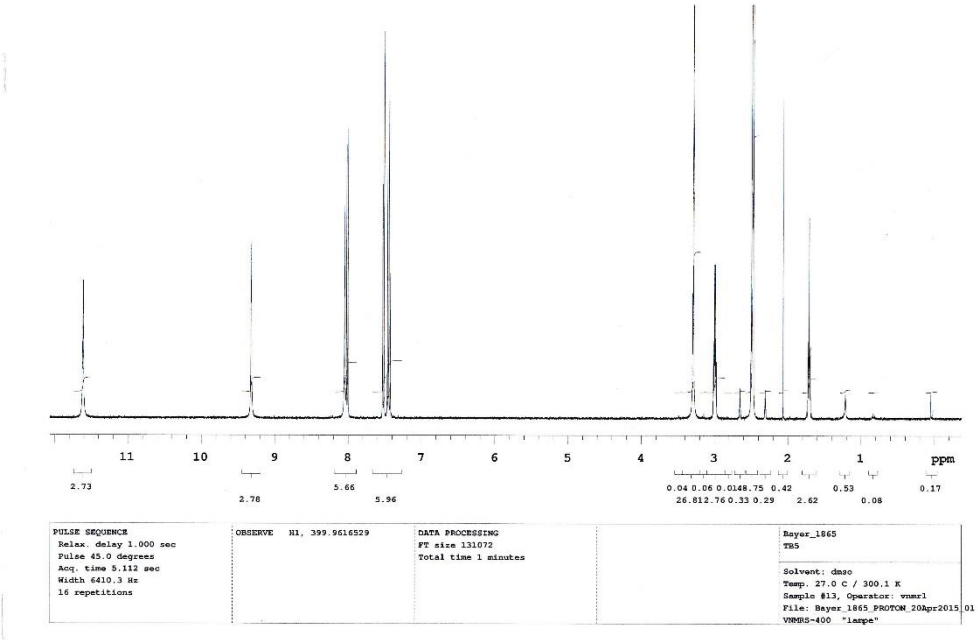

24a (TB7)

HPLC

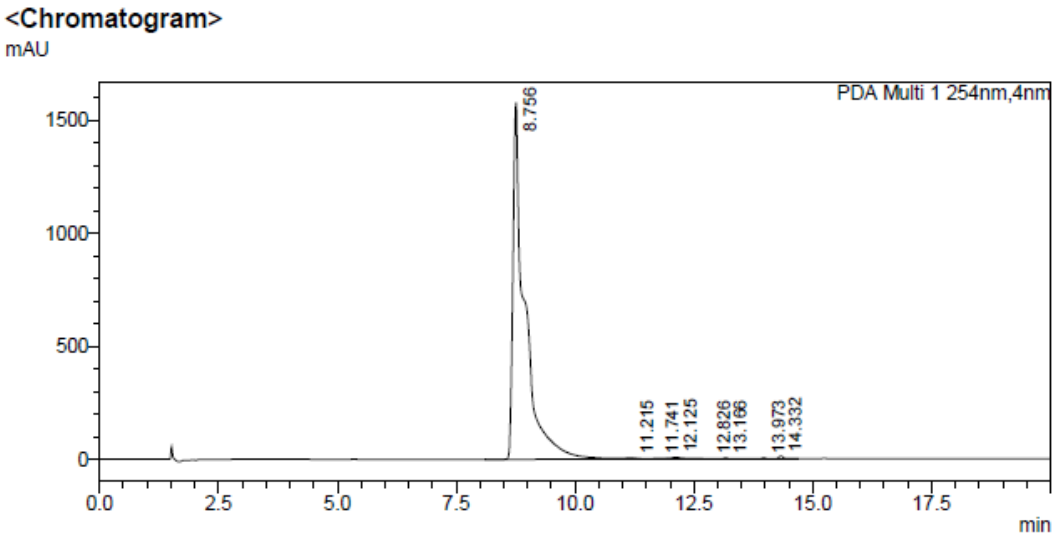

<Peak Table>

PDA Ch1 254nm

Peak#	Ret. Time	Area%	Area	Height
1	8.756	98.924	27701542	1578422
2	11.215	0.055	15269	2105
3	11.741	0.086	24202	1560
4	12.125	0.311	87193	6582
5	12.826	0.032	8887	958
6	13.166	0.112	31378	4986
7	13.973	0.167	46835	5112
8	14.332	0.313	87662	12602
Total		100.000	28002969	1612327

^{1}H-NMR

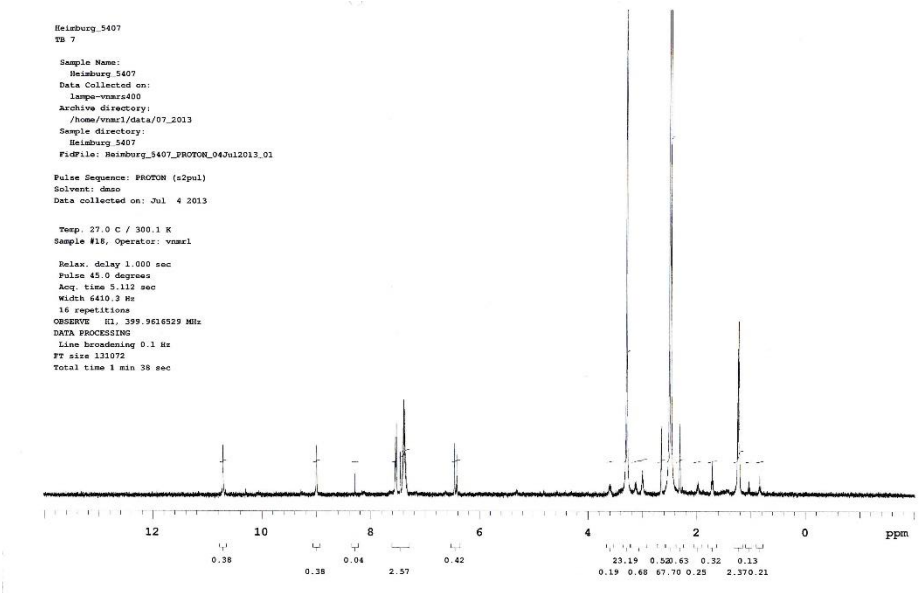

24b (TB8)

HPLC

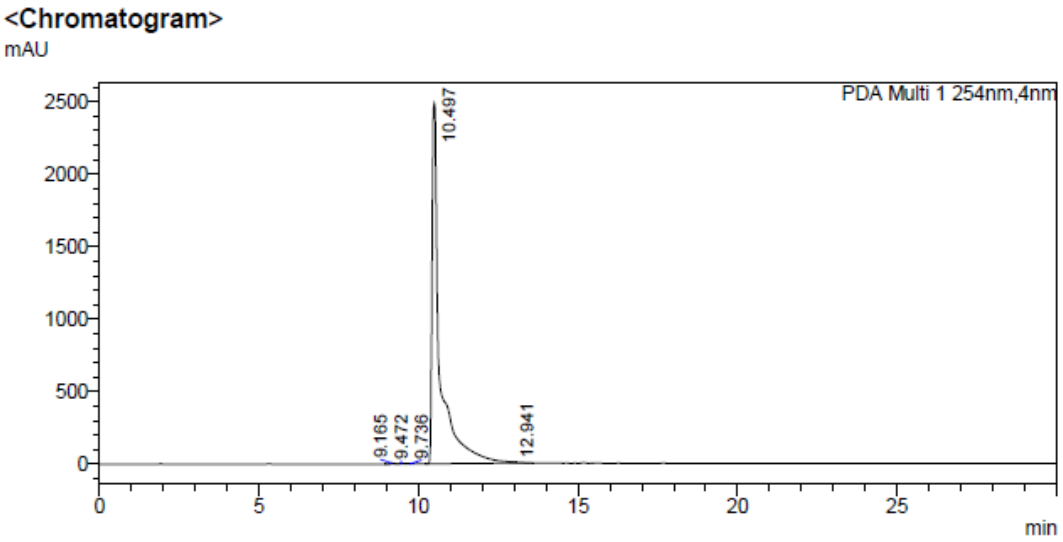

<Peak Table>

PDA Ch1 254nm

Peak#	Ret. Time	Area%	Area	Height
1	9.165	0.136	59012	5790
2	9.472	0.008	3396	487
3	9.736	0.005	2353	233
4	10.497	99.830	43403280	2487720
5	12.941	0.021	9036	1785
Total		100.000	43477078	2496016

^{1}H-NMR

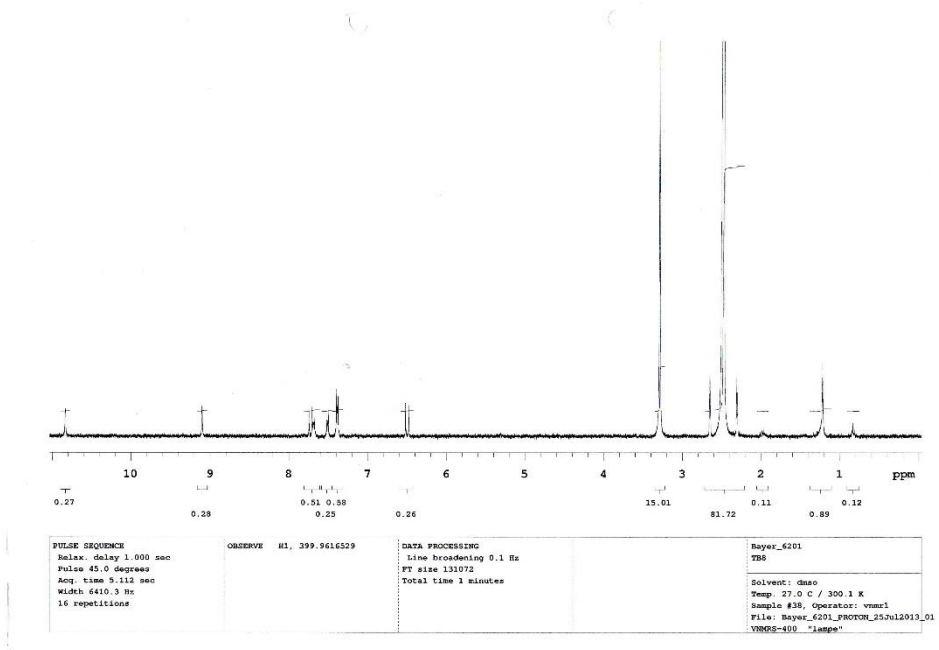

24c (TB77)

HPLC

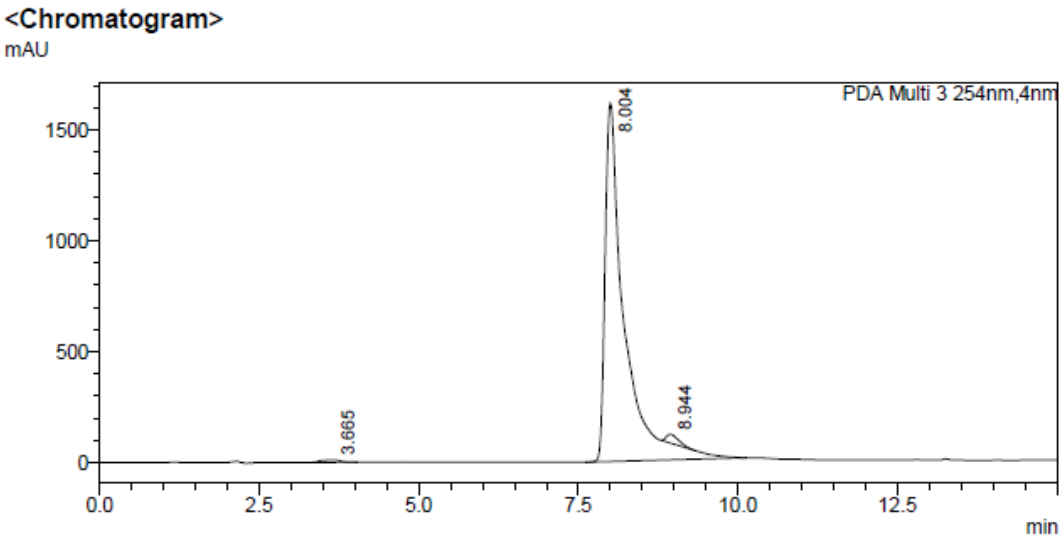

<Peak Table>

PDA Ch3 254nm

Peak#	Ret. Time	Area%
1	3.665	0.625
2	8.004	97.808
3	8.944	1.567
Total		100.000

^{1}H-NMR

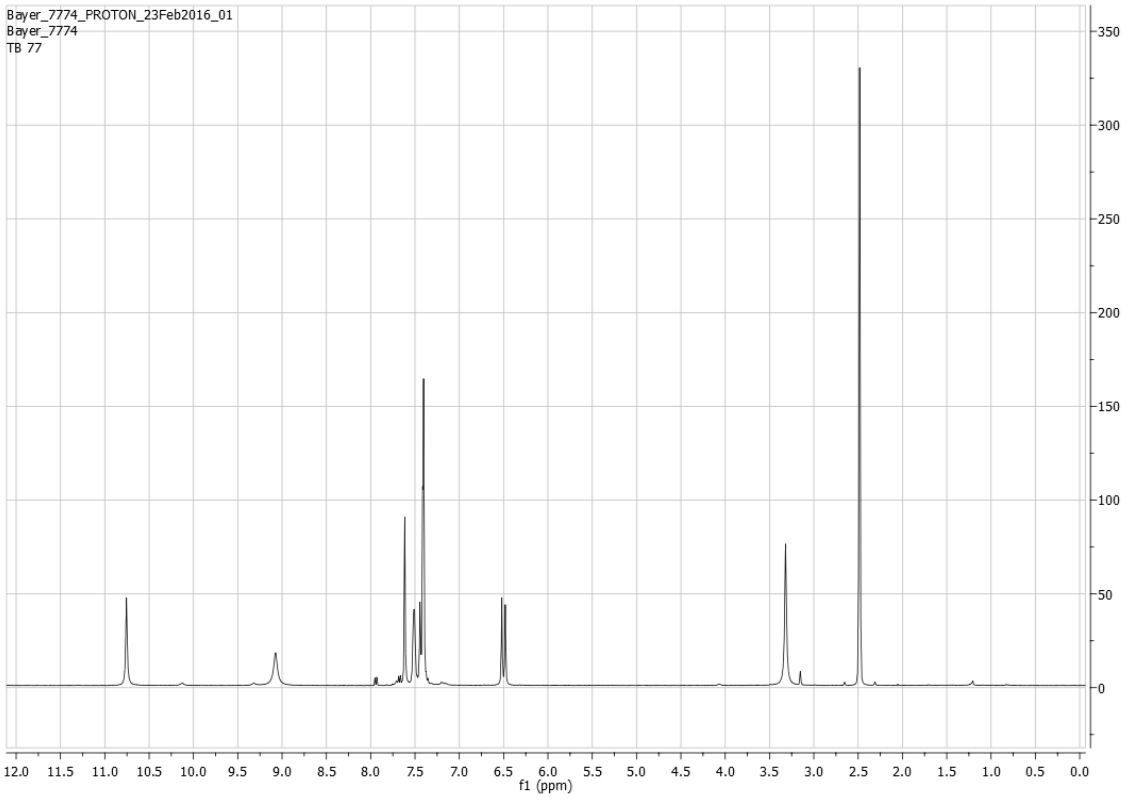

24d (TB9)

HPLC

<Chromatogram>

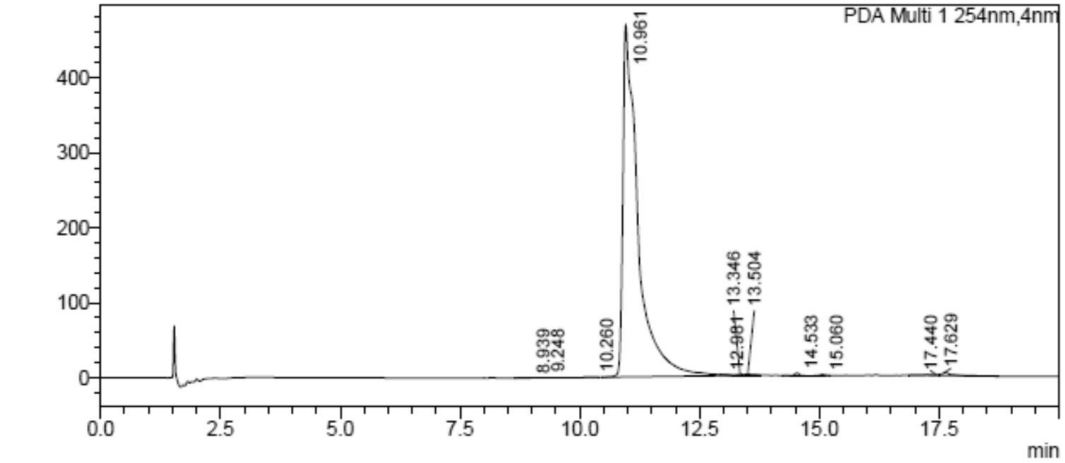

<Peak Table>

PDA Ch1 254nm

Peak#	Ret. Time	Area%	Area	Height
1	8.939	0.018	1877	133
2	9.248	0.042	4414	342
3	10.260	0.033	3489	210
4	10.961	98.649	10298376	468182
5	12.981	0.017	1790	232
6	13.346	0.062	6448	934
7	13.504	0.141	14693	1241
8	14.533	0.213	22194	3611
9	15.060	0.141	14737	1794
10	17.440	0.172	17959	1012
11	17.629	0.511	53387	4518
Total		100.000	10439363	482208

^{1}H-NMR

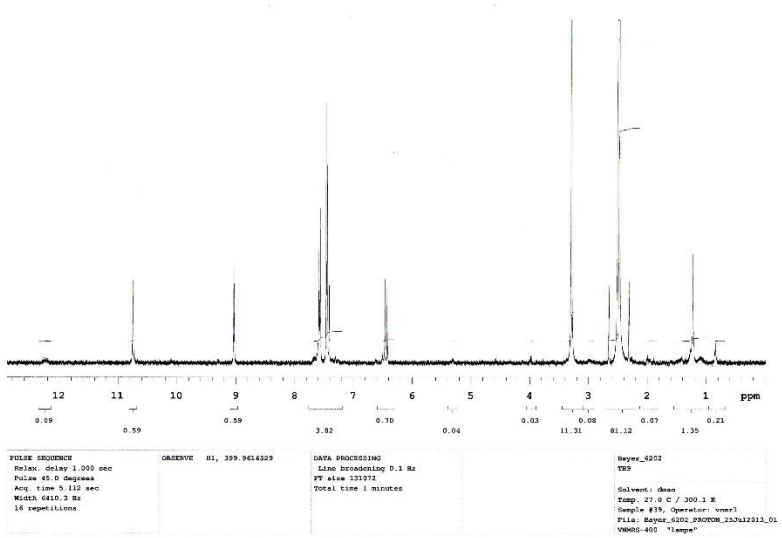

24e (TB32)

HPLC

<Chromatogram>

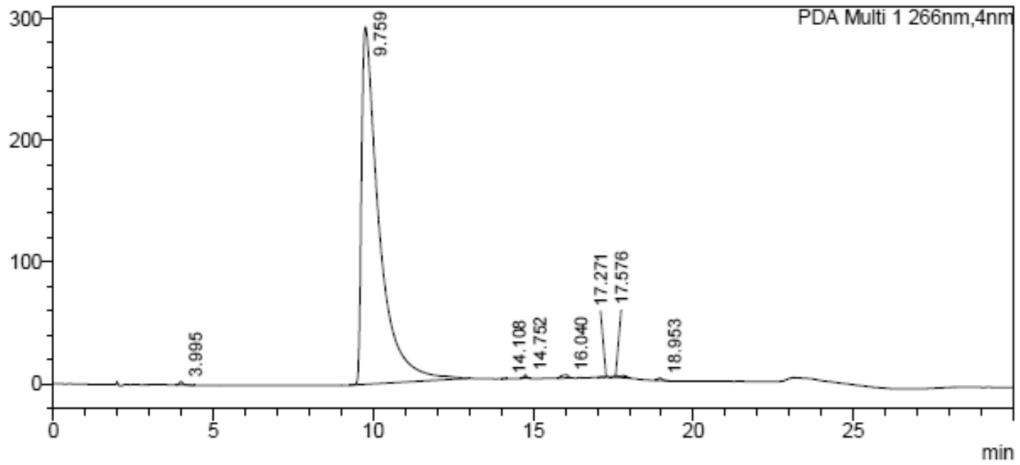

<Peak Table>

PDA Ch1 266nm

Peak#	Ret. Time	Area%	Area	Height
1	3.995	0.187	21193	2771
2	9.759	98.835	11207456	293018
3	14.108	0.021	2418	446
4	14.752	0.154	17499	2943
5	16.040	0.330	37396	2616
6	17.271	0.056	6339	699
7	17.576	0.270	30599	1638
8	18.953	0.147	16651	2114
Total		100.000	11339551	306244

^{1}H-NMR

-

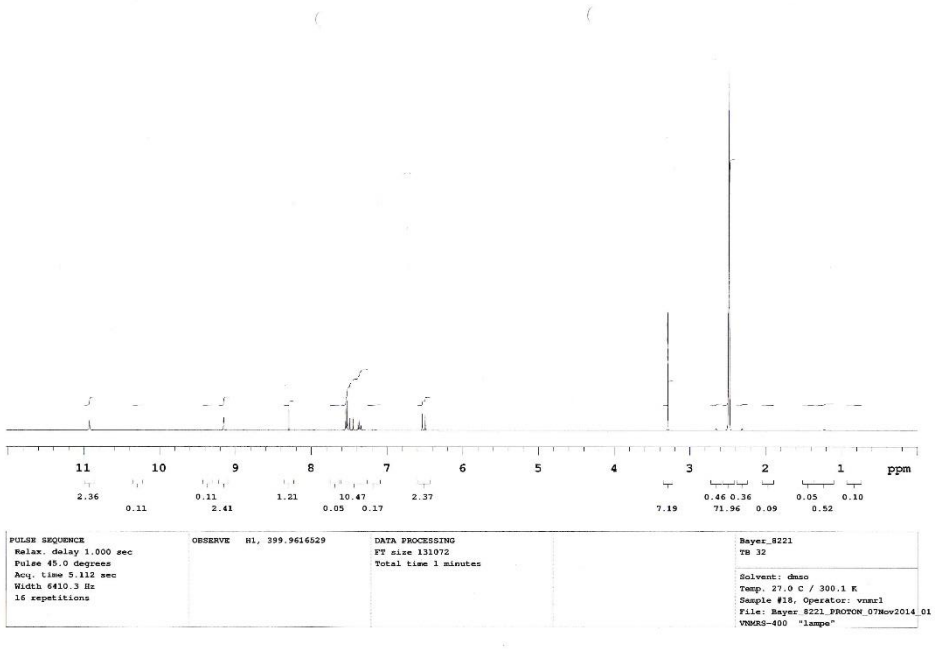

24f (TB51)

HPLC

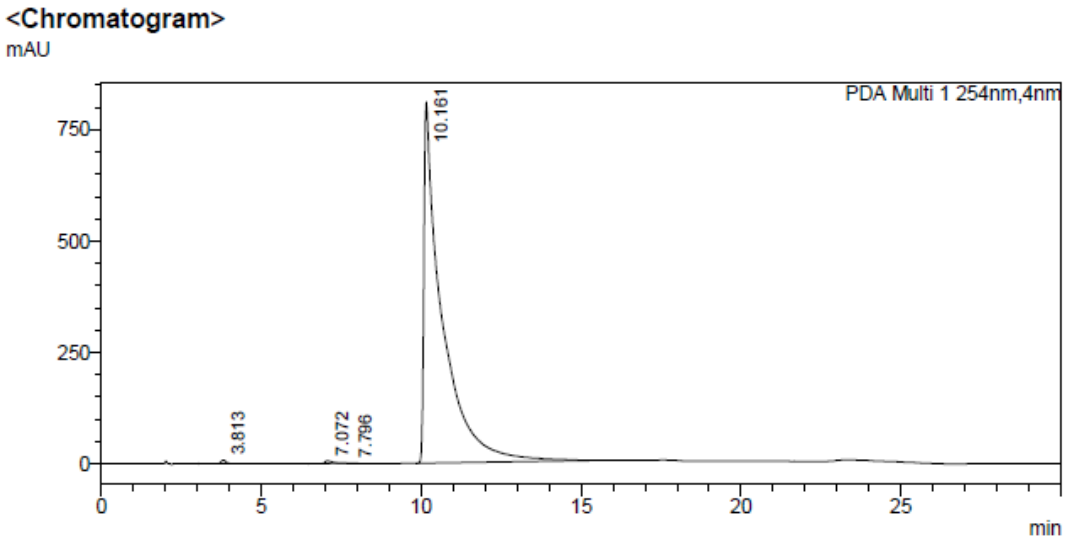

<Peak Table>

PDA Ch1 254nm

Peak#	Ret. Time	Area%	Area	Height
1	3.813	0.264	84217	8000
2	7.072	0.303	96813	6247
3	7.796	0.024	7811	854
4	10.161	99.409	31759918	807889
Total		100.000	31948758	822989

^{1}H-NMR

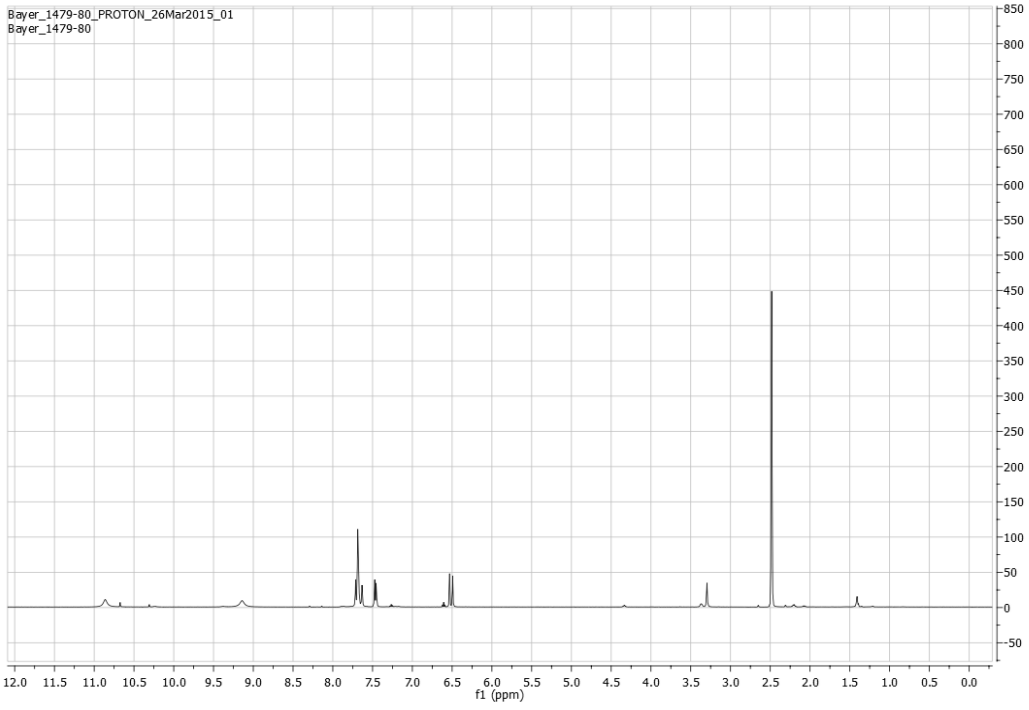

24g (TB10)

HPLC

<Chromatogram>

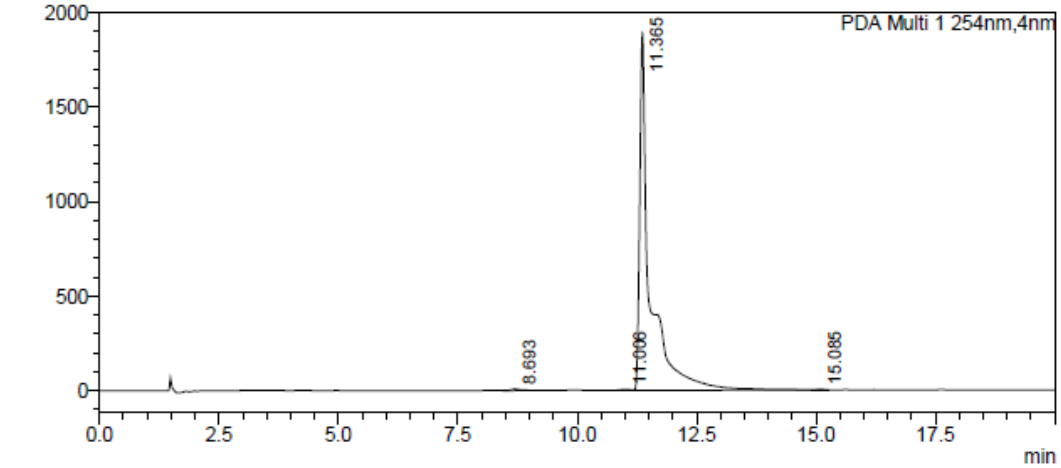

<Peak Table>

PDA Ch1 254nm

Peak#	Ret. Time	Area%	Area	Height
1	8.693	0.353	101405	8171
2	11.006	0.239	68627	5649
3	11.365	99.351	28503326	1891378
4	15.085	0.056	16055	2098
Total		100.000	28689413	1907296

^{1}H-NMR

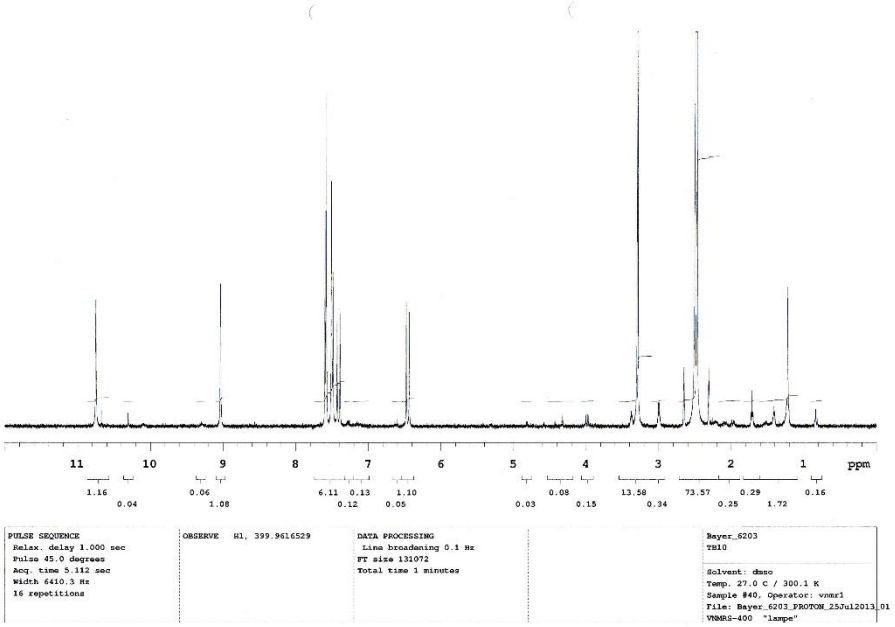

24h (TB76)

HPLC

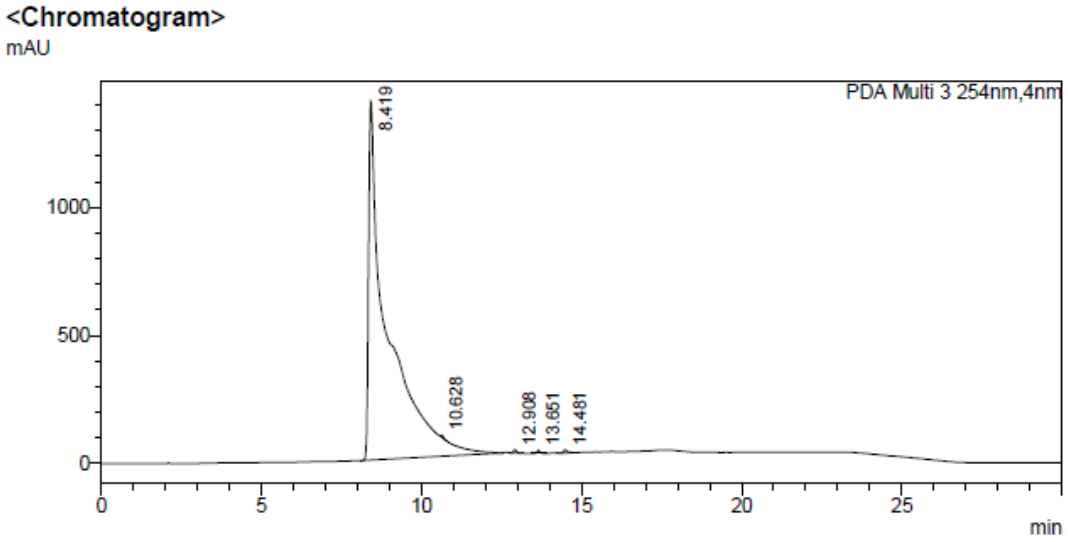

<Peak Table>

PDA Ch3 254nm

Peak#	Ret. Time	Area%	Area	Height
1	8.419	99.482	57456871	1398933
2	10.628	0.060	34529	6491
3	12.908	0.138	79838	13115
4	13.651	0.137	79282	12323
5	14.481	0.183	105724	12672
Total		100.000	57756243	1443534

^{1}H-NMR

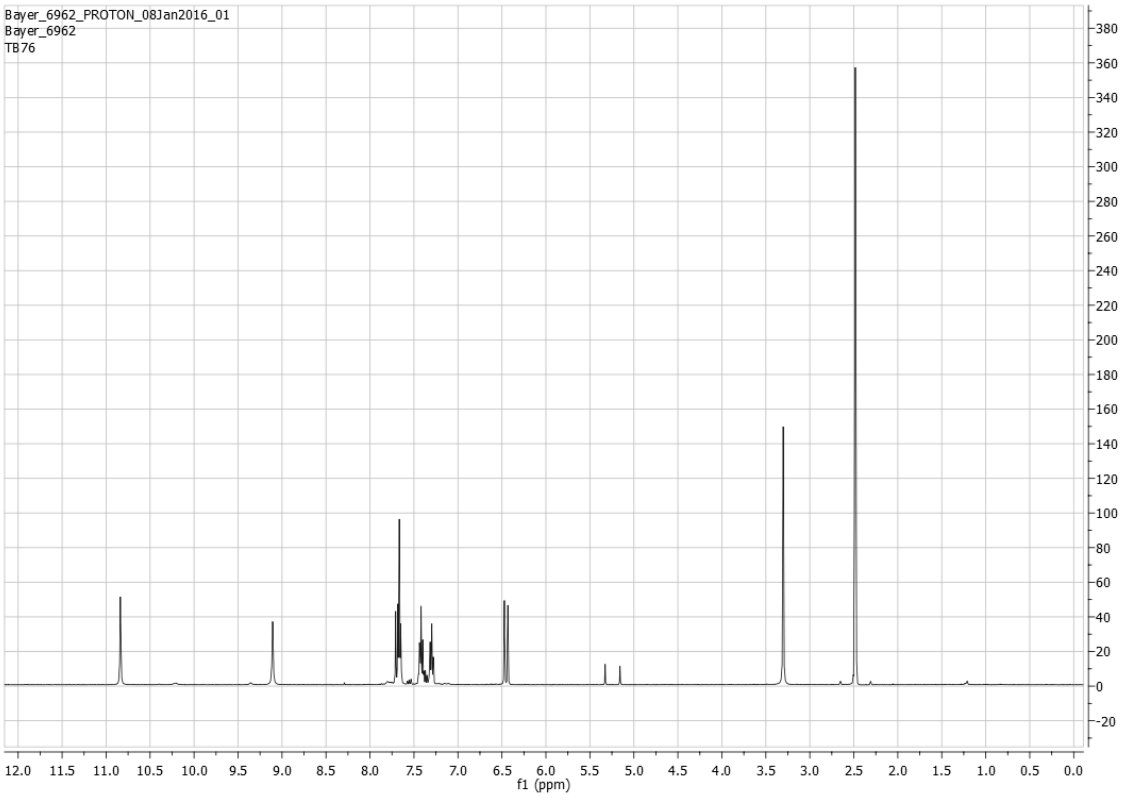

24i (TB53)

^{1}H-NMR

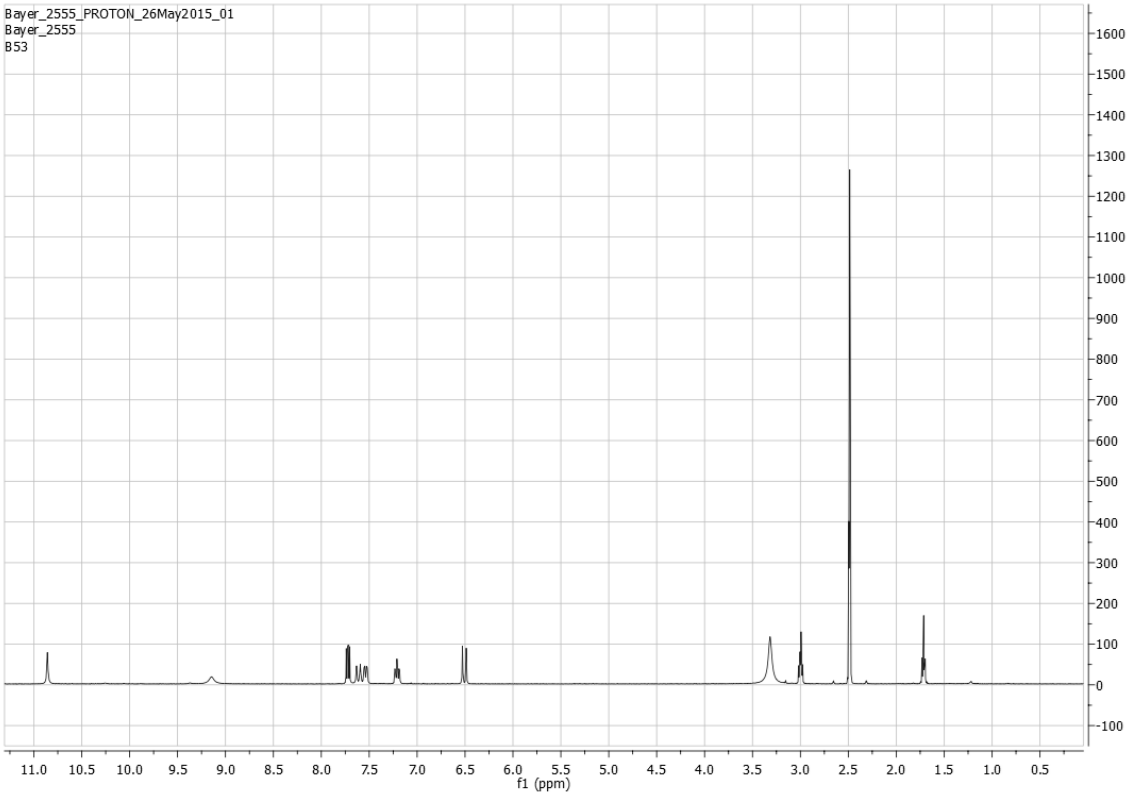

24j (TB54)

HPLC

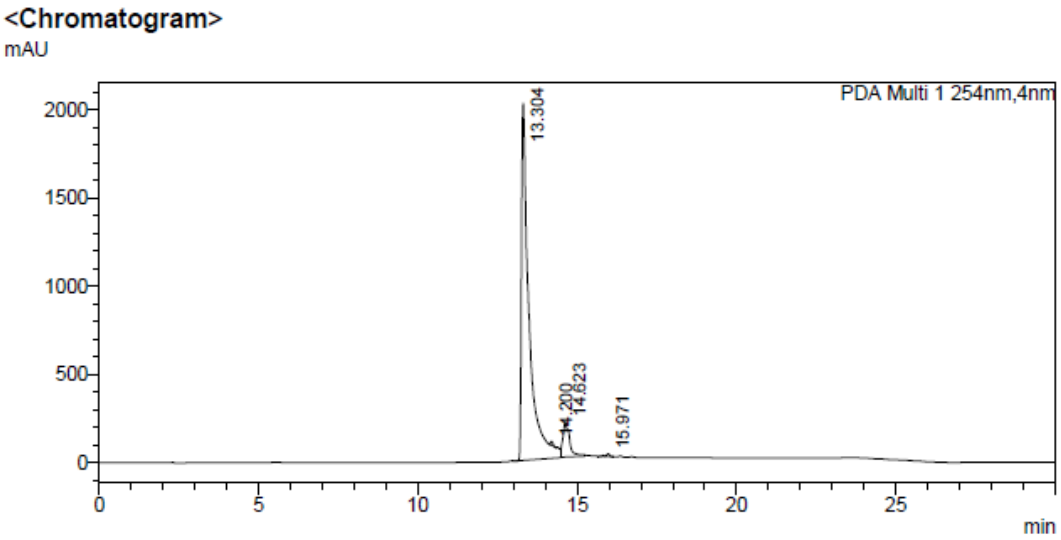

<Peak Table>

PDA Ch1 254nm

Peak#	Ret. Time	Area%	Area	Height
1	13.304	91.445	33386155	2025999
2	14.200	0.244	88913	22327
3	14.623	7.960	2906103	202898
4	15.971	0.351	128286	16240
Total		100.000	36509458	2267465

^{1}H-NMR

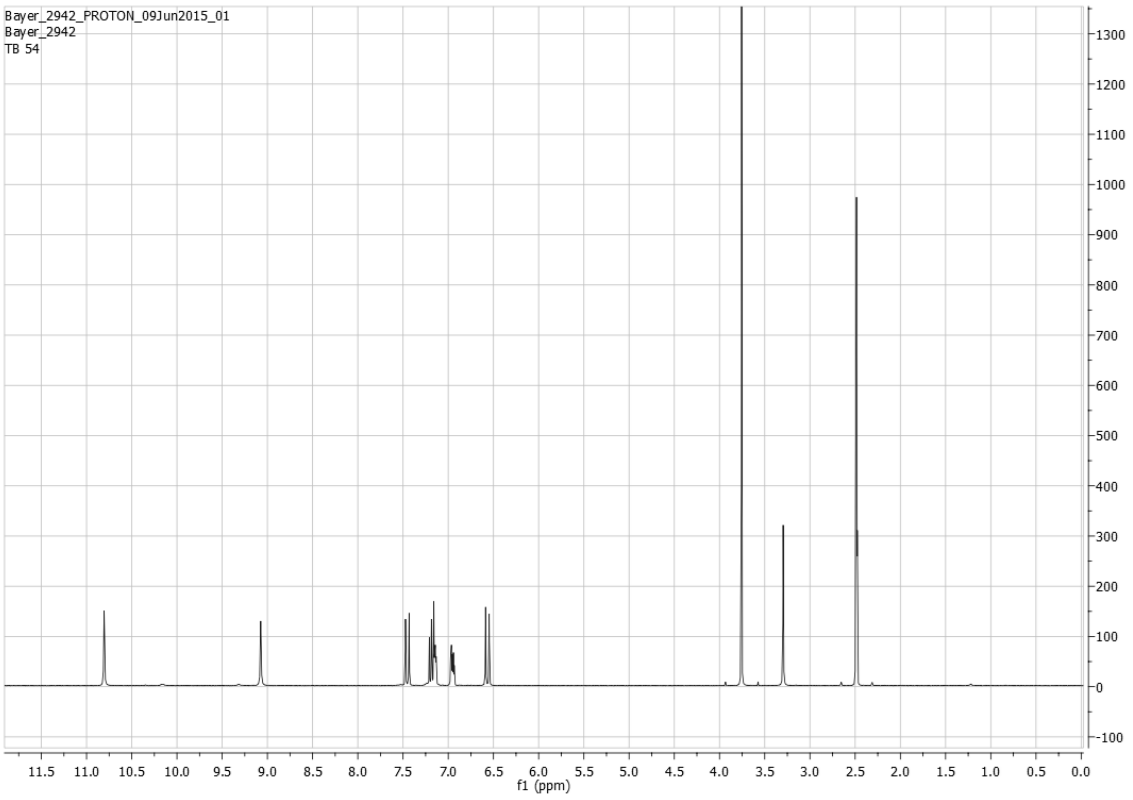

24k (TB15)

HPLC

<Chromatogram>

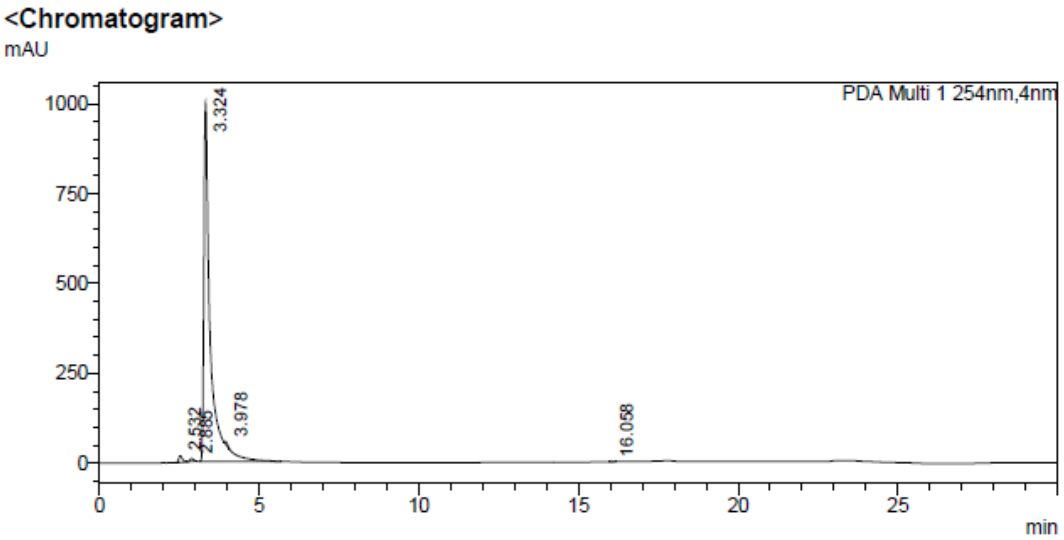

<Peak Table>

PDA Ch1 254nm

Peak#	Ret. Time	Area%	Area	Height
1	2.532	1.036	145603	18345
2	2.885	0.461	64781	8055
3	3.324	98.209	13798459	998245
4	3.978	0.267	37562	8570
5	16.058	0.027	3742	657
Total		100.000	14050147	1033872

^{1}H-NMR

.

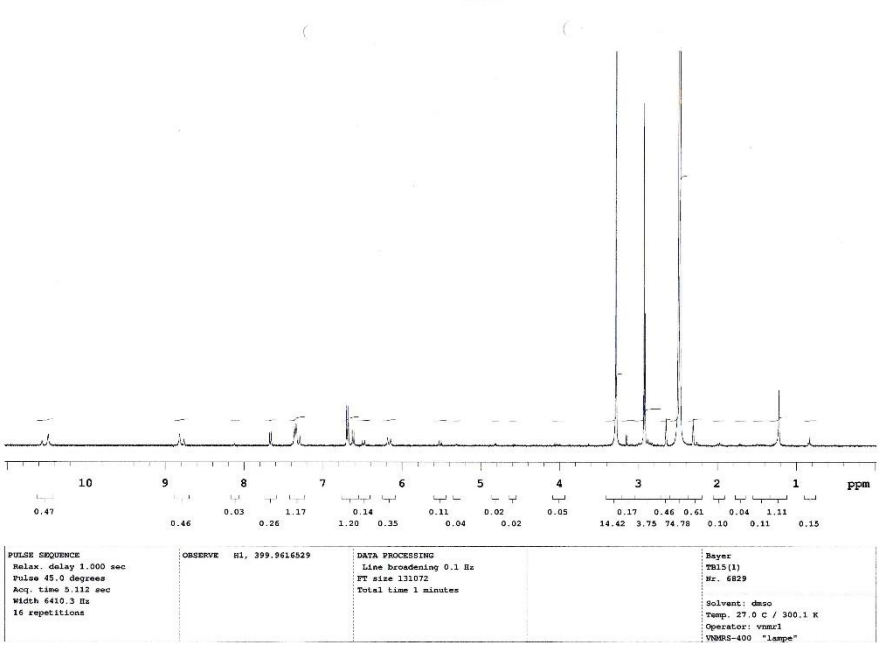

24l (TB14)

HPLC

<Chromatogram>

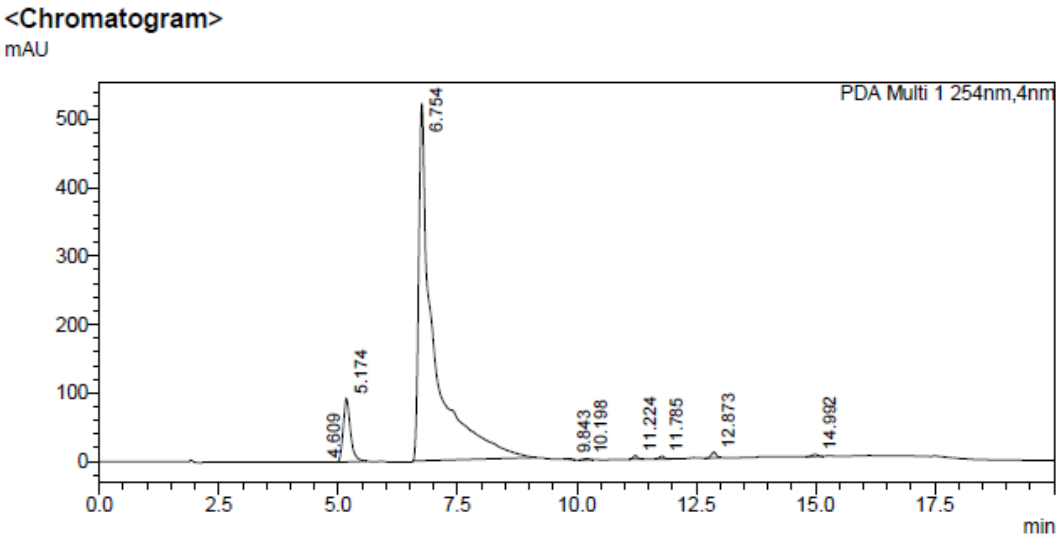

<Peak Table>

PDA Ch1 254nm

Peak#	Ret. Time	Area%	Area	Height
1	4.609	0.003	375	62
2	5.174	7.673	970387	92607
3	6.754	90.979	11506429	522718
4	9.843	0.057	7224	1212
5	10.198	0.108	13607	1930
6	11.224	0.278	35134	5545
7	11.785	0.216	27303	4062
8	12.873	0.485	61324	8580
9	14.992	0.202	25548	3177
Total		100.000	12647331	639893

^{1}H-NMR

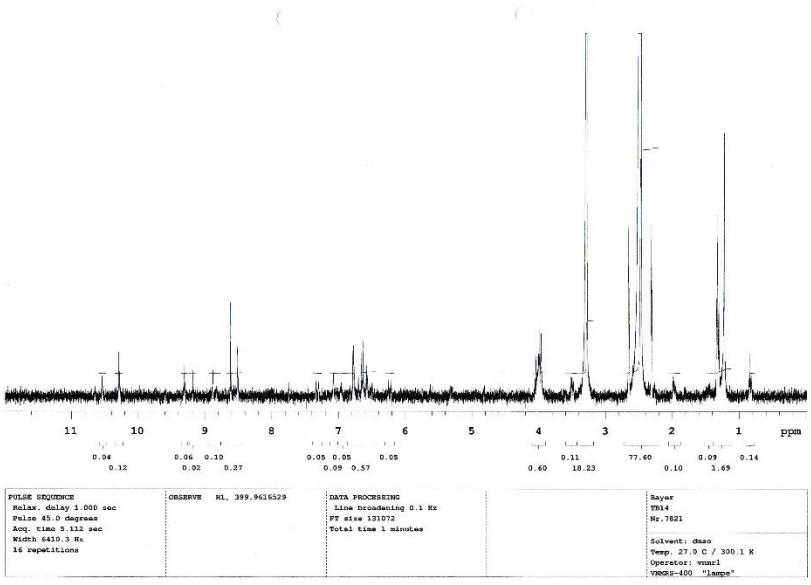

24m (TB33)

HPLC

<Chromatogram>

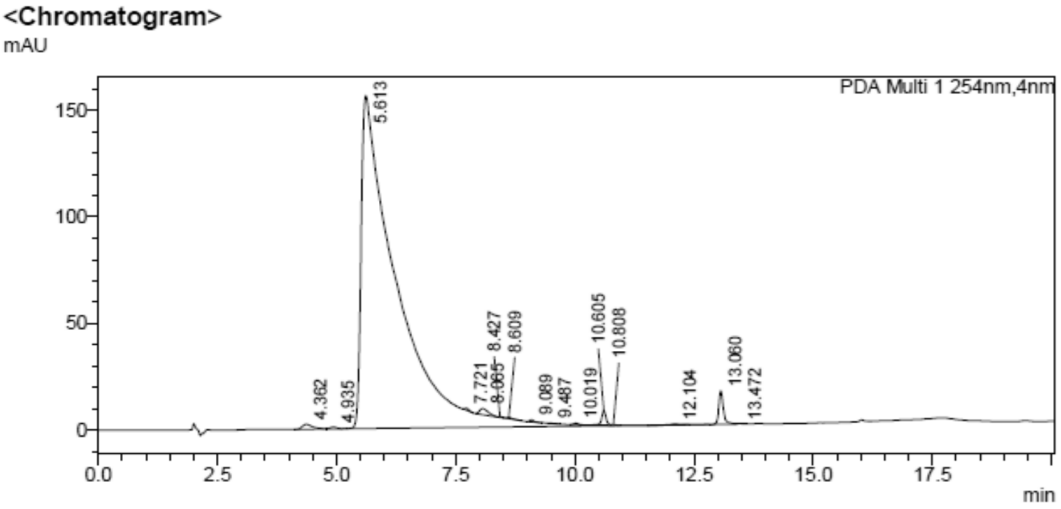

<Peak Table>

PDA Ch1 254nm

Peak#	Ret. Time	Area%	Area	Height
1	4.362	0.450	37229	2359
2	4.935	0.138	11436	984
3	5.613	96.707	8002220	155944
4	7.721	0.057	4739	917
5	8.065	0.427	35372	2823
6	8.427	0.017	1382	325
7	8.609	0.065	5405	675
8	9.089	0.063	5186	971
9	9.487	0.016	1351	152
10	10.019	0.061	5008	753
11	10.605	0.550	45485	6972
12	10.808	0.030	2492	383
13	12.104	0.126	10392	437
14	13.060	1.275	105478	15636
15	13.472	0.018	1518	194
Total		100.000	8274694	189524

^{1}H-NMR

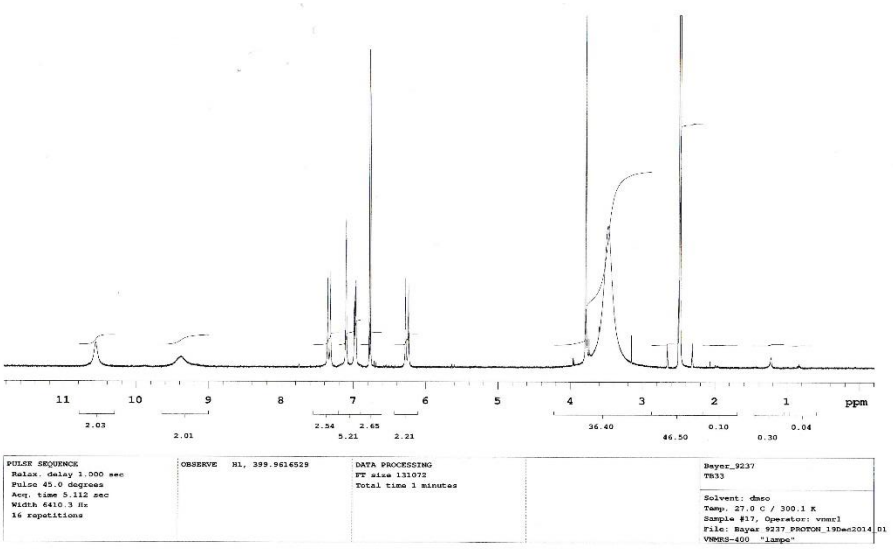

24n (TB16)

HPLC

<Chromatogram>

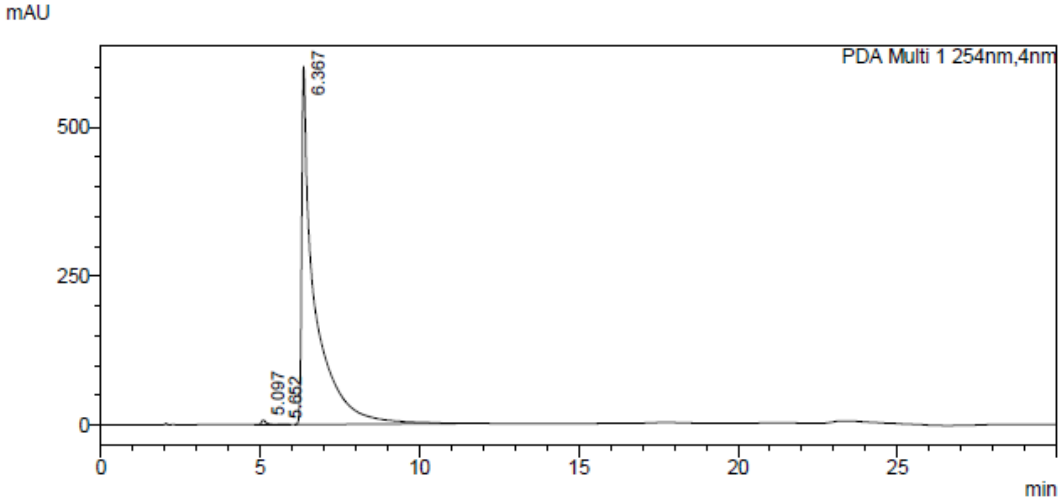

<Peak Table>

PDA Ch1 254nm

Peak#	Ret. Time	Area%	Area	Height
1	5.097	0.528	89674	7742
2	5.652	0.009	1488	186
3	6.367	99.463	16888918	602989
Total		100.000	16980080	610918

^{1}H-NMR

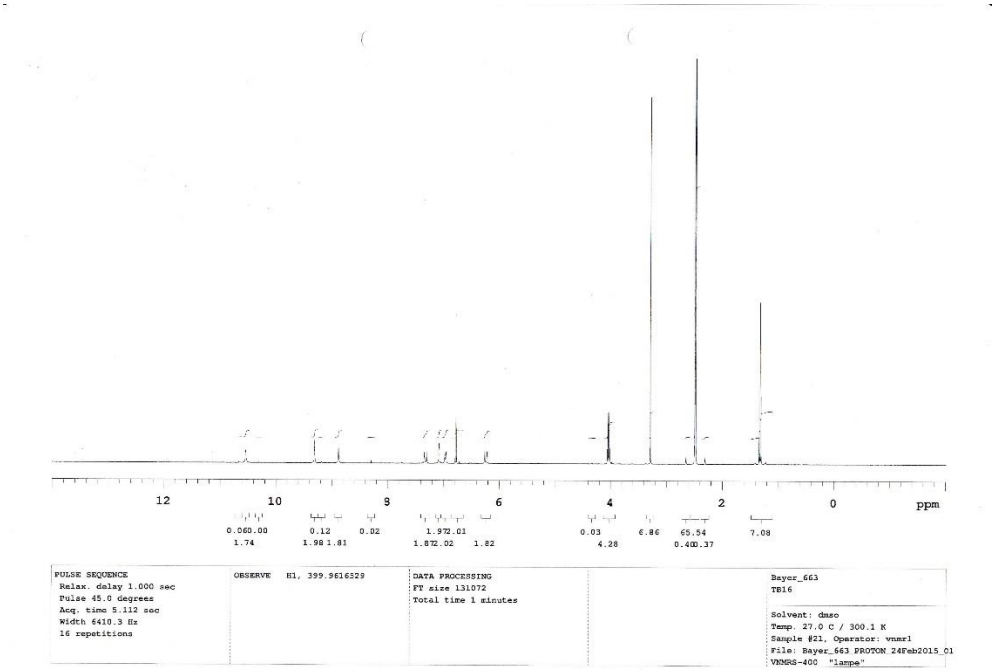

24o (TB31)

HPLC

<Chromatogram>

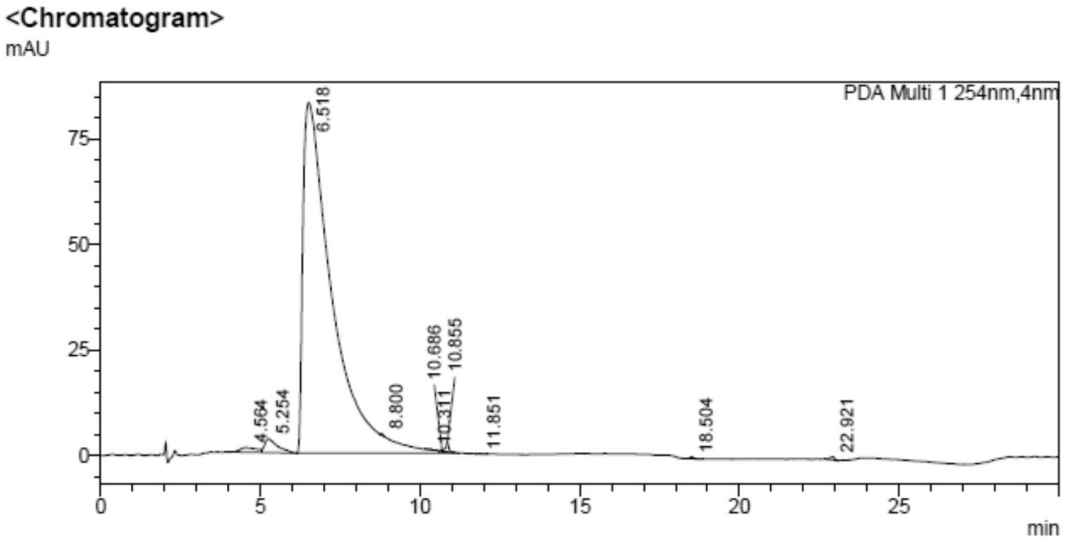

<Peak Table>

PDA Ch1 254nm

Peak#	Ret. Time	Area%	Area	Height
1	4.564	0.728	39240	1074
2	5.254	1.685	90876	3265
3	6.518	96.987	5230551	83081
4	8.800	0.023	1234	287
5	10.311	0.041	2224	273
6	10.686	0.035	1904	451
7	10.855	0.280	15103	2349
8	11.851	0.019	1049	81
9	18.504	0.065	3511	443
10	22.921	0.137	7378	738
Total		100.000	5393069	92043

^{1}H-NMR

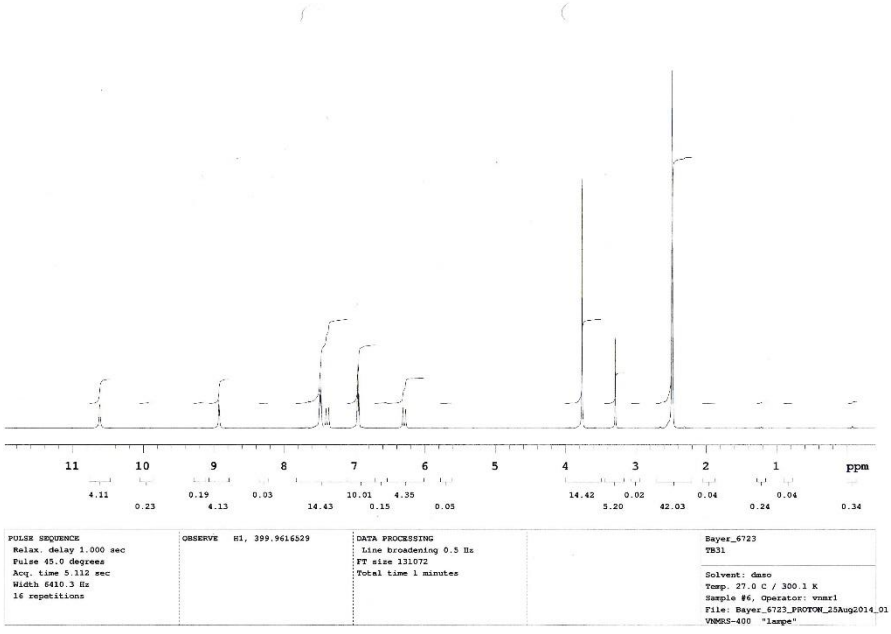

24p (TB44)

HPLC

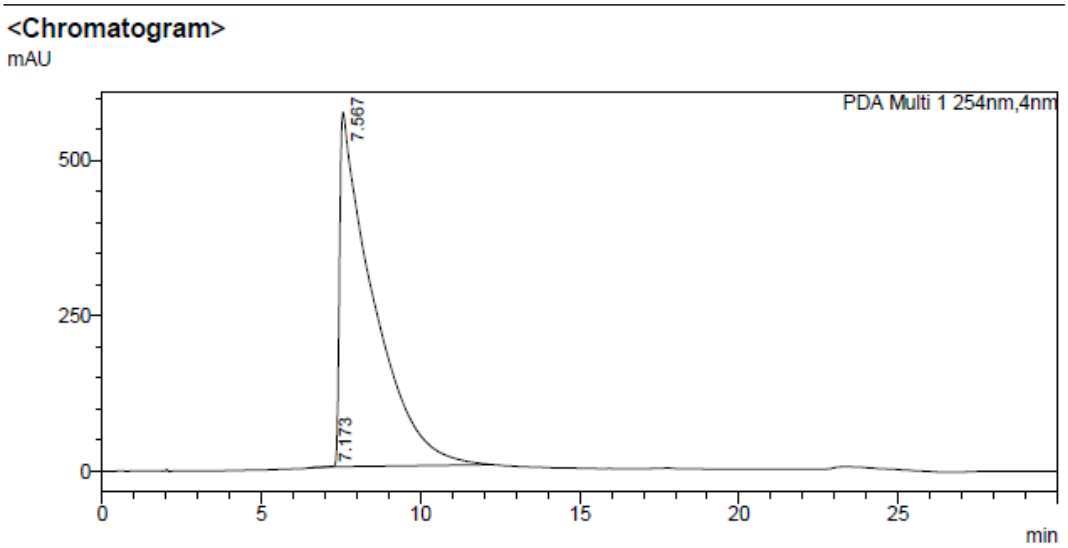

<Peak Table>

PDA Ch1 254nm

Peak#	Ret. Time	Area%	Area	Height
1	7.173	0.046	18984	1
2	7.567	99.954	41548948	570074
Total		100.000	41567932	570075

^{1}H-NMR

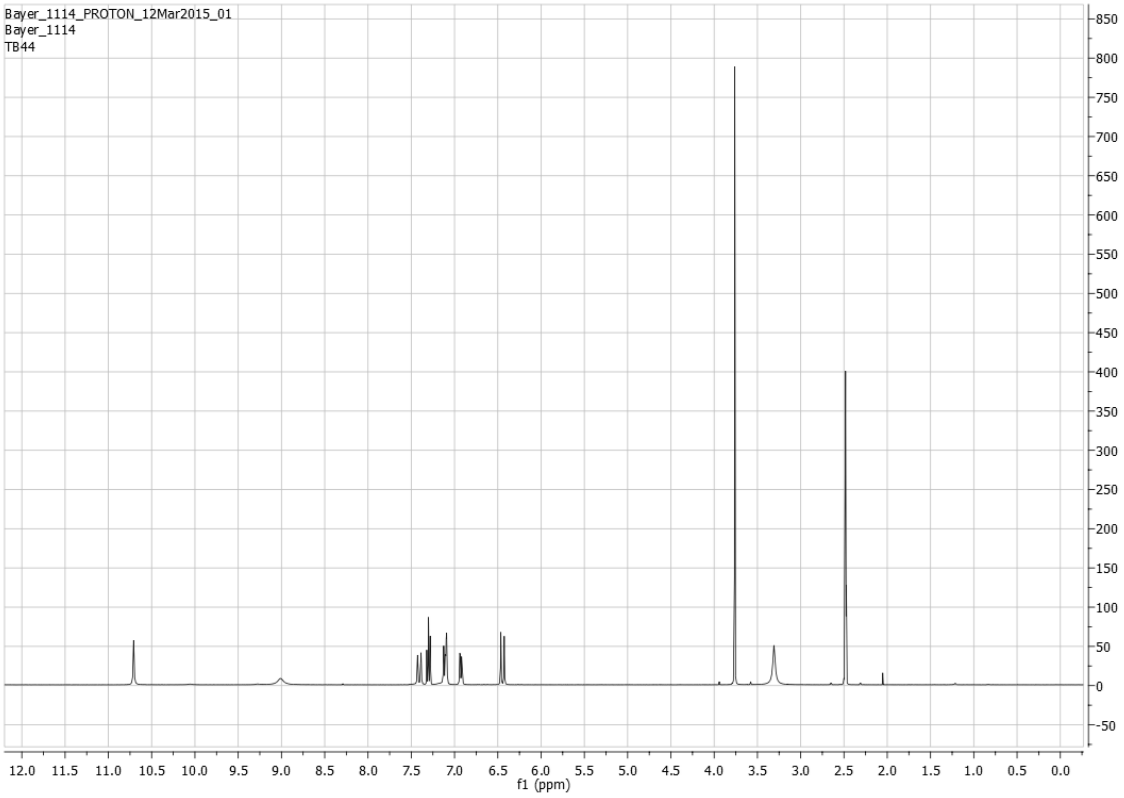

24q (TB43)

HPLC

<Chromatogram>

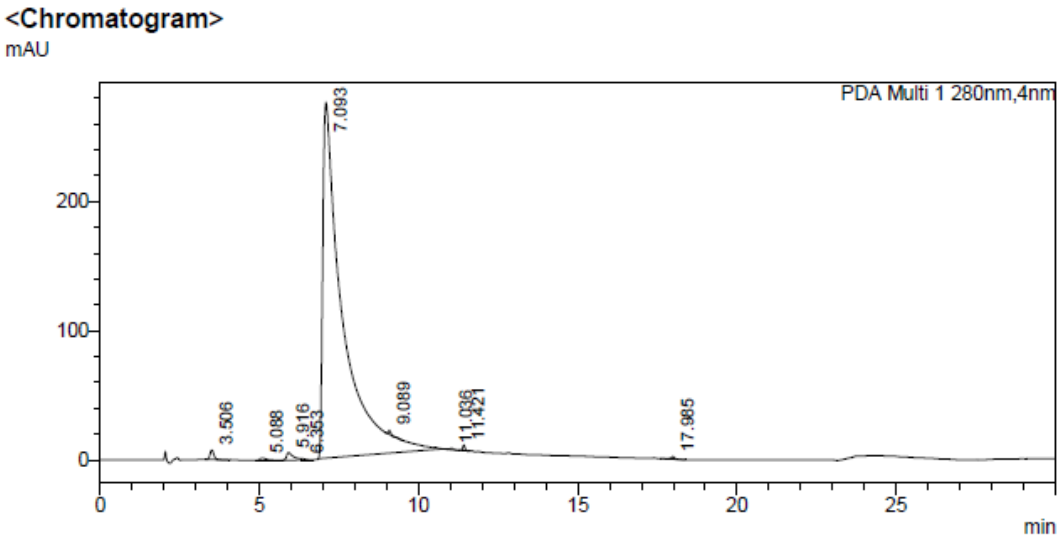

<Peak Table>

PDA Ch1 280nm

Peak#	Ret. Time	Area%	Area	Height
1	3.506	0.525	63409	7315
2	5.088	0.233	28177	1762
3	5.916	0.741	89530	6041
4	6.353	0.093	11217	1184
5	7.093	97.919	11827799	274921
6	9.089	0.095	11531	3088
7	11.036	0.057	6830	1176
8	11.421	0.192	23186	4249
9	17.985	0.145	17532	2009
Total		100.000	12079210	301744

^{1}H-NMR

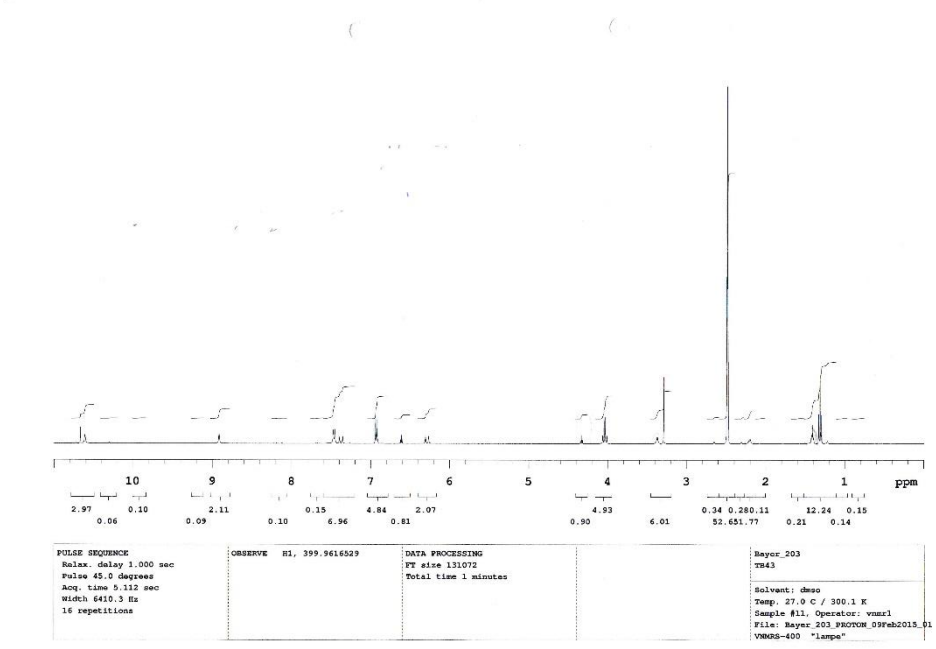

24r (TB58)

HPLC

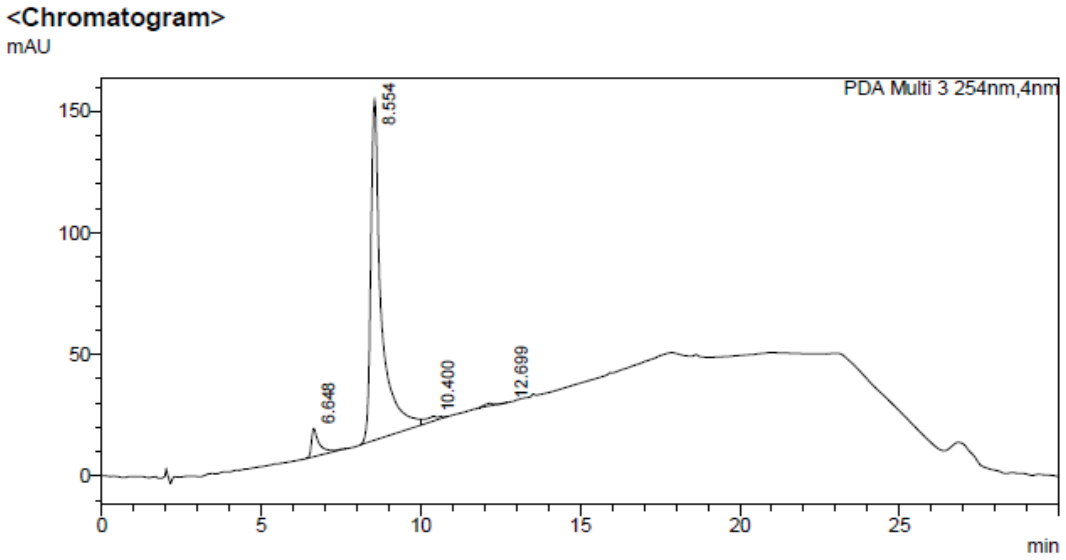

<Peak Table>

PDA Ch3 254nm

Peak#	Ret. Time	Area%
1	6.648	5.624
2	8.554	91.982
3	10.400	1.876
4	12.699	0.518
Total		100.000

^{1}H-NMR

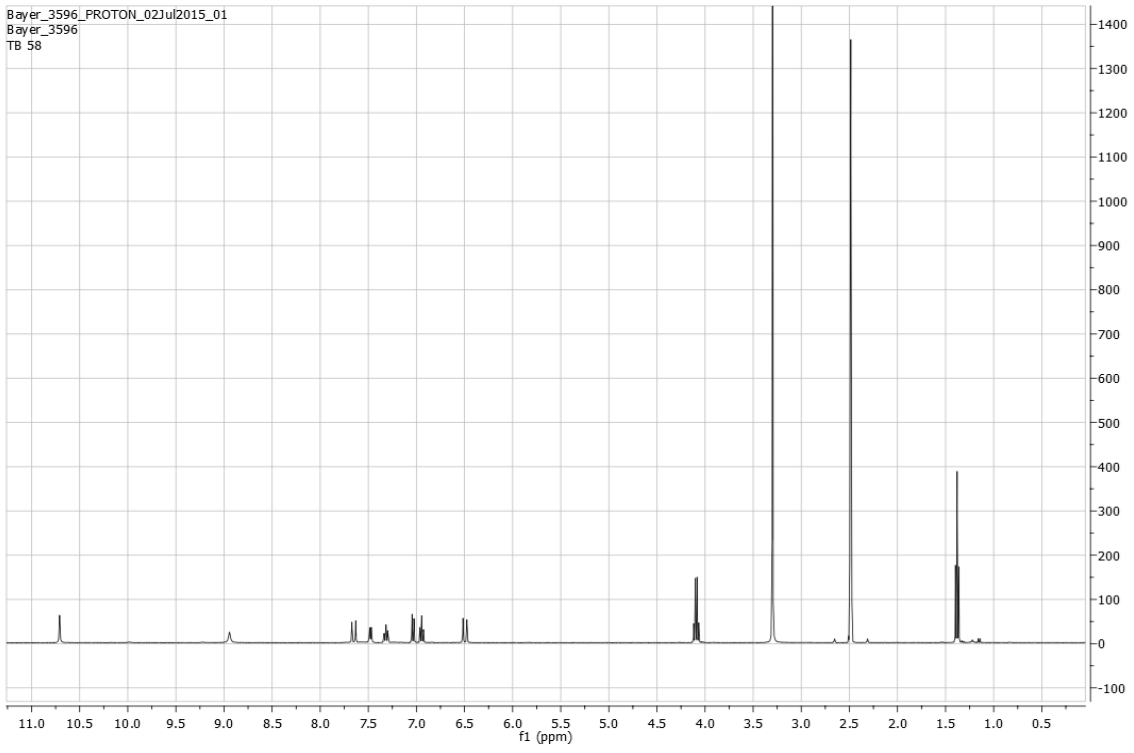

24s (TB11)

HPLC

<Chromatogram>

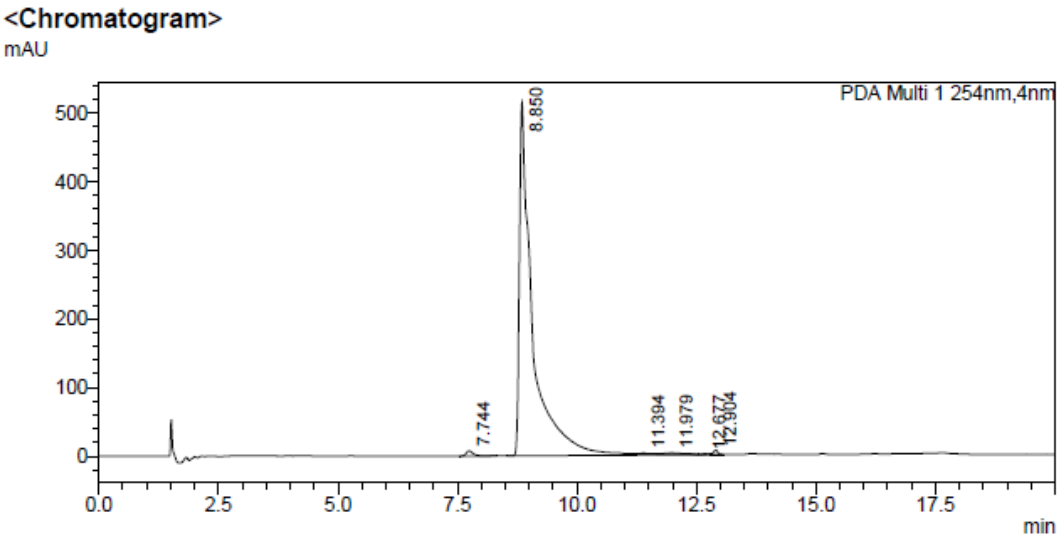

<Peak Table>

PDA Ch1 254nm

Peak#	Ret. Time	Area%	Area	Height
1	7.744	0.766	77621	7461
2	8.850	98.281	9963036	514134
3	11.394	0.068	6922	1101
4	11.979	0.432	43830	1409
5	12.677	0.071	7200	799
6	12.904	0.381	38659	6179
Total		100.000	10137269	531083

^{1}H-NMR

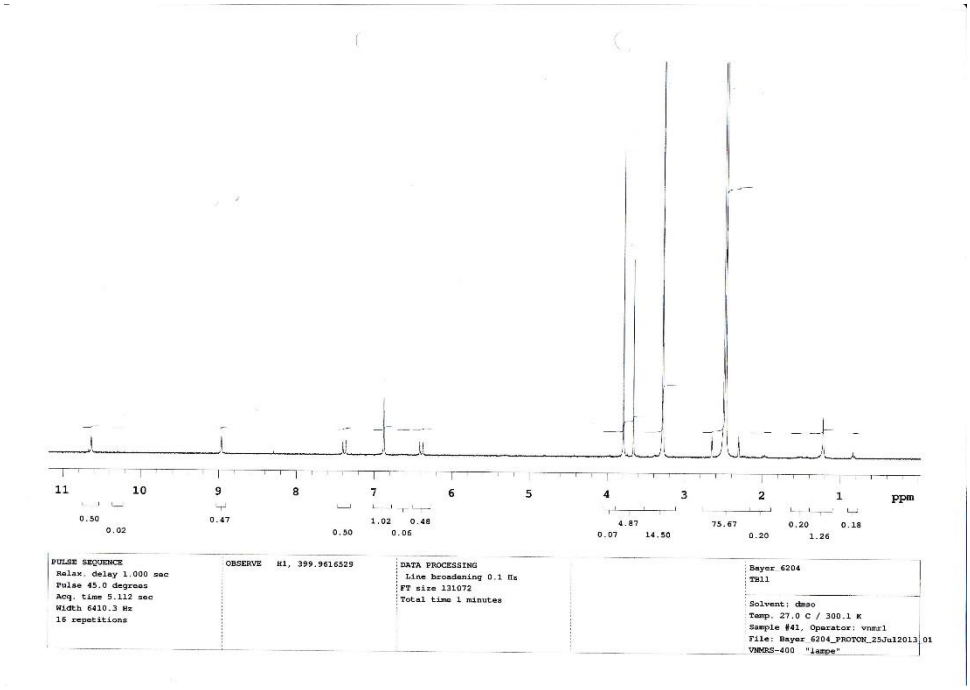

24t (TB57)

^{1}H-NMR

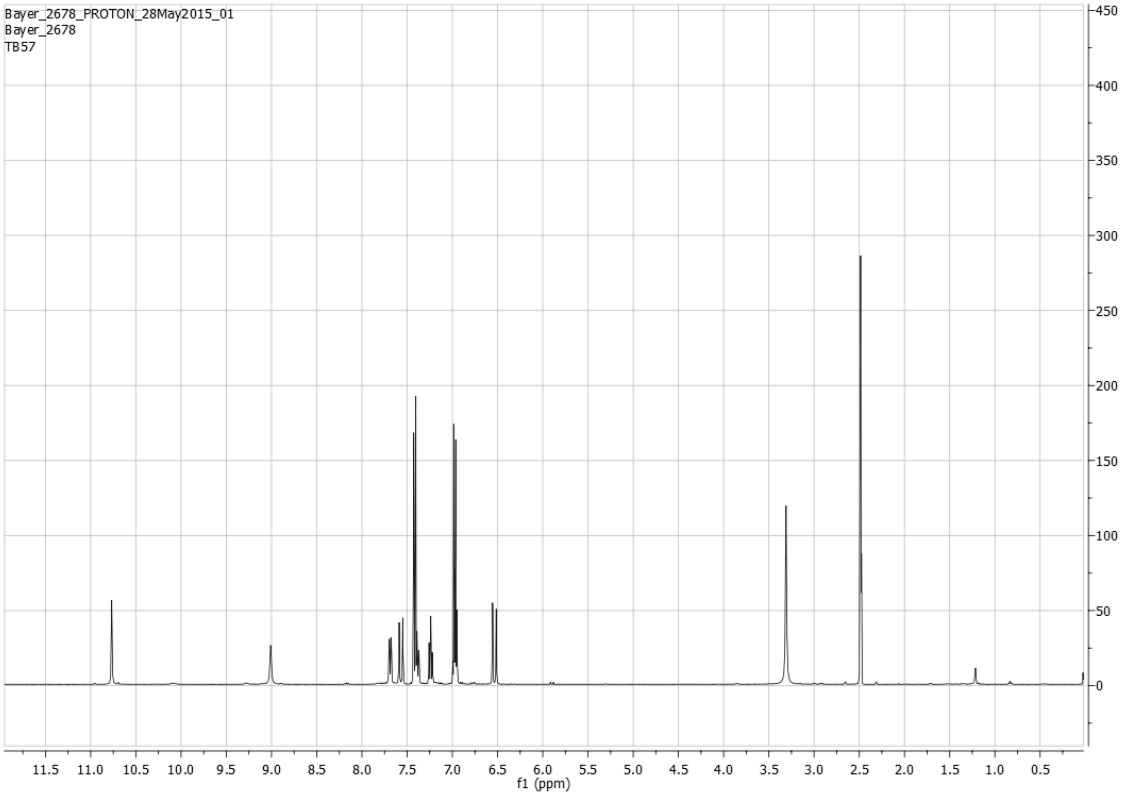

24u (TB55)

^{1}H-NMR

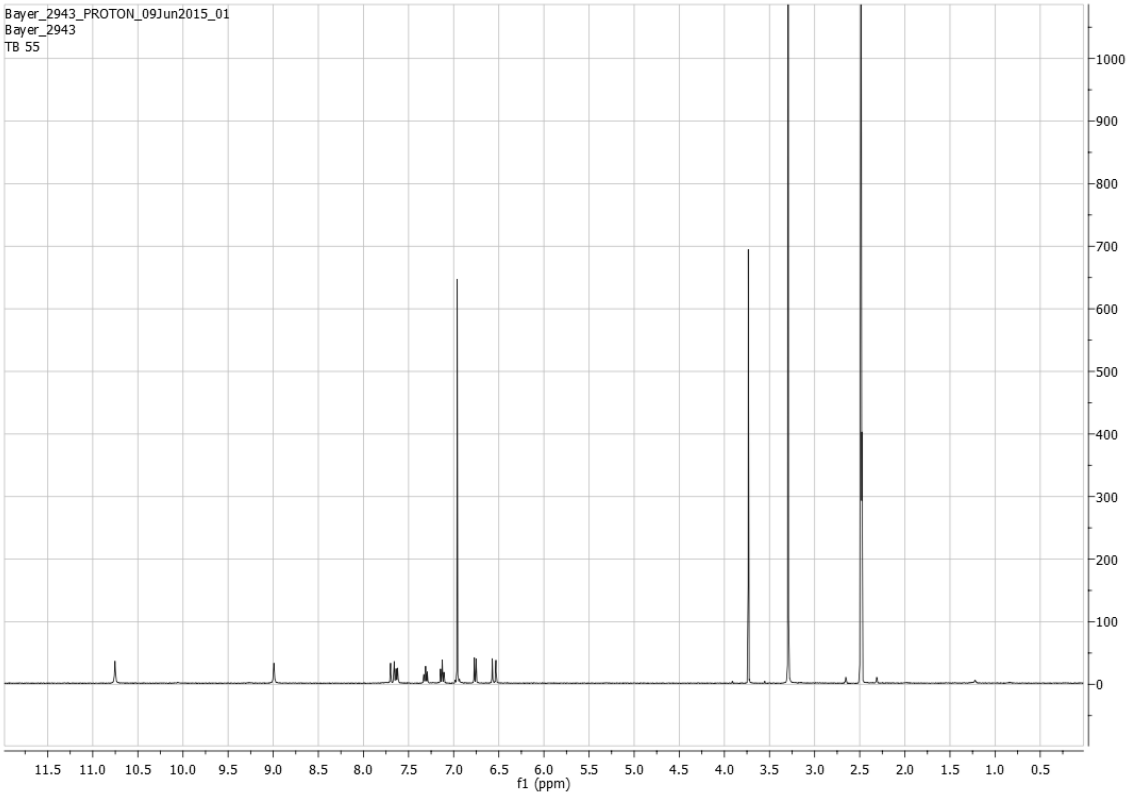

24v (TB27)

HPLC

<Chromatogram>

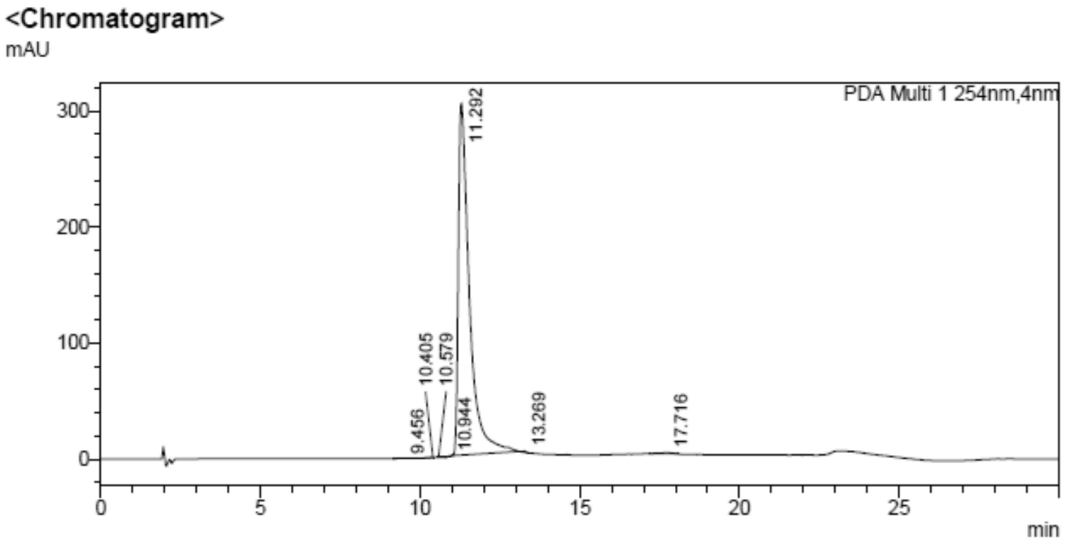

<Peak Table>

PDA Ch1 254nm

Peak#	Ret. Time	Area%	Area	Height
1	9.456	0.002	176	-1
2	10.405	-0.001	-64	10
3	10.579	-0.003	-190	53
4	10.944	0.018	1340	210
5	11.292	99.552	7279614	303103
6	13.269	0.065	4786	945
7	17.716	0.366	26740	1020
Total		100.000	7312402	305339

^{1}H-NMR

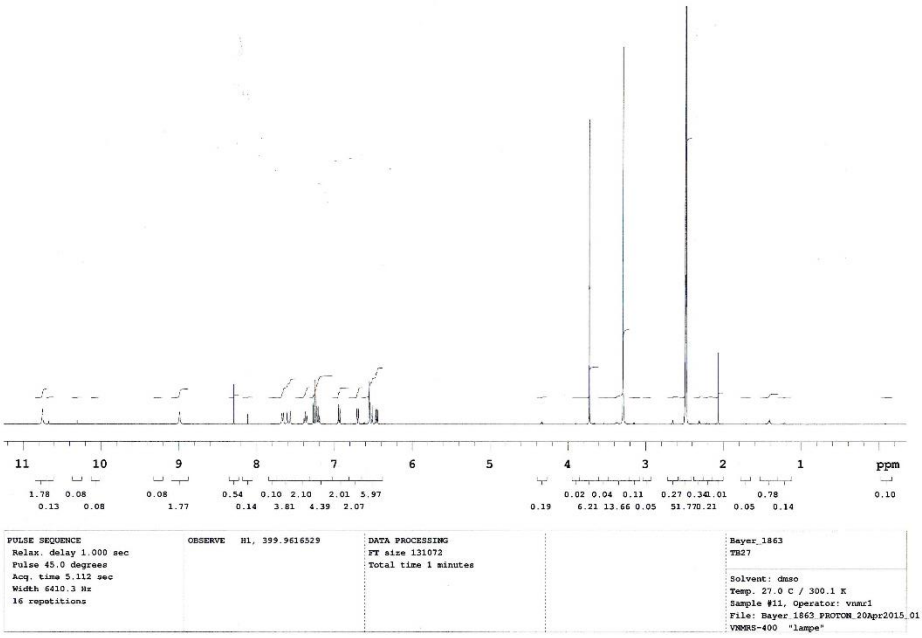

24w (TB72)

HPLC

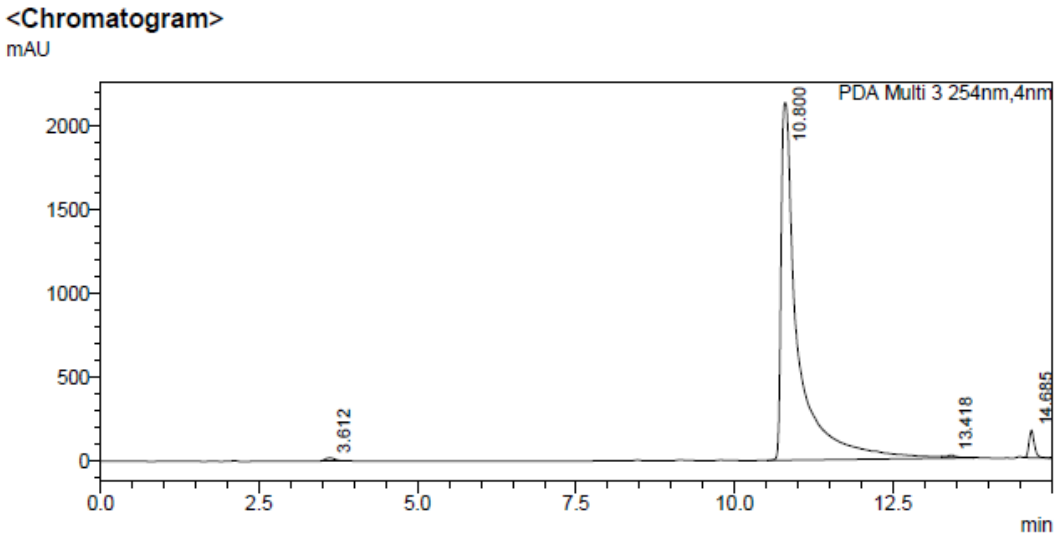

<Peak Table>

PDA Ch3 254nm

Peak#	Ret. Time	Area%
1	3.612	0.509
2	10.800	96.963
3	13.418	0.203
4	14.685	2.325
Total		100.000

^{1}H-NMR

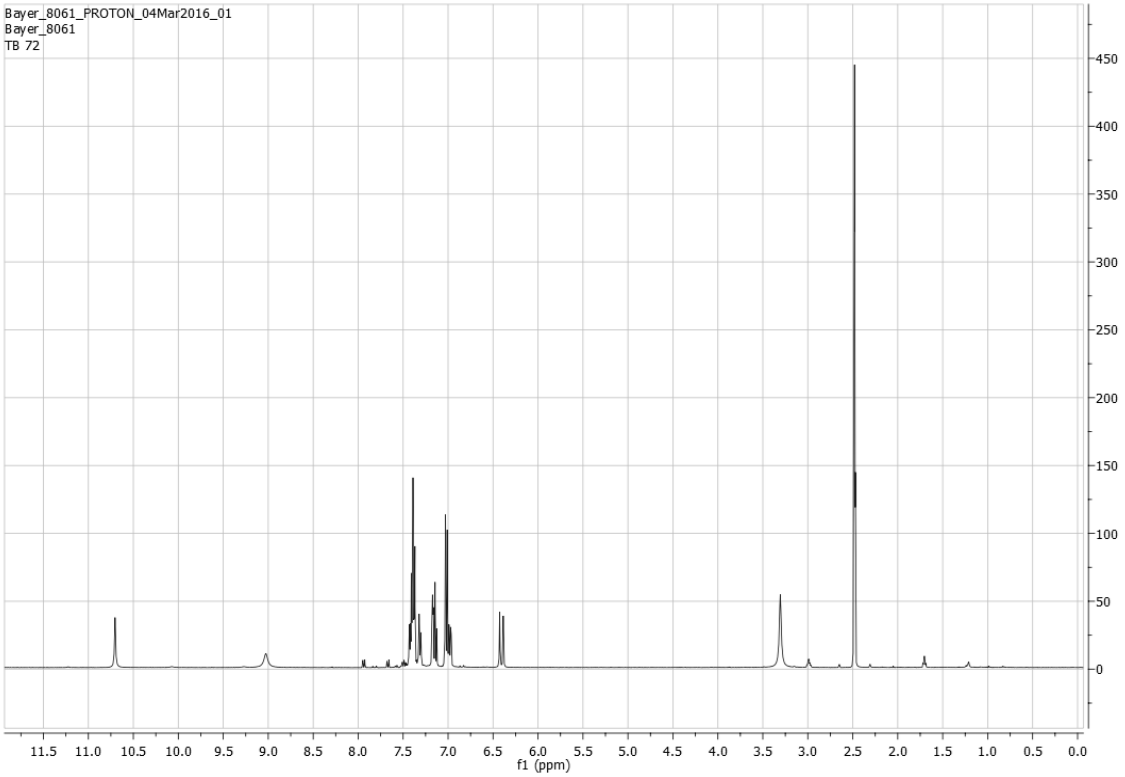

24x (TB87)

HPLC

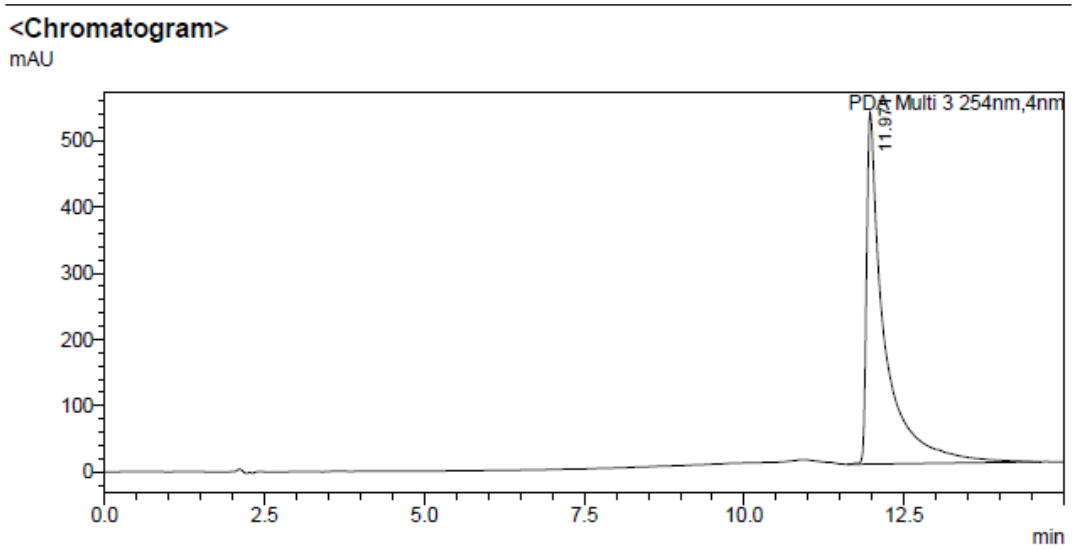

<Peak Table>

PDA Ch3 254nm

Peak#	Ret. Time	Area%
1	11.971	100.000
Total		100.000

^{1}H-NMR

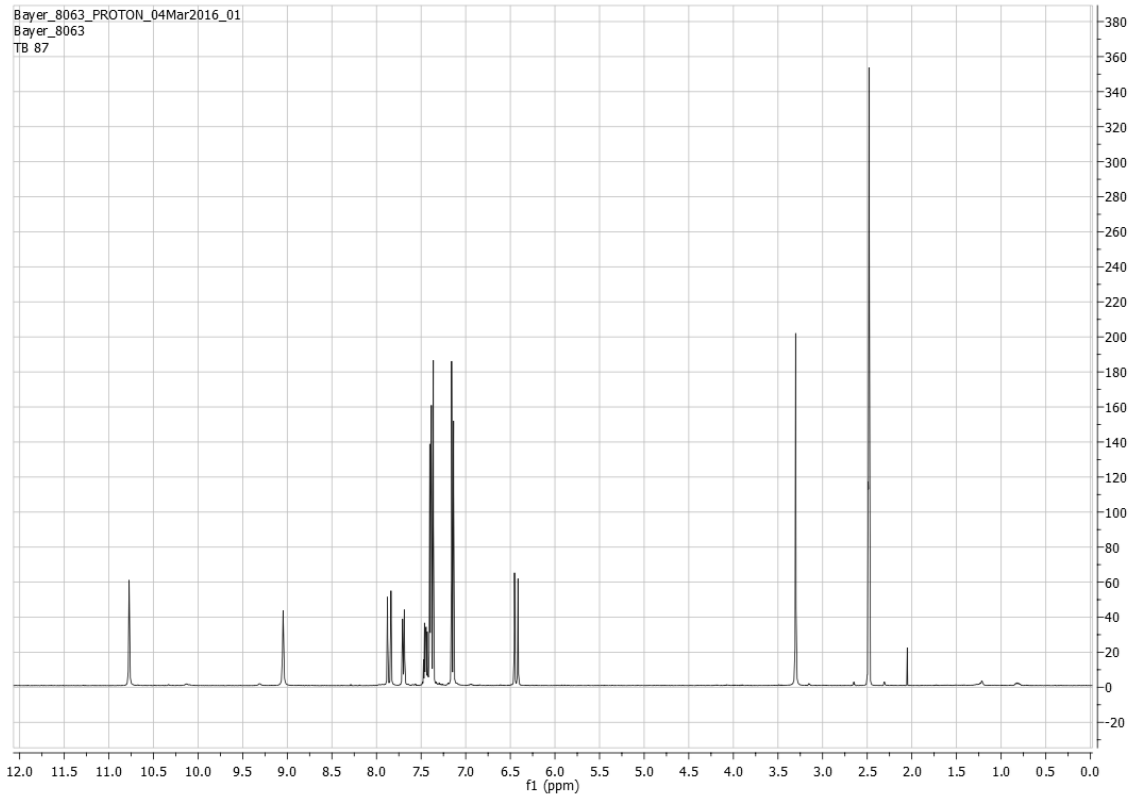

24y (TB59)

HPLC

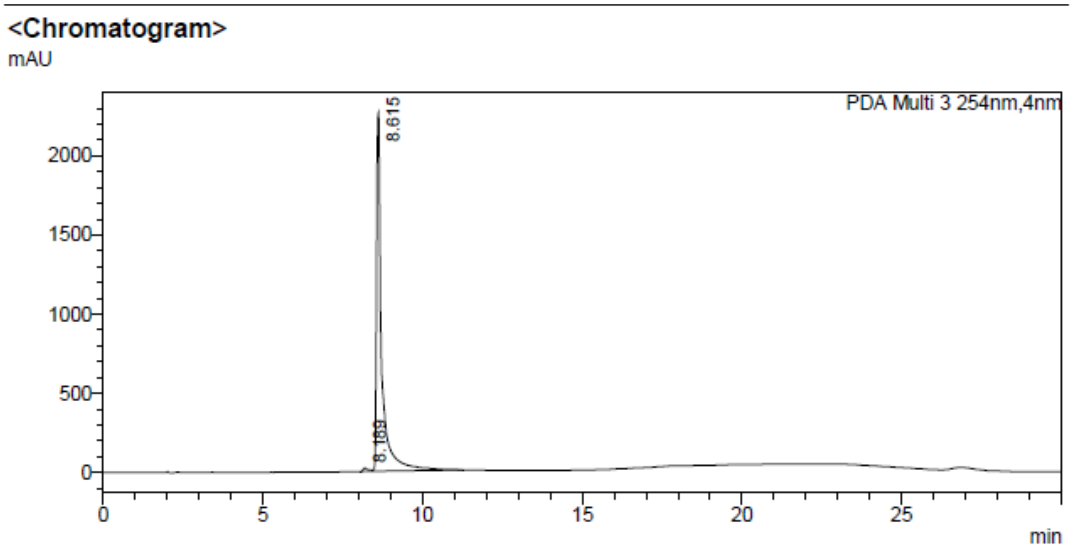

<Peak Table>

PDA Ch3 254nm

Peak#	Ret. Time	Area%
1	8.189	0.931
2	8.615	99.069
Total		100.000

^{1}H-NMR

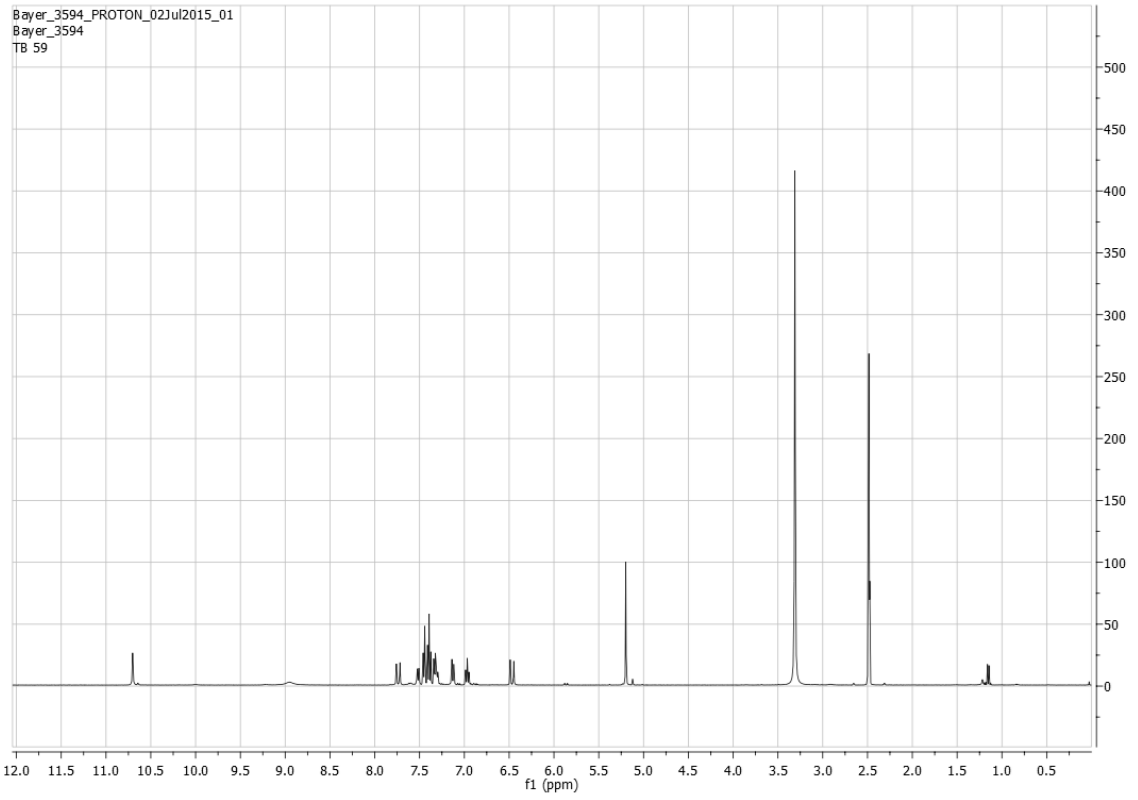

24y (TB64)

HPLC

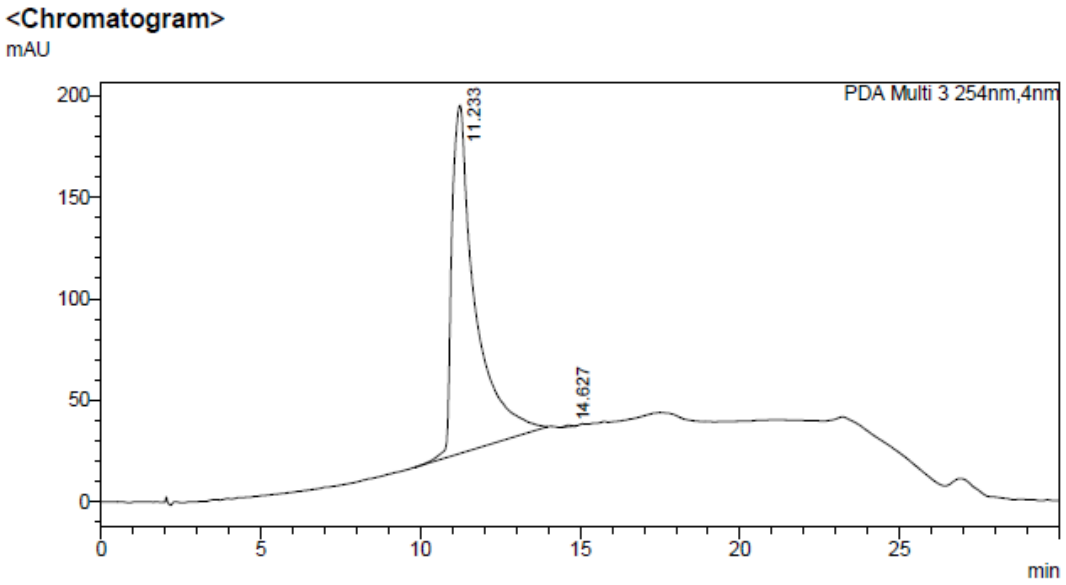

<Peak Table>

PDA Ch3 254nm

Peak#	Ret. Time	Area%
1	11.233	99.912
2	14.627	0.088
Total		100.000

^{1}H-NMR

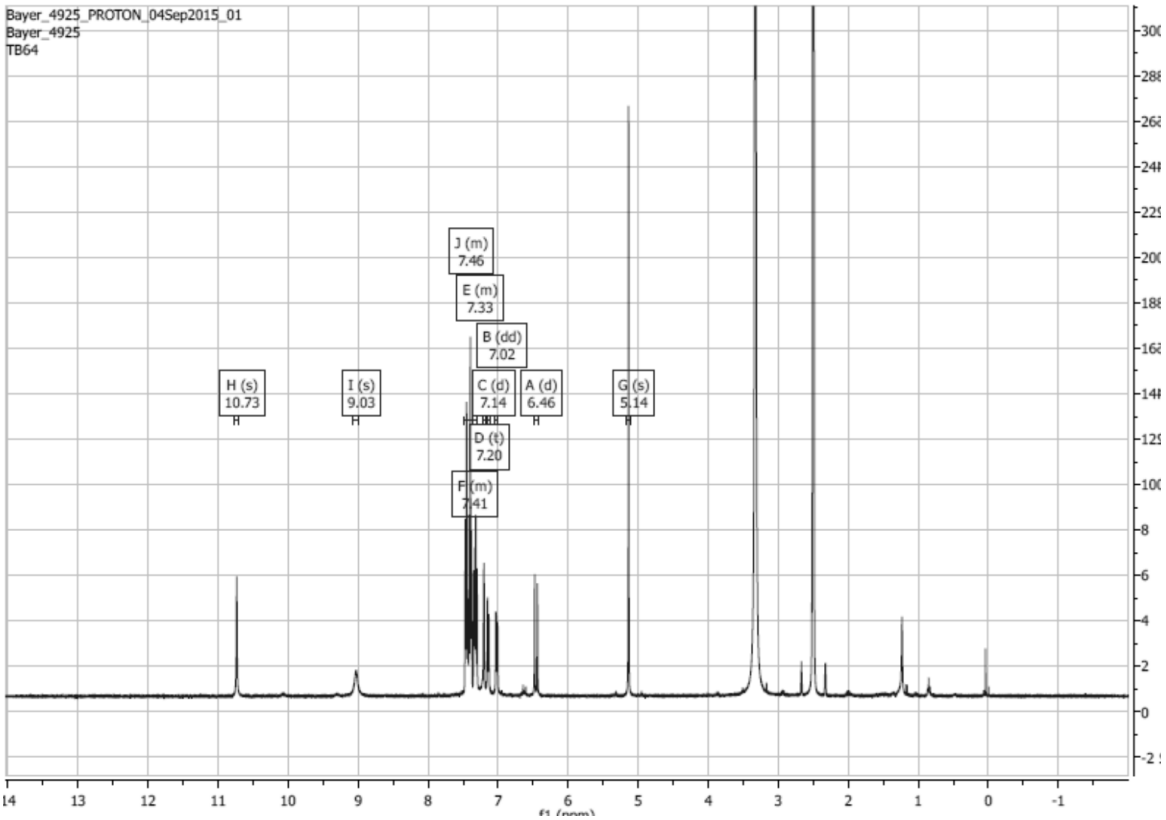

24za (TB12)

HPLC

<Chromatogram>

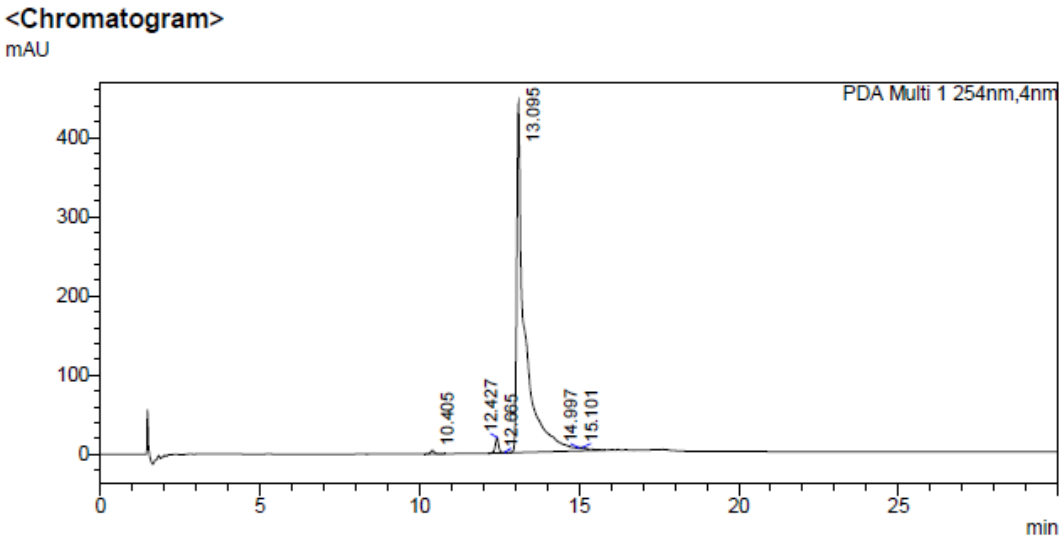

<Peak Table>

PDA Ch1 254nm

Peak#	Ret. Time	Area%	Area	Height
1	10.405	0.429	34273	4298
2	12.427	1.767	141097	19673
3	12.665	0.078	6241	623
4	13.095	97.533	7788288	441116
5	14.997	0.051	4056	758
6	15.101	0.142	11317	1436
Total		100.000	7985272	467904

^{1}H-NMR

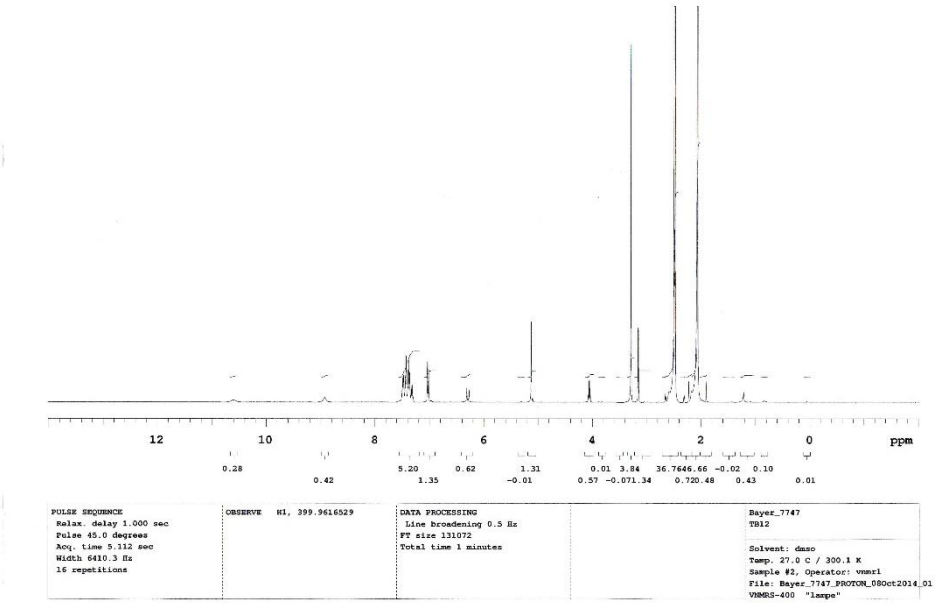

24zb (TB67)

HPLC

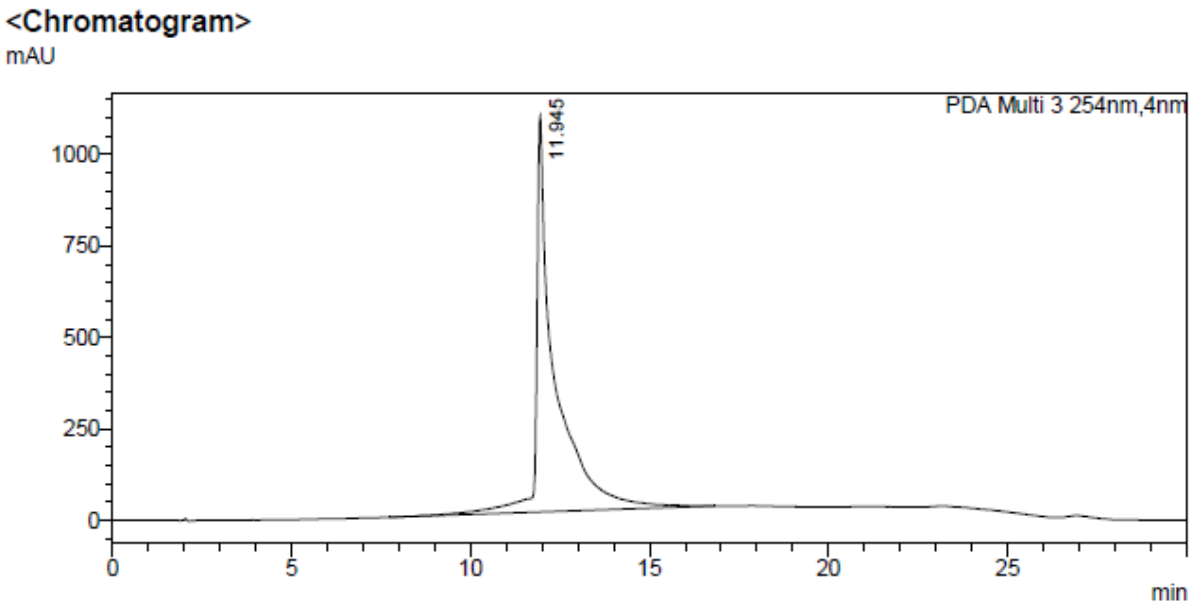

<Peak Table>

PDA Ch3 254nm

Peak#	Ret. Time	Area%
1	11.945	100.000
Total		100.000

^{1}H-NMR

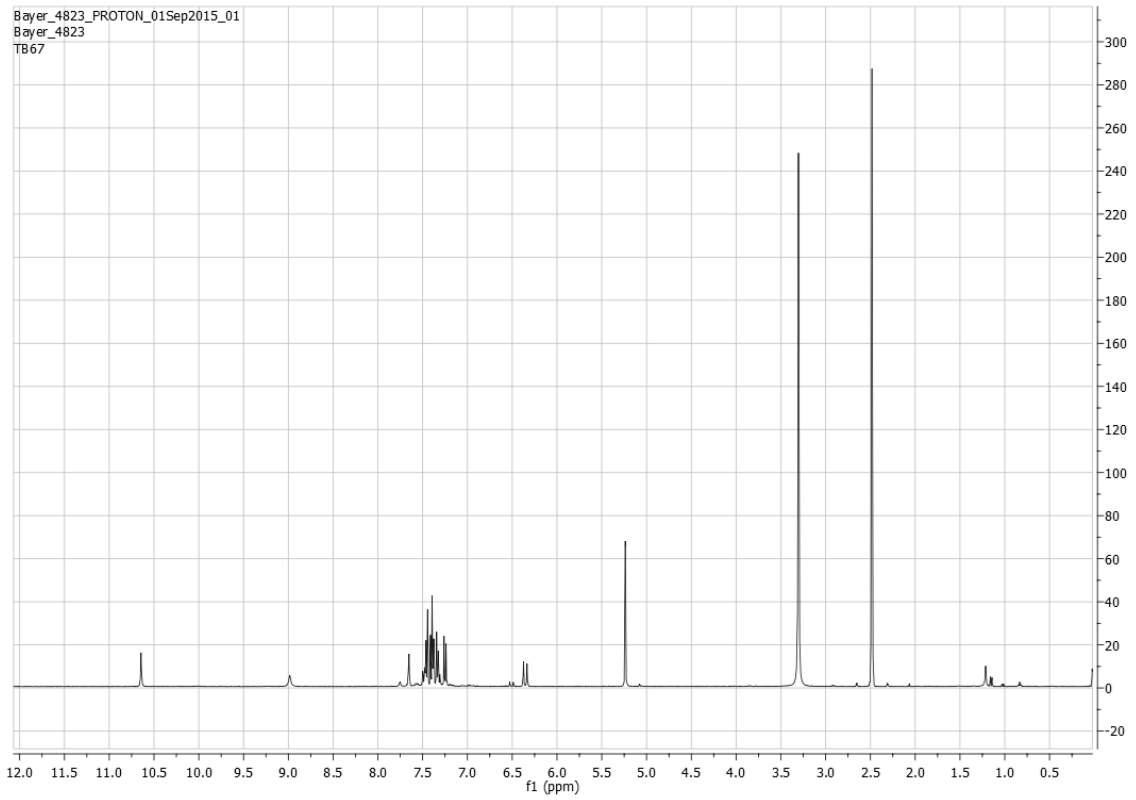

24zc (TB38)

HPLC

<Chromatogram>

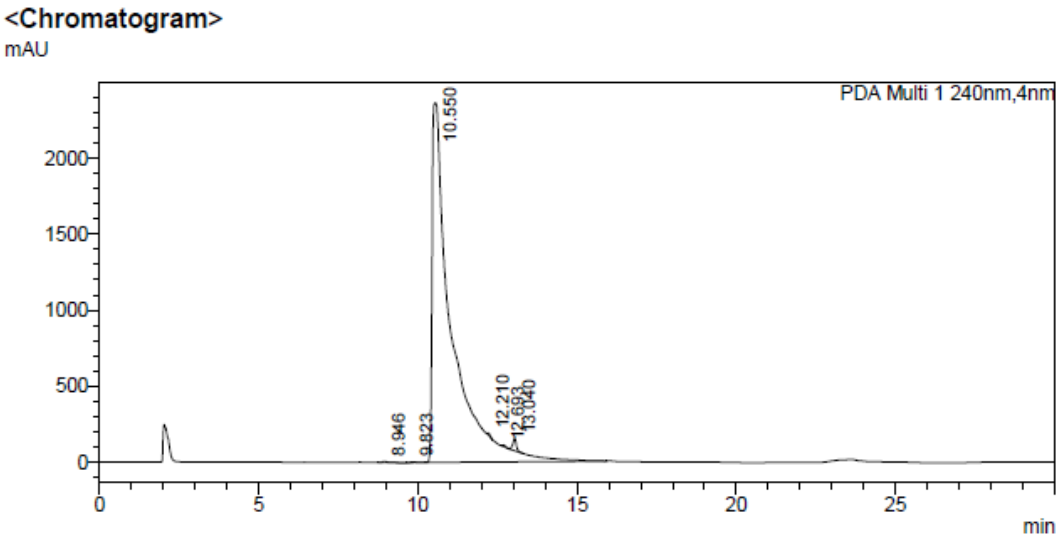

<Peak Table>

PDA Ch1 240nm

Peak#	Ret. Time	Area%	Area	Height
1	8.946	0.071	71300	7911
2	9.823	0.049	48716	4078
3	10.550	99.144	99000999	2365191
4	12.210	0.056	55845	11651
5	12.693	0.061	60462	8778
6	13.040	0.619	618249	82440
Total		100.000	99855571	2480049

^{1}H-NMR

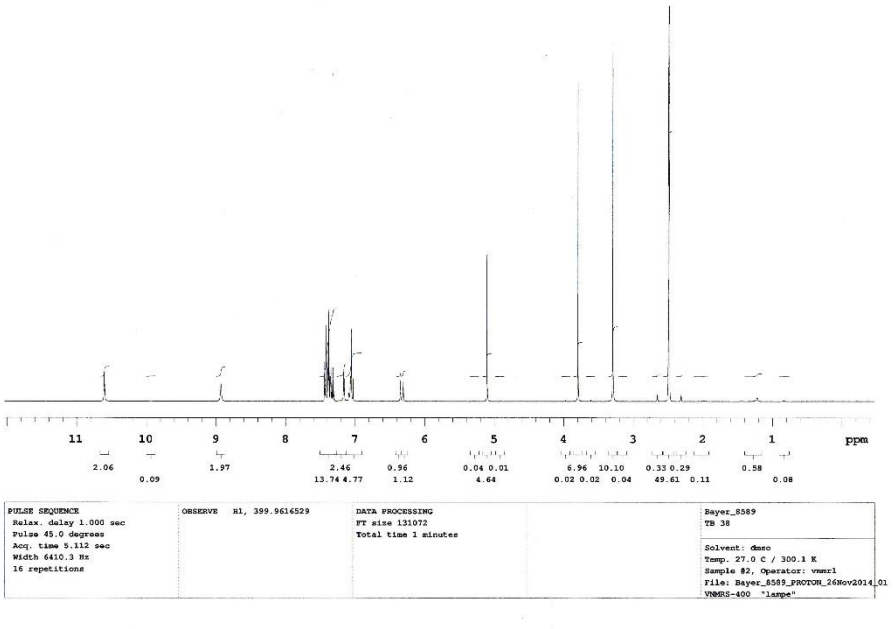

24zd (TB93)

^{1}H-NMR

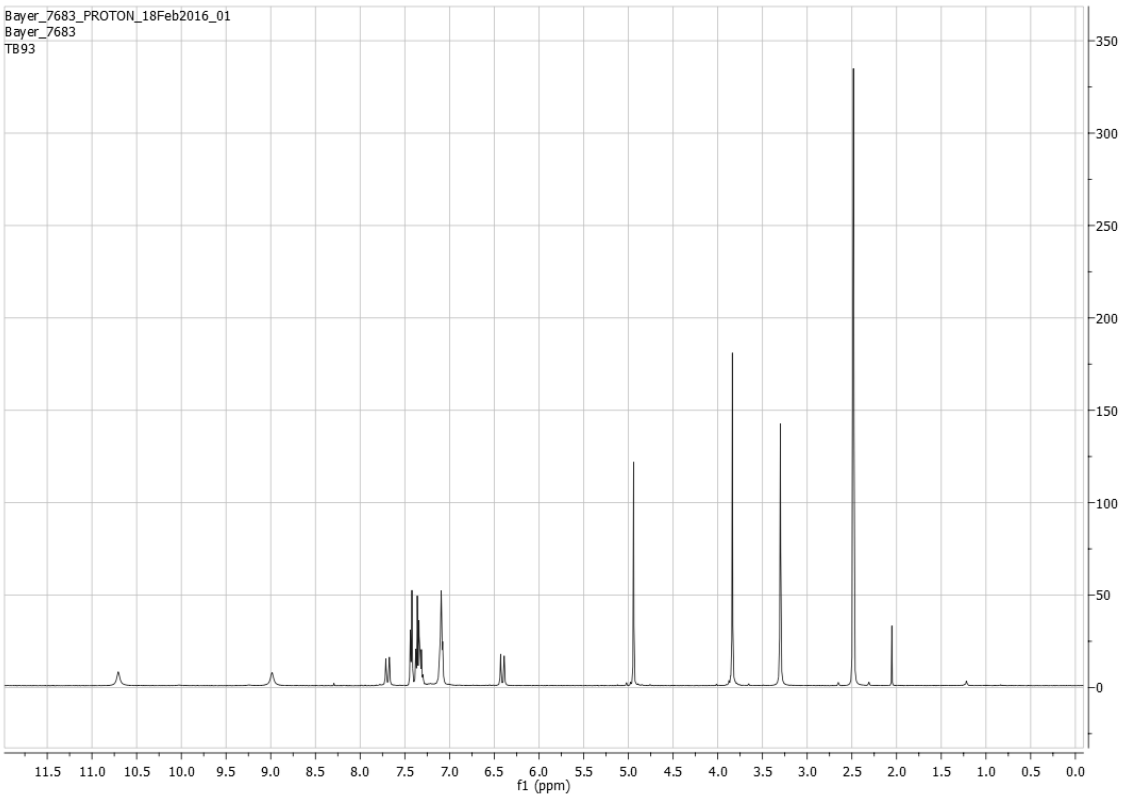

24ze (TB91)

HPLC

<Chromatogram>

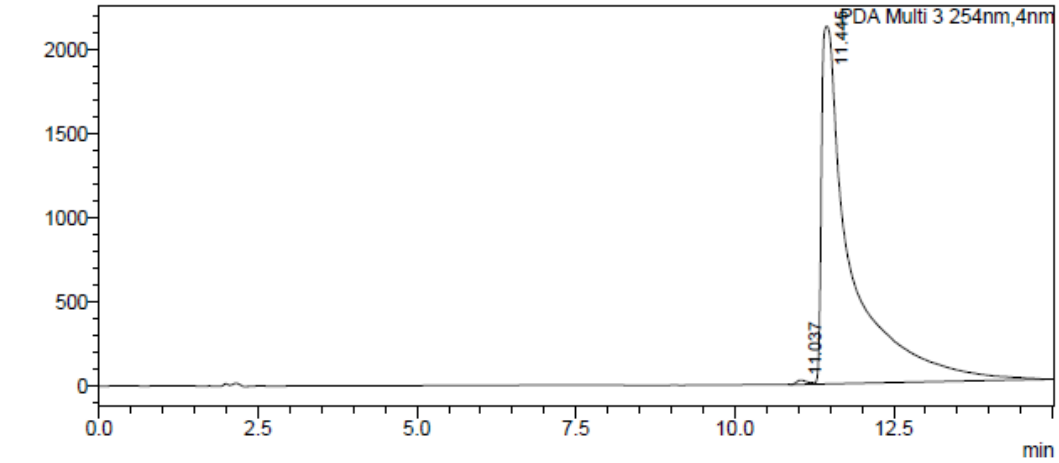

<Peak Table>

PDA Ch3 254nm

Peak#	Ret. Time	Area%
1	11.037	0.409
2	11.445	99.591
Total		100.000

^{1}H-NMR

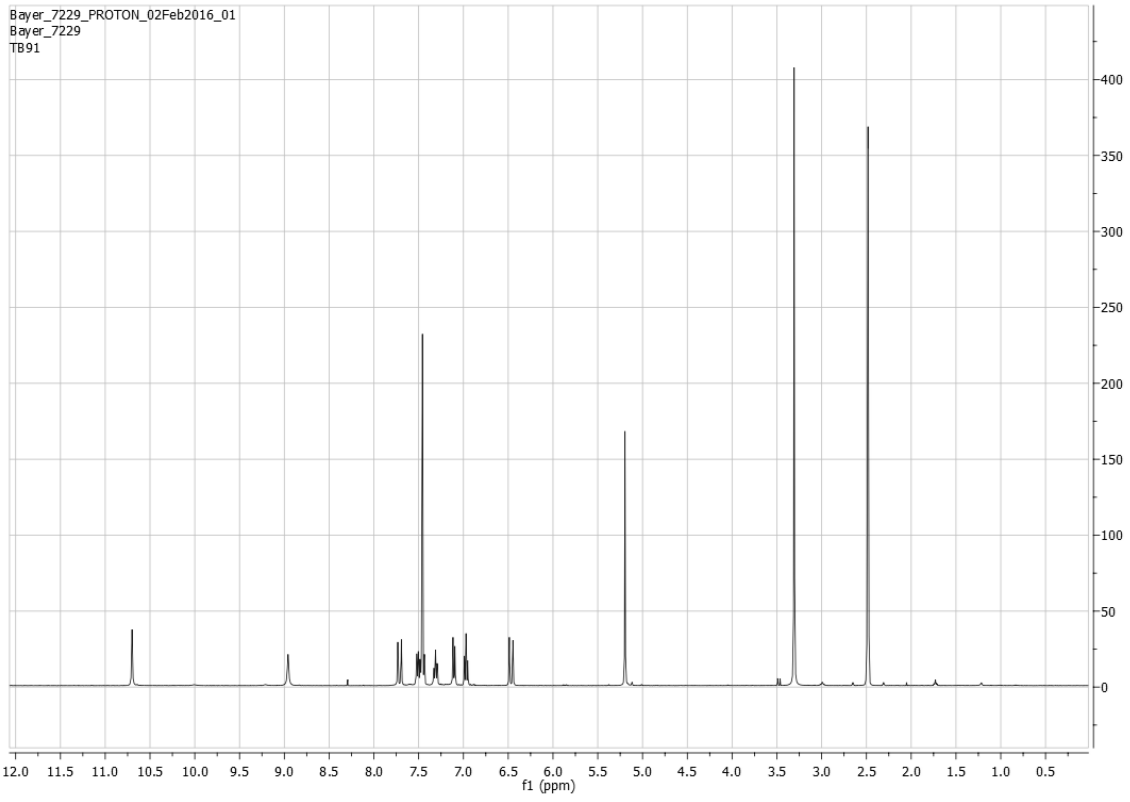

24zf (TB92)

HPLC

<Chromatogram>

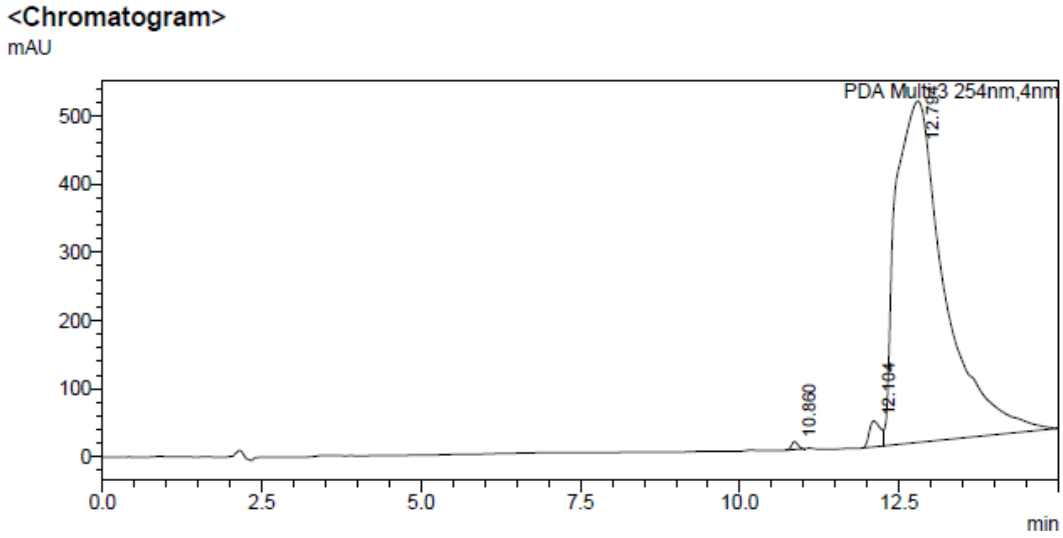

<Peak Table>

PDA Ch3 254nm

Peak#	Ret. Time	Area%
1	10.860	0.295
2	12.104	1.680
3	12.794	98.025
Total		100.000

^{1}H-NMR

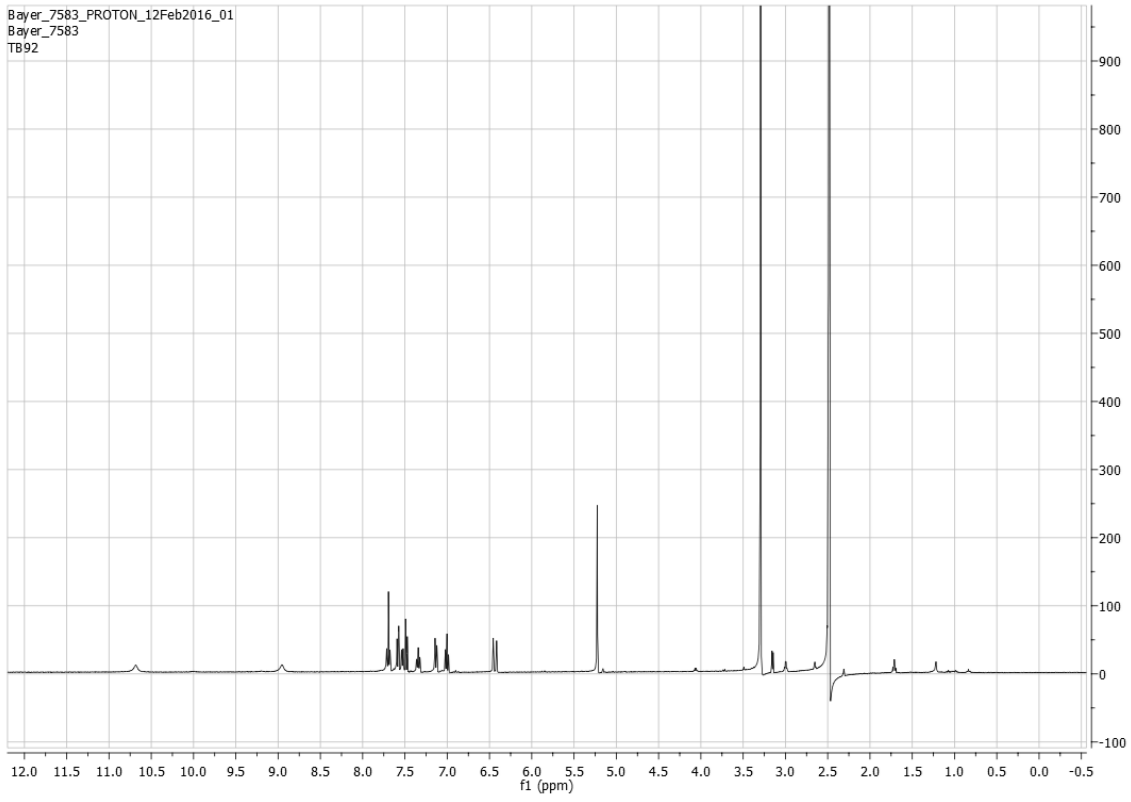

24zg (TB98)

HPLC

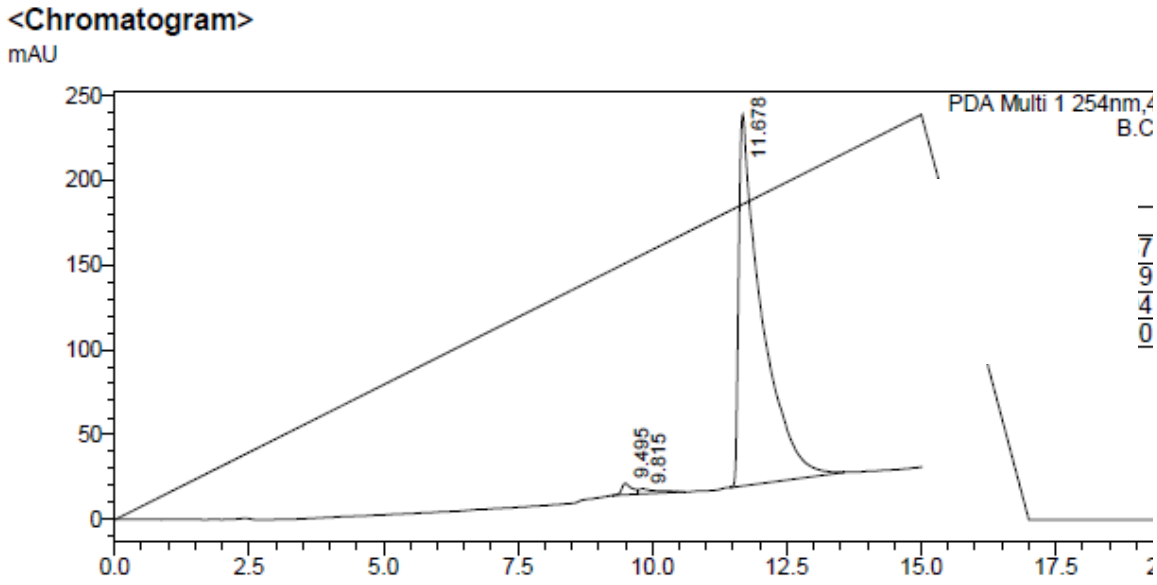

<Peak Table>

PDA Ch1 254nm

Peak#	Ret. Time	Area%
1	9.495	1.287
2	9.815	1.019
3	11.678	97.694
Total		100.000

^{1}H-NMR

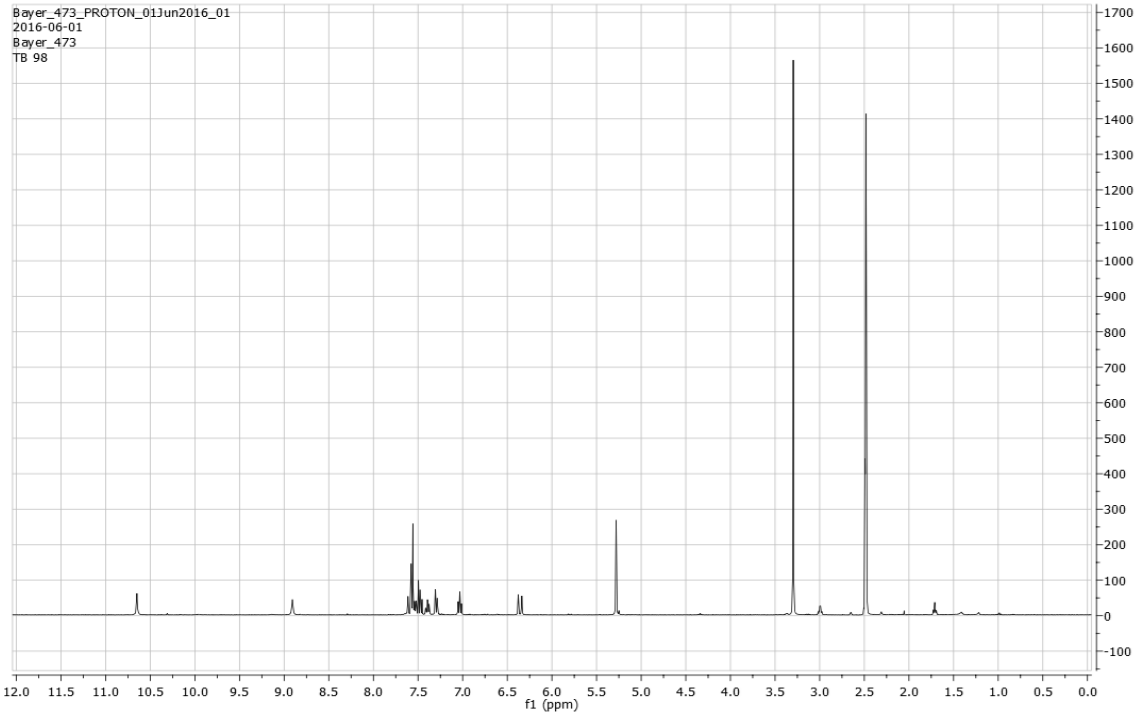

24zh (TB56)

HPLC

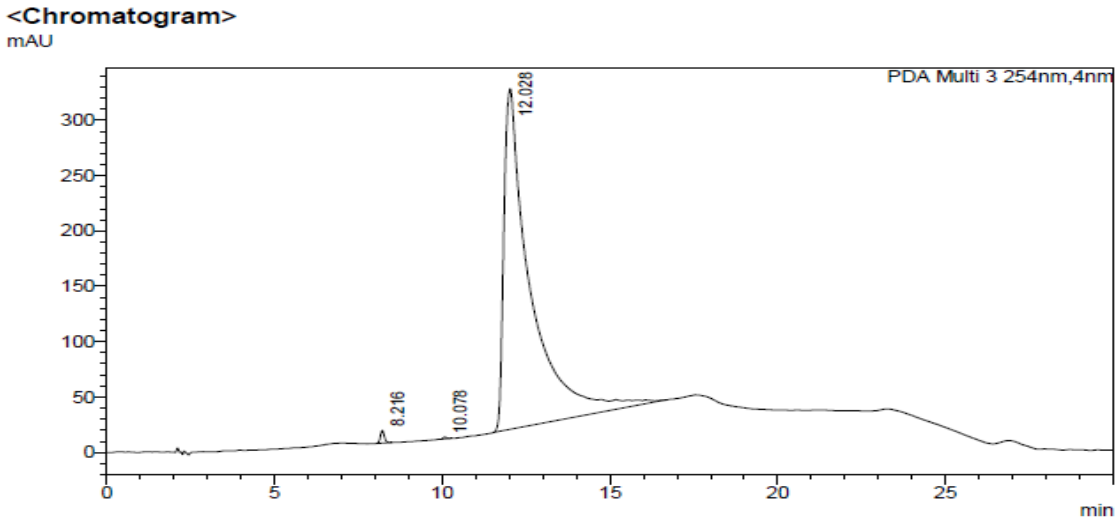

<Peak Table>

PDA Ch3 254nm

Peak#	Ret. Time	Area%
1	8.216	0.552
2	10.078	0.072
3	12.028	99.376
Total		100.000

^{1}H-NMR

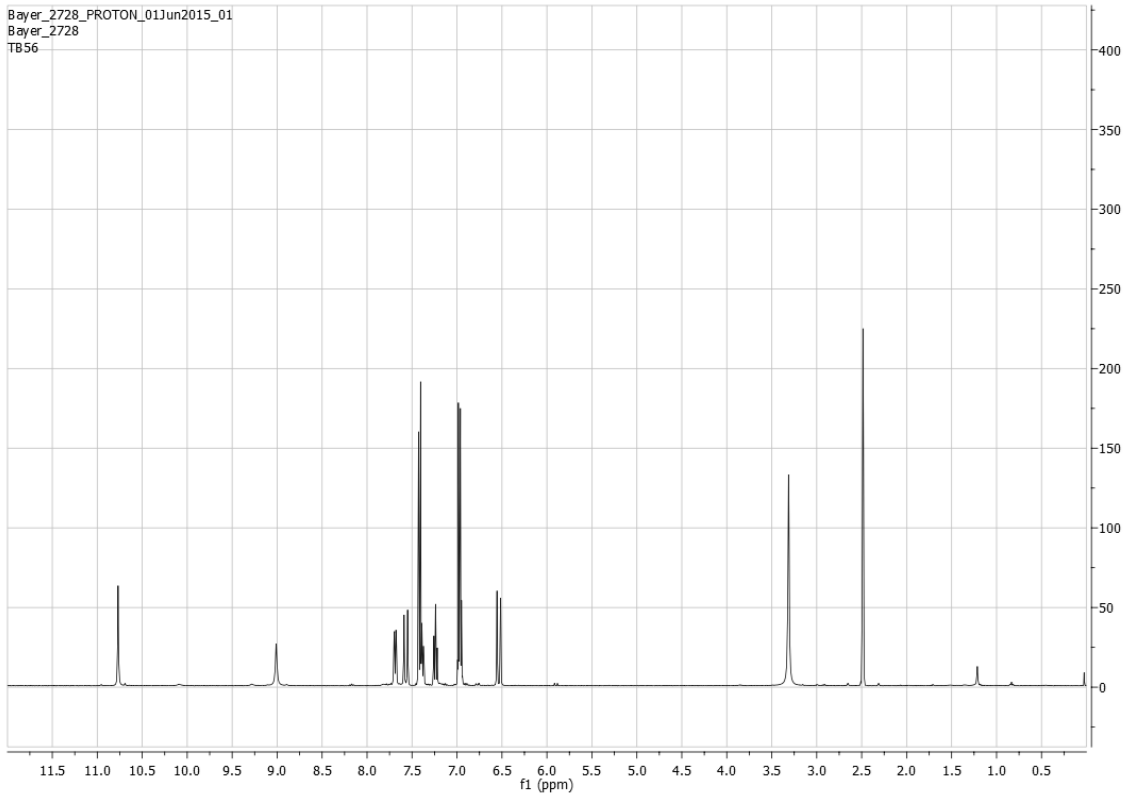

24zi (TB73)

HPLC

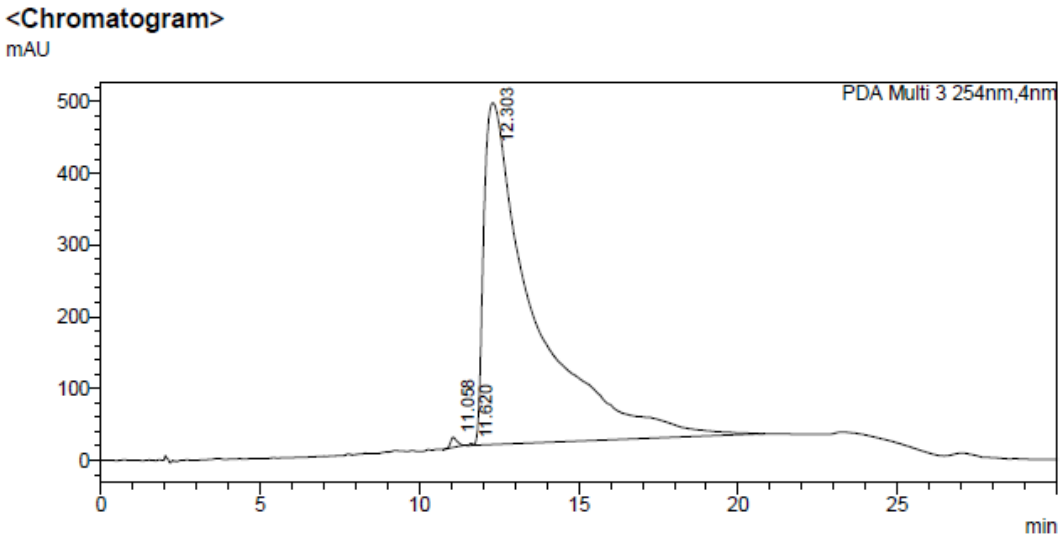

<Peak Table>

PDA Ch3 254nm

Peak#	Ret. Time	Area%
1	11.058	0.377
2	11.620	0.032
3	12.303	99.590
Total		100.000

^{1}H-NMR

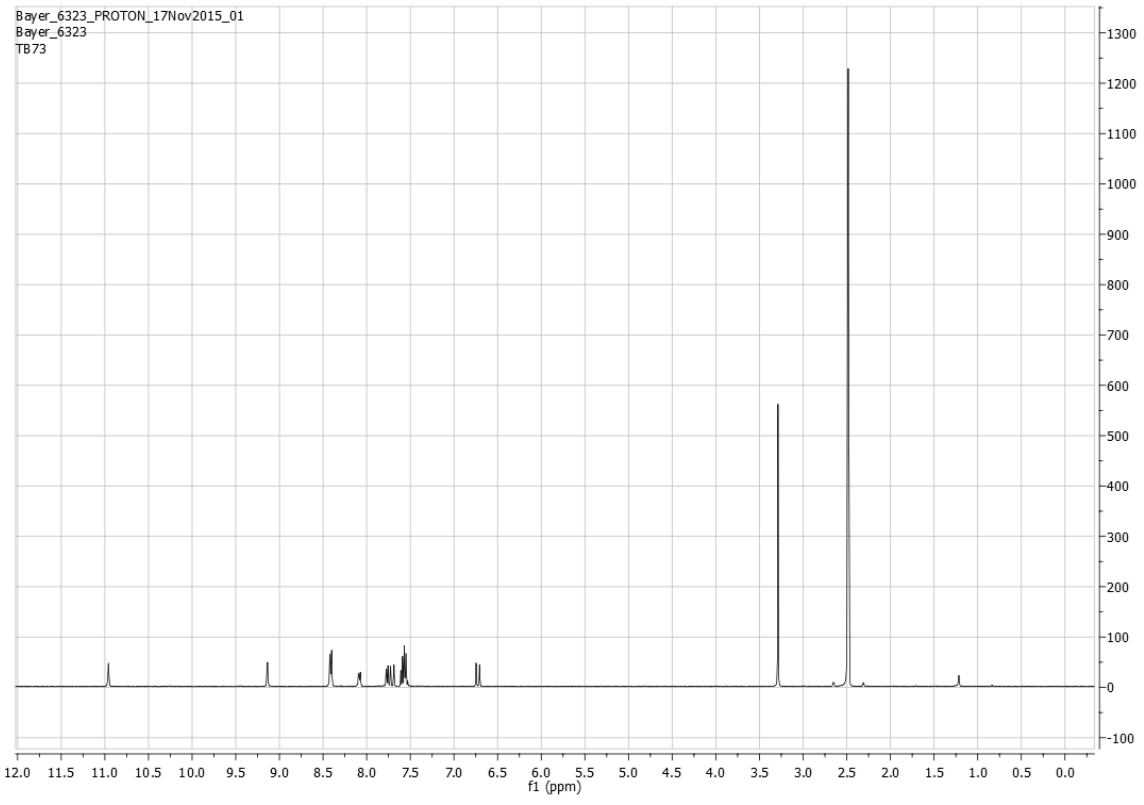

24zj (TB75)

HPLC

<Chromatogram>

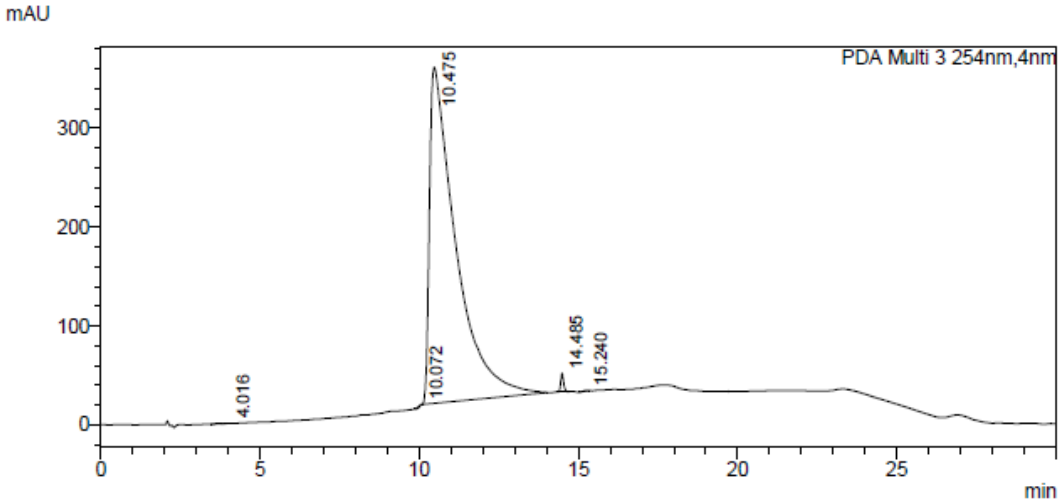

<Peak Table>

PDA Ch3 254nm

Peak#	Ret. Time	Area%	Area	Height
1	4.016	0.024	4675	-38
2	10.072	-0.010	-2021	408
3	10.475	99.381	19487959	339725
4	14.485	0.577	113080	18255
5	15.240	0.029	5730	696
Total		100.000	19609422	359046

^{1}H-NMR

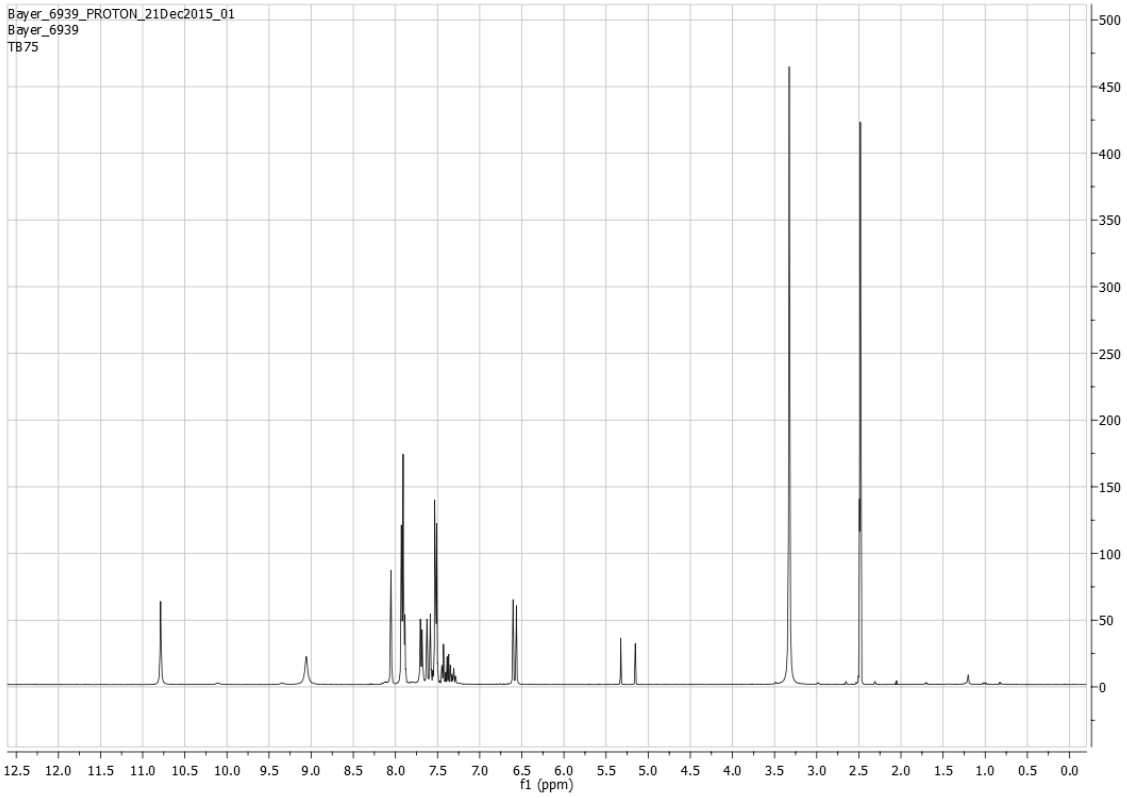

24zk (TB78)

HPLC

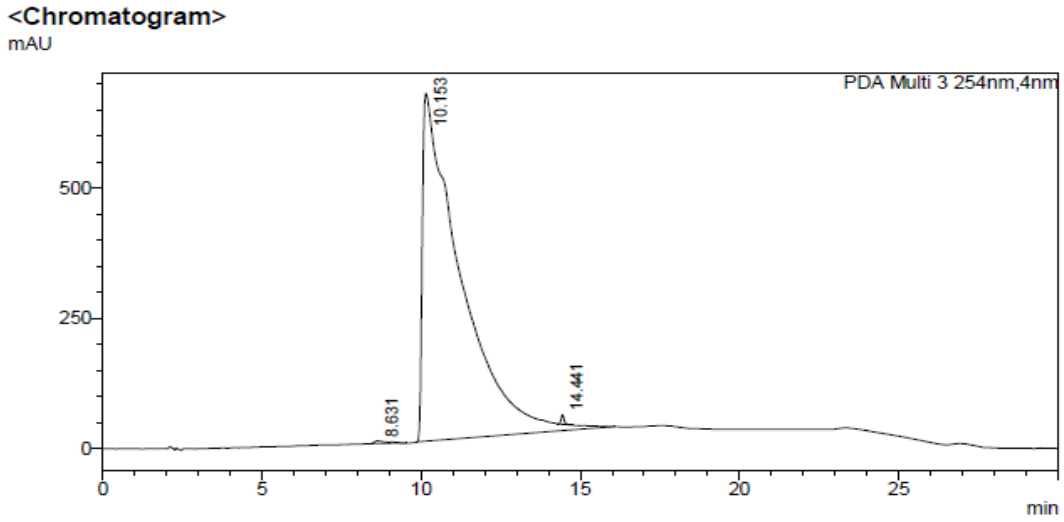

<Peak Table>

PDA Ch3 254nm

Peak#	Ret. Time	Area%
1	8.631	0.267
2	10.153	99.521
3	14.441	0.212
Total		100.000

^{1}H-NMR

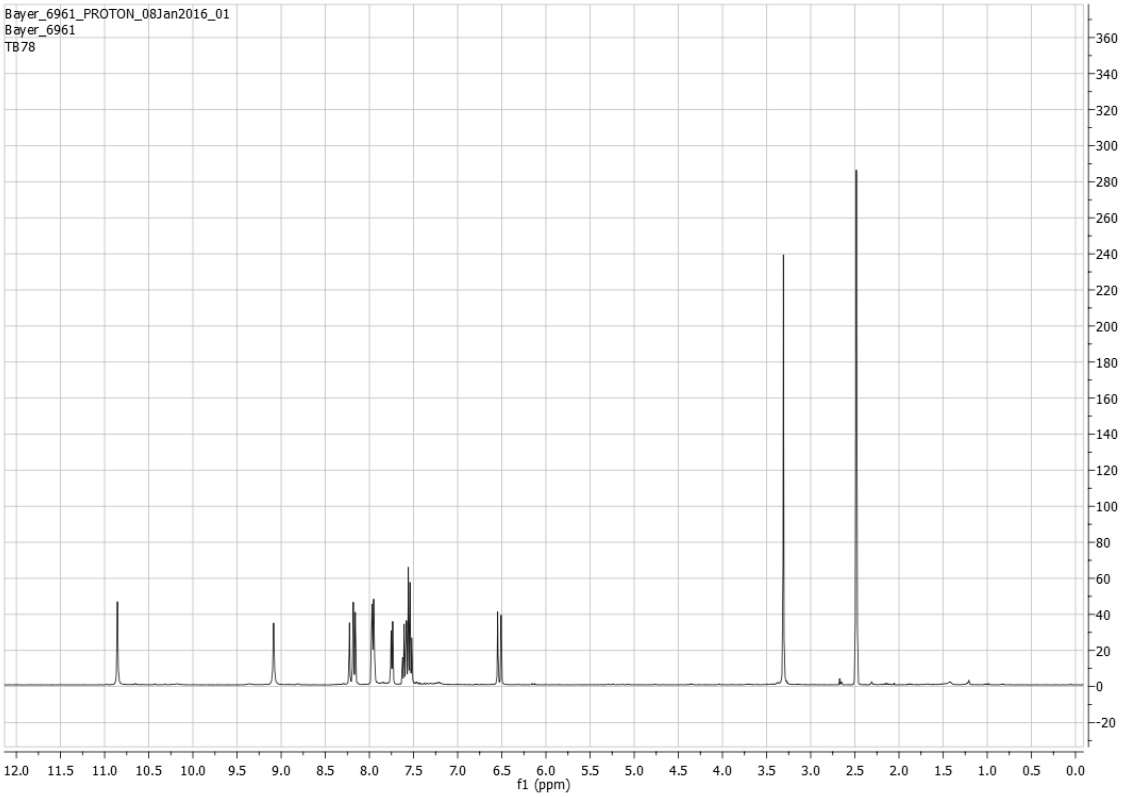

24l (TB37)

HPLC

<Chromatogram>

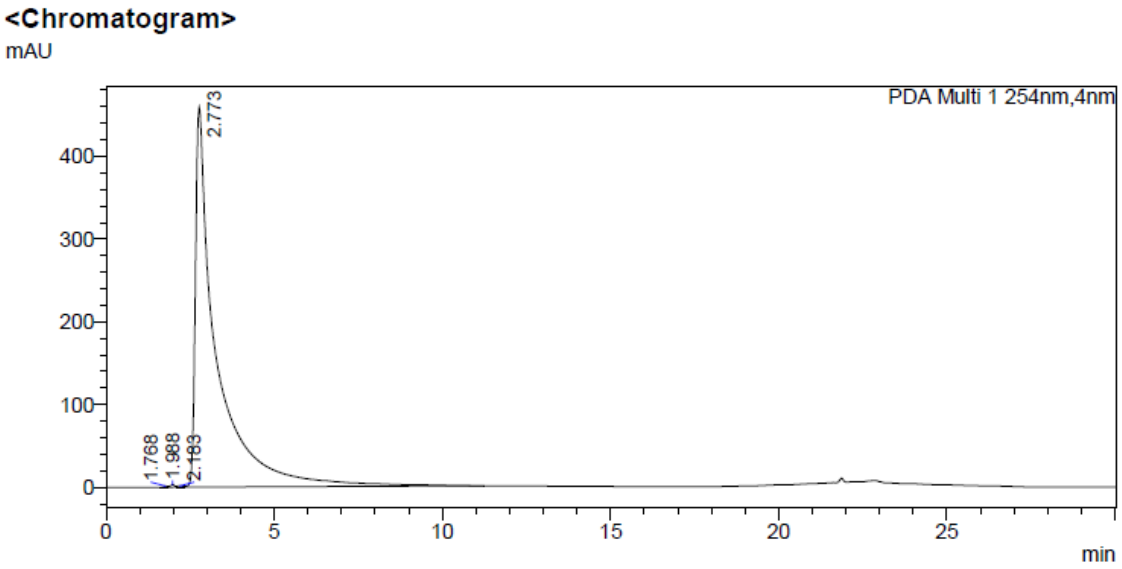

<Peak Table>

PDA Ch1 254nm

Peak#	Ret. Time	Area%	Area	Height
1	1.768	0.050	9983	1416
2	1.988	0.150	30062	3360
3	2.183	0.098	19539	1430
4	2.773	99.702	19933972	459243
Total		100.000	19993555	465449

^{1}H-NMR

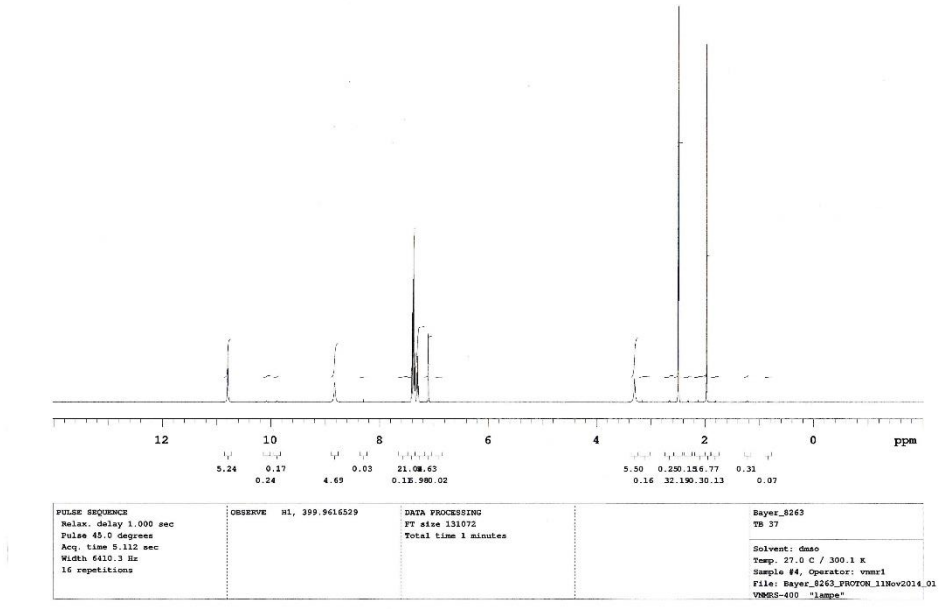

24m (TB40)

HPLC

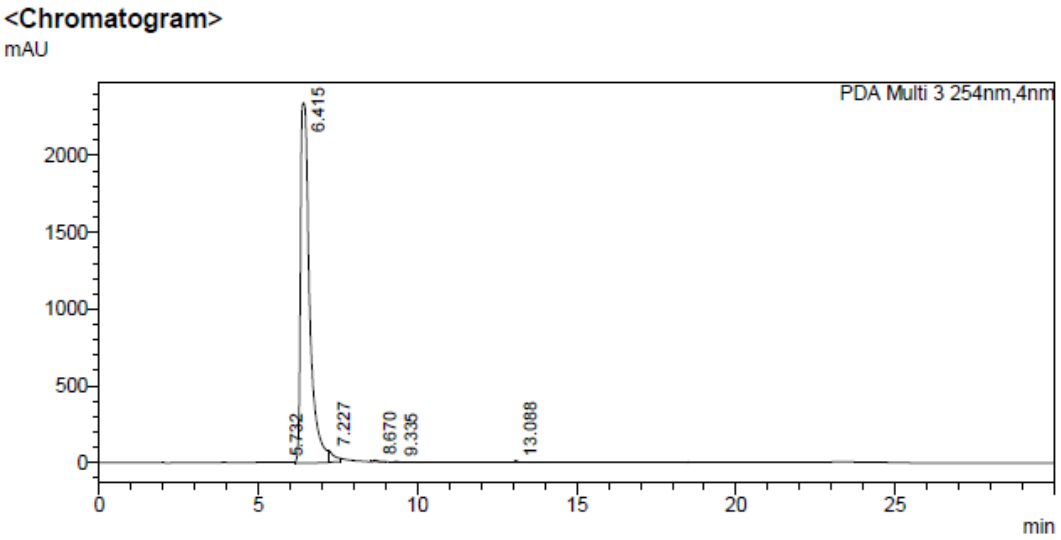

<Peak Table>

PDA Ch3 254nm

Peak#	Ret. Time	Area%	Area	Height
1	5.732	0.005	2525	414
2	6.415	97.840	46572023	2344461
3	7.227	1.791	852307	74518
4	8.670	0.147	70082	8087
5	9.335	0.070	33389	4387
6	13.088	0.147	70079	11615
Total		100.000	47600406	2443482

^{1}H-NMR

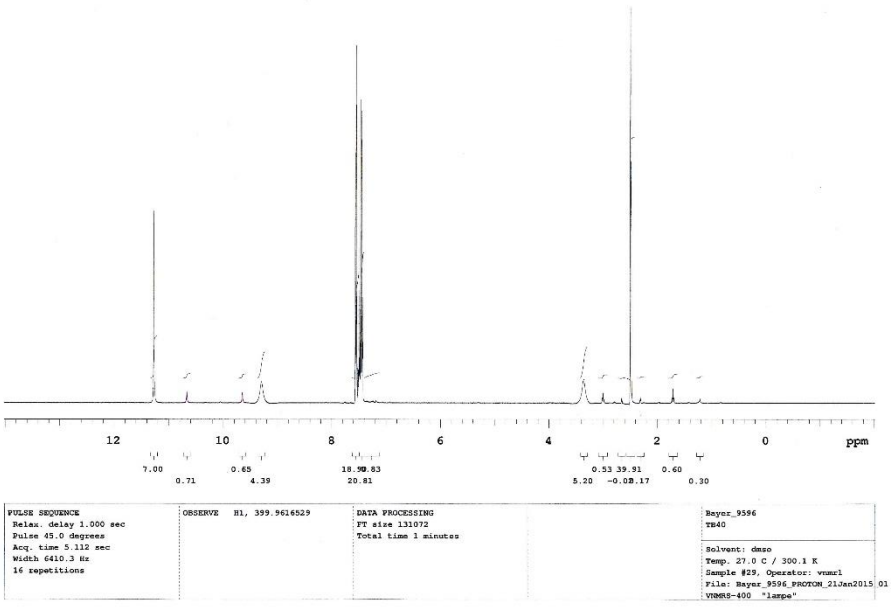

26a (TB89)

HPLC

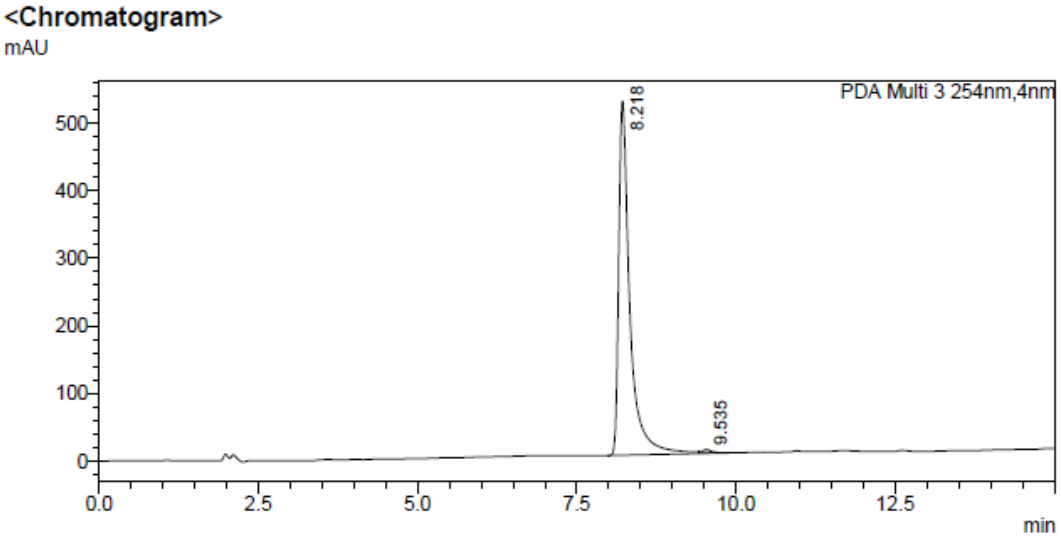

<Peak Table>

PDA Ch3 254nm

Peak#	Ret. Time	Area%
1	8.218	99.561
2	9.535	0.439
Total		100.000

^{1}H-NMR

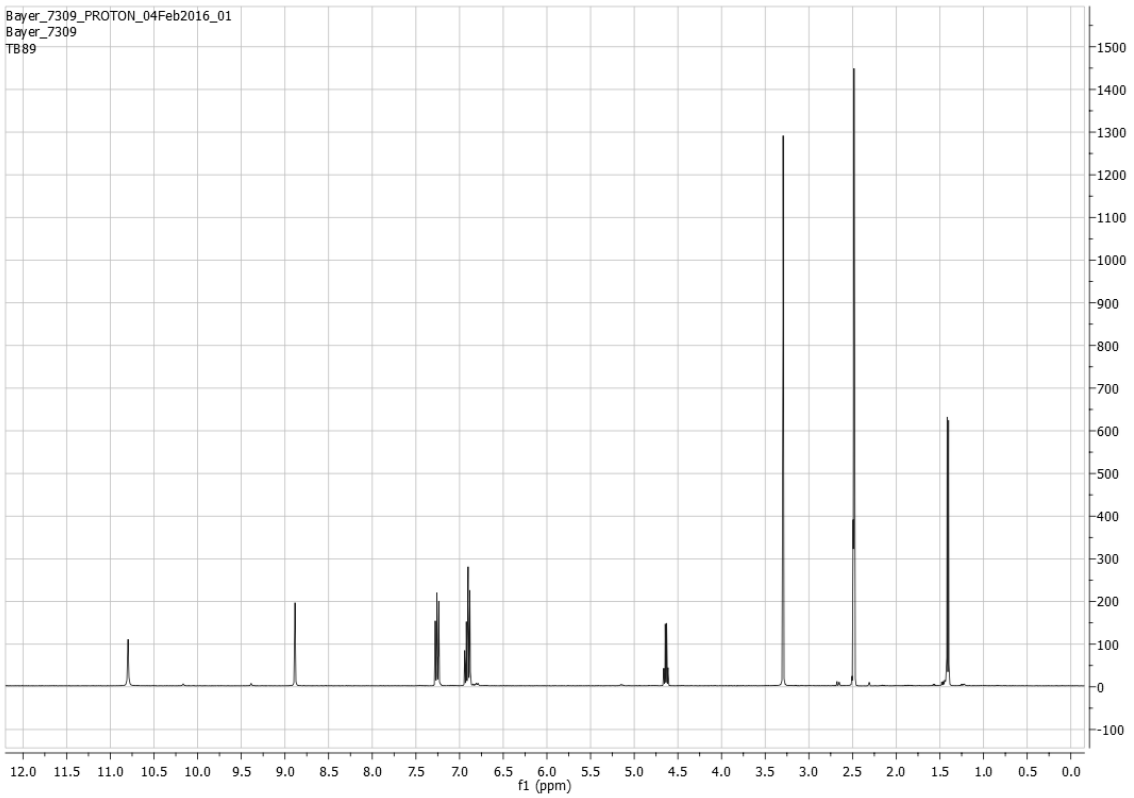

26b (TB88)

HPLC

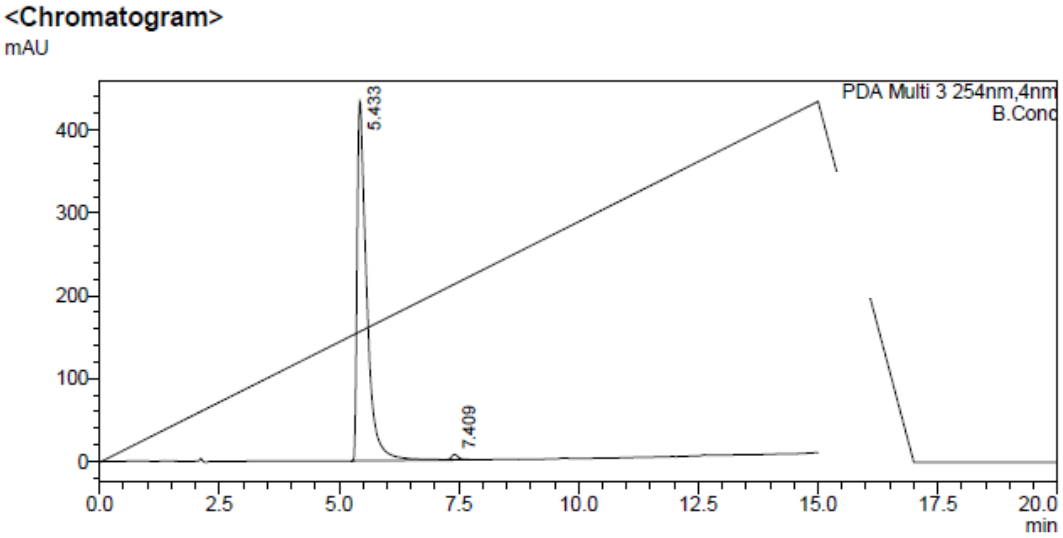

<Peak Table>

PDA Ch3 254nm

Peak#	Ret. Time	Area%
1	5.433	98.993
2	7.409	1.007
Total		100.000

^{1}H-NMR

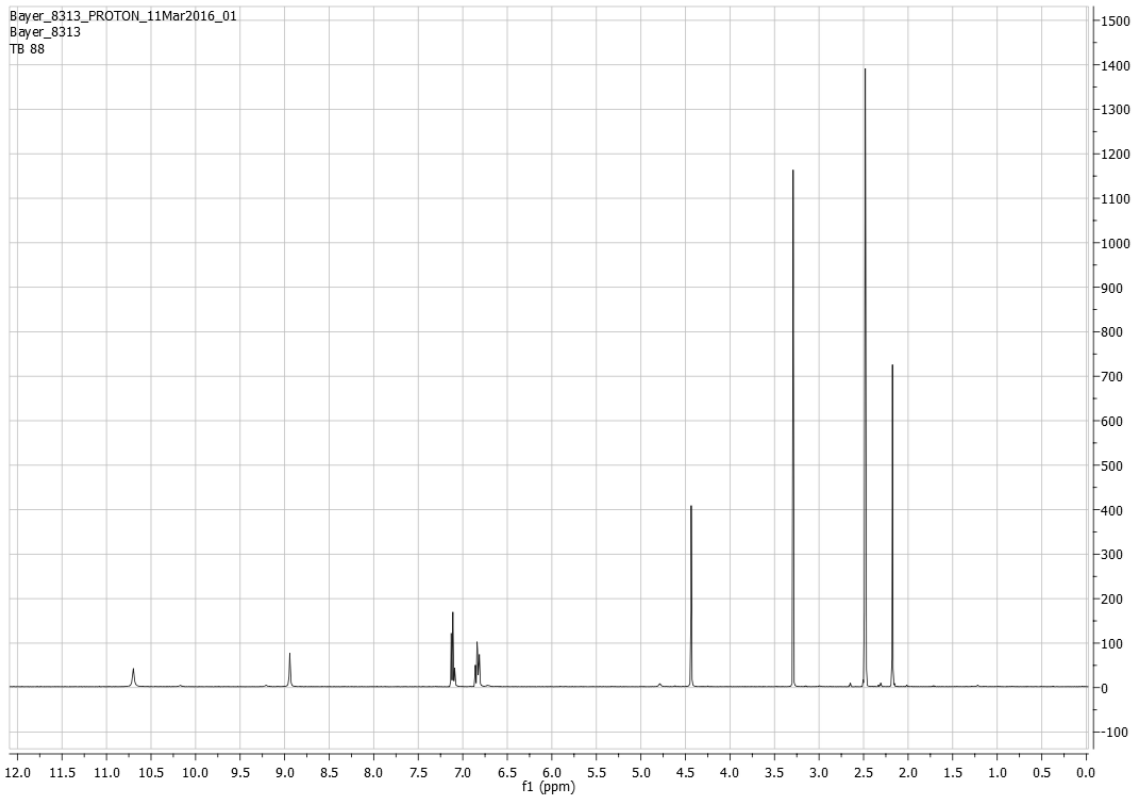

26c (TB96)

HPLC

<Chromatogram>

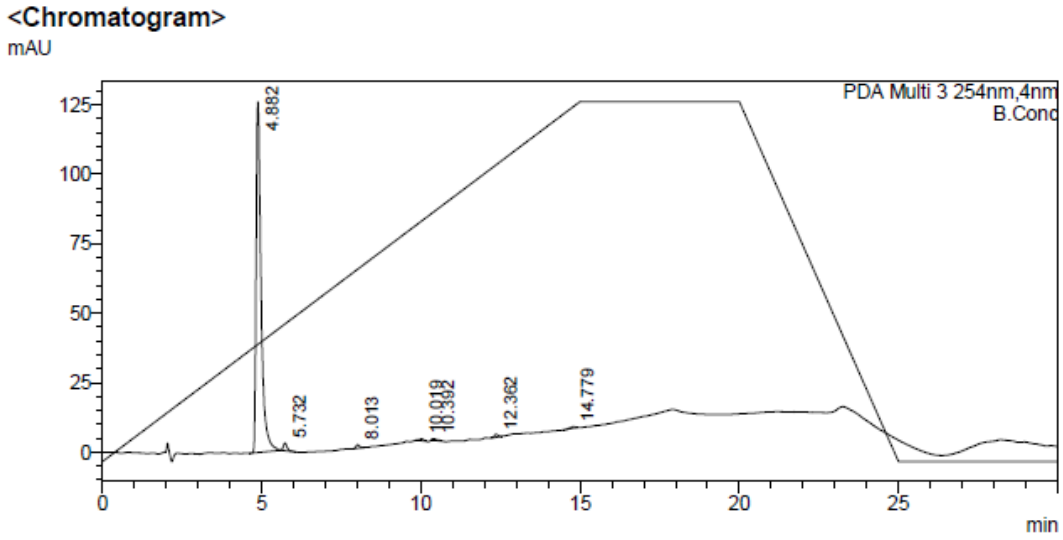

<Peak Table>

PDA Ch3 254nm

Peak#	Ret. Time	Area%	Area	Height
1	4.882	95.814	1371823	126295
2	5.732	1.567	22442	2774
3	8.013	0.659	9430	1236
4	10.019	0.413	5918	708
5	10.392	0.527	7547	703
6	12.362	0.576	8253	1088
7	14.779	0.443	6345	581
Total		100.000	1431758	133385

^{1}H-NMR

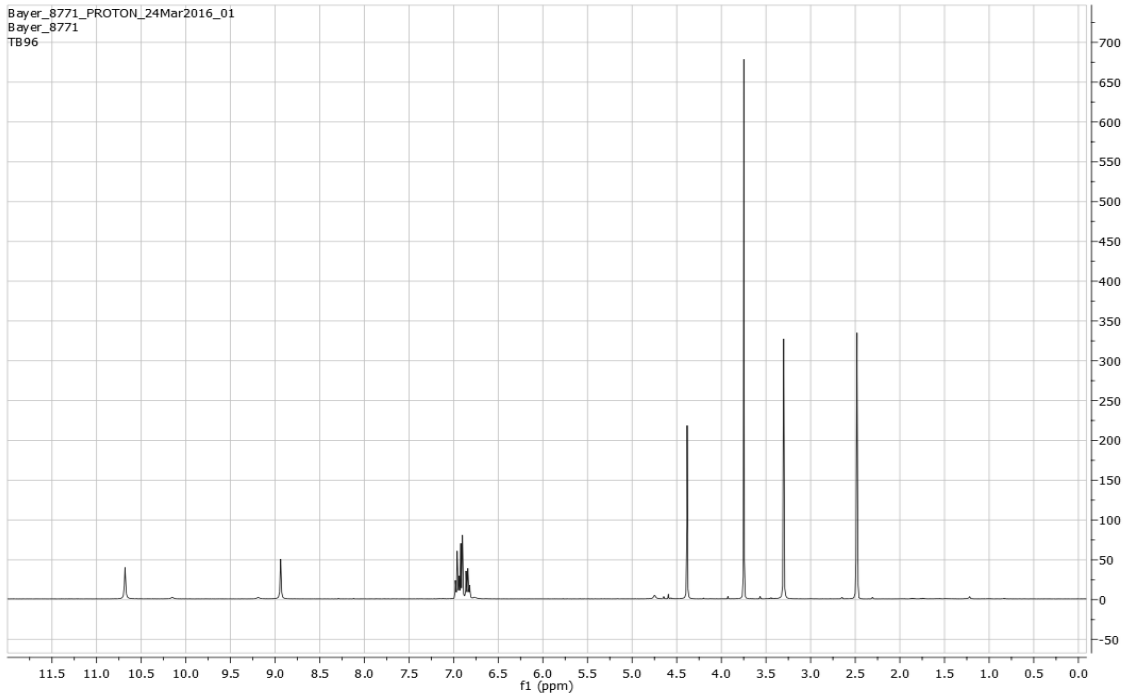

26d (TB79)

HPLC

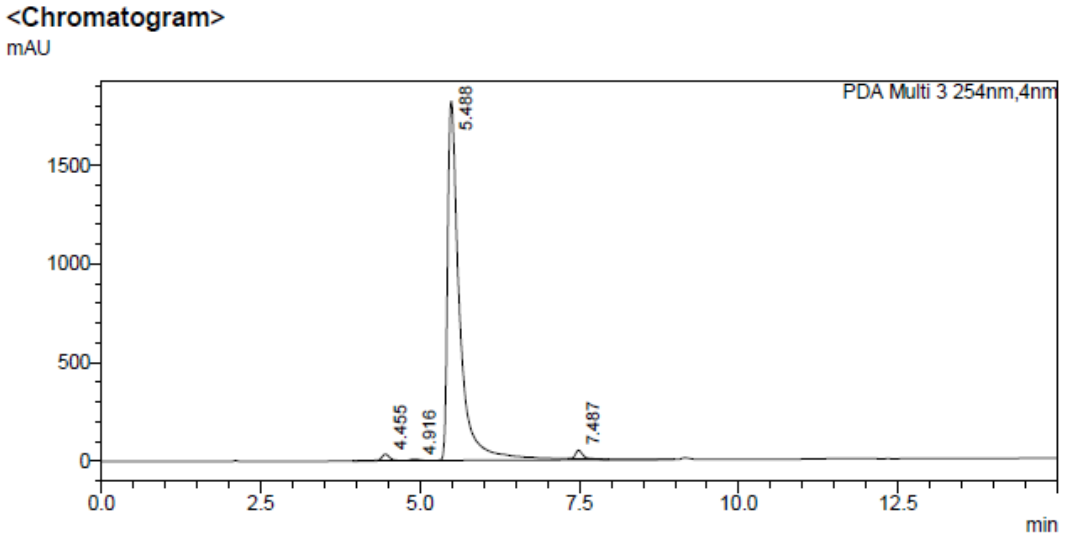

<Peak Table>

PDA Ch3 254nm

Peak#	Ret. Time	Area%
1	4.455	1.287
2	4.916	0.268
3	5.488	97.093
4	7.487	1.352
Total		100.000

^{1}H-NMR

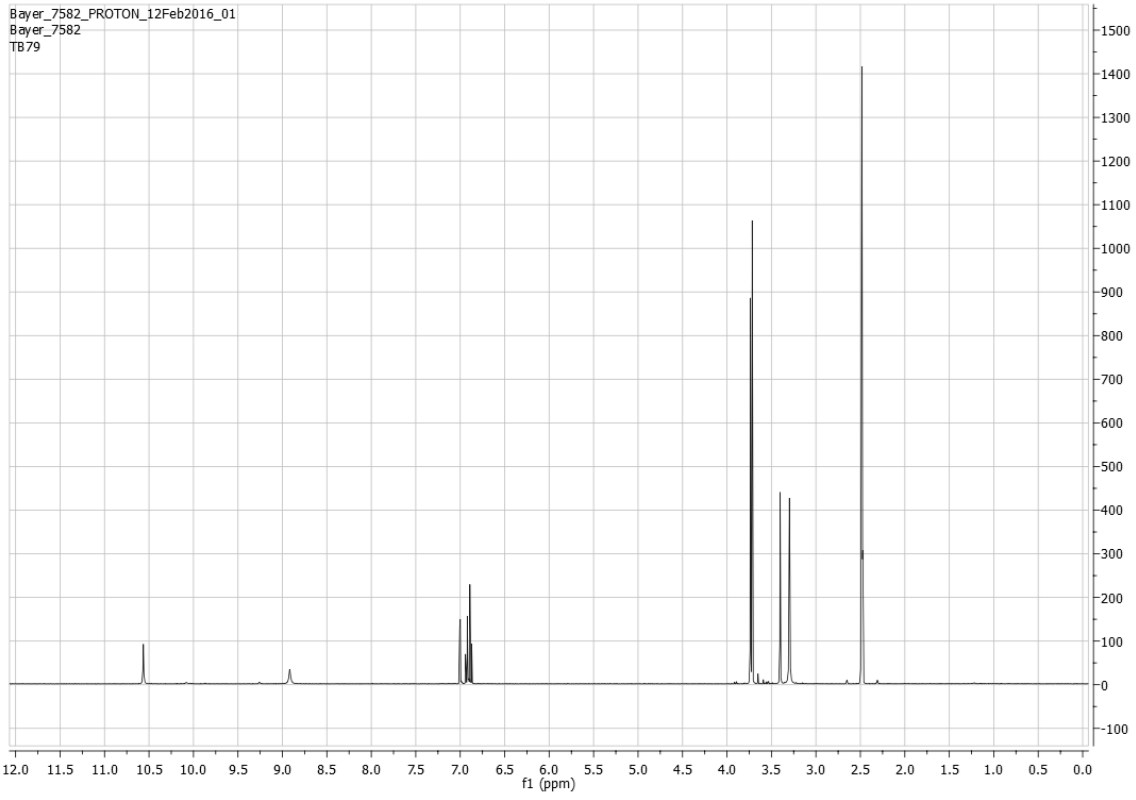

26e (TB94)

HPLC

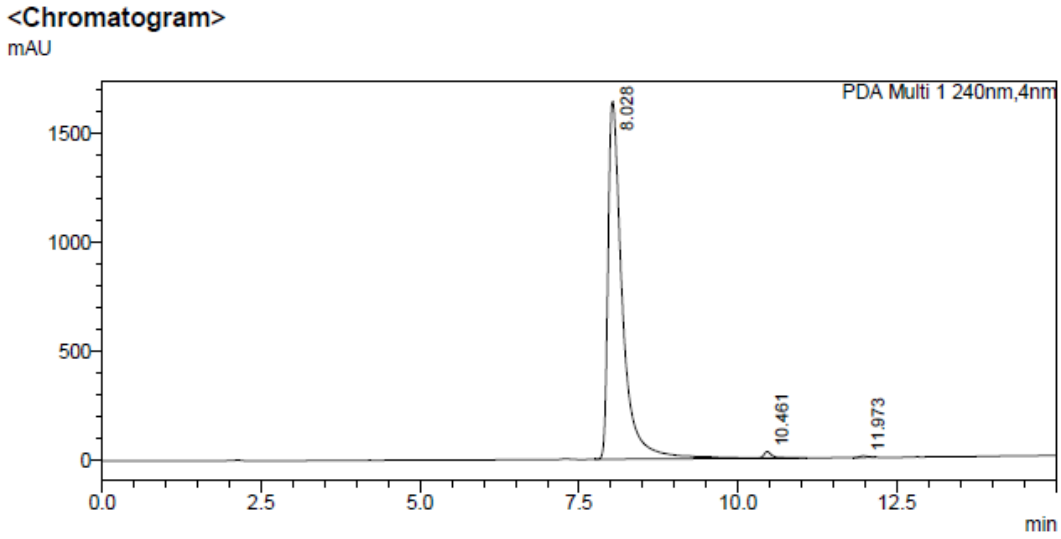

<Peak Table>

PDA Ch1 240nm

Peak#	Ret. Time	Area%
1	8.028	98.882
2	10.461	0.909
3	11.973	0.209
Total		100.000

^{1}H-NMR

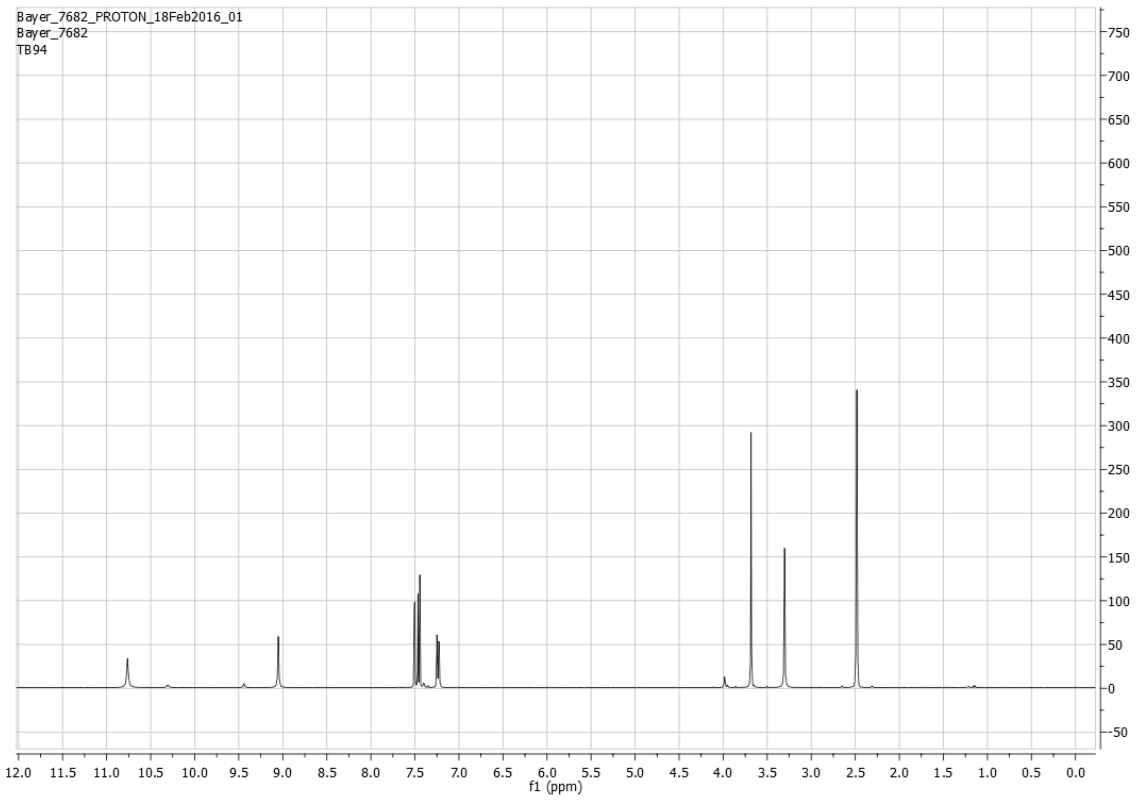

26f (TB103)

HPLC

<Chromatogram>

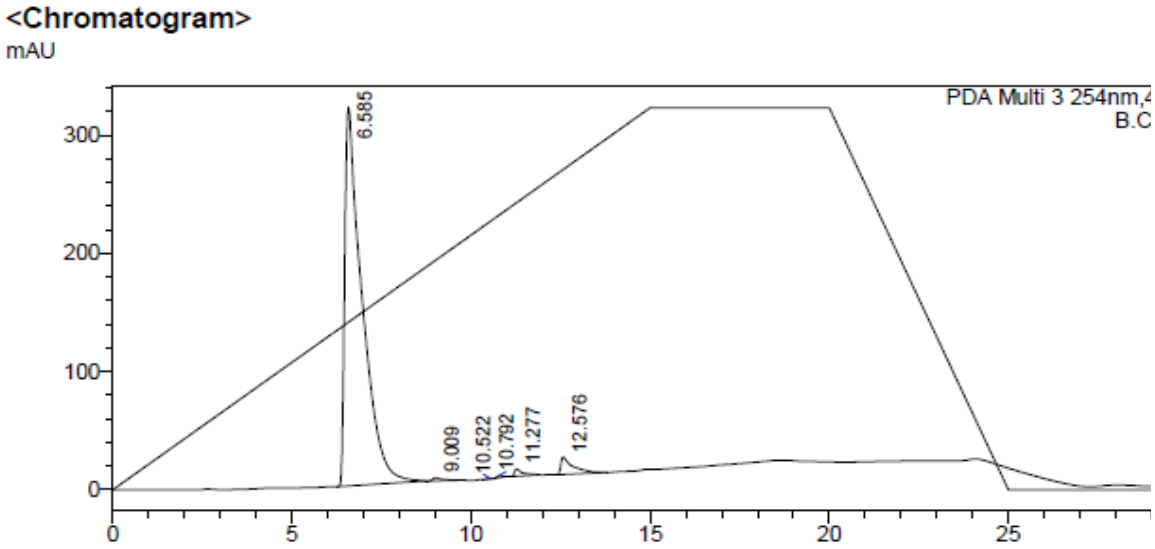

<Peak Table>

PDA Ch3 254nm

Peak#	Ret. Time	Area%	Area	Height
1	6.585	95.372	10766423	319974
2	9.009	0.446	50316	2682
3	10.522	0.035	3961	563
4	10.792	0.148	16721	1633
5	11.277	0.890	100441	6314
6	12.576	3.109	351015	14568
Total		100.000	11288876	345734

^{1}H-NMR

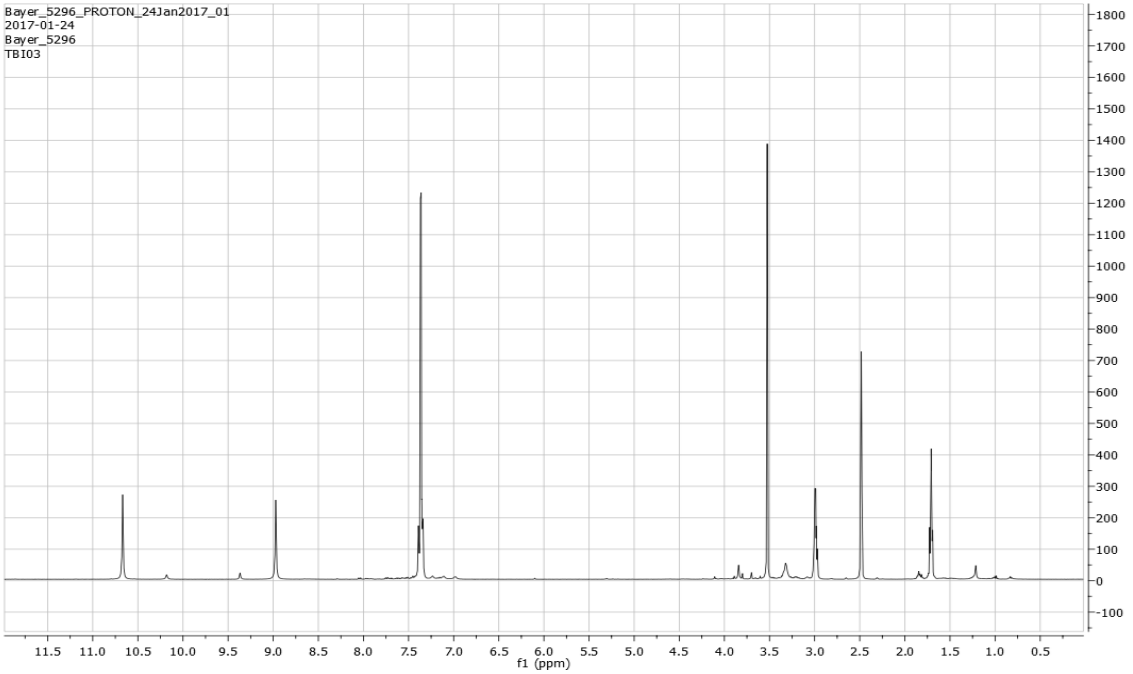

26g (TB104)

HPLC

<Chromatogram>

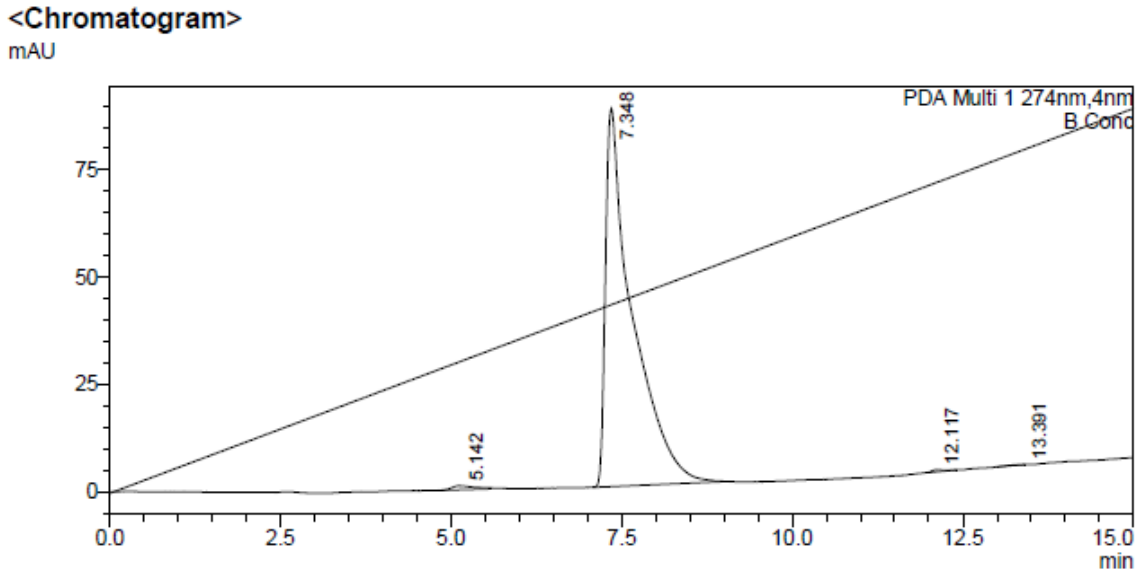

<Peak Table>

PDA Ch1 274nm

Peak#	Ret. Time	Area%	Area	Height
1	5.142	0.880	21590	918
2	7.348	98.851	2424711	88148
3	12.117	0.210	5156	469
4	13.391	0.058	1434	8
Total		100.000	2452891	89542

^{1}H-NMR

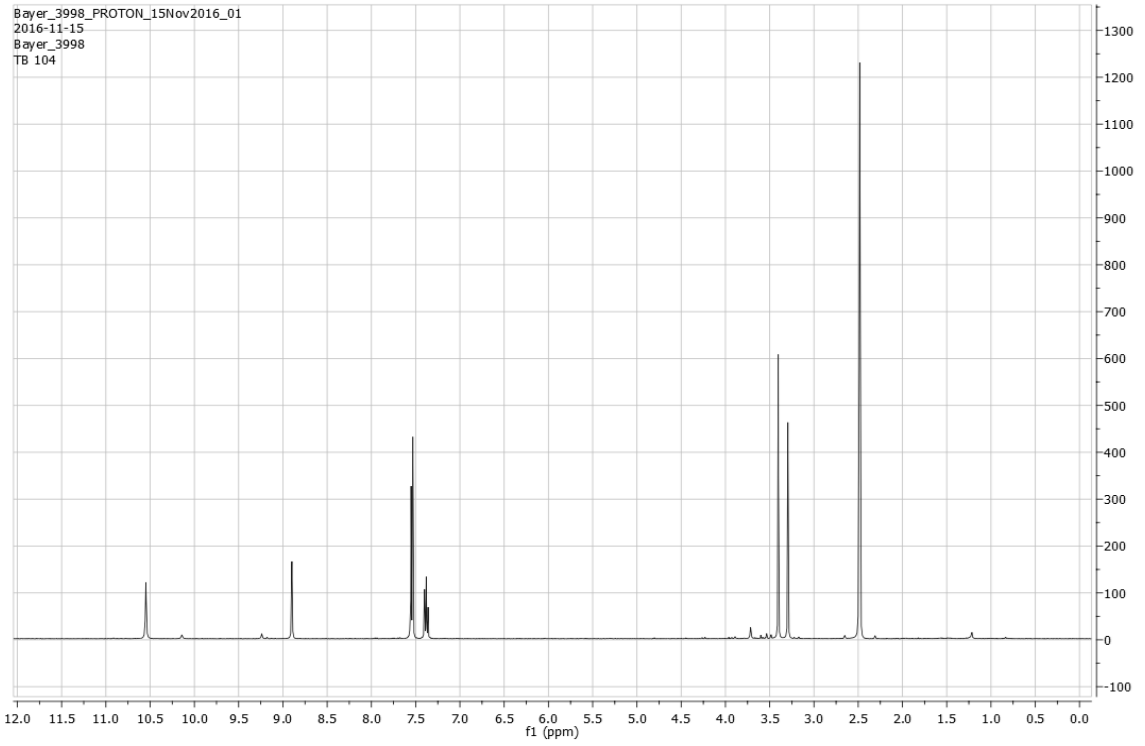

26h (TB105)

HPLC

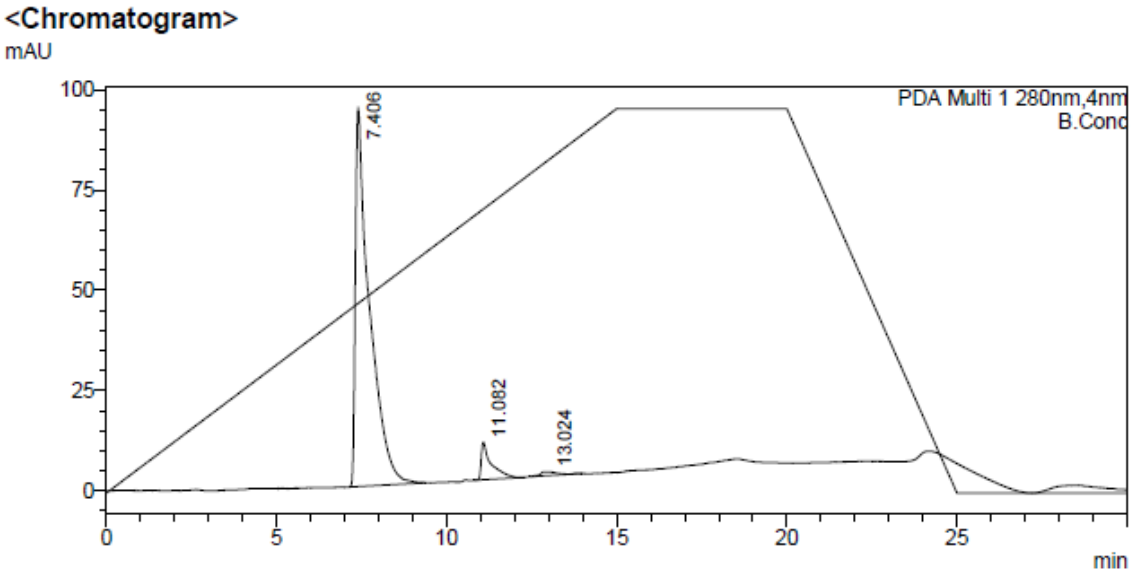

<Peak Table>

PDA Ch1 280nm

Peak#	Ret. Time	Area%	Area	Height
1	7.406	92.455	2742072	94187
2	11.082	6.486	192362	9355
3	13.024	1.060	31426	910
Total		100.000	2965861	104452

^{1}H-NMR

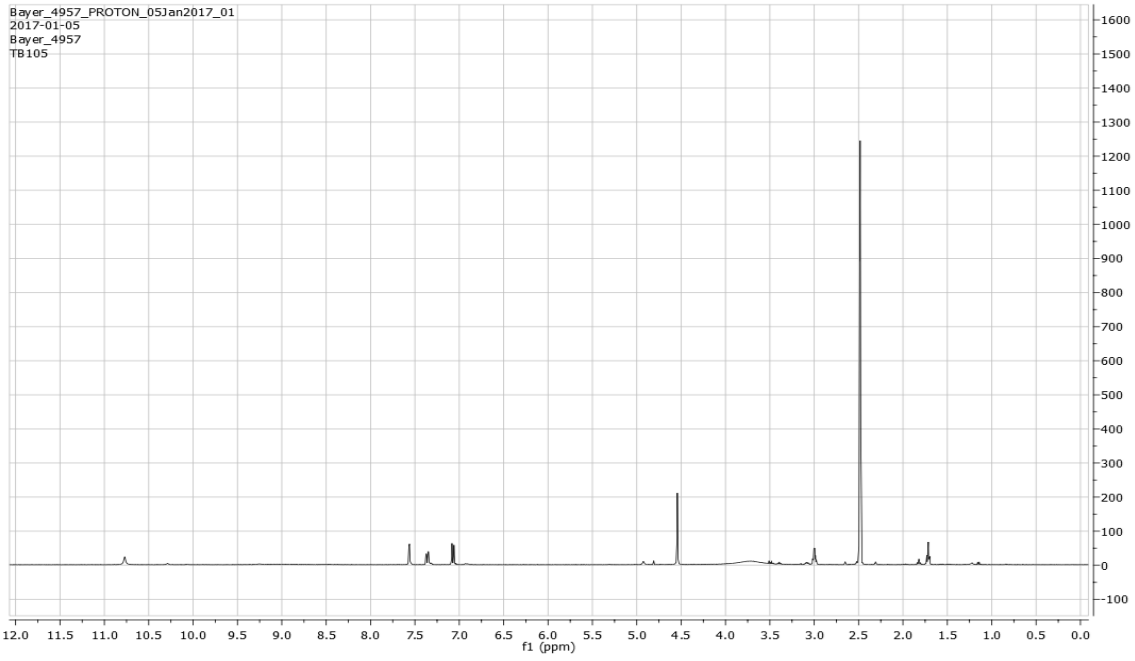

26i (TB90)

HPLC

<Chromatogram>

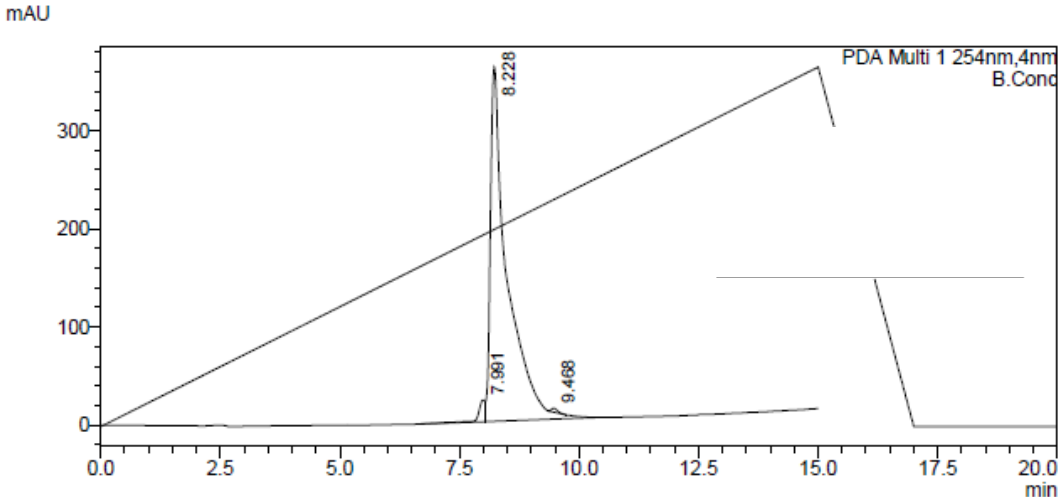

<Peak Table>

PDA Ch1 254nm

Peak#	Ret. Time	Area%
1	7.991	2.237
2	8.228	97.388
3	9.468	0.374
Total		100.000

^{1}H-NMR

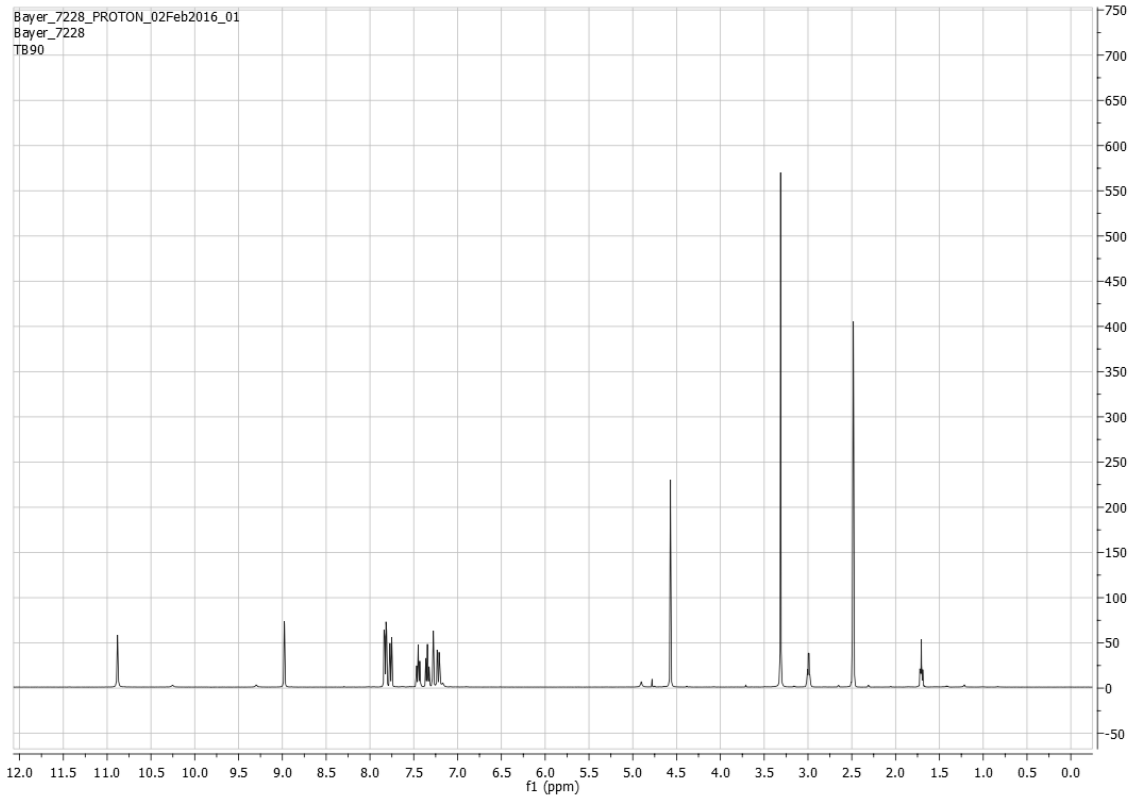

26j (TB97)

HPLC

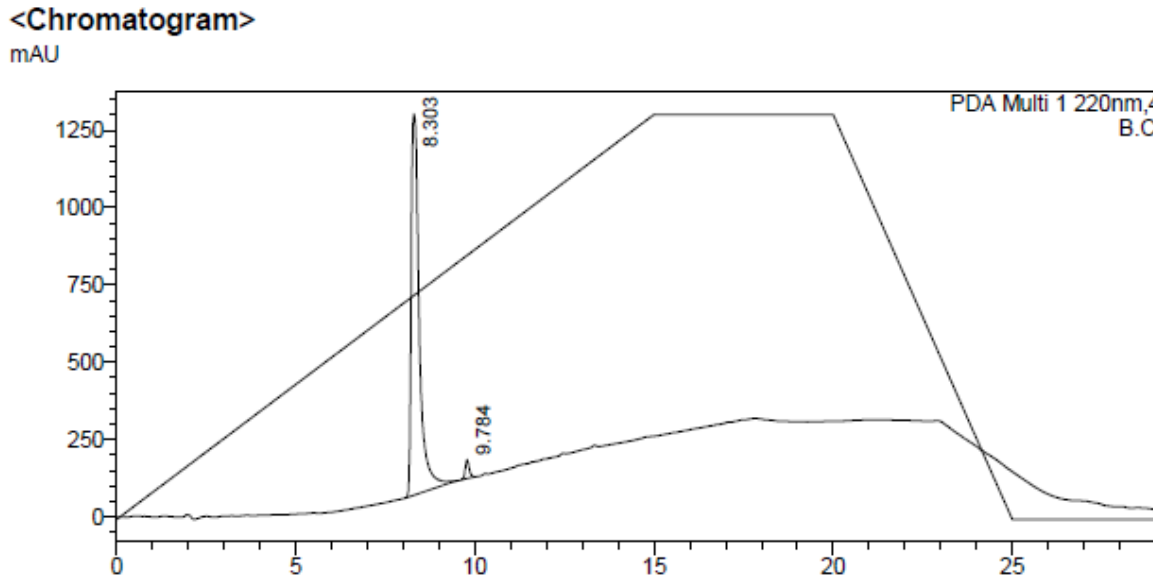

<Peak Table>

PDA Ch1 220nm

Peak#	Ret. Time	Area%	Area	Height
1	8.303	97.711	19322515	1231285
2	9.784	2.289	452719	59819
Total		100.000	19775234	1291104

^{1}H-NMR

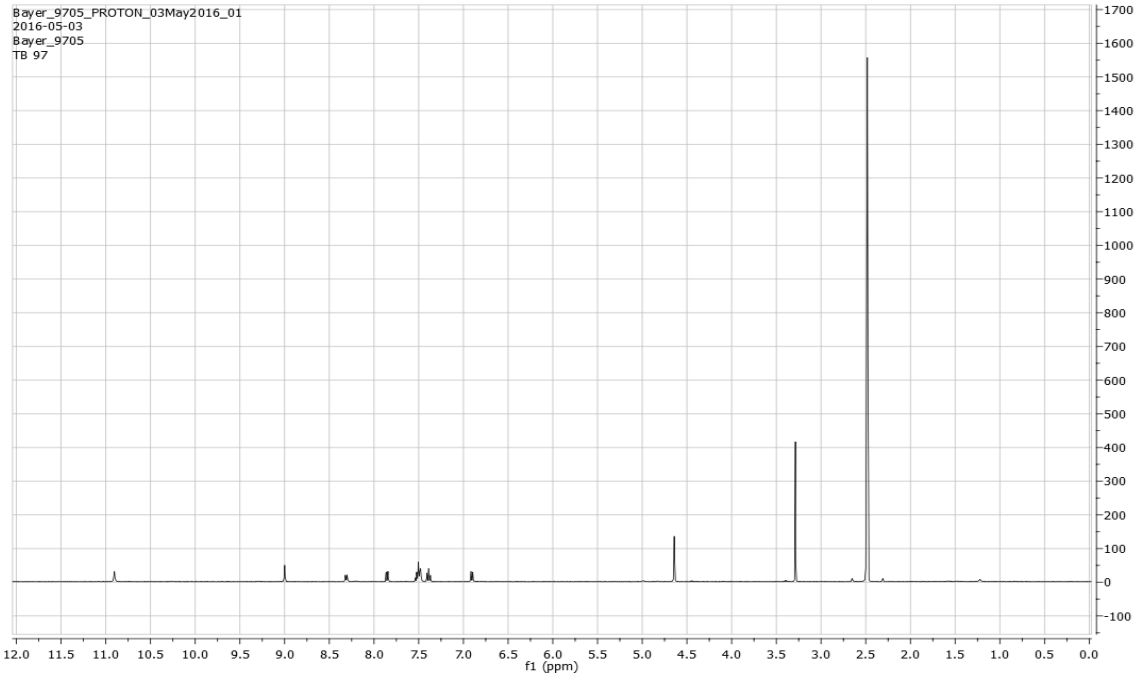

26k (TB80)

HPLC

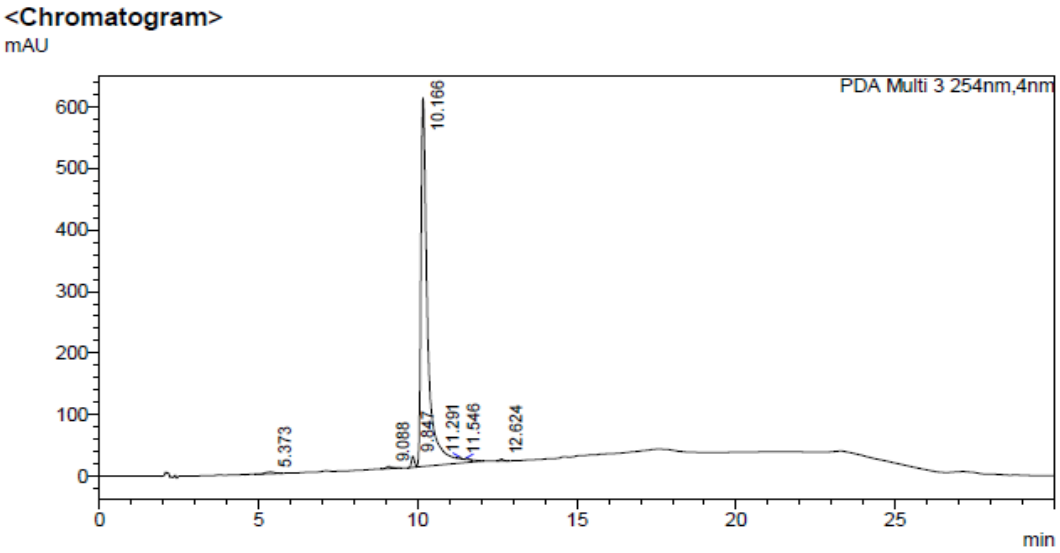

<Peak Table>

PDA Ch3 254nm

Peak#	Ret. Time	Area%
1	5.373	0.610
2	9.088	0.512
3	9.847	1.326
4	10.166	96.826
5	11.291	0.225
6	11.546	0.229
7	12.624	0.271
Total		100.000

^{1}H-NMR

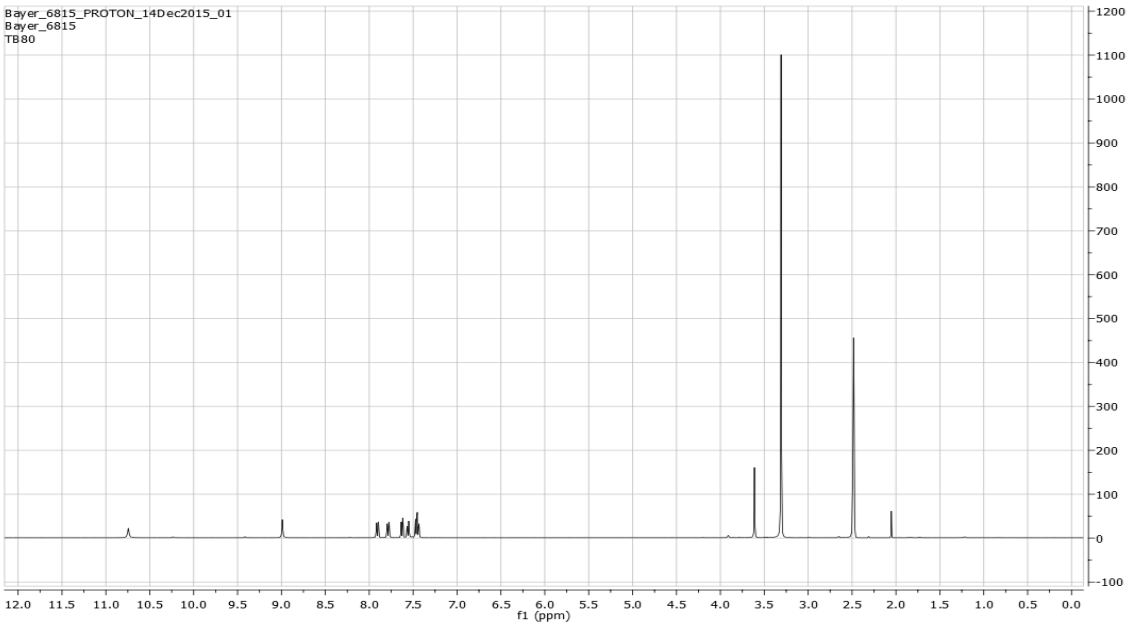

28a (TB83)

HPLC

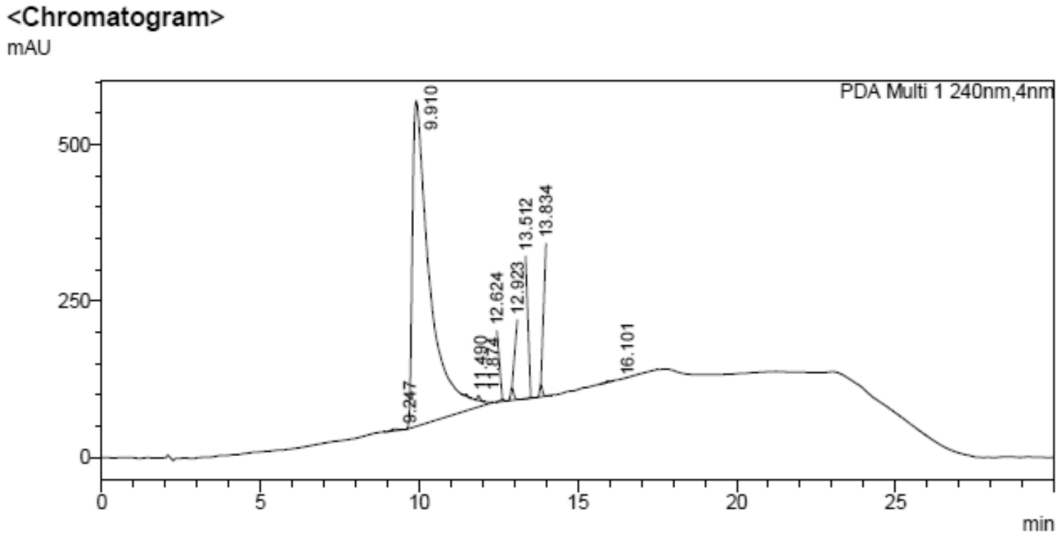

<Peak Table>

PDA Ch1 240nm

Peak#	Ret. Time	Area%	Area	Height
1	9.247	0.220	44425	2663
2	9.910	97.945	19766944	519108
3	11.490	0.059	11916	3029
4	11.874	0.223	44904	7739
5	12.624	0.155	31319	3615
6	12.923	0.684	137983	19962
7	13.512	0.050	10158	1607
8	13.834	0.586	118355	19076
9	16.101	0.077	15612	-31
Total		100.000	20181618	576767

^{1}H-NMR

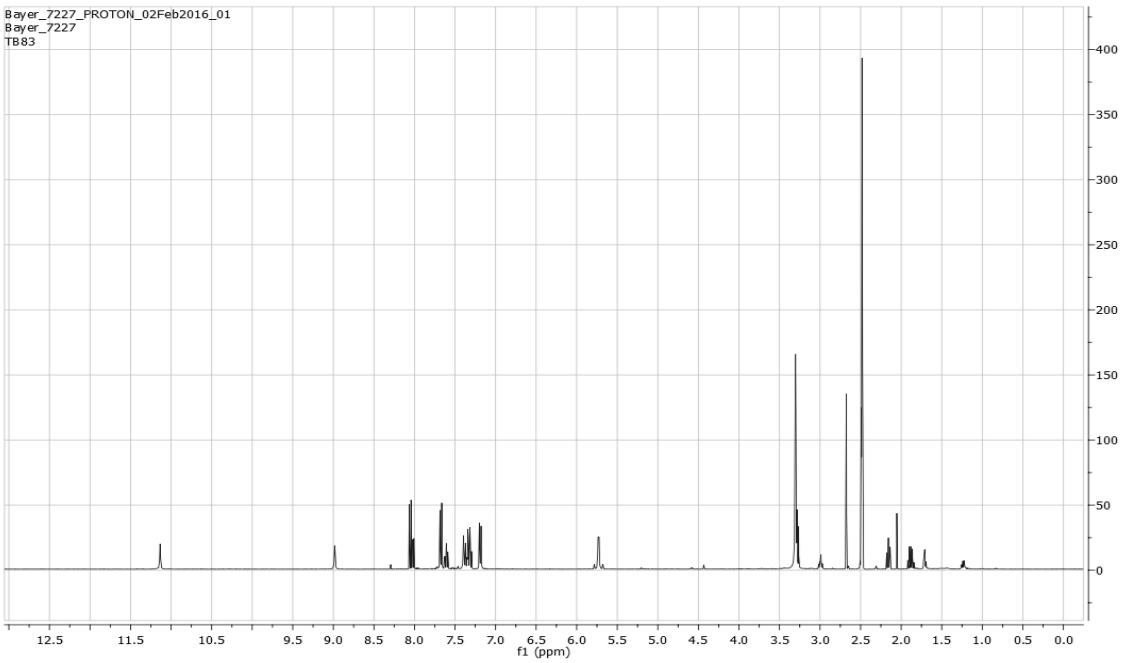

8.2 Additional Data

8.2.1 Effects on E.coli and S.cerevisae

The toxicity of some of the compounds has also been tested for *Escherichia coli* and *Saccharomyces cerevisae* with a simple agar plate test. The culture of the *E.coli* and the *S.cerevisae* cells have been incubated 24 hours and then 15 µl of a 100 µM solution of each compound was applied to each shim. Different concentrations of a positive control (in case of *E.coli*: kanamycine and in case of *S.cerevisae* cycloheximide) was applied. After another 24 hours the agar plates were examined optically (see figure 59). None of the compounds had a negative effect on either *S.cerevisae* cells or *E.coli*.The results were provided by FRANK ERDMANN, Institute of pharmacy, Martin-Luther-University, Halle.

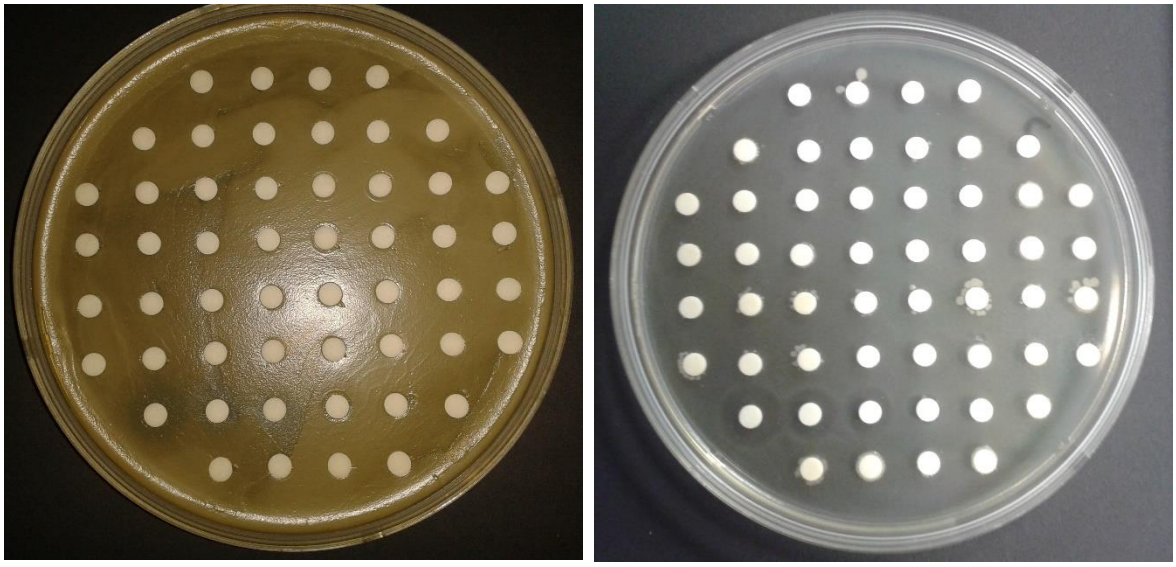

Figure 56 Results of the yeast cell and bacteria assay. On the left there is the yeast cell plate and the bayteria plate is on on the right. The second row of platelets from the bottom is a row of positive controls as described in the procedure.

List of Publications

T. Bayer, A. Chakrabarti, J. Lancelot, T. Shaik, K. Hausmann, J. Melesina, K. Schmidtkunz, M. Marek, F. Erdmann, M. Schmidt, D. Robaa, C. Romier, R.Pierce, M. Jung, W. Sippl, Synthesis, Crystallization Studies, and in vitro Characterization of Cinnamic Acid Derivatives as SmHDAC8 Inhibitors for the Treatment of Schistosomiasis. *ChemMedChem* **13,** 1517–1529 (2018).

F. Kolbinger, E. Koeneke, J. Ridinger, T. Heimburg, M. Müller, T. Bayer, W. Sippl, M. Jung, N. Gunkel, A. Miller, F. Westermann, O. Witt, I. Oehme. The HDAC6/8/10 inhibitor TH34 induces DNA damage-mediated cell death in human high-grade neuroblastoma cell lines. *Archives of Toxicology* **92,** 2649-2664 (2018)

F. Kolbinger, E. Koeneke, J. Senger., T Heimburg., T. Bayer, M. Jung, W. Sippl, M. Marek, C. Romier, N. Gunkel, A.K. Miller, P. Sehr, O. Witt, I. Oehme. Development of novel HDAC inhibitors to selectively co-inhibit HDAC8 and HDAC10 in childhood cancer *Klinische Pädiatrie* 228(03) (2018)

Luciana Ângelo de Souza, Matheus Silva e Bastos, Joice de Melo Agripino, Thiago Souza Onofre , Lourdes Fanny Apaza Calla, Tino Heimburg, Ehab Ghazy, Theresa Bayer, Victor Hugo Ferraz da Silva, Paula Dutra Ribeiro, Leandro Licursi de Oliveira, Gustavo Costa Bressan, Márcia Rogéria de Almeida Lamêgo, Abelardo Silva-Júnior, Raphael de Souza Vasconcellos, Ana Márcia Suarez-Fontes, Juliana Almeida-Silva, Marcos André Vannier-Santos, Raymond Piercee, Wolfgang Sippl and Juliana Lopes Rangel Fietto. Histone deacetylases inhibitors as new potential drugs against Leishmania braziliensis, the main causative agent of New World Tegumentary Leishmaniasis. *Biochem. Pharmacol.*, submitted

Daniel Herp, Johannes Ridinger, Dina Robaa, Stephen A. Shinsky, Karin Schmidtkunz, Talha Z. Yesiloglu, Theresa Bayer, Peter Sehr, Nikolas Gunkel, Aubry Miller, David W. Christianson, Ina Oehme, Wolfgang Sippl, Manfred Jung. First fluorescent acetylspermidine deacetylation assay for HDAC10 identifies inhibitors of neuroblastoma cell colony growth that increase lysosome accumulation. *J. Med. Chem*, submitted

Poster presentations

F. Kolbinger, E. Koeneke, J. Senger, T. Heimburg, T. Bayer, M. Jung, W. Sippl, N. Gunkel, A. Miller, P. Sehr, O. Witt , I. Oehme. Development of novel HDAC inhibitors to selectively co-inhibit HDAC8 and HDAC10 in childhood cancer. EACR Cell Death Conference, January 2016

T. Bayer, J. Melesina, A. Chakrabarti, M. Marek, C. Romier, F. Erdmann, M. Schmidt, M. Jung, W. Sippl. Synthesis and in vitro characterization of hydroxamic acids as small molecule inhibitors for epigenetic parasitic targets. Annual Meeting of the German Pharmaceutical Society – DPhG, 04.10. – 07.10.2016, Munich

T. Bayer, A. Chakrabarti , F. Erdmann, J. Lancelot, J. Melesina, M. Marek, C. Romier, M. Schmidt, M. Jung, W. Sippl. Synthesis and in vitro characterization of hydroxamic acids as small molecule inhibitors for protozoal targets. 3rd Epigenetic Spring Meeting: Chemical Biology of Epigenetics 10.03.-13.03.2016, Freiburg

T. Bayer, A. Chakrabarti , F. Erdmann, J. Lancelot, J. Melesina, M. Marek, C. Romier, M. Schmidt, M. Jung, W. Sippl. Synthesis and in vitro characterization of hydroxamic acids as small molecule inhibitors for protozoal targets. 36th European School of Medicinal Chemistry 26.06.-01.07.2016, Urbino, Italy

T. Bayer, A. Chakrabarti , F. Erdmann, J. Melesina, M. Marek, C. Romier, M. Schmidt, M. Jung, W. Sippl. Synthesis and in vitro characterization of hydroxamic acids as small molecule inhibitors for protozoal targets. DPhG Annual Meeting 2015 23.09.-25.09.2015, Düsseldorf

T. Bayer, T. Heimburg, J. Melesina, M. Marek, C. Romier, M. Schmidt, M. Jung, W. Sippl. Synthesis of hydroxamic acids as small molecule inhibitors for the schistosomial HDAC8. DPhG Annual Meeting 2013 09.10.-11.10.2013, Freiburg

Acknowledgements

I am using this opportunity to express my gratitude to everyone who has supported me throughout my Ph.D. time.

First and foremost I would like to thank Professor Wolfgang Sippl for giving me the opportunity to work on this interesting thesis. Having the opportunity to work with the many national and international collaborators was an extraordinary asset in many aspects. I would like to express my gratitude to the A-PARADDiSE Project for the funding of my work and the great collaboration of so many different specialized areas of expertise.

Dr. Matthias Schmidt deserves a special thank you for his guidance and support in the field of analysis and characterization of my compounds. Moreover I greatly appreciated the activities outside of the lab which were congresses or retreats at partnering universities or just barbecues outside of the lab rooms.

I would also like to thank Dr. Benjamin Sauer and Dr.Tino Heimburg for their assistance and dedicated effort in introducing me into the field of organic synthesis. They both shared their knowledge about synthesis and analysis of structures and also the art of composing a scientific thesis. Additionally they shared their passion for music and dancing especially at various festivals with me. I would like to thank all of the AG Schmidt for the great atmosphere, the inspiring conversations and coffee breaks and seasonal festivities.

I express my warm thanks to the working group of Prof. Sippl and Prof. Jung for inspiring meetings and seminars and the scientific exchange outside of those. I would like to thatnk all collaboration partners for the crystallization and testing of the compounds on various targets. Also I would especially like to thank Dr. Dieter Ströhl, Dr. Christian Ihling, Simone Kniesa, Manuela Woigk, Martina Mannd and Antje Herbrich-Peters for the weighing and analyzing of countless substance samples. Thank you Dr. Frank Erdmann for determining the toxicity assays for all of my compounds.

I want to thank all of the employees of the Institute of Pharmacy and the Institute of Chemistry, who have contributed to the making of this work.

Getting through my Ph.D. time required more than academic support and I have many, many people to thank for that. Here I would like to express my gratitude and appreciation for their friendship. I would like to thank - by no means exhaustive - Jonas, Tilman, Anne,

Bianca, Anni, Zara, Felix, Jan and Jenny for supporting me and dealing with the range of emotions during this time and hopefully also in the future.

Most importantly, none of this could have happened without my family. I thank my parents, brother and sister and niece for supporting me whenever needed.

Personal Declaration

Hereby, I declare that I have composed the presented thesis independently on my own and without any other resources than the ones indicated. All thoughts taken directly or indirectly from external sources are properly denoted as such.

This paper has neither been previously submitted to another authority nor has it been published yet.

Halle (Saale), 2020

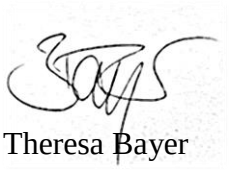

Theresa Bayer

Curriculum vitae

Personal

Name	Theresa Yasmin Charlotte Bayer
Date of birth	22.10.1986
Place of birth	Hamburg, Germany
Citizenship	German

Education

1993-1997	Grundschule Redderbarg, Hamburg, Germany
1997-2003 and 2004-2006	Carl-von-Ossietzky Gymnasium. Hamburg, Germany
2003-2004	Arthur Meighen High-School, Portage la Prairie, MB, Canada
2007-2012	Institute of Pharmacy, Martin-Luther-Universität Halle-Wittenberg, Germany
08/2008	Famulatur Bergstedter Markt Apotheke, Hamburg
09/2008	Famulatur Krankenhausapotheke Bundeswehrkrankenhaus, Hamburg
09/2010	1. Abschnitt der pharmazeutischen Prüfung
10/2012	2. Abschnitt der pharmazeutischen Prüfung
10/2012-03/2013	Pharmazeutin im Praktikum, August-Bebel-Apotheke Halle, Germany
05/2013-10/2013	Pharmazeutin im Praktikum, Inst. f. Pharmazie, Martin-Luther-Universität Halle-Wittenberg, Germany
11/2013	3. Abschnitt der pharmazeutischen Prüfung
12/2013	Approbation als Apothekerin
10/2014	Akademischer Grad: Diplom-Pharmazeutin, Martin-Luther-Universität Halle-Wittenberg, Germany

Work experience

07/2006-06/2007	Wildewood Golf and Country Club, Winnipeg, MB, Canada
12/2013-12/2018	Angestellte Apothekerin, August-Bebel-Apotheke Halle, Germany
02/2014-01/2017	Ph.D. student, Martin-Luther-Universität Halle-Wittenberg, Germany
03/2017-04/2018	Angestellte Apothekerin, Lilien-Apotheke Halle, Germany
since 05/2018	Angestellte Apothekerin / Fillialleitung, Kreuz-Apotheke Halle, Germany

Halle (Saale), 2021

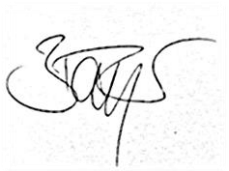

Theresa Bayer